Numerical Studies of Models for Electrokinetic Flow and Charged Solute Transport in Periodic Porous Media

Numerische Untersuchung von Modellen zum elektrokinetischen Fließgeschehen und dem Transport geladener, gelöster Substanzen in periodischen porösen Medien

Der Naturwissenschaftlichen Fakultät
der Friedrich-Alexander-Universität Erlangen-Nürnberg
zur
Erlangung des Doktorgrades Dr. rer. nat.

vorgelegt von
Florian Frank
aus Lichtenfels / Ofr.

Als Dissertation genehmigt von der Naturwissenschaftlichen Fakultät der Friedrich-Alexander-Universität Erlangen-Nürnberg.

Tag der mündlichen Prüfung:	21. November 2013
Vorsitzender des Promotionsorgans:	Prof. Dr. J. Barth
Gutachter:	Prof. Dr. P. Knabner
	Prof. Dr. F. A. Radu

Contents

List of Figures

List of Tables

Danksagung

Mit der Fertigstellung dieser Dissertationsschrift ist es an der Zeit denjenigen meinen Dank auszusprechen, die mich begleitet und unterstützt haben.

Mein besonderer Dank gilt meinem Doktorvater Herrn Prof. Dr. Peter Knabner; insbesondere für die Überlassung dieses interessanten, interdisziplinären Themas, für seine unerschöpfliche Diskussionsbereitschaft und das stetig entgegengebrachte Vertrauen. Die geführten kritischen wie inspirierenden Fachdiskussionen sowie wissenschaftlichen Streitgespräche trugen nicht nur zu der Qualität dieser Arbeit bei, sondern förderten auch meine eigene fachliche und persönliche Weiterentwicklung.

Ebenso gilt mein außerordentlicher Dank Herrn Prof. Dr. Kai Uwe Totsche vom Lehrstuhl für Hydrogeologie in Jena, der mich in großzügiger Weise seit Beginn meines Promotionsvorhabens wohlwollend förderte. Seine aufschlussreichen Anregungen zur Verknüpfung der Mathematischen Modellierung mit hydrogeologischen Anwendungen waren meinem Verständnis überaus förderlich.

Von großem Wert war mir die beratende Unterstützung von Frau Prof. Dr. Nicole Marheineke, deren Türen mir seit Beginn ihres Antritts zur Professur in Erlangen durchweg offen standen.

Ich danke den Sekretärinnen Frau Astrid Bigott und Frau Cornelia Kloss dafür, dass sie mir über all die Jahre den Rücken freihielten, indem sie stets zuverlässig und schnell Organisationsaufgaben übernahmen oder mir dazu freundlich Hilfestellung gaben. Ebenso möchte ich sowohl Frau Ina Voigt vom Lehrstuhl für Hydrogeologie in Jena als auch Frau Petra Frosch vom Promotionsbüro für die unkomplizierten und raschen Abwicklungen danken.

Für die bereitwillige Übernahme des Zweitgutachtens bedanke ich mich herzlich bei Herrn Prof. Dr. Florin Adrian Radu von der Universität Bergen in Norwegen. Ferner danke ich Herrn Prof. Dr. Johannes Jahn für die engagierte Mitwirkung als Vorsitz am Rigorosum.

Meinen derzeitigen und ehemaligen Kollegen des Lehrstuhls danke ich für das Interesse an meiner Arbeit, die Hilfsbereitschaft und vor allen Dingen für das wunderbare Arbeitsklima. Wertvolle Unterstützung erfuhr ich unter anderem durch Herrn Fabian Brunner und jüngst auch durch meine kürzlich hinzugekommenen Kollegen Herrn Tobias Elbinger, Herrn Markus Gahn und Herrn Dr. Raphael Schulz. Den Herren Dr. Vadym Aizinger,

PD Dr. Volker Grimm, PD Dr. Serge Kräutle und Dr. Alexander Prechtel möchte ich für die Zeit und die Ratschläge zur Orientierung danken, welche sich insbesondere vor verbindlichen Entscheidungen als äußerst hilfreich erwiesen. Herr Dr. Alexander Prechtel stand mir ebenfalls zusammen mit Herrn Fabian Klingbeil mit Rat und Tat bei Software- und Hardwareproblemen zur Seite.

Zweien meiner Kollegen bin ich ganz besonderen Dank schuldig: Zum einen Frau Dr. Nadja Ray, mit der ich ein Büro über mehr als vier Jahre teilte. Ihre Erläuterungen waren grundlegend für meine Einsichten in die periodische Homogenisierung sowie in die Mathematische Modellierung und haben meine Kenntnisse auf diesen Gebieten signifikant erweitert. Zum anderen Herrn Matthias Herz, mit dem ich unzählige Diskussionen quer durch die mathematischen Disziplinen führte und der sich, selbst in arbeitsreichen Zeiten, ausgiebig meiner Fragestellungen annahm. Ich möchte beiden meinen innigsten Dank aussprechen, nicht nur für die ungezwungene wie ergiebige Zusammenarbeit, sondern auch für all das, was uns in den letzten Jahren zu mehr als Kollegen hat werden lassen.

Obgleich meine Promotionszeit sehr arbeitsintensiv war und mir ein hohes Maß an persönlichem Verzicht, Fleiß und Ausdauer abverlangte, werde ich diese Zeit, die von einer offenen, familiären Atmosphäre geprägt war, stets in guter Erinnerung behalten.

Erlangen, August 2013 Florian Frank

Titel, Zusammenfassung u. Aufbau der Arbeit

Numerische Untersuchung von Modellen zum elektrokinetischen Fließgeschehen und dem Transport geladener, gelöster Substanzen in periodischen porösen Medien

Zusammenfassung. Gegenstand der vorliegenden Dissertationsschrift ist die Untersuchung von Modellen zum Fließgeschehen wässriger Elektrolytlösungen innerhalb eines porösen Mediums mit periodischer Struktur, die den Transport geladener, gelöster Stoffe berücksichtigen. Als Modell liegt das nichtstationäre Stokes-Nernst-Planck-Poisson-System (SNPP-System) zu Grunde.

Die Qualitätsbeurteilung entsprechender *gemittelter* Modelle ist von allgemeinem Interesse, da Simulationen, welche die Geometrie der porösen Matrix auf der Porenskala auflösen, unter ökonomischen Gesichtspunkten nicht praktikabel sind. Die verschiedenen, zu untersuchenden, gemittelten Modelle beschreiben in Abhängigkeit der gewählten Skalierung mit variabler Präzision das effektive makroskopische Verhalten der betrachteten elektrokinetischen Phänomene. Die zugrundeliegenden partiellen Differentialgleichungen beinhalten effektive Tensoren, deren analytische Darstellung durch die Mittelung von Lösungen von Hilfsproblemen gewonnen wird. Diese sogenannten Zellprobleme sind auf kleinen Gebieten definiert, welche die periodische Struktur der porösen Matrix widerspiegeln.

Ein Schwerpunkt dieser Arbeit liegt sowohl in der qualitativen als auch quantitativen Untersuchung des Homogenisierungsprozesses mittels umfangreicher numerischer Studie, d. h. der Konvergenzeigenschaften des SNPP-Systems für verschwindende Mikrostruktur. Zu diesem Zweck werden numerische Verfahren vorgeschlagen, welche in der Lage sind, das nichtstationäre, vollgekoppelte / nichtlineare SNPP-System sowie die entsprechenden gemittelten Systeme präzise und effizient zu lösen. Die Diskretisierung erfolgt

vollimplizit in der Zeit; während im Ort zweidimensionale gemischte Finite Elemente benutzt werden, die lokal massenerhaltend bezüglich der Konzentrationen der geladenen Teilchen sind. Bezüglich der Diskretisierungsparameter sind die Verfahren von optimaler Ordnung. Dies wird zum einen numerisch gezeigt und zum anderen rigoros durch eine a-priori-Fehlerabschätzung bewiesen.

Schließlich befasst sich die Arbeit mit der numerischen Umsetzung einer Erweiterung des SNPP-Systems, welches Anlagerungs- und Auflösungsprozesse an der Oberfläche der betrachteten, lokal-periodischen porösen Matrix einbezieht. Die hierdurch entstehende veränderliche Mikrostruktur beeinflusst das Fließgeschehen und somit auch den Stofftransport. Die Lösung des zugehörigen Zweiskalenmodells, welches jene Abhängigkeiten zwischen den Skalen umfasst, wird auf beiden Skalen durch gemischte Finite Elemente approximiert. Simulationen veranschaulichen das Zusammenspiel zwischen Stofftransport, veränderlicher Mikrostruktur und Fließgeschehen.

Aufbau der Arbeit nach Kapiteln. In Kapitel 2 werden die mathematischen Modelle, die Gegenstand der numerischen und analytischen Untersuchungen in der vorliegenden Arbeit sind, vorgestellt. Zunächst wird das in Abschnitt 1.1 eingeführte, dimensionslose SNPP-System in einen Zweiskalenkontext unter Verwendung einer periodischen Mikrostruktur eingebettet. Durch Einbezug von Skalierungsparametern erhält man eine Familie von skalierten SNPP-Systemen. Es werden »äquivalente«, gemittelte partielle Differentialgleichungssyteme aufgeführt, welche das effektive makroskopische Verhalten der betrachteten Phänomene sinnvoll beschreiben. Die Art dieser Homogenisierungsergebnisse, die als Darcy-Nernst-Planck-Poisson-Systeme (DNPP-Systeme) bezeichnet werden, hängen von den gewählten Skalierungsparametern ab. Diese beinhalten unter anderem effektive Tensoren, die man durch die Mittelung der Lösungen von sogenannten Zellproblemen erhält. Letztere sind auf kleinen Gebieten definiert, welche die periodische Geometrie des Feststoffanteils der porösen Matrix abbilden. Schließlich wird der Zusammenhang zwischen der Geometrie der porösen Matrix und den effektiven Tensoren veranschaulicht.

In Kapitel 3 wird eine voll-zeitimplizite gemischte Finite-Element-Diskretisierung ausgearbeitet, die Raviart-Thomas-Elemente beliebiger Ordnung verwendet. Das Hauptresultat dieses Kapitels ist eine a-priori-Abschätzung für den Gesamtdiskretisierungsfehler des betrachteten Systems. Der zugehörige Beweis greift auf ein bestehendes Existenzresultat für das SNPP-System in nichtgemischter Form zurück. Daher ist es zunächst erforderlich zu zeigen, dass die Lösung der gemischten Formulierung ebenfalls Lösung der nichtgemischten ist. Mit dem nun zur Verfügung stehenden Existenzresultat werden a-priori-Abschätzungen

für die Teilsysteme gezeigt, welche in Kombination schließlich den Beweis des Haupttheorems liefern.

Kapitel 4 stellt ein implementierbares volldiskretes numerisches Verfahren vor, welches die Lösung des skalierten SNPP-Systems sowie die assoziierter SNPP-Systeme in zwei Raumdimensionen zu approximieren vermag. Zunächst werden zwei Linearisierungsschemata – ein iteratives Splitting- und ein Newton-Verfahren – vorgestellt und anhand des zeitdiskreten SNPP-Systems erläutert. Einer auf die praktische Anwendbarkeit bezogenen Diskussion folgend, fällt die Wahl auf das iterative Splitting-Schema, das insbesondere auch analog auf die homogenisierten Systeme anwendbar ist. Durch dieses zerfallen die nichtlinearen, zeitdiskreten Systeme in lineare Teilsysteme, die entweder von Konvektions-Diffusions-Typ oder von Stokes-Typ sind. Erstere werden im Raum mittels Raviart-Thomas-Elemente niedrigster Ordnung, letztere mittels Taylor-Hood-Elemente diskretisiert. Das resultierende numerische Gesamtverfahren ist voll-zeitimplizit und bezüglich chemischer Spezies lokal massenerhaltend.

In Kapitel 5 wird das Verifizierungsverfahren MMS auf die Implementierungen der im vorherigen Kapitel vorgestellten Diskretisierungsverfahren angewendet. Die numerischen Schemata für die vollgekoppelten/nichtlinearen SNPP- und DNPP Systeme werden verifiziert, indem die anhand der Konvergenzabschätzungen für die linearen Teilsysteme zu erwartenden optimalen Gitterkonvergenzordnungen numerisch belegt werden. Insbesondere wird dadurch implizit auch die Konvergenz des inbegriffenen iterativen Splitting-Schemas nachgewiesen. Zudem wird durch die numerisch bestimmten Konvergenzraten gezeigt, dass die in Kapitel 3 gezeigte a-priori-Fehlerabschätzung des SNPP-Systems für Raviart-Thomas Elemente niedrigster Ordnung gültig ist.

Die Verifikation der Diskretisierungsverfahren aller betrachteten Systeme stellt die Grundlage für die numerische Untersuchung aller zur Diskussion stehenden Systeme in Kapitel 6 dar. Gegenstand dieses Kapitels ist der Vergleich der Lösungen der auf der Porenskala gültigen SNPP-Systeme mit denen der entsprechenden DNPP-Systeme, welche auf einer gemittelten Skala definiert sind. Aus diesem Grund muss zuvor ein geeignetes Testszenario erarbeitet werden, welches insbesondere die Definition des perforierten Gebiets, auf welchem die SNPP-Probleme formuliert sind, beinhaltet. Anhand von anschließenden Simulationen wird das Lösungsverhalten hinsichtlich derer physikalischen Bedeutung für verschiedene Skalierungen diskutiert. Der Kern dieses Kapitels stellt sowohl die qualitative als auch quantitative Untersuchung der Konvergenzraten dar, mit denen die Lösungen der Porenskalenmodelle gegen die der entsprechenden effektiven Modelle konvergieren. Um die

auf verschiedenen Gittern definierten Lösungen zu vergleichen, wird ein Verfahren benutzt, welches auf einem Gitter definierte diskrete Lösungen auf ein anderes Gitters projiziert.

Kapitel 7 befasst sich mit der numerischen Simulation eines Zweiskalenszenarios, welches die effektive Kolloiddynamik in einer aus einer Phase bestehenden Flüssigkeit innerhalb eines porösen Mediums beschreibt. Das zugrundeliegende Porenskalenproblem ist eine Erweiterung des bekannten SNPP-Systems, das Anlagerungs- und Ablösungsprozesse berücksichtigt, die eine veränderliche Mikrostruktur der porösen Matrix nach sich ziehen. Die in diesem Kapitel vorgestellte numerische Zweiskalenmethode greift auf die Diskretisierungen von Kapitel 4 zurück. Abschließende Simulationen zeigen das Zusammenspiel zwischen Stofftransport, sich veränderlicher Mikrostruktur und Fließgeschehen.

Für die Simulationen der in dieser Dissertationsschrift betrachteten Modelle wurde das numerische Werkzeug *HyPHM* geschrieben, dessen Umfang im Anhang A aufgeführt ist.

Bereits publizierte Beiträge. Teile der vorliegenden Dissertationsschrift konnten bereits in den Zeitschriftenartikeln F. Frank, N. Ray, & P. Knabner (2011) »Numerical investigation of homogenized Stokes–Nernst–Planck–Poisson systems« und N. Ray, T. van Noorden, F. Frank, & P. Knabner (2012c) »Multiscale modeling of colloid and fluid dynamics in porous media including an evolving microstructure« publiziert werden. Die dort präsentierten numerischen Ergebnisse stammen vom Autor dieser Dissertationsschrift und basieren auf den im Weiteren beschriebenen algorithmischen und numerischen Konzepten und Implementierungsstrategien. Die Homogenisierungsresultate wurden maßgeblich von Nadja Ray im Rahmen ihrer Promotion erarbeitet (siehe Ray 2013).

Abstract

We consider the dynamics of dilute electrolytes and of dissolved charged particles within a periodic porous medium at the pore scale, which is described by the non-stationary Stokes–Nernst–Planck–Poisson (SNPP) system.

Since simulations that resolve the geometry of the solid matrix at the pore scale are not feasible in practice, a major interest lies in the quality assessment of corresponding *averaged* models. Depending on the chosen scaling, the different averaged models under investigation reasonably describe to a greater or lesser extent the effective macroscopic behavior of the phenomena considered. The underlying partial differential equations include effective tensors, the closed-form expression of which is provided by averaging of the solutions of auxiliary problems. These so-called cell problems are defined on small domains reflecting the periodic geometry of the solid matrix.

The main objectives are both the qualitative and the quantitative investigation of homogenization processes by means of an extensive numerical study, i. e., of the convergence properties of the SNPP systems for vanishing microstructure. To this end, numerical schemes are proposed that are capable of solving accurately and efficiently the non-stationary, fully coupled / nonlinear SNPP system and also the corresponding averaged systems. The discretization is performed fully implicitly in time, while using mixed finite elements in two space dimensions, which are locally mass conservative with respect to the concentration of charged particles. The schemes are of optimal order in the discretization parameters, which is demonstrated numerically and also shown rigorously by an a priori error estimate for the overall discretization error.

Subsequently, the thesis proceeds with the numerical realization of an extension to the SNPP system allowing for attachment and detachment processes on the surface of the considered locally periodic solid matrix. The resulting evolving microstructure has an impact on the liquid flow and thus consequently on the solute transport. The corresponding two-scale model, which contains these inter-scale dependencies, is approached numerically using mixed finite elements on both scales. Simulations illustrate the interplay between solute transport, evolving microstructure, and liquid flow.

Chapter 1

Introduction

Section 1.1 gives a brief phenomenological description of the non-stationary *Stokes–Nernst–Planck–Poisson (SNPP) system* consisting of coupled / nonlinear partial differential equations. This continuum model is well-accepted for the description of the dynamics of dilute electrolytes and dissolved charged particles in small channels and thus also within a porous medium at the *pore scale* (cf., e. g., Kirby 2010; Masliyah & Bhattacharjee 2006; Probstein 2003). The SNPP system and derived or related systems are still topic of recent publications, especially in the mathematical disciplines of numerics (Allaire et al. 2013; Bauer et al. 2011, 2012; Johannesson 2009; Paz-García et al. 2011), of numerical analysis (Prohl & Schmuck 2009, 2010), of analysis (Berg & Findlay 2011; Herz et al. 2012; Roubíček 2005a, 2006; Schmuck 2009), and of homogenization theory (Allaire et al. 2010, 2013; Looker & Carnie 2006; Moyne & Murad 2002, 2006; Ray et al. 2012a; Schmuck 2011, 2013).

At the end of Section 1.1, a *nondimensionalization procedure* of the SNPP system leads to the *dimensionless SNPP system* revealing characteristic numbers that describe the ratio of the magnitudes of the different physical processes incorporated in the model. Subsequently, powers of the *scale parameter* ε take the place of the characteristic quantities, which give rise to introduce the *scaled SNPP system*. This system depends on the chosen *scaling parameters* α, β, γ, and thus represents an entire family of scaled systems. Ray et al. (2012a) used a *periodic homogenization* procedure to derive averaged systems that are valid on the *field scale*. The description of these systems is postponed to Chapter 2. The scaled SNPP system together with three averaged systems (for three fixed sets of (α,β,γ)) are the main objects of the numerical investigations in this work. In order to give the reader a better insight of the homogenization process and of the nature of homogenized models in general, Section 1.2 briefly introduces the formal *method of two-scale asymptotic expansion*. The chapter closes with an outline of this thesis in Section 1.3.

Guideline for the reader. Where relevant, we state the dimensions of physical quantities by their associated SI units. Lists of the SI units and derived units, of the physical quantities, and of the mathematical symbols that are used in this thesis are found in Appendix B. Numbered theorems, hypotheses, definitions and so on are emphasized in italics. Proofs to theorems, propositions or lemmas are closed with the symbol □, numbered examples and remarks with the symbol △.

We consider two distinct continuum scales within this thesis: the *pore scale* and the *field scale*. Depending on the context, if we speak of *microscopic* quantities we refer to the pore scale, whereas the terms *macroscopic*, *effective*, *homogenized*, and *upscaled* refer to the field scale.

1.1 Pore-Scale Model and Nondimensionalization

Phenomenological description of the pore-scale model. We consider a rigid porous medium saturated with a single Newtonian liquid acting as a solvent, which we assume to be isothermal, incompressible, and electrically neutral. We call the solid part of the medium the *solid matrix*—one may think of concrete, ceramics, metal foam, or soil for instance. We assume further that the pore space of the porous medium is connected.

For the following considerations, we take the presence of an applied or induced *electric field* $\boldsymbol{E}$ [V m^{-1}] into account. The movement of a viscous Newtonian liquid at low Reynolds numbers Re [−] (cf. (1.12b)) fulfills laminar flow conditions that are allowed to be postulated when dealing with small channels as provided by the solid matrix. If in addition $\mathrm{Re} \ll 1$, the *liquid velocity* field $\boldsymbol{u}$ [m s^{-1}] and the *pressure* distribution p [Pa] is described fairly precise by the *momentum equation* for Stokes flow:

$$-\mu\,\Delta\boldsymbol{u} + \boldsymbol{\nabla} p \;=\; \boldsymbol{f}_{\mathrm{E}} \quad [\mathrm{Pa\,m^{-1}}]\,. \tag{1.1}$$

Here, μ [Pa s], the *dynamic viscosity* of the liquid, is a constant, since the liquid was considered Newtonian. The quantity $\boldsymbol{f}_{\mathrm{E}}$ [N m^{-3}] denotes the *electric body force per unit volume* acting on the liquid. This force density comprises the *charge density* ρ_{E} [C m^{-3}], which is described in more detail below (cf. (1.9)), and the electric field $\boldsymbol{E}$, which both are time and space dependent quantities:

$$\boldsymbol{f}_{\mathrm{E}} \;=\; \rho_{\mathrm{E}}\,\boldsymbol{E} \quad [\mathrm{N\,m^{-3}}]\,. \tag{1.2}$$

Equation (1.2) is termed the *Lorentz relation*.

If we further consider the liquid to be incompressible then the liquid's *mass density* ρ [kg m^{-3}] is constant with respect to time and space. This yields the *incompressibility condition*

$$\boldsymbol{\nabla} \cdot \boldsymbol{u} \;=\; 0 \quad [\mathrm{s}^{-1}] \tag{1.3}$$

that together with the previous equations yields the *Stokes equations* {(1.1), (1.3)}.

For this section, we consider an arbitrary number of possibly charged *chemical species* (cf. McNaught & Wilkinson 1997) in the liquid, ranging from nano-size to colloidal size, all of which are represented by their *molar densities/molar concentrations* c_i [mol m^{-3}]. The integers z_i denote the respective *charge numbers/valences* (z_i is equal to zero for uncharged species). Note that by using this approach, the particles are not treated as "matter" in the classical meaning, since the particles' volumes are neglected, while only the particles' molar masses are considered. Nevertheless, the approach is acceptable provided that dilute solutions are considered, as done in this work. The motion of species i is described by the total *molar flux* $\boldsymbol{j}_i$ [mol m^{-2} s^{-1}]. This quantity is a measure for the amount of moles passing locally though a small area per time interval. The relation between time evolution and spatial spreading of the ith chemical species is given by the *mass conservation equation*

$$\partial_t c_i + \boldsymbol{\nabla} \cdot \boldsymbol{j}_i \;=\; r_i(\boldsymbol{c}) \quad [\mathrm{mol\,m^{-3}\,s^{-1}}] \,. \tag{1.4}$$

Here, we considered in addition *reaction rates* r_i [mol m^{-3} s^{-1}] acting on the vector of all concentrations $\boldsymbol{c}$, and thus the governing equations of change for chemical species are coupled in general. In many mathematical models, the reaction rates are of empirical nature and represent the amount of different types of transformation of matter, such as growth or decay, biological processes, sorption to the solid matrix, etc. (cf. Prechtel 2005, and references cited therein).

The molar flux $\boldsymbol{j}_i$ appearing in (1.4) originates from the three following hydrophysical processes that we take into account: Brownian motion of particles leads to a balancing of concentration differences on the continuum scale. The involving *diffusive flux* $\boldsymbol{j}_i^{\mathrm{diffusion}}$ [mol m^{-2} s^{-1}] is assumed to obey *Fick's law* for diffusion, which postulates that this flux is directly proportional to the negative concentration gradient with an empirical constant D_i [m^2 s^{-1}] that is called *diffusivity* or *diffusion coefficient*:

$$\boldsymbol{j}_i^{\mathrm{diffusion}} \;=\; -D_i\, \boldsymbol{\nabla} c_i \quad [\mathrm{mol\,m^{-2}\,s^{-1}}] \,.$$

The quantity D_i is a scalar depending only on the particle size of the ith species, provided that an isothermal, homogeneous liquid is considered. In addition to diffusion, mass is transported due to liquid movement. The associated molar flux is called the *advective flux*

$$\boldsymbol{j}_i^{\text{advection}} = \boldsymbol{u}\, c_i \quad [\text{mol m}^{-2}\,\text{s}^{-1}]$$

with $\boldsymbol{u}$ being the liquid velocity according to {(1.1), (1.3)}. Eventually, when charged species are subjected to an electric field $\boldsymbol{E}$, an additional mass transfer takes place along or against the field direction. This transfer is called *electromigration*, *electric drift*, or *electrophoresis*, and the associated molar flux reads

$$\boldsymbol{j}_i^{\text{migration}} = v_i\, z_i\, F\, \boldsymbol{E}\, c_i \quad [\text{mol m}^{-2}\,\text{s}^{-1}]\,,$$

where F [C mol^{-1}] is the *Faraday constant* (cf. Tab. B.2, p. 142). The proportionality factor v_i [mol s kg^{-1}] is called the *electrical mobility* of the ith species, which is a measure for the ability to be moved through the liquid in response to an electric field. The mobility directly relates to the diffusivity of a considered species by the *Nernst–Einstein equation*

$$D_i = R\,T\,v_i \quad [\text{m}^2\,\text{s}^{-1}] \tag{1.5}$$

with *gas constant* R [J K^{-1} mol^{-1}] and *temperature* T [K]. The process of advective transport, sometimes together with electromigration, is often also called *convection*. The molar fluxes due to diffusion, advection, and migration are additive, i. e., $\boldsymbol{j}_i = \boldsymbol{j}_i^{\text{diffusion}} + \boldsymbol{j}_i^{\text{advection}} + \boldsymbol{j}_i^{\text{migration}}$, and altogether, we arrive with (1.5), $F = e\,N_\text{A}$, and $R = k_\text{B}\,N_\text{A}$ (cf. Tab. B.2, p. 142) at the formulas for the total molar fluxes

$$\boldsymbol{j}_i = -D_i\,\boldsymbol{\nabla} c_i + \left(\boldsymbol{u} + \frac{D_i\,z_i\,e}{k_\text{B}\,T}\boldsymbol{E}\right) c_i \quad [\text{mol m}^{-2}\,\text{s}^{-1}]\,. \tag{1.6}$$

Especially when electromigration is taken into account, the system {(1.4), (1.6)} is called the *Nernst–Planck equations*.

The electric field $\boldsymbol{E}$ is the negative gradient of the *electric potential* ϕ [V] (also *electric field potential*, *electrostatic potential*, *voltage*), or vice versa, ϕ is the solution of the equation

$$\boldsymbol{E} = -\boldsymbol{\nabla}\phi \quad [\text{V m}^{-1}]\,. \tag{1.7}$$

Defined as the gradient of a scalar, the vector field $\boldsymbol{E}$ is curl free.

Charge carried by chemical species acts on the electric field as a source or a sink due to *Gauss's law* for electricity:

$$\boldsymbol{\nabla} \cdot (\epsilon \boldsymbol{E}) \;=\; \rho_{\mathrm{E}} \quad [\mathrm{V}]\,, \tag{1.8}$$

where ϵ [$\mathrm{C\,V^{-1}\,m^{-1}}$] denotes the *electric permittivity* of the liquid that is constant for our assumptions. In an electrolyte solution consisting of a neutral solvent, the charge density ρ_{E}, which already appeared in {(1.1), (1.2)} is given by

$$\rho_{\mathrm{E}} \;=\; F \sum_i z_i\, c_i \quad [\mathrm{C\,m^{-3}}]\,. \tag{1.9}$$

Inserting (1.7) into (1.8) yields an equation of Poisson type; and as found in the literature (see below), we refer to the system {(1.7), (1.8)} as the *Poisson equation*. On the surface of the solid matrix we prescribe either a *surface potential* ϕ_{D} [V] or a *surface charge density* σ [$\mathrm{C\,m^{-2}}$] claiming that $\epsilon \boldsymbol{E} \cdot \boldsymbol{\nu} = \sigma$ holds, where $\boldsymbol{\nu}$ [−] denotes the unit normal on the surface (cf. Rem. 2.2).

The system of fully coupled, nonlinear partial differential equations {(1.1), (1.3), (1.6), (1.4), (1.7), (1.8)} is called the *Stokes–Nernst–Planck–Poisson (SNPP) system*. We refer the interested reader to the monographies of Kirby (2010), Masliyah & Bhattacharjee (2006), and Probstein (2003) for more detailed information. One well-established simplification mainly used in the mathematical analysis of the SNPP system (cf. Samson et al. 1999, and references cited therein), but not used in this thesis, is the hypothesis of an *electroneutrality* condition

$$\sum_i z_i\, c_i \;=\; 0 \quad [\mathrm{mol\,m^{-3}}]\,. \tag{1.10}$$

The system under consideration in this work, which is valid on the pore scale, is a nondimensional formulation of the above SNPP system for the special case of two oppositely charged species with the same valence (the liquid is in this case called a *symmetric elecrolyte*). Prior to the nondimensionalization procedure, various types of possible boundary conditions are defined and discussed.

Boundary conditions. The SNPP system {(1.1), (1.3), (1.6), (1.4), (1.7), (1.8)} is defined on a time–space cylinder. In order to complete the mathematical problem, besides initial conditions for c_i describing the concentration distribution in the spatial domain at the time level at which the physical processes begin, additional conditions must be imposed at the

boundaries of the considered domain. These boundary conditions either prescribe the values or the spatial derivatives of the unknowns of the SNPP system and have to be compliant with the conservation description. The boundary conditions used in this thesis are well-known in literature and will be made explicit whenever needed.

For the physical meanings of the various boundary conditions for the *Stokes* subsystems, we refer the interested reader to the monographies of Elman et al. (2005, Chap. 5), Gross & Reusken (2011, Sec. 1.2), and Remark 4.17. Boundary conditions for the *Darcy* equation that emerges from the Stokes equations by means of a homogenization procedure (cf. Sec. 2.2) are treated in Logan (2001, Sec. 5.2.2), Kinzelbach (1992, Sec. 2.3), Bear (1972, Sec. 7.1), Domenico & Schwartz (1998, Sec. 4.4), and Spitz & Moreno (1996, Sec. 2.4). In Logan (2001, Sec. 2.7.2), Kinzelbach (1992, pp. 32, 177, 206), Domenico & Schwartz (1998, Sec. 14.3), and Spitz & Moreno (1996, Sec. 3.4), the different types of boundary conditions for *transport* processes are discussed (cf. also Rem. 4.7 for Neumann conditions), while a discussion on boundary conditions of the *Poisson* subsystem is found in Kirby (2010, Sec. 5.1.7) and in Remark 2.2.

Nondimensionalization. Instead of treating the SNPP system as described above, we consider a representative nondimensionalized model containing dimensionless unknowns in combination with resubstitution laws for the reconstruction of the original physical unknowns. The SNPP system in dimensionless form is valid for arbitrary but fixed (pore) scales, as long as the assumptions made in the derivation of the model above are not violated. One key advantage here is that the nondimensionalized model reveals so-called *characteristic numbers* describing the ratio between the physical phenomena modeled by the SNPP system (e. g., between advective and diffusive transport). In Chapter 2, the characteristic numbers will be substituted by variable scaling parameters, and thus, various effective models are obtained in a homogenization procedure. The monographies of Probstein (2003, Sec. 3.5) and Kirby (2010, Appx. E) give a well-formulated introduction to the nondimensionalization technique.

Let L [m] be a *characteristic length*, t_c [s] be a *characteristic time*, U [$\mathrm{m\,s^{-1}}$] a *characteristic velocity*, and C [$\mathrm{mol\,m^{-3}}$] a *characteristic concentration*. In order to rewrite system {(1.1), (1.3), (1.6), (1.4), (1.7), (1.8)} (relations (1.2), (1.9) substituted) in terms of *dimensionless variables*, the following scalings are used:

$$t = t_c\, t^*\,, \qquad \boldsymbol{x} = L\, \boldsymbol{x}^*\,,$$

$$\boldsymbol{u} = U\,\boldsymbol{u}^*\,, \qquad \boldsymbol{j}_i = C\,U\,\boldsymbol{j}_i^*\,, \qquad \boldsymbol{E} = \frac{k_\mathrm{B}\,T}{e\,L}\,\boldsymbol{E}^*\,,$$
$$p - p_0 = \rho\,U^2\,p^*\,, \qquad c_i = C\,c_i^*\,, \qquad \phi - \phi_0 = \frac{R\,T}{F}\,\phi^* = \frac{k_\mathrm{B}\,T}{e}\,\phi^*\,.$$

Here, the asterix marks the respective reduced dimensionless variables. The data p_0 and ϕ_0 define a convenient reference state. Even though the choice of scaling is an arbitrary one in the mathematical sense, a physical meaningful scaling was chosen (see references cited above). Taking into account that $\partial_t = \partial_{t^*}/t_\mathrm{c}$, $\boldsymbol{\nabla} = \boldsymbol{\nabla}^*/L$, and $\Delta = \Delta^*/L^2$ by the chain rule, we arrive at the following *nondimensionalized SNPP system*:

$$-\frac{1}{\mathrm{Re}}\,\Delta^*\boldsymbol{u}^* + \boldsymbol{\nabla}^* p^* = \frac{R\,T\,C}{\rho\,U^2}\left(\sum z_i\,c_i^*\right)\boldsymbol{E}^* \qquad [-]\,, \tag{1.11a}$$
$$\boldsymbol{\nabla}^*\cdot\boldsymbol{u}^* = 0 \qquad [-]\,, \tag{1.11b}$$
$$\boldsymbol{j}_i^* = -\frac{1}{\mathrm{Pe}}\,\boldsymbol{\nabla}^* c_i^* + \left(\boldsymbol{u}^* + \frac{z_i}{\mathrm{Pe}}\boldsymbol{E}^*\right)c_i^* \qquad [-]\,, \tag{1.11c}$$
$$\mathrm{St}\,\frac{\partial c_i^*}{\partial t^*} + \boldsymbol{\nabla}^*\cdot\boldsymbol{j}_i^* = \frac{L}{C\,U}\,r_i(C\,\boldsymbol{c}^*) \qquad [-]\,, \tag{1.11d}$$
$$\boldsymbol{E}^* = -\boldsymbol{\nabla}^*\phi^* \qquad [-]\,, \tag{1.11e}$$
$$\boldsymbol{\nabla}^*\cdot\boldsymbol{E}^* = \frac{F^2\,C\,L^2}{R\,T\,\epsilon}\left(\sum z_i\,c_i^*\right) \qquad [-]\,. \tag{1.11f}$$

In (1.11), the following *characteristic numbers* are used:

$$\textit{mass Péclet number}\ \mathrm{Pe}_i := \frac{L\,U}{D_i}\,, \tag{1.12a}$$
$$\textit{Reynolds number}\ \mathrm{Re} := \frac{\rho\,U\,L}{\mu} = \frac{U\,L}{\nu}\,, \tag{1.12b}$$
$$\textit{Strouhal number}\ \mathrm{St} := \frac{L}{t_\mathrm{c}\,U}\,. \tag{1.12c}$$

We define the natural characteristic time t_c with relation to the velocity by $U = L/t_\mathrm{c}$, which yields a Strouhal number equal to one. With $r_i^*(\boldsymbol{c}^*) := \frac{L}{C\,U}\,r_i(C\,\boldsymbol{c}^*)$, we write the second part of (1.11d) as

$$\frac{\partial c_i^*}{\partial t^*} + \boldsymbol{\nabla}^*\cdot\boldsymbol{j}_i^* = r_i^*(\boldsymbol{c}^*)\,. \tag{1.12d}$$

The characteristic quantities have to be defined prior to the solving of the nondimensionalized system. In practice, these quantities are often chosen in a way that the nondimensionalized initial and / or boundary data equal one in some regions. After solving a dimensionless

problem, the original physical unknowns are obtained again by resubsitution using the scaling equations defined above. Note that the obtained nondimensional model is not unique, in the sense that there is some freedom of expressing characteristic scales in terms of other ones (cf. *Buckingham π theorem*, Buckingham 1914).

1.2 The Concept of Periodic Homogenization

The main tasks of periodic homogenization is the study and the averaging of partial differential equations with rapidly oscillating coefficients. The underlying differential equations may describe, e. g., inhomogeneous materials with an idealized *periodic* microstructure. By means of a limiting process, *effective* partial differential equations are obtained describing the *average* macroscopic behavior of the considered quantities. These equations contain effective "smooth" coefficients, which are determined by means of the solutions of auxiliary problems defined on so-called *cells* representing the local heterogeneities of the microscale.

This work deals indeed with the numerical investigation of homogenization results, of the original, non-homogenized models, and of homogenization processes in general. However, the application of homogenization methods is not part of this thesis. Nevertheless we illustrate the basic concepts by giving a short example of how the *method of two-scale asymptotic expansion* is applied and further accompany this with visualizations of problem solutions. This homogenization technique is a simple one and is only of *formal* nature. However, the technique is often used as a first step in the proofs of *rigorous* homogenization methods (see end of this section) in order to "guess" the averaged limit problems. For a short introduction into the method of two-scale asymptotic expansion, we refer to the lecture notes of G. Allaire (Allaire 2010a,b). For a brief overview of upscaling methods in general, we refer the reader to the thesis of Ray (2013, Sec. 3.1.1 ff.)

Example 1.1 (Two-scale asymptotic expansion). Let the domain $\Omega_\varepsilon \subset \mathbb{R}^2$ be a disk with boundary $\partial\Omega$ and with an associated characteristic material property that is periodic in each spatial direction as illustrated in Figure 1.1. This characteristic property shall be represented by a *representative unit cell* $Y =]0, 1[^2$. We define the parameter $\varepsilon \ll 1$—to which we refer to as the *scale parameter* in the following—equal to the length of one period in Ω_ε. The physical model that we consider in this example is the stationary *Darcy equation*,

$$\boldsymbol{u}_\varepsilon = -K_\varepsilon(\boldsymbol{x})\,\boldsymbol{\nabla} h_\varepsilon \qquad \text{in } \Omega_\varepsilon\,, \tag{1.13a}$$

$$\boldsymbol{\nabla}\cdot\boldsymbol{u}_\varepsilon = f \qquad \text{in } \Omega_\varepsilon\,, \tag{1.13b}$$

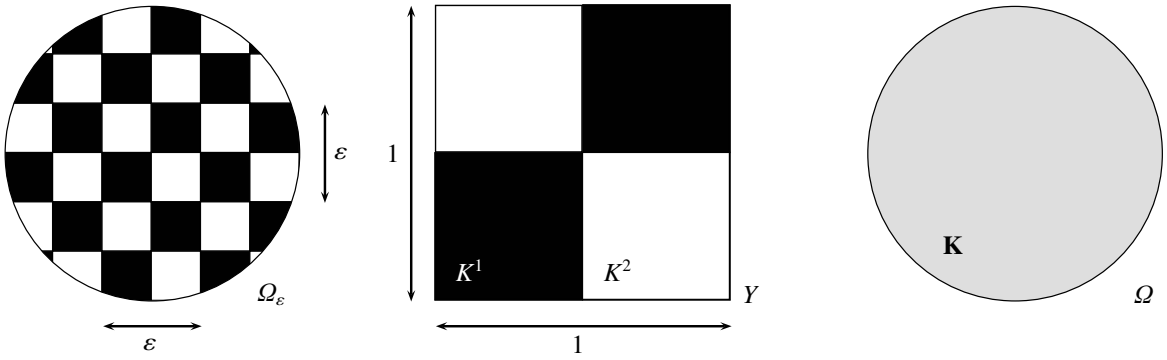

Figure 1.1. The domain Ω_ε with oscillating, piecewise constant hydraulic conductivity K^i (K^1 *black areas*, K^2 *white areas*), the representative unit cell Y containing a section of Ω_ε, and the domain Ω associated with an averaged hydraulic conductivity $\mathbf{K}$.

which itself can be derived from the steady-state Navier–Stokes equations (Bear & Cheng 2010, Sec. 4.2.2) or the Stokes equations (Allaire 2010a, Sec. 1.1) by the method of two-scale asymptotic expansion. The problem (1.13) is supplemented with appropriate boundary conditions of Dirichlet type and/or Neumann type on $\partial\Omega$ (cf. Sec. 1.1). This system of equations describes the averaged horizontal liquid movement (i. e., orthogonally to gravitational direction) within a saturated porous medium for an incompressible liquid (cf., e. g., Bear & Cheng 2010, Sec. 4.1; Spitz & Moreno 1996, Sec. 2.2.2; Domenico & Schwartz 1998, Sec. 3.3). Here, $\boldsymbol{u}_\varepsilon$ [$\mathrm{m\,s^{-1}}$] stands for the liquid velocity—the so-called *Darcy flux* or *specific discharge*—h_ε [m] for the *piezometric head*, K_ε [$\mathrm{m\,s^{-1}}$] for the *hydraulic conductivity* (often also denoted by the symbol k_f), which is a function of the permeability of the solid matrix and of the viscosity of the considered liquid, and f [$\mathrm{s^{-1}}$] for a *source/sink* or *well/drain* (assumed here to be a constant). Alternatively, the system (1.13) may also describe the displacement h_ε of an elastic plate or membrane fixed at its boundary and subjected to a transversal load of intensity f (Chen 2005, Sec. 1.1.1; Ern & Guermond 2004, Sec. 3.3.1).

In our example, the data for (1.13) are chosen as follows: let $f :\equiv 1$ and the coefficient K_ε be piecewise constant:

$$K_\varepsilon(\boldsymbol{x}) :\equiv \left\{ \begin{array}{ll} K^1\,, & \left\lfloor 2x_1/\varepsilon \right\rfloor + \left\lfloor 2x_2/\varepsilon \right\rfloor \text{ is an even integer} \\ K^2\,, & \text{otherwise} \end{array} \right\},$$

where $\lfloor\cdot\rfloor$ denotes the floor function. The oscillating coefficient $K_\varepsilon = K_\varepsilon(\boldsymbol{x})$ is εY-periodic in Ω_ε. We define the hydraulic conductivity K on the unit cell Y as

$$K\left(\frac{\boldsymbol{x}}{\varepsilon}\right) \coloneqq K_\varepsilon(\boldsymbol{x})$$

and denote its Y-periodic extension with the same symbol. Next, we postulate that the solution of (1.13) can be expressed in terms of power series in ε:

$$\boldsymbol{u}_\varepsilon(\boldsymbol{x}) = \sum_{k=0}^{\infty} \varepsilon^k \boldsymbol{u}_k\left(\boldsymbol{x}, \frac{\boldsymbol{x}}{\varepsilon}\right) \qquad \text{and} \qquad h_\varepsilon(\boldsymbol{x}) = \sum_{k=0}^{\infty} \varepsilon^k h_k\left(\boldsymbol{x}, \frac{\boldsymbol{x}}{\varepsilon}\right) \tag{1.14}$$

with $\boldsymbol{u}_\varepsilon$, h_ε being Y-periodic in the second argument. In addition to the "macroscopic variable" $\boldsymbol{x}$, a "microscopic variable" $\boldsymbol{y}$ is defined, connected to $\boldsymbol{x}$ by $\boldsymbol{y} \coloneqq \boldsymbol{x}/\varepsilon$.

The system (1.13) is interpreted as series of problems in ε yielding a series of solutions $\{(\boldsymbol{u}_\varepsilon, h_\varepsilon)\}_\varepsilon$ that possibly converges toward a limiting solution for $\varepsilon \to 0$. The formal homogenization by two-scale asymptotic expansion amounts to find an *effective equation* that admits this limit as its solution. In the following, the effective equation for $(\boldsymbol{u}_0, h_0)$ as given in (1.14) is derived. One has to be aware of the fact that—since (1.14) is a heuristic assumption—it is not guaranteed that $(\boldsymbol{u}_0, h_0)$ approximates $\lim_{\varepsilon\to 0}(\boldsymbol{u}_\varepsilon, h_\varepsilon)$ reasonably accurate.

With the aim to separate both scales and to derive an effective equation, the ansatz (1.14) is inserted into (1.13), taking into account the chain rule

$$\boldsymbol{\nabla}_{\boldsymbol{x}} \cdot \Big(\boldsymbol{u}_k(\boldsymbol{x}, \boldsymbol{y})\Big) = \Big(\boldsymbol{\nabla}_{\boldsymbol{x}} \cdot \boldsymbol{u}_k + \varepsilon^{-1} \boldsymbol{\nabla}_{\boldsymbol{y}} \cdot \boldsymbol{u}_k\Big)(\boldsymbol{x}, \boldsymbol{y})$$

(analogously $\boldsymbol{\nabla}_{\boldsymbol{x}} h_k$) and identifying the coefficients of the resulting series in ε to zero. Thus, the flux equation of order ε^{-1} associated with (1.13a) reads

$$\mathbf{0} = -K(\boldsymbol{y})\, \boldsymbol{\nabla}_{\boldsymbol{y}} h_0(\boldsymbol{x}, \boldsymbol{y}) \,.$$

Hence, h_0 is a macroscopic quantity, i. e., $h_0(\boldsymbol{x}, \boldsymbol{y}) \equiv h_0(\boldsymbol{x})$. The flux equation of order ε^0 together with the scalar equation of order ε^{-1} yield the mixed system

$$\boldsymbol{u}_0(\boldsymbol{x}, \boldsymbol{y}) = -K(\boldsymbol{y}) \Big(\boldsymbol{\nabla}_{\boldsymbol{y}} h_1(\boldsymbol{x}, \boldsymbol{y}) + \boldsymbol{\nabla}_{\boldsymbol{x}} h_0(\boldsymbol{x})\Big) \,, \tag{1.15a}$$

$$\boldsymbol{\nabla}_{\boldsymbol{y}} \cdot \boldsymbol{u}_0(\boldsymbol{x}, \boldsymbol{y}) = 0 \,. \tag{1.15b}$$

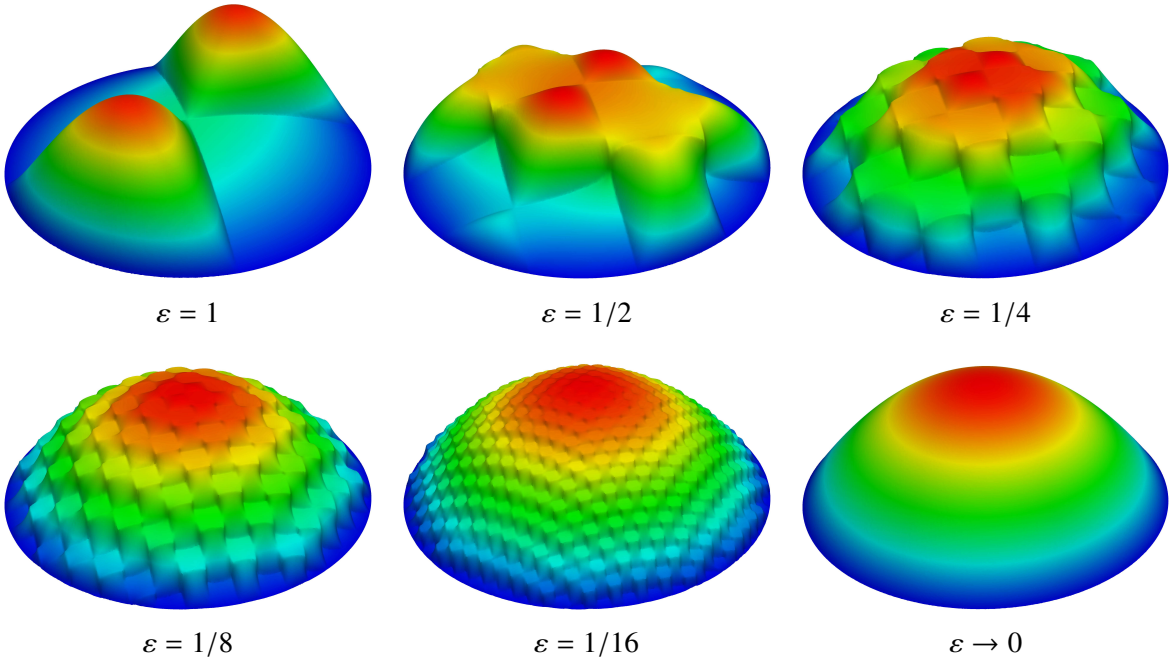

Figure 1.2. Distribution of the piezometric head for $\varepsilon = 1, 1/2, \ldots, 1/16$ and for the limit $\varepsilon \to 0$.

We continue with the decomposition of the variables $\boldsymbol{u}_0$ and h_1 in a product term with a microscopic and a macroscopic factor. To this end, we define the following auxiliary problem, the so-called *cell problem*: for $j \in \{1, 2\}$, seek $(\boldsymbol{\xi}_j, \zeta_j)$ such that

$$\boldsymbol{\xi}_j = -K(\boldsymbol{y})\left(\boldsymbol{\nabla}_{\boldsymbol{y}}\zeta_j + \boldsymbol{e}_j\right) \qquad \text{in } Y\,, \tag{1.16a}$$

$$\boldsymbol{\nabla}_{\boldsymbol{y}} \cdot \boldsymbol{\xi}_j = 0 \qquad \text{in } Y \tag{1.16b}$$

with $(\boldsymbol{\xi}_j, \zeta_j)$ componentwise periodic in Y and $\fint_Y \zeta_j(\boldsymbol{y})\,\mathrm{d}\boldsymbol{y} = 0$, $j \in \{1, 2\}$, $\boldsymbol{e}_j$ being the jth unit vector in $\mathbb{R}^2$. Note that the constraint $\fint_Y \zeta_j(\boldsymbol{y})\,\mathrm{d}\boldsymbol{y} = 0$ ensures uniqueness of the unknowns ζ_j. The values of these average integrals can be chosen arbitrarily, since only the flux unknowns $\boldsymbol{\xi}_j$ are of concern when computing the averaged coefficient of the homogenized problem (cf. (1.20)). Owing to the linearity of (1.15), the pair $(\boldsymbol{u}_0, h_1)$ can now be expressed in terms of the cell solutions $(\boldsymbol{\xi}_j, \zeta_j)$:

$$(\boldsymbol{u}_0, h_1)(\boldsymbol{x}, \boldsymbol{y}) = \sum_{j=1}^{2} (\boldsymbol{\xi}_j, \zeta_j)(\boldsymbol{y})\, \partial_{x_j} h_0(\boldsymbol{x}) \quad \Leftrightarrow \quad \begin{pmatrix} \boldsymbol{u}_0 \\ h_1 \end{pmatrix}(\boldsymbol{x}, \boldsymbol{y}) = \begin{bmatrix} \boldsymbol{\xi}_1 & \boldsymbol{\xi}_2 \\ \zeta_1 & \zeta_2 \end{bmatrix}(\boldsymbol{y})\, \boldsymbol{\nabla}_{\boldsymbol{x}} h_0(\boldsymbol{x})\,. \tag{1.17}$$

This can easily be confirmed by inserting $\boldsymbol{u}_0$ and h_1 from (1.17) into (1.15) and using the equations (1.16) of the cell problem. Eventually, the scalar equation of order ε^0 reads

$$\boldsymbol{\nabla}_{\boldsymbol{x}} \cdot \boldsymbol{u}_0(\boldsymbol{x}, \boldsymbol{y}) + \boldsymbol{\nabla}_{\boldsymbol{y}} \cdot \boldsymbol{u}_1(\boldsymbol{x}, \boldsymbol{y}) \;=\; f \;. \tag{1.18}$$

Owing to the periodicity of the unit cell Y, we find that

$$\int_Y \boldsymbol{\nabla}_{\boldsymbol{y}} \cdot \boldsymbol{u}_1(\boldsymbol{x}, \boldsymbol{y}) \, \mathrm{d}\boldsymbol{y} \;=\; \int_{\partial Y} \boldsymbol{u}_1(\boldsymbol{x}, \boldsymbol{y}) \cdot \boldsymbol{\nu} \, \mathrm{d}s_{\boldsymbol{y}} \;=\; 0$$

due to the divergence theorem. Thus, taking the Y-average of (1.18) yields the effective scalar equation

$$\boldsymbol{\nabla}_{\boldsymbol{x}} \cdot \bar{\boldsymbol{u}}_0(\boldsymbol{x}) \;=\; |Y| \, f \;=\; f \qquad \text{in } \Omega \,, \tag{1.19a}$$

where we define $\bar{\boldsymbol{u}}_0 \coloneqq \fint_Y \boldsymbol{u}_0(\boldsymbol{x}, \boldsymbol{y}) \, \mathrm{d}\boldsymbol{y}$. We also take the Y-average of $\boldsymbol{u}_0$ in (1.17) in order to obtain the effective flux equation

$$\bar{\boldsymbol{u}}_0(\boldsymbol{x}) \;=\; -\mathbf{K} \, \boldsymbol{\nabla}_{\boldsymbol{x}} h_0(\boldsymbol{x}) \qquad \text{in } \Omega \tag{1.19b}$$

with $\mathbf{K}$, the *hydraulic conductivity tensor*, defined by the negative Y-average of the consisting of columns $\boldsymbol{\xi}_j$, where $\boldsymbol{\xi}_j$ are the solutions of the cell problem (1.16):

$$\mathbf{K} \;=\; -\fint_Y \left[\boldsymbol{\xi}_1 \middle| \boldsymbol{\xi}_2 \right] \, \mathrm{d}\boldsymbol{y} \;. \tag{1.20}$$

In Equations (1.19a) and (1.19b) we write Ω instead of Ω_ε to emphasize the invariance of the associated conductivity $\mathbf{K}$ with respect to ε (although the two domains are identical in the mathematical sense).

In conclusion, the system (1.19) is just as the original system (1.13) of Darcy type, but includes an effective hydraulic conductivity coefficient $\mathbf{K}$ rather than an oscillating one. Note that the right-hand side of (1.13b) and the boundary conditions of (1.13) keep unaffected in the homogenization process, since the right hand-side, the boundary data, and the boundary itself, respectively, do not depend on the scaling parameter ε.

Figure 1.2 illustrates the two-dimensional distribution of the piezometric head in Ω_ε due to (1.13) for decreasing scale parameter ε and the limit distribution of the effective equations (1.19). In the computations, a homogeneous Dirichlet condition for the piezometric head is chosen on the boundary $\partial\Omega$ and the values $K^1 = 5\mathrm{E}-2$ and $K^2 = 1$ are used. The computed hydraulic conductivity tensor $\mathbf{K}$ is approximately equal to $2.16\,\mathbf{I}$, $\mathbf{I}$ denoting

the unit matrix in $\mathbb{R}^2$. In fact, the tensor reduces to a scalar, since there is no preferential flow direction due to the checkerboard-like ordered conductivity distribution (i. e., we have obtained an isotropic medium in the homogenization process). △

In the following chapter, the mathematical models that are the object of the numerical investigations in Chapters 3 to 6 are presented. The three included averaged models were derived by Ray et al. (2012a) with the *method of two-scale convergence*, which was introduced by Nguetseng (1989) and further developed by Allaire (1992). In contrast to the method of two-scale asymptotic expansion, this method is *rigorous* in the mathematical sense, i. e., the existence of the two-scale limit is implicitly proven.

1.3 Outline of the Thesis

All mathematical models that are the object of the numerical and analytical investigations of this work are outlined in Chapter 2. Initially, the dimensionless SNPP system that was introduced in Section 1.1 is embedded into a periodic two-scale framework. A family of scaled SNPP systems is obtained by the inclusion of a set of scaling parameters. We state "equivalent" averaged systems of the partial differential equations that may reasonably describe the effective macroscopic behavior of the phenomena considered. The type of these homogenization results that we refer to as Darcy–Nernst–Planck–Poisson (DNPP) systems depends on the choice of the chosen scaling parameters. They incorporate, inter alia, effective tensors that are obtained by averaging the solutions of so-called cell problems defined on small domains representing the periodic geometry of the solid part of the porous matrix. The correlation between the geometry of the solid part and the effective tensors is illustrated.

A fully time-implicit mixed finite element discretization of one specific DNPP system using Raviart–Thomas elements of arbitrary order is elaborated in Chapter 3. The main result of this chapter is an a priori estimate of the overall discretization error of the considered system. Its proof exploits an established existence result for the DNPP system in non-mixed form. Therefore, it is necessary to show the implication of the solution of the mixed formulation toward the solution of the non-mixed formulation. With this existence result at hand, a priori error estimates for the subsystems are shown and their combination concludes the proof of the main theorem.

Chapter 4 presents an implementable fully discrete numerical scheme capable of approximating the solutions of the scaled SNPP systems and the associated DNPP systems in two space dimensions. First, two linearization schemes—an iterative splitting scheme and

the Newton scheme—are explained by taking the example of the time-discrete SNPP system. A discussion on their practical usability reveals that the iterative splitting scheme is the method of choice, which is also applicable for the homogenized systems in an analogous way. By means of this, the nonlinear, time-discrete systems decompose into linear subsystems that are either of convection–diffusion type or of Stokes type. Problems of the first type are discretized in space using lowest-order Raviart–Thomas elements, while the latter are discretized using mixed finite elements due to Taylor and Hood. The overall numerical scheme is fully time-implicit and is locally mass conservative with respect to the chemical species.

In Chapter 5, the method of manufactured solutions is applied to the implemented discretization schemes illustrated in the previous chapter. The overall numerical schemes for the fully coupled / nonlinear SNPP system and DNPP systems are verified by capturing numerically the optimal grid convergence orders that are expected based on convergence estimates for the linear subproblems. In particular, this also verifies implicitly the convergence of the iterative splitting scheme. In addition, the numerically estimated orders of convergence show that the a priori error estimate for the DNPP system of Chapter 3 is valid for lowest order Raviart–Thomas elements.

The verification of the discretization schemes for all systems under consideration is the basis for the numerical investigations that follow in Chapter 6. This chapter aims at the comparison of solutions of the SNPP systems, which are valid on the pore scale, with those of their associated averaged-scale DNPP systems. On that account, a suitable test scenario has to be defined in advance, in particular including the definition of a perforated domain on which the SNPP problems are defined. Based on subsequent simulations, the behavior of the solutions with regard to their physical meanings is discussed for different scalings. The crucial part of this chapter is the qualitative and also the quantitative study of the convergence rates according to which the pore-scale solutions converge toward their upscaled equivalents. For this purpose, a grid-to-grid projection algorithm is used in order to compare the solutions, which are defined on different grids.

Chapter 7 is dedicated to the numerical simulation of a two-scale scenario describing colloidal dynamics and single-phase liquid flow within a porous medium at an averaged scale. The underlying pore-scale SNPP problem is an extension to the one already known taking into account attachment and detachment processes, which result in an evolving microstructure of the solid matrix. The numerical two-scale scheme presented in this chapter draws on the discretizations of Chapter 4. Concluding simulations reveal the interplay between solute transport, evolving microstructure, and liquid flow.

In order to perform simulations of the models considered in this work, the numerical toolbox *HyPHM* was newly written, which is outlined in Appendix A.

Chapter 2

Mathematical Models under Consideration

This chapter starts with the introduction of a periodic two-scale framework, in which the dimensionless SNPP system is embedded. Based on this, we state "equivalent" averaged systems of partial differential equations that reasonably describe the effective *macroscopic* behavior of the phenomena considered. These systems that we refer to as *Darcy–Nernst–Planck–Poisson (DNPP) systems*, are the recent homogenization results of Ray et al. (2012a) (see also Ray 2013), obtained by the method of two-scale convergence.

In Section 2.1, we first describe the postulated idealized periodic geometry of the considered underlying solid matrix and proceed with the introduction of the *scaled* SNPP system describing the dynamics of charged particles at the *pore scale*. The introduced scalings by powers of the *scale parameter* ε realize a weighting of the different electrokinetic processes that is adjusted by *scaling parameters* α, β, γ. In Section 2.2, we summarize the homogenization results of Ray et al. (2012a), who used the method of two-scale convergence for the rigorous transition to the limit $\varepsilon \to 0$ of the transient, nonlinear scaled SNPP system for different choices of scaling parameters. The derived DNPP systems incorporate, inter alia, *effective tensors*, which are obtained by averaging the solutions of so-called *cell problems* defined on small domains that represent the periodic geometry of the solid part of the porous matrix. In addition to that, we discuss the correlation between pore geometry and effective tensors.

2.1 The Pore-Scale Problem / The SNPP System

Geometric setting. We consider a bounded domain $\Omega \subset \mathbb{R}^d$, $d \in \{2, 3\}$ with the *exterior boundary* $\partial\Omega$ and an associated periodic microstructure defined by the unit cell $Y =]0, 1[^d$, see Figure 2.1. The *representative unit cell* Y with the *exterior boundary* ∂Y is decomposed into two open sets: the *liquid part* Y_l and the *solid part* Y_s such that $\overline{Y} = \overline{Y}_l \cup \overline{Y}_s$ and

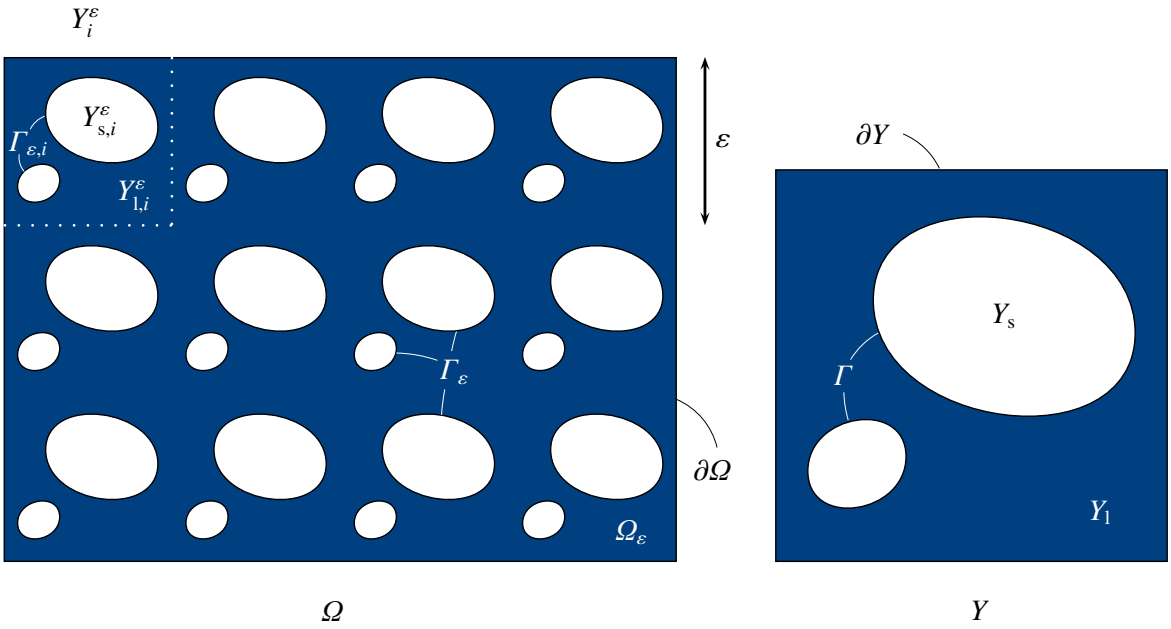

Figure 2.1. Periodic representation of a porous medium (*left*) and of the standard unit cell Y (*right*).

$Y_\mathrm{l} \cap Y_\mathrm{s} = \emptyset$ (the symbol $\overline{\ }$ denotes the topological closure). Furthermore, let $|Y_\mathrm{l}|$ denote the (Lebesgue) measure of Y_l. The *interior boundary* Γ within the unit cell is defined by $\Gamma := \overline{Y}_\mathrm{l} \cap \overline{Y}_\mathrm{s}$. In particular, we assume that the interior boundary Γ does not intersect the exterior boundary ∂Y of the unit cell Y and that the liquid part is connected. The characteristic ratio of pore size that is determined by the size of the underlying microstructure and the domain size $|\Omega|$ is denoted by ε. We call $\varepsilon \ll 1$ the *scale parameter* and assume the macroscopic domain Ω to be covered by a regular mesh of size ε consisting of ε-scaled and shifted cells Y_i^ε that are divided into an analogously scaled liquid part, solid part, and boundary. Let us denote those by $Y_{\mathrm{l},i}^\varepsilon$, $Y_{\mathrm{s},i}^\varepsilon$, and $\Gamma_{\varepsilon,i}$, respectively. The liquid part / pore space, the solid part / porous matrix, and the *interior boundary* Γ_ε of the porous medium are defined by

$$\Omega_\varepsilon := \bigcup_i Y_{\mathrm{l},i}^\varepsilon\,, \qquad \Omega\backslash\overline{\Omega}_\varepsilon := \bigcup_i Y_{\mathrm{s},i}^\varepsilon\,, \qquad \text{and} \qquad \Gamma_\varepsilon := \bigcup_i \Gamma_{\varepsilon,i}\,,$$

respectively. Consequently, since we assume that Ω is completely covered by ε-scaled unit cells Y_i^ε and, in particular, since the solid part is not allowed to intersect the exterior boundary, $\partial\Omega \cap \Gamma_\varepsilon = \emptyset$ holds. We mark all functions defined on Ω_ε with the index $_\varepsilon$ and denote the *outward unit normal* by ν. Furthermore, the open time interval $]0, T[$ is abbreviated by J, $T > 0$ denoting the end time.

Model equations. Recall the dimensionless SNPP system (1.11) describing the dynamics of charged particles within a porous medium at the pore scale in a continuum mechanical sense. For the remainder of this thesis, we restrict our considerations to a symmetric electrolyte solution that is composed of one positively and one negatively charged species represented by associated positive (+) and negative (−) *molar concentrations* $c_\varepsilon^\pm$, respectively. The notation $\pm$ (and $\mp$) is used as an abbreviation in order to formulate equations for both positively and negatively charged particles in one line (all the corresponding upper signs have to be interpreted as the first equation and all the lower signs as the second equation). In addition, we consider a simple mass-conserving reaction $r^\pm(c_\varepsilon^+, c_\varepsilon^-) := \mp c_\varepsilon^+ \pm c_\varepsilon^-$ (cf. (1.12d), p. 7) that couples both transport problems. This reaction translates to the stoichiometric equation $A^+ \rightleftharpoons A^-$ with rate coefficients equal to one.

A nondimensionalization result (cf. Sec. 1.1; Ray 2013, Sec. 2.1.3 and Rem. 4.1; van de Ven 1989, p. 83ff.) motivates the following scalings of the different terms with respect to the scale parameter ε introducing the *scaling parameters* $\alpha, \beta, \gamma \in \mathbb{R}_0^+$. The resulting family of scaled SNPP systems has the following form:

Problem 2.1 (Family of SNPP problems).

$$
\begin{aligned}
-\varepsilon^2 \Delta \boldsymbol{u}_\varepsilon + \boldsymbol{\nabla} p_\varepsilon &= \varepsilon^\beta \boldsymbol{E}_\varepsilon (c_\varepsilon^+ - c_\varepsilon^-) && \text{in } J \times \Omega_\varepsilon\,, && \text{(2.1a)}\\
\boldsymbol{\nabla} \cdot \boldsymbol{u}_\varepsilon &= 0 && \text{in } J \times \Omega_\varepsilon\,, && \text{(2.1b)}\\
\boldsymbol{u}_\varepsilon &= \boldsymbol{0} && \text{on } J \times \Gamma_\varepsilon\,, && \text{(2.1c)}\\
\boldsymbol{j}_\varepsilon^\pm &= -\boldsymbol{\nabla} c_\varepsilon^\pm + (\boldsymbol{u}_\varepsilon \pm \varepsilon^\gamma \boldsymbol{E}_\varepsilon)\, c_\varepsilon^\pm && \text{in } J \times \Omega_\varepsilon\,, && \text{(2.1d)}\\
\partial_t c_\varepsilon^\pm + \boldsymbol{\nabla} \cdot \boldsymbol{j}_\varepsilon^\pm &= \mp (c_\varepsilon^+ - c_\varepsilon^-) && \text{in } J \times \Omega_\varepsilon\,, && \text{(2.1e)}\\
\boldsymbol{j}_\varepsilon^\pm \cdot \boldsymbol{\nu} &= 0 && \text{on } J \times \Gamma_\varepsilon\,, && \text{(2.1f)}\\
\boldsymbol{E}_\varepsilon &= -\varepsilon^\alpha \boldsymbol{\nabla} \phi_\varepsilon && \text{in } J \times \Omega_\varepsilon\,, && \text{(2.1g)}\\
\boldsymbol{\nabla} \cdot \boldsymbol{E}_\varepsilon &= c_\varepsilon^+ - c_\varepsilon^- && \text{in } J \times \Omega_\varepsilon\,, && \text{(2.1h)}\\
\left\{ \begin{aligned} \boldsymbol{E}_\varepsilon \cdot \boldsymbol{\nu} &= \varepsilon \sigma\,, \quad \alpha = 0 \\ \phi_\varepsilon &= \phi_{\mathrm{D}}\,, \quad \alpha = 2 \end{aligned} \right\} && && \text{on } J \times \Gamma_\varepsilon\,. && \text{(2.1i)}
\end{aligned}
$$

The system (2.1) is completed with exterior boundary conditions on $J \times \partial\Omega$ and initial conditions for $c_\varepsilon^\pm$ on $\{0\} \times \Omega_\varepsilon$ that are specified in Section 6.1. This family of pore-scale problems is similar to the problem of Example 1.1 on p. 8 with the difference that the fine-scale dependency is essentially produced by the periodic solid matrix and not by the coefficients per se.

Remark 2.2 (Interior boundary conditions for the Poisson problem). For the parameters $\alpha = 0$ and $\alpha = 2$, the Poisson subsystem {(2.1g), (2.1h)} is supplemented with an interior boundary condition of Neumann and of Dirichlet type, respectively (cf. (2.1i)). This boundary condition is associated either with the *surface charge density* σ or with the *surface potential* ϕ_D, which correspondingly relates to the so-called *ζ-potential* of the solid matrix (for a detailed discussion, see Kirby 2010, Sec. 5.1.7). In applications, these data can be obtained, for instance, by measurements. For simplicity, we assume $\sigma, \phi_D : J \times \Gamma_\varepsilon \to \mathbb{R}$ to be given constants. This assumption can be relaxed in a straightforward way using standard assumptions for the regularity of the functions σ, ϕ_D. △

2.2 The Homogenized Problems / The DNPP Systems

Cell problems. The DNPP systems under consideration are the homogenization results of the family of SNPP systems (2.1) for the limit $\varepsilon \to 0$. By using the following definition of cell problems and effective tensors that is an equivalent reformulation of Ray et al.'s (2012, Def. 4.4), we are able to quote the main homogenization theorems (cf. Thm. 2.5, Thm. 2.8).

Definition 2.3 (Effective tensors and cell problems). *Let $\boldsymbol{e}_j$ denote the jth unit vector in $\mathbb{R}^d$. The space-averaged (stationary) macroscopic* diffusion/permittivity tensor *is represented by a matrix $\mathbf{D} \in \mathbb{R}^{d,d}$ that is composed of the negative Y-average of the column vectors $\boldsymbol{q}_1, \dots, \boldsymbol{q}_d$ as follows:*

$$\mathbf{D} = -\int_{Y_1} \left[\boldsymbol{q}_1 \middle| \dots \middle| \boldsymbol{q}_d\right] \mathrm{d}\boldsymbol{y} \,, \tag{2.2a}$$

where $(\boldsymbol{q}_j, u_j)$, $j \in \{1, \dots, d\}$ solve the stationary cell problems

$$\begin{aligned} \boldsymbol{q}_j &= -\boldsymbol{\nabla} u_j - \boldsymbol{e}_j && \text{in } Y_1 \,, \\ \boldsymbol{\nabla} \cdot \boldsymbol{q}_j &= 0 && \text{in } Y_1 \,, \\ \boldsymbol{q}_j \cdot \boldsymbol{\nu} &= 0 && \text{on } \Gamma \end{aligned} \tag{2.2b}$$

with $(\boldsymbol{q}_j, u_j)$ componentwise periodic in Y and $\fint_{Y_1} u_j \,\mathrm{d}\boldsymbol{y} = 0$, $j \in \{1, \dots, d\}$.

The space-averaged (stationary) macroscopic permeability tensor *is represented by a matrix* $\mathbf{K} \in \mathbb{R}^{d,d}$ *that is composed of the* Y*-average of the column vectors* $\boldsymbol{w}_1, \ldots, \boldsymbol{w}_d$ *as follows:*

$$\mathbf{K} = \int_{Y_1} \left[\boldsymbol{w}_1 \middle| \ldots \middle| \boldsymbol{w}_d \right] \, \mathrm{d}\boldsymbol{y} \,, \tag{2.3a}$$

where $(\boldsymbol{w}_j, \pi_j)$, $j \in \{1, \ldots, d\}$ *solve the stationary* cell problems

$$\begin{aligned} -\Delta \boldsymbol{w}_j + \boldsymbol{\nabla} \pi_j &= \boldsymbol{e}_j && \text{in } Y_1 \,, \\ \boldsymbol{\nabla} \cdot \boldsymbol{w}_j &= 0 && \text{in } Y_1 \,, \\ \boldsymbol{w}_j &= \mathbf{0} && \text{on } \Gamma \end{aligned} \tag{2.3b}$$

with $(\boldsymbol{w}_j, \pi_j)$ *componentwise periodic in* Y *and* $\int_{Y_1} \pi_j \, \mathrm{d}\boldsymbol{y} = 0$, $j \in \{1, \ldots, d\}$.

Furthermore, let $(\boldsymbol{\eta}, \varphi)$ *be the solution of the following stationary* cell problem*:*

$$\begin{aligned} \boldsymbol{\nabla} \cdot \boldsymbol{\eta} &= 1 && \text{in } Y_1 \,, \\ \boldsymbol{\eta} &= -\boldsymbol{\nabla} \varphi && \text{in } Y_1 \,, \\ \varphi &= 0 && \text{on } \Gamma \end{aligned} \tag{2.4}$$

with $(\boldsymbol{\eta}, \varphi)$ *componentwise periodic in* Y.

The tensors defined in (2.2a) and (2.3a) are symmetric and positive definite (Cioranescu & Donato 1999; Hornung 1997). Note that the cell problems (2.2b), (2.3b), (2.4) are given here in the *mixed* formulation as opposed to the original form in Ray et al. (2012a). This is owed to the numerical solution approach presented in this thesis that is applied to these equations, which is based on the mixed formulation (cf. Chap. 4).

Next, we state an example that provides the reader an insight of how solutions of cell problems look and of the correlation between cell geometry and effective tensors.

Example 2.4 (Permeability tensors for various geometries). Figure 2.2 visualizes the solutions of the family of cell problems (2.3b) ($d = 2$) for a representitive cell Y with solid part Y_s as used in Allaire et al. (2013). This geometric setting violates the assumptions made in Section 2.1, but nevertheless produces a macroscopic domain with a connected liquid part and the setting is indeed feasible for numerical computations. The set of equations (2.3b) suggests interpreting the solution of the cell problems as velocities of a Stokes flow driven by body force densities pointing into the two coordinate directions. In

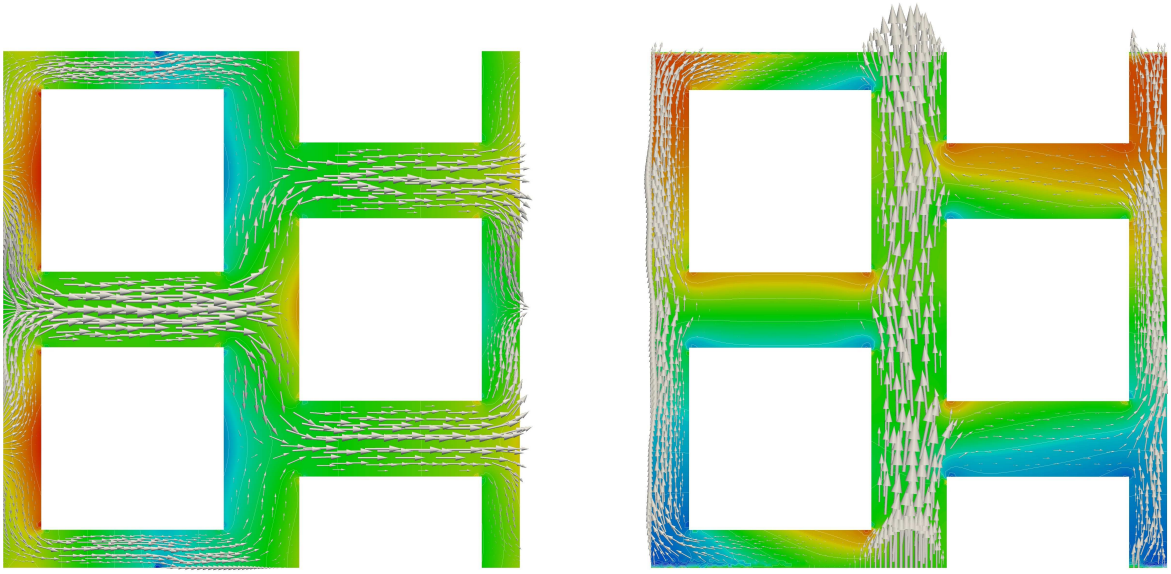

Figure 2.2. Illustration of the two cell solutions $(\boldsymbol{w}_j, \pi_j)$ in Y_l satisfying (2.3b).

particular, the tensor as defined in (2.3b) (and also the one defined in (2.2b)) is a function only of the solid part's geometry.

Some values of the effective tensor $\mathbf{K}$ are listed in Figure 2.3. Those are computed according to (2.3a) for $d = 2$ by solving the two cell problems (2.3b) numerically for different cell geometries. The representative cell Y in Figure 2.3 (a) contains a solid part Y_s with the shape of a square. Since this cell is symmetric in both coordinate axes, the computed tensor simplifies virtually to a scalar. This tensor is invariant in shiftings of Y_s within Y due to the periodic setting (cf. Fig. 2.3 (b)). Doubling the volume of the solid part Y_s entails a smaller-scaled tensor (cf. Fig. 2.3 (c)). The cell in (d) contains the geometry as already illustrated in Figure 2.2. Note that the volume $|Y_\mathrm{s}|$ of the solid part in (d) equals that in (c). Two crucial observations are made: on the one hand, the magnitude of the tensor is much smaller, on the other hand the tensor is no longer isotropic. The latter fact is obvious, since the geometry as in (d) prefers a Stokes flow in x_2 direction compared to that in x_1 direction (cf. Fig. 2.2). The reduction of the magnitude of the tensor is explained by the increase of the solid's surface, at which the Stokes velocity tends to zero due to the no-slip boundary condition on Γ as given in (2.3b). Eventually, (e) and (f) illustrate the dependency of the tensor $\mathbf{K}$ on the directional alignment of a fixed obstacle.

Note that all computed tensors are indeed symmetric and positive definite as stated by the theory. △

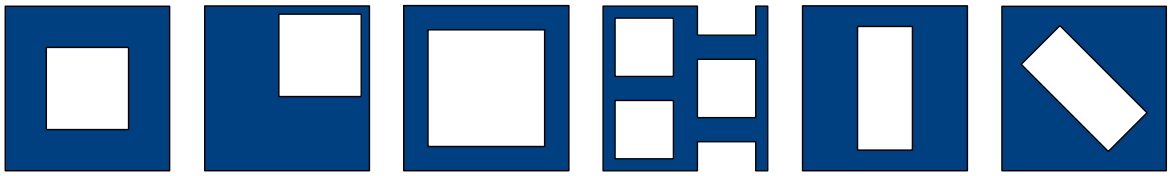

$\begin{bmatrix} 1.307 & 0 \\ 0 & 1.307 \end{bmatrix}$ $\begin{bmatrix} 1.307 & 0 \\ 0 & 1.307 \end{bmatrix}$ $\begin{bmatrix} .238 & 0 \\ 0 & .238 \end{bmatrix}$ $\begin{bmatrix} .038 & 0 \\ 0 & .050 \end{bmatrix}$ $\begin{bmatrix} .248 & 0 \\ 0 & 2.576 \end{bmatrix}$ $\begin{bmatrix} .870 & -.175 \\ -.175 & .870 \end{bmatrix}$

3/4 (a) 3/4 (b) 1/2 (c) 1/2 (d) 3/4 (e) 3/4 (f)

Figure 2.3. Computed permeability tensors for different cell geometries (cf. Expl. 2.4). Here, the regions of the cells that are highlighted in color illustrate the liquid parts Y_1. The listed tensors are scaled and have to be mutliplied by a factor of 100. The third row lists the porosity $|Y_1|$ of the cells (cf. comment after Thm. 2.5).

2.2.1 Homogenized Limit Systems for a Neumann Condition on the Interior Boundary Γ_ε in Poisson's Equation

For this paragraph, we consider the case of $\alpha = 0$, i. e., we assume a Neumann boundary condition for the electric potential on the interior boundary Γ_ε (cf. (2.1i)). This corresponds to a physical problem in which the surface charge density of the porous medium is prescribed. The next theorem is a homogenization result of Ray et al. (2012a) in mixed form:

Theorem 2.5 (Homogenization result 1). *Let $\alpha = 0$ and let $(\boldsymbol{u}_\varepsilon, p_\varepsilon, c_\varepsilon^+, c_\varepsilon^-, \phi_\varepsilon)$ be a weak solution of Problem 2.1. Then the two-scale limits $\phi_0, c_0^\pm$, and the Y_1-average $\bar{\boldsymbol{u}}_0$ of the two-scale limit $\boldsymbol{u}_0$ satisfy the following averaged equations:*

$$\bar{\boldsymbol{u}}_0 = -\mathbf{K}\left(\nabla p_0 - \begin{Bmatrix} \mathbf{D}^{-1}\boldsymbol{E}_0(c_0^+ - c_0^-), & \beta = 0 \\ 0, & \beta > 0 \end{Bmatrix}\right) \quad \text{in } J \times \Omega, \tag{2.5a}$$

$$\nabla \cdot \bar{\boldsymbol{u}}_0 = 0 \quad \text{in } J \times \Omega, \tag{2.5b}$$

$$\boldsymbol{j}_0^\pm := -\mathbf{D}\nabla c_0^\pm + \bar{\boldsymbol{u}}_0 c_0^\pm \pm \begin{Bmatrix} \boldsymbol{E}_0\, c_0^\pm, & \gamma = 0 \\ 0, & \gamma > 0 \end{Bmatrix} \quad \text{in } J \times \Omega, \tag{2.5c}$$

$$|Y_1|\,\partial_t c_0^\pm + \nabla \cdot \boldsymbol{j}_0^\pm = \mp |Y_1|\,(c_0^+ - c_0^-) \quad \text{in } J \times \Omega, \tag{2.5d}$$

$$\boldsymbol{E}_0 := -\mathbf{D}\nabla\phi_0 \quad \text{in } J \times \Omega, \tag{2.5e}$$

$$\nabla \cdot \boldsymbol{E}_0 = |Y_1|\,(c_0^+ - c_0^-) + \bar{\sigma} \quad \text{in } J \times \Omega \tag{2.5f}$$

with $\bar{\sigma} := -\int_\Gamma \sigma \,\mathrm{d}s_{\boldsymbol{y}}$.

Proof. See Ray et al. (2012a, Thms. 4.6, 4.8, 4.10). □

The ratio of pore volume (which equals the liquid volume in our setting by assumption, see Section 1.1) to the total volume is called the *porosity* (cf., e. g., Domenico & Schwartz 1998, Sec. 2.1). Since we consider a macroscopic domain completely covered with unit cells of the same geometry, the porosity equals $|Y_l|$. Note that the exterior boundary conditions on $J \times \partial\Omega$ that complete the system (2.5) are the same as the ones chosen in Problem 2.1.

Remark 2.6 (Problem specifications). For $\beta = 0$, we derive an *extended Darcy's law* (cf. {(2.5a), (2.5b)}; we call this an "extended Darcy's law" due to the presence of the drift term $\mathbf{D}^{-1}\boldsymbol{E}_0(c_0^+ - c_0^-)$, active for $\beta = 0$). Along with the pressure gradient, an additional forcing term occurs due to the electric potential. In the case of $\beta > 0$, the electric potential has no influence on the macroscopic velocity, which is then determined by a standard Darcy's law.

Table 2.1 gives an overview of the different types of limit systems that are obtained for a (fixed) scaling parameter of $\alpha = 0$. The four cases, which depend on the choice of the parameters β and γ can be classified as follows: for $\gamma = 0$, the transport of the concentrations is given by the Nernst–Planck equations. In the case of $\gamma > 0$, the electric potential has no direct influence on the macroscopic concentrations. The equations for the concentrations simplify to a convection–diffusion–reaction system. Depending on the choice of β, the upscaling procedure yields either a fully coupled system of effective partial differential equations or provides averaged equations that are coupled only in one direction. △

Remark 2.7 (Effective coefficients). The family of auxiliary cell problems (2.2b) yields the effective coefficient $\mathbf{D}$. Hence, the diffusion tensor in (2.5c) and the permittivity tensor in (2.5e) are identical. This is due to the constant parameters such as the electric permittivity and the diffusivity that we have suppressed for ease of presentation. △

2.2.2 Homogenized Limit Systems for a Dirichlet Condition on the Interior Boundary Γ_ε in Poisson's Equation

In this paragraph, we consider the case of $\alpha = 2$, i. e., we assume a Dirichlet boundary condition for the electric potential on the interior boundary Γ_ε (cf. (2.1i)). This corresponds to a physical problem in which the surface potential of the porous medium is prescribed. In

	$\beta = 0$	$\beta > 0$
$\gamma = 0$	extended Darcy's law Nernst–Planck equations Poisson equation	Darcy's law Nernst–Planck equations Poisson equation
$\gamma > 0$	extended Darcy's law advection–diffusion equations Poisson equation	Darcy's law advection–diffusion equations Poisson equation

Table 2.1. The different types of limit systems for fixed scaling parameter $\alpha = 0$.

geoscience applications, this boundary condition relates to the specification of the so-called ζ-potential. For technical reasons, Ray et al. (2012a) demanded that the *volume additivity constraint*

$$c_\varepsilon^+(t,\boldsymbol{x}) + c_\varepsilon^-(t,\boldsymbol{x}) \;=\; 1 \quad \text{for a. e. } (t,\boldsymbol{x}) \in J \times \Omega_\varepsilon \tag{2.6}$$

holds in the case of a Dirichlet boundary condition in (2.1i), which is a common assumption for the system (2.1) (cf., e. g., Roubíček 2005b). Note that this constraint is not necessary in the case of a Neumann boundary condition in (2.1i). We define the *transformed electric potential* $\phi_\varepsilon - \phi_D =: \phi_\varepsilon^{\text{hom}} : \Omega_\varepsilon \to \mathbb{R}$. Since ϕ_D is a constant in space, $\phi_\varepsilon^{\text{hom}}$ satisfies the following set of equations:

$$\begin{aligned}
\boldsymbol{E}_\varepsilon &= -\varepsilon^2 \nabla \phi_\varepsilon^{\text{hom}} && \text{in } J \times \Omega_\varepsilon\,, \\
\nabla \cdot \boldsymbol{E}_\varepsilon &= c_\varepsilon^+ - c_\varepsilon^- && \text{in } J \times \Omega_\varepsilon\,, \\
\phi_\varepsilon^{\text{hom}} &= 0 && \text{in } J \times \Gamma_\varepsilon\,.
\end{aligned}$$

Theorem 2.8 (Homogenization result 2). *Let $\alpha = 2$ and let $(\boldsymbol{u}_\varepsilon, p_\varepsilon, c_\varepsilon^+, c_\varepsilon^-, \phi_\varepsilon)$ be a weak solution of Problem 2.1. Then the two-scale limits $\phi_0^{\text{hom}}, c_0^\pm$, and the Y_1-average $\bar{\boldsymbol{u}}_0$ of the two-scale limit $\boldsymbol{u}_0$ satisfy the following averaged equations for $\beta \geq 1$, $\gamma \geq 1$:*

$$\begin{aligned}
\bar{\boldsymbol{u}}_0 &= -\mathbf{K} \nabla p_0 && \text{in } J \times \Omega\,, && \text{(2.7a)} \\
\nabla \cdot \bar{\boldsymbol{u}}_0 &= 0 && \text{in } J \times \Omega\,, && \text{(2.7b)} \\
\boldsymbol{j}_0^\pm &:= -\mathbf{D} \nabla c_0^\pm + \bar{\boldsymbol{u}}_0\, c_0^\pm && \text{in } J \times \Omega\,, && \text{(2.7c)} \\
|Y_1|\, \partial_t c_0^\pm + \nabla \cdot \boldsymbol{j}_0^\pm &= \mp |Y_1|\, (c_0^+ - c_0^-) && \text{in } J \times \Omega\,, && \text{(2.7d)} \\
\bar{\phi}_0^{\text{hom}} &= |Y_1| \left(\fint_{Y_1} \varphi \, \mathrm{d}\boldsymbol{y} \right) (c_0^+ - c_0^-) && \text{in } J \times \Omega\,, && \text{(2.7e)}
\end{aligned}$$

where φ is the partial solution of the cell problem (2.4).

Proof. See Ray et al. (2012a, Thms. 4.12, 4.14, 4.16). □

Note that the exterior boundary conditions on $J \times \partial\Omega$ that complete the pore-scale system (2.1) are not affected by the homogenization process and thus are similar to the ones for the averaged systems (2.7) and (2.5).

Remark 2.9 (Problem specifications). The transport of the concentrations is determined by a convection–diffusion–reaction system and the liquid flow is obtained by a standard Darcy's law. The electric potential is directly given in terms of the concentration fields whereas no back coupling to liquid flow and transport occurs. Note that no explicit representation of the electric field $\boldsymbol{E}_0$ is given here and that the actual averaged electric potential $\bar{\phi}_0$ can be obtained as follows:

$$\bar{\phi}_0 \;=\; \overline{\phi_0^{\mathrm{hom}} + \phi_{\mathrm{D}}} \;=\; \int_{Y_{\mathrm{l}}} \phi_0^{\mathrm{hom}} + \phi_{\mathrm{D}} \,\mathrm{d}\boldsymbol{y} \;=\; |Y_{\mathrm{l}}| \left(\fint_{Y_{\mathrm{l}}} \varphi \,\mathrm{d}\boldsymbol{y} \right) (c_0^+ - c_0^-) + |Y_{\mathrm{l}}|\, \phi_{\mathrm{D}} \,. \tag{2.8}$$

△

Chapter 3

Error Analysis of one DNPP System

For the numerical analysis, from the three DNPP systems under investigation, we consider the one that contains the highest number of nonlinear coupling terms. This is the homogenization result for the scaling parameters $\alpha = \beta = \gamma = 0$, i. e., the system (2.5) (cf. Thm. 2.5, p. 23). For the sake of presentation, we set the (constant and stationary) quantity $|Y_\ell|$ equal to one without loss of generality and complete the problem with boundary conditions on $\partial\Omega$:

$$
\begin{aligned}
\bar{\boldsymbol{u}}_0 &= -\mathbf{K}\boldsymbol{\nabla} p_0 + \mathbf{K}\mathbf{D}^{-1}\boldsymbol{E}_0(c_0^+ - c_0^-) && \text{in } J\times\Omega\,, && \text{(3.1a)}\\
\boldsymbol{\nabla}\cdot\bar{\boldsymbol{u}}_0 &= 0 && \text{in } J\times\Omega\,, && \text{(3.1b)}\\
\boldsymbol{j}_0^\pm &= -\mathbf{D}\boldsymbol{\nabla} c_0^\pm + \bar{\boldsymbol{u}}_0 c_0^\pm \pm \boldsymbol{E}_0 c_0^\pm && \text{in } J\times\Omega\,, && \text{(3.1c)}\\
\partial_t c_0^\pm + \boldsymbol{\nabla}\cdot\boldsymbol{j}_0^\pm &= r^\pm(c_0^+, c_0^-) && \text{in } J\times\Omega\,, && \text{(3.1d)}\\
\boldsymbol{E}_0 &= -\mathbf{D}\boldsymbol{\nabla}\phi_0 && \text{in } J\times\Omega\,, && \text{(3.1e)}\\
\boldsymbol{\nabla}\cdot\boldsymbol{E}_0 &= c_0^+ - c_0^- + \bar{\sigma} && \text{in } J\times\Omega\,, && \text{(3.1f)}\\
\bar{\boldsymbol{u}}_0\cdot\boldsymbol{\nu} &= 0 && \text{on } J\times\partial\Omega\,, && \text{(3.1g)}\\
c_0^\pm &= 0 && \text{on } J\times\partial\Omega\,, && \text{(3.1h)}\\
\phi_0 &= \phi_\mathrm{D} && \text{on } J\times\partial\Omega\,, && \text{(3.1i)}\\
c_0^\pm &= c_0^{\pm,0} && \text{on } \{0\}\times\Omega && \text{(3.1j)}
\end{aligned}
$$

with $c_0^{\pm,0}$ satisfying the boundary conditions (3.1h). The assumptions on the data of (3.1) are slightly relaxed with respect to the original homogenization result and will be specified further in Hypotheses 3.12. For the remainder of this chapter, we write $(\boldsymbol{u}, p, \boldsymbol{j}^+, c^+, \boldsymbol{j}^-, c^-, \boldsymbol{E}, \phi)$ instead of $(\bar{\boldsymbol{u}}_0, p_0, \boldsymbol{j}_0^+, c_0^+, \boldsymbol{j}_0^-, c_0^-, \boldsymbol{E}_0, \phi_0)$.

In Section 3.1, we first recall some definitions and properties of used function spaces, their norms, and some elementary inequalities. Furthermore, we introduce notations that are used in Section 3.2, where an *a priori error estimate* of optimal order is shown for

the time-implicit mixed finite element discretization of system (3.1). More precisely, if $(\boldsymbol{u}, p, \boldsymbol{j}^+, c^+, \boldsymbol{j}^-, c^-, \boldsymbol{E}, \phi)$ denotes the solution of the (weak) continuous formulation and $(\boldsymbol{u}_h^n, p_h^n, \boldsymbol{j}_h^{+,n}, c_h^{+,n}, \boldsymbol{j}_h^{-,n}, c_h^{-,n}, \boldsymbol{E}_h^n, \phi_h^n)$ the solution of the respective fully discrete formulation after n time steps, we prove an a priori estimate for the $L^2(\Omega)$ discretization error at the time level t_n, roughly of the form

$$\begin{aligned}\max_{m\in\{1,\dots,n\}} \|\boldsymbol{u}_h^m - \boldsymbol{u}(t_m)\|^2 + \max_{m\in\{1,\dots,n\}} \|p_h^m - p(t_m)\|^2 + \sum_{i\in\{+,-\}} \tau \sum_{m=1}^{m} \|\boldsymbol{j}_h^{i,m} - \boldsymbol{j}^i(t_m)\|^2 \\ + \sum_{i\in\{+,-\}} \max_{m\in\{1,\dots,n\}} \|c_h^{i,m} - c^i(t_n)\|^2 + \max_{m\in\{1,\dots,n\}} \|\boldsymbol{E}_h^m - \boldsymbol{E}(t_m)\|^2 + \max_{m\in\{1,\dots,n\}} \|\phi_h^m - \phi(t_m)\|^2 \\ \leq\ C\,(\boldsymbol{u}, p, \boldsymbol{j}^+, c^+, \boldsymbol{j}^-, c^-, \boldsymbol{E}, \phi)\left(\tau^2 + h^{2k+2}\right),\end{aligned}$$

provided that the solution of the continuous problem is sufficiently smooth. Here, C is a constant depending on derivatives of the continuous unknowns, on the boundary data, on the initial data, and on the smoothness of the domain Ω, but not on the time step size τ, nor on the mesh size h. The integer k stands for the chosen order of approximation spaces according to Raviart and Thomas.

3.1 Preliminaries and Notation

Throughout this chapter, let $\Omega \subset \mathbb{R}^d$, $d \in \{2, 3\}$ be a polygonally bounded, convex domain with boundary $\partial\Omega$ (i. e., in particular $\partial\Omega$ is of class $C^{0,1}$ ("Lipschitz boundary")), where $\boldsymbol{\nu}$ denotes, as usual, the outward unit normal. The (open) time interval $]0, T[$ with initial time zero and end time $T > 0$ is denoted by J.

Sobolev spaces. We use the standard notation for Sobolev spaces (Adams & Fournier 2003; Evans 2010). Let $L^p(\Omega)$ denote the space of Lebesgue-measurable functions, which pth power is Lebesgue-integrable on Ω, i. e., for which the norm

$$\|v\|_{L^p(\Omega)} \coloneqq \begin{Bmatrix} \left(\int_\Omega |v(\boldsymbol{x})|^p \,\mathrm{d}\boldsymbol{x}\right)^{1/p}, & 1 \leq p < \infty \\ \operatorname{ess\,sup}_{\boldsymbol{x}\in\Omega} |v(\boldsymbol{x})|, & p = \infty \end{Bmatrix}$$

is finite. Moreover, in the quotient space $L^2(\Omega)/\mathbb{R}$, two elements of $L^2(\Omega)$ are identified if and only if their difference is constant. Let $H^k(\Omega)$ be the set of k-times differentiable functions in $L^2(\Omega)$ with weak derivatives in $L^2(\Omega)$, equipped with the usual scalar prod-

uct $(\cdot\,,\,\cdot)_{H^k(\Omega)}$, $k \in \mathbb{N}_0$ (cf. Wu et al. 2006, Def. 1.3.2; Ern & Guermond 2004, Thm. B.27). Let the space $H^{1/2}(\partial\Omega)$ contain those functions on the boundary $\partial\Omega$ for which the norm

$$\|v\|^2_{H^{1/2}(\partial\Omega)} \;:=\; \int_{\partial\Omega} |v(\boldsymbol{x})|^2 \,\mathrm{d}\boldsymbol{x} + \int_{\partial\Omega}\int_{\partial\Omega} \frac{|v(\boldsymbol{x}) - v(\boldsymbol{y})|^2}{|\boldsymbol{x}-\boldsymbol{y}|^{d+1}} \,\mathrm{d}\boldsymbol{x}\,\mathrm{d}\boldsymbol{y}$$

is finite and let $H^{-1/2}(\partial\Omega)$ denote its dual space (cf. Adams 1975, Chap. 7, p. 208). We define by $\boldsymbol{H}^k(\Omega) := (H^k(\Omega))^d = H^k(\Omega;\mathbb{R}^d)$ the space of vector-valued functions $\boldsymbol{v} = (v_1,\dots,v_d)^{\mathrm{T}} : \Omega \to \mathbb{R}^d$, which components are in $H^k(\Omega)$ equipped with the norm and the scalar product

$$\|\boldsymbol{v}\|^2_{\boldsymbol{H}^k(\Omega)} \;:=\; \sum_{i=1}^{d} \|v_i\|^2_{H^k(\Omega)} \qquad \text{and} \qquad (\boldsymbol{v}\,,\,\boldsymbol{w})_{\boldsymbol{H}^k(\Omega)} \;:=\; \sum_{i=1}^{d} (v_i\,,\,w_i)_{H^k(\Omega)}\,, \tag{3.2}$$

respectively. Furthermore, let $\boldsymbol{H}^{k,\mathrm{div}}(\Omega) := \{\boldsymbol{v} \in \boldsymbol{H}^k(\Omega);\ \boldsymbol{\nabla}\cdot\boldsymbol{v} \in H^k(\Omega)\}$ for $k \in \mathbb{N}_0$. With the scalar product

$$(\boldsymbol{v}_1\,,\,\boldsymbol{v}_2)_{\boldsymbol{H}^{k,\mathrm{div}}(\Omega)} \;=\; (\boldsymbol{v}_1\,,\,\boldsymbol{v}_2)_{\boldsymbol{H}^k(\Omega)} + (\boldsymbol{\nabla}\cdot\boldsymbol{v}_1\,,\,\boldsymbol{\nabla}\cdot\boldsymbol{v}_2)_{H^k(\Omega)}$$

for $\boldsymbol{v}_1, \boldsymbol{v}_2 \in \boldsymbol{H}^{k,\mathrm{div}}(\Omega)$ and induced norm $\|\cdot\|^2_{\boldsymbol{H}^{k,\mathrm{div}}(\Omega)} = (\cdot\,,\,\cdot)_{\boldsymbol{H}^{k,\mathrm{div}}(\Omega)}$, the space $\boldsymbol{H}^{k,\mathrm{div}}(\Omega)$ is a Hilbert space.

In general, we denote by $(\cdot\,,\,\cdot)_V$ the scalar product in the Hilbert space V and by $\langle\cdot\,,\,\cdot\rangle_{V',V}$ the duality pairing between V and its dual V'. In proofs, we occasionally suppress the subindex for $V = L^2(\Omega)$ or $\boldsymbol{L}^2(\Omega)$ and simply write $\|\cdot\|$ and $(\cdot\,,\,\cdot)$.

We continue with the definition of spaces containing time-dependent functions. With V being a Banach space, the space $L^p(J;V)$ consists of Bochner-measurable, V-valued functions such that the norm

$$\|v\|_{L^p(J;V)} \;:=\; \begin{Bmatrix} \left(\int_J \|v(t,\cdot)\|_V^p \,\mathrm{d}t\right)^{1/p}, & 1 \le p < \infty \\ \operatorname{ess\,sup}_{t\in J} \|v(t,\cdot)\|_V, & p = \infty \end{Bmatrix}$$

is finite, which makes $L^p(J;V)$ a Banach space. For the case of $V = L^p(\Omega)$, we identify $L^p(J\times\Omega) = L^p(J;V)$.

An overview of notation used in this context is found in Table B.8 on p. 147.

Theorem 3.1 (Trace and normal trace). *Let Ω be a domain as considered above.*

(i) *The* trace operator $\gamma_0 : H^1(\Omega) \ni w \mapsto w|_{\partial\Omega} \in H^{1/2}(\partial\Omega)$ *is a linear and continuous mapping, i. e., $\gamma_0 \in \mathcal{L}(H^1(\Omega); H^{1/2}(\partial\Omega))$. Furthermore, γ_0 is surjective.*

(ii) *The* normal trace operator $\gamma_\nu : \boldsymbol{H}^{\mathrm{div}}(\Omega) \ni \boldsymbol{v} \mapsto \boldsymbol{v} \cdot \boldsymbol{\nu}|_{\partial\Omega} \in H^{-1/2}(\partial\Omega)$ *is a linear and continuous mapping, i. e.,* $\gamma_\nu \in \mathcal{L}(\boldsymbol{H}^{\mathrm{div}}(\Omega); H^{-1/2}(\partial\Omega))$. *In particular,*

$$\|\boldsymbol{v} \cdot \boldsymbol{\nu}\|_{H^{-1/2}(\partial\Omega)} \leq \|\gamma_\nu\| \, \|\boldsymbol{v}\|_{\boldsymbol{H}^{\mathrm{div}}(\Omega)} \tag{3.3}$$

holds with $\|\gamma_\nu\| = \|\gamma_\nu\|_{\mathcal{L}(\boldsymbol{H}^{\mathrm{div}}(\Omega);H^{-1/2}(\partial\Omega))} = 1$. *Furthermore,* γ_ν *is surjective.*

Proof. See Girault & Raviart (1986, Thm. 1.5, Thm. 2.5, and Cor. 2.8). □

A useful consequence is the following formula for partial integration.

Corollary 3.2 (Green). *Let* $\boldsymbol{v} \in \boldsymbol{H}^{\mathrm{div}}(\Omega)$. *Then* $\boldsymbol{v} \cdot \boldsymbol{\nu}|_{\partial\Omega} \in H^{-1/2}(\partial\Omega)$ *and there holds*

$$\forall w \in H^1(\Omega), \quad (\boldsymbol{\nabla} \cdot \boldsymbol{v}\,,\, w)_{L^2(\Omega)} + (\boldsymbol{v}\,,\, \boldsymbol{\nabla} w)_{L^2(\Omega)} \;=\; \langle \boldsymbol{v} \cdot \boldsymbol{\nu}\,,\, w \rangle_{H^{-1/2}(\partial\Omega),H^{1/2}(\partial\Omega)} \,. \tag{3.4}$$

If, in addition, $\boldsymbol{v} \cdot \boldsymbol{\nu}|_{\partial\Omega} \in L^2(\partial\Omega)$, we can identify the duality pairing in (3.4) by $\int_{\partial\Omega} \boldsymbol{v} \cdot \boldsymbol{\nu}\, w = (\boldsymbol{v} \cdot \boldsymbol{\nu}\,,\, w)_{L^2(\partial\Omega)}$. Then, in particular, $\langle \cdot\,,\, \cdot \rangle_{H^{-1/2}(\partial\Omega),H^{1/2}(\partial\Omega)}$ is a continuous extension of the inner product $(\cdot\,,\, \cdot)_{L^2(\partial\Omega)}$, since $(H^{1/2}(\partial\Omega), L^2(\partial\Omega), H^{-1/2}(\partial\Omega))$ is a Gelfand triple (cf. Roubíček 2005b, Sec. 7.2).

With Theorem 3.1 we are able to define the following *constrained ansatz spaces*:

$$\boldsymbol{H}^{\mathrm{div}}_a(\Omega) \;\coloneqq\; \left\{ \boldsymbol{v} \in \boldsymbol{H}^{\mathrm{div}}(\Omega);\; \boldsymbol{v} \cdot \boldsymbol{\nu} = a \;\text{ on } \partial\Omega \right\}, \quad H^1_b(\Omega) \;\coloneqq\; \left\{ w \in H^1(\Omega);\; w = b \;\text{ on } \partial\Omega \right\},$$

where $a \in H^{-1/2}(\partial\Omega)$ and $b \in H^{1/2}(\partial\Omega)$. The spaces $\boldsymbol{H}^{\mathrm{div}}_0(\Omega)$ and $H^1_0(\Omega)$ therefore consist of functions with vanishing normal trace and vanishing trace, respectively.

In the error analysis presented in Section 3.2, we require the following version of the discrete Gronwall lemma:

Lemma 3.3 (Discrete Gronwall). *Let* $(a_k)_{k\in\mathbb{N}}$, $(b_k)_{k\in\mathbb{N}}$ *be nonnegative sequences of real numbers,* (b_n) *non-decreasing, and* c *be a (fixed) positive constant. If* (a_n) *satisfies*

$$\forall\, n \in \mathbb{N}, \quad a_n \;\leq\; b_n + c \sum_{m=1}^{n-1} a_m \,,$$

then

$$\forall n \in \mathbb{N}, \quad a_n \;\leq\; (1 + c)^n b_n \,.$$

Proof. See Girault & Raviart (1979, Lem. 2.4). □

Note that the sum is zero for $n = 1$ by definition.

We recall some elementary inequalities that are frequently used in the numerical analysis in this work. For further generalizations, we refer to the monographies of Adams & Fournier (2003) and Wu et al. (2006).

Young inequality. For positive numbers a, b, there holds for all $\delta > 0$ that

$$ab \;\leq\; \frac{\delta}{2}a^2 + \frac{1}{2\delta}b^2 \,.$$

Minkowski inequality. Let $1 \leq p < \infty$. If $f, g \in L^p(\Omega)$, then $f + g \in L^p(\Omega)$ and

$$\|f + g\|_{L^p(\Omega)} \;\leq\; \|f\|_{L^p(\Omega)} + \|g\|_{L^p(\Omega)} \,.$$

The discrete version for sequences of real numbers $(a_k)_{k\in\mathbb{N}}$, $(b_k)_{k\in\mathbb{N}}$ reads:

$$\left(\sum_k |a_k + b_k|^p\right)^{1/p} \;\leq\; \left(\sum_k |a_k|^p\right)^{1/p} + \left(\sum_k |b_k|^p\right)^{1/p} \,.$$

Hölder inequality. Let $1 \leq p, q, r \leq \infty$ and $\frac{1}{p} + \frac{1}{q} = \frac{1}{r}$. If $f \in L^p(\Omega)$, $g \in L^q(\Omega)$, then $fg \in L^r(\Omega)$ and

$$\|fg\|_{L^r(\Omega)} \;\leq\; \|f\|_{L^p(\Omega)}\, \|g\|_{L^q(\Omega)} \,.$$

In particular, $r = 1$, $p = q = 2$ yields the Cauchy–Schwarz inequality:

$$(f\,,\, g)_{L^2(\Omega)} \;\leq\; \|fg\|_{L^1(\Omega)} \;\leq\; \|f\|_{L^2(\Omega)}\, \|g\|_{L^2(\Omega)} \,.$$

The discrete version for sequences of real numbers $(a_k)_{k\in\mathbb{N}}$, $(b_k)_{k\in\mathbb{N}}$ reads:

$$\left(\sum_k |a_k b_k|^r\right)^{1/r} \;\leq\; \left(\sum_k |a_k|^p\right)^{1/p} \left(\sum_k |b_k|^q\right)^{1/q} \,.$$

Jensen inequality. We only state the special case for powers and uniform distributions here. Let $p \geq 1$ and let $f : \Omega \to \mathbb{R}_0^+$. Then

$$\left(\fint f\right)^p \;\leq\; \fint f^p \qquad \text{and} \qquad \left(\fint f\right)^{1/p} \;\geq\; \fint f^{1/p} \,,$$

where $\fint \cdot$ denotes the integral mean (cf. Tab. B.7, p. 146). The discrete version for $a_k \in \mathbb{R}_0^+$ reads:

$$\left(\frac{1}{n}\sum_{k=1}^{n} a_k\right)^p \leq \frac{1}{n}\sum_{k=1}^{n} a_k^p \qquad \text{and} \qquad \left(\frac{1}{n}\sum_{k=1}^{n} a_k\right)^{1/p} \geq \frac{1}{n}\sum_{k=1}^{n} a_k^{1/p} .$$

Triangulation of the domain. Let $\mathcal{T}_h$ be a *regular family of decompositions* (Ciarlet 1991, (H1), p. 131) into closed *d-simplices* T of characteristic size h (also called *fineness* or *mesh size*) such that $\overline{\Omega} = \cup T$. For the treatment of curved domains in the context of finite element methods for second-order problems we refer to Ciarlet (1991, Chap. VI). Let $\mathcal{E}_\Omega$ denote the set of interior edges (faces for $d = 3$), $\mathcal{E}_{\partial\Omega}$ the set of exterior edges (faces for $d = 3$), $\mathcal{E}_\Omega \cup \mathcal{E}_{\partial\Omega} =: \mathcal{E} = \{E\}$, and $\boldsymbol{\nu}_E$ the unit normal on E under global orientation that, for $E \in \mathcal{E}_{\partial\Omega}$, points outward Ω (cf. Fig. 3.1). Triangulation and grid related symbols are found in Table B.6 on p. 145.

Local discrete spaces. We denote by $\mathbb{P}_k(T)$ the space of polynomials of degree at most k on a simplex $T \in \mathcal{T}_h$ and define by

$$\begin{aligned} \mathbb{RT}_k(T) &:= \mathbb{P}_k(T)^d \oplus \boldsymbol{x}\mathbb{P}_k(T) \\ &= \{\boldsymbol{v}_h : T \to \mathbb{R}^d;\ \boldsymbol{v}_h(\boldsymbol{x}) = a\,\boldsymbol{x} + \boldsymbol{b}\,,\ a \in \mathbb{P}_k(T)\,,\ \boldsymbol{b} \in \mathbb{P}_k(T)^d\} \end{aligned} \tag{3.5}$$

the *local Raviart–Thomas space* of order k (Nédélec 1980; Raviart & Thomas 1977; Thomas 1977). We state some properties of the local discrete spaces in the following lemma.

Lemma 3.4 (Properties of local discrete spaces).

(i) $\dim \mathbb{RT}_k(T) = d\binom{k+d}{k} + \binom{k+d-1}{k}$.

(ii) $\dim \mathbb{P}_k(T) = \binom{k+d}{d}$.

(iii) *Let* $\boldsymbol{v}_h \in \mathbb{RT}_k(T)$, *then* $\forall E \subset T$, $\boldsymbol{v}_h \cdot \boldsymbol{\nu}_E \in \mathbb{P}_k(E)$.

(iv) *Let* $\boldsymbol{v}_h \in \mathbb{RT}_k(T)$ *such that* $\boldsymbol{\nabla} \cdot \boldsymbol{v}_h = 0$, *then* $\boldsymbol{v}_h \in \mathbb{P}_k(T)^d$.

(v) $\mathbb{P}_{k-1}(T)^d \subset \mathbb{RT}_{k-1}(T) \subset \mathbb{P}_k(T)^d$ *for* $k \geq 1$.

Proof. For properties (i)–(iv) see Durán (2008, Lem. 3.1), for property (v) see Roberts & Thomas (1991). □

Definition 3.5 (Jump). *Consider an interior edge (or face) $E \in \mathcal{E}_\Omega$ and two d-simplices $T_1, T_2 \in \mathcal{T}_h$ sharing E, i. e., $E = T_1 \cap T_2$. Let $\boldsymbol{\nu}_E$ be the unit normal on E under global orientation (cf. Fig. 3.1). For a vector-valued quantity $\boldsymbol{w} \in \prod_{T\in\mathcal{T}_h} \boldsymbol{H}^{\mathrm{div}}(T)$, we define the* jump $[\![\cdot]\!]_E$ *on E by*

$$[\![\boldsymbol{w}]\!]_E \coloneqq \gamma_{\boldsymbol{\nu}_E}(\boldsymbol{w}|_{T_1}) - \gamma_{\boldsymbol{\nu}_E}(\boldsymbol{w}|_{T_2}) .$$

Now consider an exterior edge $E \in \mathcal{E}_{\partial\Omega}$. Recall that $\boldsymbol{\nu}_E$ denotes the unit normal exterior to Ω in this case. We define $[\![\boldsymbol{w}]\!]_E \coloneqq \gamma_{\boldsymbol{\nu}_E}(\boldsymbol{w}|_{T\supset E})$.

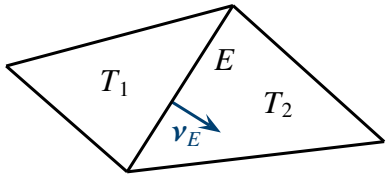

Figure 3.1. Two adjacent triangles T_1, T_2 sharing an edge E which has an oriented unit normal $\boldsymbol{\nu}_E$.

Global discrete spaces. We define by

$$\mathbb{P}_k(\mathcal{T}_h) \coloneqq \{w_h : \Omega \to \mathbb{R};\ \forall T \in \mathcal{T}_h,\ w_h|_T \in \mathbb{P}_k(T)\} \tag{3.6}$$

the global polynomial space on the triangulation $\mathcal{T}_h$, which is discontinuous on interior edges / faces. Clearly, $\mathbb{P}_k(\mathcal{T}_h) \subset L^2(\Omega)$. The *global Raviart–Thomas space* of order k is defined by

$$\begin{aligned}\mathbb{RT}_k(\mathcal{T}_h) &\coloneqq \boldsymbol{H}^{\mathrm{div}}(\Omega) \cap \prod_{T\in\mathcal{T}_h} \mathbb{RT}_k(T) \\ &= \left\{ \boldsymbol{v}_h : \Omega \to \mathbb{R}^d;\ \forall T \in \mathcal{T}_h,\ \boldsymbol{v}_h|_T \in \mathbb{RT}_k(T);\ \forall E \in \mathcal{E}_\Omega,\ [\![\boldsymbol{v}_h]\!]_E = 0 \right\} .\end{aligned} \tag{3.7}$$

Thus, the constraint $[\![\boldsymbol{v}_h]\!]_E = 0$—i. e., the normal components of $\boldsymbol{v}_h$ are continuous across the interior edges—ensures that $\mathbb{RT}_k(\mathcal{T}_h) \subset \boldsymbol{H}^{\mathrm{div}}(\Omega)$ (Raviart & Thomas 1977, p. 297). Note that in general, these functions are not continuous in each component.

We refer to Definition 4.14 for closed-form expressions of the basis functions and the degrees of freedom for $\mathbb{RT}_0(\mathcal{T}_h)$ in two space dimensions.

Global interpolation operators. Let the projectors $\boldsymbol{\Pi}_h^k : \boldsymbol{H}^{\mathrm{div}}(\Omega) \cap \prod_{T\in\mathcal{T}_h} \boldsymbol{H}^1(T) \ni \boldsymbol{v} \mapsto \boldsymbol{\Pi}_h^k \boldsymbol{v} \in \mathbb{RT}_k(\mathcal{T}_h)$ and $P_h^k : L^2(\Omega) \ni w \mapsto P_h^k w \in \mathbb{P}_k(\mathcal{T}_h)$ be the *global interpolation operators*

due to Raviart and Thomas (Brezzi & Fortin 1991; Durán 2008). Clearly, $\boldsymbol{\Pi}_h^k$ and P_h^k are each the identity operator on $\mathbb{RT}_k(\mathcal{T}_h)$ and $\mathbb{P}_k(\mathcal{T}_h)$, respectively. The projector P_h^k is defined as follows:

Definition 3.6 (Projector properties 1). *Let P_h^k be the orthogonal $L^2(\Omega)$ projector on $\mathbb{P}_k(\mathcal{T}_h)$, i. e.,*

$$\forall w_h \in \mathbb{P}_k(\mathcal{T}_h), \quad \left(P_h^k w\,,\, w_h\right)_{L^2(\Omega)} \;=\; (w\,,\, w_h)_{L^2(\Omega)} \tag{3.8}$$

for $w \in L^2(\Omega)$.

The projector $\boldsymbol{\Pi}_h^k$ is defined by means of local $\mathbb{RT}_k(T)$ projections, the definition of which can be found, e. g., in Durán (2008). The projector has the following property:

Lemma 3.7 (Projector properties 2). *The projector $\boldsymbol{\Pi}_h^k$ fulfills the following orthogonality: for $\boldsymbol{v} \in \boldsymbol{H}^{\mathrm{div}}(\Omega) \cap \prod_{T\in\mathcal{T}_h} \boldsymbol{H}^1(T)$ given,*

$$\forall w_h \in \mathbb{P}_k(\mathcal{T}_h), \quad \left(\boldsymbol{\nabla}\cdot\boldsymbol{\Pi}_h^k\boldsymbol{v}\,,\, w_h\right)_{L^2(\Omega)} \;=\; (\boldsymbol{\nabla}\cdot\boldsymbol{v}\,,\, w_h)_{L^2(\Omega)}\,. \tag{3.9}$$

Proof. See (Durán 2008, Lem. 3.5). □

In other words, $(P_h^k - I)w$ and $\boldsymbol{\nabla}\cdot(\boldsymbol{\Pi}_h^k - \boldsymbol{I})\boldsymbol{v}$ are orthogonal to $\mathbb{P}_k(\mathcal{T}_h)$.

Lemma 3.8 (Commuting diagram property). *The following diagram commutes:*

$$\begin{array}{ccc} \boldsymbol{H}^{\mathrm{div}}(\Omega) \cap \prod_{T\in\mathcal{T}_h} \boldsymbol{H}^1(T) & \xrightarrow{\boldsymbol{\nabla}\cdot} & L^2(\Omega) \\ \Big\downarrow{\scriptstyle \boldsymbol{\Pi}_h^k} & & \Big\downarrow{\scriptstyle P_h^k} \\ \mathbb{RT}_k(\mathcal{T}_h) & \xrightarrow[\boldsymbol{\nabla}\cdot]{} & \mathbb{P}_k(\mathcal{T}_h) \end{array}$$

Proof. See Durán (2008, (38)) and also Ern & Guermond (2004, Lem. 1.41 and Prop. 1.98). □

In short, this means that $\boldsymbol{\nabla}\cdot\boldsymbol{\Pi}_h^k = P_h^k\,\boldsymbol{\nabla}\cdot$ and, in particular, that $\boldsymbol{\nabla}\cdot\mathbb{RT}_k(\mathcal{T}_h) = \mathbb{P}_k(\mathcal{T}_h)$. Note that the divergence operator in Lemma 3.8 is surjective:

Lemma 3.9. *Given $w_h \in \mathbb{P}_k(\mathcal{T}_h)$, there exists $\boldsymbol{v}_h \in \mathbb{RT}_k(\mathcal{T}_h)$ such that $\boldsymbol{\nabla} \cdot \boldsymbol{v}_h = w_h$ and*

$$\|\boldsymbol{v}_h\|_{\boldsymbol{H}^{\mathrm{div}}(\Omega)} \leq C_\Omega \|w_h\|_{L^2(\Omega)} \tag{3.10}$$

holds with a constant C_Ω depending only on Ω.

Proof. See Raviart & Thomas (1977, Thm. 4, p. 310) or Chen (2005, Lem. 3.7, p. 164). □

With this result we can write (3.8) as

$$\forall \boldsymbol{v}_h \in \mathbb{RT}_k(\mathcal{T}_h), \quad \left(P_h^k w\,,\, \boldsymbol{\nabla} \cdot \boldsymbol{v}_h\right)_{L^2(\Omega)} = (w\,,\, \boldsymbol{\nabla} \cdot \boldsymbol{v}_h)_{L^2(\Omega)}\,. \tag{3.11}$$

The $\mathbb{RT}_k(\mathcal{T}_h)$ and $\mathbb{P}_k(\mathcal{T}_h)$ finite element spaces have the following approximation properties:

Lemma 3.10 (Projection errors). *For any $\boldsymbol{v} \in \boldsymbol{H}^{l,\mathrm{div}}(\Omega)$ and $w \in H^l(\Omega)$, there exist constants $C > 0$ independent of h such that for $l \in \{1, \ldots, k+1\}$,*

$$\begin{aligned}
\|\boldsymbol{\nabla} \cdot (\boldsymbol{\Pi}_h^k - \boldsymbol{I})\boldsymbol{v}\|_{L^2(\Omega)} &\leq C h^l |\boldsymbol{\nabla} \cdot \boldsymbol{v}|_{H^l(\Omega)}\,,\\
\|(\boldsymbol{\Pi}_h^k - \boldsymbol{I})\boldsymbol{v}\|_{\boldsymbol{L}^2(\Omega)} &\leq C h^l |\boldsymbol{v}|_{\boldsymbol{H}^l(\Omega)}\,,\\
\|(P_h^k - I)w\|_{L^2(\Omega)} &\leq C h^l |w|_{H^l(\Omega)}\,.
\end{aligned}$$

Proof. See Brezzi & Fortin (1991, Prop. 3.9, p. 132) and Quarteroni & Valli (1994, Sec. 3.4.2, Eqn. (3.5.24)). □

Time discretization. Let $0 =: t_0 < t_1 < \ldots < t_N := T$ be an equidistant decomposition of the time interval J and let $\tau := T/N$ denote the *time step size*. The assumption of even time step sizes in this chapter is for an easy presentation and not necessary for the analysis that follows.

For fully discrete functions v_h^n, $n \in \{1, \ldots, N\}$, we define the *backward difference quotient* by

$$\overline{\partial} v_h^n := \frac{v_h^n - v_h^{n-1}}{\tau}\,. \tag{3.12}$$

Analogously, for a continuous function, we set $\overline{\partial} v(t_n) := (v(t_n) - v(t_{n-1}))/\tau$.

With the definition (3.12), the well-known Taylor expansion with integral remainder yields the following useful identities entering the proof of Proposition 3.24:

Corollary 3.11 (FTC / Taylor). *Let $v \in H^1(\,]t_{n-1}, t_n[\,)$. Then*

$$\overline{\partial} v(t_n) \;=\; \frac{1}{\tau}\int_{t_{n-1}}^{t_n} \partial_t v(s)\,\mathrm{d}s \;=\; \fint_{t_{n-1}}^{t_n} \partial_t v(s)\,\mathrm{d}s\,. \tag{3.13a}$$

Let $v \in H^2(\,]t_{n-1}, t_n\,[)$. Then

$$(\partial_t - \overline{\partial}) v(t_n) \;=\; \frac{1}{\tau}\int_{t_{n-1}}^{t_n} (s - t_{n-1})\,\partial_{tt} v(s)\,\mathrm{d}s \;=\; \fint_{t_{n-1}}^{t_n} (s - t_{n-1})\,\partial_{tt} v(s)\,\mathrm{d}s\,. \tag{3.13b}$$

3.2 Discretization and Convergence Analysis

The hypotheses imposed on the data of system (3.1) are as follows:

Hypotheses 3.12 (Hypotheses on the data).

(H1) *The inverse of the coefficient $\mathbf{D} \in \mathbb{R}^{d,d}$ is bounded and positive definite, i. e., there exist strictly positive constants D_α, D_∞, such that*

$$\begin{aligned} &\forall \boldsymbol{\xi} \in \mathbb{R}^d\,, && \boldsymbol{\xi}\cdot\mathbf{D}^{-1}\boldsymbol{\xi} \;\geq\; D_\alpha |\boldsymbol{\xi}|^2\,,\\ &\forall \boldsymbol{\xi}_1, \boldsymbol{\xi}_2 \in \mathbb{R}^d\,, && \boldsymbol{\xi}_1\cdot\mathbf{D}^{-1}\boldsymbol{\xi}_2 \;\leq\; D_\infty |\boldsymbol{\xi}_1||\boldsymbol{\xi}_2|\,. \end{aligned}$$

(H2) *The hypothesis* (H1) *holds for the coefficient $\mathbf{K}$ with the constants K_α, K_∞.*

(H3) *The nonlinear coefficients $r^\pm$ are globally Lipschitz continuous.*

(H4) *The initial data $c^{\pm,0}$ are bounded and nonnegative, i. e.,*

$$c^{\pm,0} \in L^\infty(\Omega) \qquad \text{and} \qquad c^{\pm,0}(\boldsymbol{x}) \;\geq\; 0 \quad \text{for a. e. } \boldsymbol{x} \in \Omega\,.$$

(H5) *The coefficient ϕ_D is bounded in $H^1(J; H^{1/2}(\partial\Omega))$.*

(H6) *The coefficient $\bar{\sigma}$ is bounded in $L^\infty(J \times \Omega)$.*

Note that the symmetry and positive definiteness of the matrices in hypotheses (H1) and (H2) imply the symmetry and positive definiteness of their inverses (e. g., Knabner & Barth 2012, Thm. 4.135).

Some of the items in Hypotheses 3.12 are naturally satisfied:

Remark 3.13 (Satisfied hypotheses of the DNPP problem). The homogenization result (2.5) (cf. Thm. 2.5, p. 23) naturally satisfies some of the assumptions on the data: the symmetry and positive definiteness of the upscaled tensors $\mathbf{D}$ and $\mathbf{K}$ as postulated in (H1) and (H2) holds for Problem 3.14 (cf. Def. 2.3 and Cioranescu & Donato (1999) and Hornung (1997)). Being defined as $-\int_\Gamma \sigma \, \mathrm{d}s_{\boldsymbol{y}}$, the boundedness of the coefficient $\bar{\sigma}$ directly follows from the boundedness of σ on the interior cell boundary Γ. △

The error analysis of this section deals with the discretization of the following *mixed weak continuous problem* that is derived by multiplication of the flux equations of (3.1) by the inverse tensors and by using the Green formula (3.4):

Problem 3.14 (Mixed weak continuous DNPP problem). *Let the data* $\mathbf{D}$, $\mathbf{K}$, $r^\pm$, $c^{\pm,0}$, ϕ_D, $\bar{\sigma}$ *be given and let the hypotheses* (H1)–(H6) *hold. Seek* $(\boldsymbol{u}, p, \boldsymbol{j}^+, c^+, \boldsymbol{j}^-, c^-, \boldsymbol{E}, \phi)$ *with* $\boldsymbol{u} \in L^2(J; \boldsymbol{H}^{\mathrm{div}}_0(\Omega))$, $p \in L^2(J; L^2(\Omega)/\mathbb{R})$, $\boldsymbol{j}^\pm \in L^2(J; \boldsymbol{H}^{\mathrm{div}}(\Omega))$, $c^\pm \in L^\infty(J \times \Omega) \cap H^1(J; L^2(\Omega))$, $\boldsymbol{E} \in L^\infty(J; \boldsymbol{H}^{\mathrm{div}}(\Omega))$, $\phi \in L^\infty(J; L^2(\Omega))$ *such that for a. e.* $t \in J$,

$$\forall \boldsymbol{v} \in \boldsymbol{H}^{\mathrm{div}}(\Omega), \quad -\left(\mathbf{K}^{-1}\boldsymbol{u}(t)\,,\,\boldsymbol{v}\right) + \left(\boldsymbol{\nabla}\cdot\boldsymbol{v}\,,\,p(t)\right) \;=\; -\left(\mathbf{D}^{-1}\boldsymbol{E}(t)\,(c^+(t)-c^-(t))\,,\,\boldsymbol{v}\right), \tag{3.14a}$$

$$\forall w \in L^2(\Omega), \quad \left(\boldsymbol{\nabla}\cdot\boldsymbol{u}(t)\,,\,w\right) \;=\; 0\,, \tag{3.14b}$$

$$\forall \boldsymbol{v} \in \boldsymbol{H}^{\mathrm{div}}(\Omega), \quad -\left(\mathbf{D}^{-1}\boldsymbol{j}^\pm(t)\,,\,\boldsymbol{v}\right) + \left(\boldsymbol{\nabla}\cdot\boldsymbol{v}\,,\,c^\pm(t)\right) + \left(\mathbf{D}^{-1}(\boldsymbol{u}(t)\pm\boldsymbol{E}(t))c^\pm(t)\,,\,\boldsymbol{v}\right) \;=\; 0\,, \tag{3.14c}$$

$$\forall w \in L^2(\Omega), \quad \left(\partial_t c^\pm(t)\,,\,w\right) + \left(\boldsymbol{\nabla}\cdot\boldsymbol{j}^\pm(t)\,,\,w\right) \;=\; \left(r^\pm(c^+(t),c^-(t))\,,\,w\right), \tag{3.14d}$$

$$\forall \boldsymbol{v} \in \boldsymbol{H}^{\mathrm{div}}(\Omega), \quad -\left(\mathbf{D}^{-1}\boldsymbol{E}(t)\,,\,\boldsymbol{v}\right) + \left(\boldsymbol{\nabla}\cdot\boldsymbol{v}\,,\,\phi(t)\right) \;=\; \langle \boldsymbol{v}\cdot\boldsymbol{\nu}\,,\,\phi_\mathrm{D}(t)\rangle_{H^{-1/2}(\partial\Omega),H^{1/2}(\partial\Omega)}\,, \tag{3.14e}$$

$$\forall w \in L^2(\Omega), \quad \left(\boldsymbol{\nabla}\cdot\boldsymbol{E}(t)\,,\,w\right) \;=\; \left(c^+(t)-c^-(t)+\bar{\sigma}(t)\,,\,w\right) \tag{3.14f}$$

with $c^\pm$ *satisfying* $\forall w \in L^2(\Omega)$, $\left(c^\pm(0)-c^{\pm,0}\,,\,w\right) \;=\; 0$.

We call the solution of Problem 3.14 the *true solution* in contrast to the solution of the below defined discrete problem, which we call the *discrete solution*.

The formulation of the fully discrete counterpart of Problem 3.14 contains the following *cut-off operator* (Barbeiro & Wheeler 2010; Sun & Wheeler 2005; Sun et al. 2002):

Definition 3.15 (Cut-off operator). *For* $w \in L^p(\Omega)$, $1 \le p \le \infty$ *and fixed* $M \in \mathbb{R}^+$, *let* $\mathcal{M} : L^p(\Omega) \ni w \mapsto \mathcal{M}(w) \in L^\infty(\Omega)$ *be an operator such that for a. e.* $\boldsymbol{x} \in \Omega$,

$$\mathcal{M}(w)(\boldsymbol{x}) \;=\; \min\left\{|w(\boldsymbol{x})|,\, M\right\}$$

holds.

Lemma 3.16 (Properties of the cut-off operator). *Let $1 \leq p \leq \infty$. The following statements hold:*

(i) $\forall w \in L^p(\Omega),\ \|\mathcal{M}(w)\|_{L^\infty(\Omega)} \leq M$.

(ii) *Let $w \in L^\infty(\Omega)$. If M satisfies $\|w\|_{L^\infty(\Omega)} \leq M$, then $\mathcal{M}(w) = w$.*

(iii) *The operator $\mathcal{M}(\cdot)$ is globally Lipschitz continuous on $L^p(\Omega)$ with a Lipschitz constant equal to one, i. e.,*

$$\forall v, w \in L^p(\Omega), \quad \|\mathcal{M}(v) - \mathcal{M}(w)\|_{L^p(\Omega)} \ \leq\ \|v - w\|_{L^p(\Omega)}.$$

Proof. The properties (i) and (ii) are obvious. Property (iii) follows from the pointwise Lipschitz continuity $|\mathcal{M}(v)(\boldsymbol{x}) - \mathcal{M}(w)(\boldsymbol{x})| \leq |v(\boldsymbol{x}) - w(\boldsymbol{x})|$ for a. e. $\boldsymbol{x} \in \Omega$ taking the essential supremum on both sides for $p = \infty$ and taking both sides to the power p and integration over Ω for $1 \leq p < \infty$. A sketch of the proof of the pointwise property (iii), i. e., for $p = \infty$, is given in Sun et al. (2002). □

The cut-off operator $\mathcal{M}$ is a crucial tool in the error analysis that follows. However, the associated numerical scheme is not defined properly yet as long as no *explicit* expression for the cut-off level M is given that does not depend on the true solution itself. Especially, it has to be ensured that M is chosen sufficiently large such that the property (ii) of Lemma 3.16 holds for the partial true solutions $c^\pm(t)$. This means, in particular, that an L^∞ a priori estimate is necessary providing an L^∞ bound depending only on the data. To this end, we show that solutions of Problem 3.14 also solve Problem 3.17 in order to allow the exploitation of the estimate (iii) of Theorem 3.18 yielding the demanded explicit bound. The so obtained validity of Theorem 3.18 yields furthermore the existence and uniqueness of solutions of Problem 3.14 and also the nonnegativity of concentrations.

Before we continue with discretization of Problem 3.14, which is based on the mixed formulation of system (3.1), we cite an existence result of Herz et al. (2012) that yields an explicit bound for $\sum_{i\in\{+,-\}} \|c^\pm\|_{L^\infty(J\times\Omega)}$. The weak problem under investigation of Herz et al. (2012) derives from the *non-mixed* formulation of {(3.1c), (3.1d), (3.1e), (3.1f)} and reads as follows:

Problem 3.17 (Non-mixed weak continuous DNPP problem). *Let the data* $\mathbf{D}$, $\mathbf{K}$, $r^\pm$, $c^{\pm,0}$, ϕ_D, $\bar{\sigma}$ *be given and let the hypotheses* (H1)–(H6) *hold. Seek* $(\boldsymbol{u}, p, c^+, c^-, \phi)$ *with*

$\boldsymbol{u} \in L^2(J; \boldsymbol{H}^{\mathrm{div}}_0(\Omega))$, $p \in L^2(J; L^2(\Omega)/\mathbb{R})$, $c^\pm \in L^\infty(J \times \Omega) \cap L^2(J; H^1_0(\Omega)) \cap H^1(J; H^{-1}(\Omega))$, $\phi \in L^\infty(J; H^2(\Omega) \cap H^1_{\phi_\mathrm{D}}(\Omega))$ *such that for a. e.* $t \in J$,

$$\forall \boldsymbol{v} \in \boldsymbol{H}^{\mathrm{div}}_0(\Omega), \quad -\left(\mathbf{K}^{-1}\boldsymbol{u}(t)\,,\,\boldsymbol{v}\right) + (\boldsymbol{\nabla}\cdot\boldsymbol{v}\,,\,p(t)) \;=\; ((c^+(t)-c^-(t))\,\boldsymbol{\nabla}\phi\,,\,\boldsymbol{v})\,, \tag{3.15a}$$

$$\forall w \in L^2(\Omega), \quad (\boldsymbol{\nabla}\cdot\boldsymbol{u}(t)\,,\,w) \;=\; 0\,, \tag{3.15b}$$

$$\forall z \in H^1_0(\Omega), \quad \langle \partial_t c^\pm(t)\,,\,z\rangle_{H^{-1}(\Omega),H^1_0(\Omega)} + (\mathbf{D}\,\boldsymbol{\nabla}c^\pm(t)\,,\,\boldsymbol{\nabla}z) - (\boldsymbol{u}(t)\,c^\pm(t)\,,\,\boldsymbol{\nabla}z) \tag{3.15c}$$

$$\pm\,(\mathbf{D}\,c^\pm(t)\boldsymbol{\nabla}\phi(t)\,,\,\boldsymbol{\nabla}z) \;=\; (r^\pm(c^+(t),c^-(t))\,,\,z)\,,$$

$$\forall w \in L^2(\Omega), \quad (\boldsymbol{\nabla}\cdot\mathbf{D}\,\boldsymbol{\nabla}\phi(t)\,,\,w) \;=\; (c^+(t)-c^-(t)+\bar{\sigma}(t)\,,\,w) \tag{3.15d}$$

with $c^\pm$ *satisfying* $\forall w \in L^2(\Omega)$, $\left(c^\pm(0)-c^{\pm,0}\,,\,w\right) \;=\; 0$.

We summarize the most important results of Herz et al. (2012) in the following theorem:

Theorem 3.18 (Existence, uniqueness, nonnegativity, and L^∞ stability). *Let* $(\boldsymbol{u}, p, c^+, c^-, \phi)$ *be the solution of Problem 3.17 and let* (H1)–(H6) *hold. Then the following statements hold:*

(i) *The solution* $(\boldsymbol{u}, p, c^+, c^-, \phi)$ *of Problem 3.17* uniquely exists.

(ii) *The partial solutions* $c^\pm$ *are* nonnegative, *i. e.,*

$$c^\pm(t,\boldsymbol{x}) \;\geq\; 0 \quad \text{for a. e. } (t,\boldsymbol{x}) \in J \times \Omega\,.$$

(iii) *The following estimate holds for arbitrary end time* $T \in]0,\infty[$ *:*

$$\sum_{i\in\{+,-\}} \|c^i\|_{L^\infty(J\times\Omega)} \;\leq\; C(c^{\pm,0},\bar{\sigma},\Omega,T)\,, \tag{3.16}$$

with $C(c^{\pm,0},\bar{\sigma},\Omega,T) > 0$ *depending only on* $\|c^{\pm,0}\|_{L^\infty(\Omega)}$, *on* $\|\bar{\sigma}\|_{L^\infty(J\times\Omega)}$, *on coefficients of the Sobolev embedding theorem, and on the end time* T.

Proof. See Herz et al. (2012, Thms. 3.4, 3.10, 3.11 and Remarks 2.2, 3.7). Item (iii) can be deduced as follows: from (Herz et al. 2012, Thm. 3.5) we have

$$\sum_{i\in\{+,-\}} \|c^i\|_{L^\infty(J\times\Omega)} \;\leq\; C_\mathrm{M} \sum_{i\in\{+,-\}} \|c^i\|_{L^2(J\times\Omega)} + 4 \sum_{i\in\{+,-\}} \|c^{i,0}\|_{L^\infty(\Omega)}$$

with a constant $C_{\mathrm{M}} > 0$ depending only on $\|\bar{\sigma}\|_{L^\infty(J\times\Omega)}$ and on coefficients of the Sobolev embedding theorem. Application of Gronwall's lemma to the parabolic estimate (Herz et al. 2012, Remark 3.6)

$$\frac{\mathrm{d}}{\mathrm{d}t}\sum_{i\in\{+,-\}}\|c^i(t)\|_{L^2(\Omega)} + \sum_{i\in\{+,-\}}\|\boldsymbol{\nabla} c^i(t)\|_{\boldsymbol{L}^2(\Omega)} \;\leq\; \frac{2}{D_\alpha}\|\bar{\sigma}\|_{L^\infty(J\times\Omega)}\sum_{i\in\{+,-\}}\|c^i(t)\|_{L^2(\Omega)}$$

yields

$$\forall t\in J\,,\quad \sum_{i\in\{+,-\}}\|c^i(t)\|_{L^2(\Omega)} \;\leq\; \exp\left(\frac{2T}{D_\alpha}\right)\sum_{i\in\{+,-\}}\|c^{i,0}\|_{L^2(\Omega)}\,,$$

which, inserted in the first equation, closes the proof. □

Proposition 3.19 (Mixed solution is non-mixed solution). *Let* $(\boldsymbol{u}, p, \boldsymbol{j}^+, c^+, \boldsymbol{j}^-, c^-, \boldsymbol{E}, \phi)$ *be a solution of Problem 3.14. Then the partial solution* $(\boldsymbol{u}, p, c^+, c^-, \phi)$ *is a solution of Problem 3.17. In particular,* $c^\pm \in L^2(J; H^1_0(\Omega))$ *and* $\phi \in L^\infty(J; H^2(\Omega)\cap H^1_{\phi_{\mathrm{D}}}(\Omega))$ *holds.*

Proof. In this proof we frequently use the fact that the tensors $\mathbf{D}$ and $\mathbf{K}$ have an inverse $\mathbf{D}^{-1}$ and $\mathbf{K}^{-1}$, respectively, due to (H1), (H2). We denote by $\mathcal{D}(\Omega)$ the space of infinitely differentiable functions with compact support on Ω, and by $\mathcal{D}'(\Omega)$ the space of distributions (cf. Ern & Guermond 2004, Sec. B.2).

We test (3.14e) with $\boldsymbol{v}\in\mathcal{D}(\Omega)^d \subset \boldsymbol{H}^{\mathrm{div}}(\Omega)$:

$$\forall \boldsymbol{v}\in\mathcal{D}(\Omega)^d\,,\quad \left(\mathbf{D}^{-1}\boldsymbol{E}(t)\,,\,\boldsymbol{v}\right) \overset{(3.14\mathrm{e})}{=} (\phi(t)\,,\,\boldsymbol{\nabla}\cdot\boldsymbol{v}) \;=\; -\langle\boldsymbol{\nabla}\phi(t)\,,\,\boldsymbol{v}\rangle_{\mathcal{D}'(\Omega)^d,\mathcal{D}(\Omega)^d}\,, \tag{3.17}$$

which is the defining equation for $\boldsymbol{\nabla}\phi(t)$, i. e., $\boldsymbol{\nabla}\phi(t)$ in the distributional sense is a function: $-\boldsymbol{\nabla}\phi(t) = \mathbf{D}^{-1}\boldsymbol{E}(t)$ for a. e. $t\in J$. Since $\|\mathbf{D}^{-1}\boldsymbol{E}\|_{L^\infty(J;\boldsymbol{L}^2(\Omega))} \leq \|\mathbf{D}^{-1}\|_{\mathbf{L}^\infty(\Omega)}\,\|\boldsymbol{E}\|_{L^\infty(J;\boldsymbol{L}^2(\Omega))} < \infty$ due to (H1) and $\boldsymbol{L}^2(\Omega)\supset\boldsymbol{H}^{\mathrm{div}}(\Omega)$, it follows that $\boldsymbol{\nabla}\phi\in L^\infty(J;\boldsymbol{L}^2(\Omega))$. From $\phi\in L^\infty(J;L^2(\Omega))$ given, we consequently infer that $\phi\in L^\infty(J;H^1(\Omega))$. Owing to $\mathcal{D}(\Omega)\subset L^2(\Omega)$ dense (cf. Ern & Guermond 2004, Thm. B.14; Wu et al. 2006, Cor. 1.1.1), the variational equation

$$\forall\boldsymbol{v}\in\boldsymbol{L}^2(\Omega)\,,\quad \left(\mathbf{D}^{-1}\boldsymbol{E}(t)\,,\,\boldsymbol{v}\right) \;=\; -(\boldsymbol{\nabla}\phi(t)\,,\,\boldsymbol{v}) \tag{3.18}$$

holds. Next, we show that $\phi(t) = \phi_{\mathrm{D}}(t)$ for a. e. $t\in J$, which was demanded implicitly in Problem 3.17 by the constrained ansatz space $H^1_{\phi_{\mathrm{D}}}(\Omega)$ and explicitly in Problem 3.14 by

a boundary integral: using the fact that (3.18) also holds for $\boldsymbol{v} \in \boldsymbol{H}^{\mathrm{div}}(\Omega) \subset \boldsymbol{L}^2(\Omega)$ and application of Green's formula yields

$$\begin{aligned}\forall \boldsymbol{v} \in \boldsymbol{H}^{\mathrm{div}}(\Omega)\,, \quad \langle \boldsymbol{v}\cdot\boldsymbol{\nu}\,,\,\phi(t)\rangle_{H^{-1/2}(\partial\Omega),H^{1/2}(\partial\Omega)} &\overset{(3.4)}{=} (\phi(t)\,,\,\nabla\cdot\boldsymbol{v}) + (\nabla\phi(t)\,,\,\boldsymbol{v}) \\ &\overset{(3.18)}{=} (\phi(t)\,,\,\nabla\cdot\boldsymbol{v}) - \left(\mathbf{D}^{-1}\boldsymbol{E}(t)\,,\,\boldsymbol{v}\right) \overset{(3.14e)}{=} \langle \boldsymbol{v}\cdot\boldsymbol{\nu}\,,\,\phi_{\mathrm{D}}(t)\rangle_{H^{-1/2}(\partial\Omega),H^{1/2}(\partial\Omega)}\,.\end{aligned}$$

In order to prove that $\phi(t)$ is also in $H^2(\Omega)$, we test (3.14f) with $w \in \mathcal{D}(\Omega) \subset L^2(\Omega)$:

$$\begin{aligned}\forall w \in \mathcal{D}(\Omega)\,, \quad (c^+(t) - c^-(t) + \bar{\sigma}(t)\,,\,w) &\overset{(3.14f)}{=} (\nabla\cdot\boldsymbol{E}(t)\,,\,w) \\ &= -(\boldsymbol{E}(t)\,,\,\nabla w) \overset{(3.18)}{=} (\mathbf{D}\nabla\phi(t)\,,\,\nabla w) \;=\; -\langle \nabla\cdot\mathbf{D}\nabla\phi(t)\,,\,w\rangle_{\mathcal{D}'(\Omega),\mathcal{D}(\Omega)}\,,\end{aligned}$$

which shows that the distributional divergence of $\mathbf{D}\nabla\phi(t)$ is a function. Because $c^\pm$ and $\bar{\sigma}$ are element of $L^\infty(J;L^2(\Omega)) \supset L^\infty(J\times\Omega)$ from assumption and due to (H6), respectively, we conclude—taking the previous considerations into account—that $\phi \in L^\infty(H^2(\Omega)\cap H^1_{\phi_{\mathrm{D}}}(\Omega))$. Thus $\phi(t)$ is a partial solution of (3.15d) for a. e. $t \in J$.

With (3.18) and owing to $c^\pm \in L^\infty(J\times\Omega)$, the mixed variational subsystems {(3.15a), (3.15b)} and {(3.14a), (3.14b)} coincide. Hence, $(\boldsymbol{u}(t), p(t)) \in \boldsymbol{H}^{\mathrm{div}}_0(\Omega) \times L^2(\Omega)/\mathbb{R}$ is also a partial solution of {(3.15a), (3.15b)}.

It remains to show that $c^\pm(t)$ are partial solutions of the non-mixed variational equation (3.15c). We test (3.14c) with $\boldsymbol{v} \in \mathcal{D}(\Omega)^d \subset \boldsymbol{H}^{\mathrm{div}}(\Omega)$:

$$\begin{aligned}\forall \boldsymbol{v} \in \mathcal{D}(\Omega)^d\,, \quad \left(\mathbf{D}^{-1}\left(\boldsymbol{j}^\pm(t) - (\boldsymbol{u}(t)\pm\boldsymbol{E}(t))c^\pm(t)\right),\boldsymbol{v}\right) &\overset{(3.14c)}{=} (c^\pm(t)\,,\,\nabla\cdot\boldsymbol{v}) \\ &= -\langle \nabla c^\pm(t)\,,\,\boldsymbol{v}\rangle_{\mathcal{D}'(\Omega)^d,\mathcal{D}(\Omega)^d}\,, \quad (3.19)\end{aligned}$$

i. e., $\nabla c^\pm(t)$ in the distributional sense is a function. Using the Minkowski and the Hölder inequalities, we obtain

$$\begin{aligned}&\left\|\mathbf{D}^{-1}\left(\boldsymbol{j}^\pm(t) - (\boldsymbol{u}(t)\pm\boldsymbol{E}(t))c^\pm(t)\right)\right\|_{\boldsymbol{L}^2(\Omega)} \\ &\qquad \overset{(H1)}{\leq} \|\mathbf{D}^{-1}\|_{\mathbf{L}^\infty(\Omega)}\left(\|\boldsymbol{j}^\pm(t)\|_{\boldsymbol{L}^2(\Omega)} + \|\boldsymbol{u}(t)\pm\boldsymbol{E}(t)\|_{\boldsymbol{L}^2(\Omega)}\|c^\pm(t)\|_{L^\infty(\Omega)}\right) \;<\; \infty\,.\end{aligned}$$

Hence, $\nabla c^\pm(t) \in \boldsymbol{L}^2(\Omega)$ and thus $c^\pm(t) \in H^1(\Omega)$ for a. e. $t \in J$. In particular, (3.19) also holds in the $\boldsymbol{L}^2(\Omega)$ sense. With this result, $c^\pm \in L^2(J;H^1(\Omega))$ is easily shown:

$$\|c^\pm\|^2_{L^2(J;H^1(\Omega))} \;=\; \int_J \|c^\pm(s)\|^2_{H^1(\Omega)}\,\mathrm{d}s \;=\; \|c^\pm\|^2_{L^2(J\times\Omega)} + \int_J \|\nabla c^\pm(s)\|^2_{\boldsymbol{L}^2(\Omega)}\,\mathrm{d}s$$

$$
\begin{aligned}
&\overset{(3.19)}{=} \|c^{\pm}\|^2_{L^2(J\times\Omega)} + \int_J \left\| \mathbf{D}^{-1}\Big(\boldsymbol{j}^{\pm}(s) - (\boldsymbol{u}(s) \pm \boldsymbol{E}(s))c^{\pm}(s) \Big) \right\|^2_{\boldsymbol{L}^2(\Omega)} \mathrm{d}s \\
&\leq \|c^{\pm}\|^2_{L^2(J\times\Omega)} + \|\mathbf{D}^{-1}\|^2_{\mathbf{L}^\infty(\Omega)} \|\boldsymbol{j}^{\pm} - (\boldsymbol{u} \pm \boldsymbol{E})c^{\pm}\|^2_{\boldsymbol{L}^2(J\times\Omega)} \\
&\leq \|c^{\pm}\|^2_{L^2(J\times\Omega)} + 2\|\mathbf{D}^{-1}\|^2_{\mathbf{L}^\infty(\Omega)} \Big(\|\boldsymbol{j}^{\pm}\|^2_{\boldsymbol{L}^2(J\times\Omega)} + \|\boldsymbol{u} \pm \boldsymbol{E}\|^2_{\boldsymbol{L}^2(J\times\Omega)} \|c^{\pm}(t)\|^2_{L^\infty(J\times\Omega)} \Big) \\
&< \infty \,,
\end{aligned}
$$

where, inter alia, the discrete Jensen inequality was used. Equation (3.14c) also holds for $\boldsymbol{v} \in \mathcal{D}(\Omega)^d \subset \boldsymbol{H}^{\mathrm{div}}_0(\Omega)$. We test (3.14c) with $\boldsymbol{v} = \mathbf{D}^{\mathrm{T}}\boldsymbol{\nabla} w$, where $w \in \mathcal{D}(\Omega)$, use (H1), and apply Green's formula to the first and the second term:

$$
\forall w \in \mathcal{D}(\Omega) \,, \quad (\boldsymbol{\nabla} \cdot \boldsymbol{j}^{\pm}(t) \,,\, w) \;=\; (\mathbf{D}\boldsymbol{\nabla} c^{\pm}(t) \,,\, \boldsymbol{\nabla} w) - ((\boldsymbol{u}(t) \pm \boldsymbol{E}(t))c^{\pm}(t) \,,\, \boldsymbol{\nabla} w) \,. \tag{3.20}
$$

Note that the second scalar product is meaningful due to the above shown regularity. Since $\mathcal{D}(\Omega) \subset L^2(\Omega)$, we may substitute (3.20) into (3.14d):

$$
\begin{aligned}
\forall w \in \mathcal{D}(\Omega) \,, \quad (\partial_t c^{\pm}(t) \,,\, w) + (\mathbf{D}\boldsymbol{\nabla} c^{\pm}(t) \,,\, \boldsymbol{\nabla} w) - ((\boldsymbol{u}(t) \pm \boldsymbol{E}(t))c^{\pm}(t) \,,\, \boldsymbol{\nabla} w) \\
= \; (r^{\pm}(c^+(t), c^-(t)) \,,\, w)
\end{aligned} \tag{3.21}
$$

for a. e. $t \in J$. Since $\mathcal{D}(\Omega) \subset H^1_0(\Omega)$ dense with respect to $\|\cdot\|_{H^1(\Omega)}$ (Evans 2010, Sec. 5.2.2), (3.21) also holds for $w \in H^1_0(\Omega)$. Using that $\boldsymbol{E}(t) = -\mathbf{D}\boldsymbol{\nabla}\phi(t)$ holds in $\boldsymbol{L}^2(\Omega)$ for a. e. $t \in J$, as shown above, and noting that

$$
\forall w \in H^1_0(\Omega) \,, \quad (\partial_t c^{\pm}(t) \,,\, w) \;=\; \langle \partial_t c^{\pm}(t) \,,\, w \rangle_{H^{-1}(\Omega), H^1_0(\Omega)} \,,
$$

since $\partial_t c^{\pm}(t) \in L^2(\Omega)$ by the definition of Problem 3.14 and $(H^1_0(\Omega), L^2(\Omega), H^{-1}(\Omega))$ is a Gelfand triple, it follows that the partial solutions $c^{\pm}(t)$ of Problem 3.14 solve the non-mixed variational equation (3.15c) of Problem 3.17. □

From Proposition 3.19 it follows immediately the following corollary:

Corollary 3.20. *Theorem 3.18 also holds true for the solution* $(\boldsymbol{u}, p, \boldsymbol{j}^+, c^+, \boldsymbol{j}^-, c^-, \boldsymbol{E}, \phi)$ *of Problem 3.14.*

We continue with the formulation of the fully discrete problem. Recall (3.12)—the definition of the backward difference quotient. We assume that the (stationary) upscaled coefficients, namely $\mathbf{D}$, $\mathbf{K}$, and $\bar{\sigma}$ are sufficiently precisely precomputed such that a discretization error in

these coefficients is negligible. The discrete boundary data $\phi_{\mathrm{D},h}^n$ is considered to be a "good approximation" of $\phi_{\mathrm{D}}(t_n)$.

Owing to Corollary 3.20, the use of the cut-off operator $\mathcal{M}$ according to Definition 3.15 is now admissible for the definition of the *fully discrete weak problem*:

Problem 3.21 (Mixed weak discrete DNPP problem). *Let $c_h^{\pm,0} := P_h^k c^{\pm,0}$. For $n \in \{1, \dots, N\}$, seek $(\boldsymbol{u}_h^n, p_h^n, \boldsymbol{j}_h^{+,n}, c_h^{+,n}, \boldsymbol{j}_h^{-,n}, c_h^{-,n}, \boldsymbol{E}_h^n, \phi_h^n) \in (\mathbb{RT}_k(\mathcal{T}_h) \times \mathbb{P}_k(\mathcal{T}_h))^4$ such that*

$$\forall \boldsymbol{v}_h \in \mathbb{RT}_k(\mathcal{T}_h), \quad -\left(\mathbf{K}^{-1}\boldsymbol{u}_h^n, \boldsymbol{v}_h\right) + \left(\boldsymbol{\nabla}\cdot\boldsymbol{v}_h, p_h^n\right) = -\left(\mathbf{D}^{-1}\boldsymbol{E}_h^n\, \mathcal{M}(c_h^{+,n} - c_h^{-,n}), \boldsymbol{v}_h\right), \tag{3.22a}$$

$$\forall w_h \in \mathbb{P}_k(\mathcal{T}_h), \quad \left(\boldsymbol{\nabla}\cdot\boldsymbol{u}_h^n, w_h\right) = 0, \tag{3.22b}$$

$$\forall \boldsymbol{v}_h \in \mathbb{RT}_k(\mathcal{T}_h), -\left(\mathbf{D}^{-1}\boldsymbol{j}_h^{\pm,n}, \boldsymbol{v}_h\right) + \left(\boldsymbol{\nabla}\cdot\boldsymbol{v}_h, c_h^{\pm,n}\right) + \left(\mathbf{D}^{-1}(\boldsymbol{u}_h^n \pm \boldsymbol{E}_h^n)\mathcal{M}(c_h^{\pm,n}), \boldsymbol{v}_h\right) = 0, \tag{3.22c}$$

$$\forall w_h \in \mathbb{P}_k(\mathcal{T}_h), \quad \left(\overline{\partial} c_h^{\pm,n}, w_h\right) + \left(\boldsymbol{\nabla}\cdot\boldsymbol{j}_h^{\pm,n}, w_h\right) = \left(r^{\pm}(c_h^{+,n}, c_h^{-,n}), w_h\right), \tag{3.22d}$$

$$\forall \boldsymbol{v}_h \in \mathbb{RT}_k(\mathcal{T}_h), \quad -\left(\mathbf{D}^{-1}\boldsymbol{E}_h^n, \boldsymbol{v}_h\right) + \left(\boldsymbol{\nabla}\cdot\boldsymbol{v}_h, \phi_h^n\right) = \left(\boldsymbol{v}_h\cdot\boldsymbol{\nu}, \phi_{\mathrm{D},h}^n\right)_{L^2(\partial\Omega)}, \tag{3.22e}$$

$$\forall w_h \in \mathbb{P}_k(\mathcal{T}_h), \quad \left(\boldsymbol{\nabla}\cdot\boldsymbol{E}_h^n, w_h\right) = \left(c_h^{+,n} - c_h^{-,n} + \bar{\sigma}, w_h\right), \tag{3.22f}$$

where the cut-off level M for the cut-off operator $\mathcal{M}$ is chosen equal to the right-hand side of (3.16) *in Theorem 3.18* (iii).

The cutting off of the terms in {(3.22a), (3.22c)} is necessary here in order to bound the respective scalar products uniformly in h. Note that it would also be possible to cut off the fluxes $\boldsymbol{u}_h^n$ and $\boldsymbol{E}_h^n$. However, we could not access analytical results that provide $\boldsymbol{L}^\infty$ a priori estimates for $\boldsymbol{u}$ or $\boldsymbol{E}$.

In the context of a priori error analysis it is admissible to make further assumptions on the regularity of the true solution that is to be approximated.

Hypotheses 3.22 (Hypotheses on the true solution and on the initial data).
Let $l_1, \dots, l_6 \in \{1, \dots, k+1\}$ be fixed integers (k as in Prob. 3.21).

(H7) *For the partial true solution $(\boldsymbol{u}, p)$ it additionally holds that*
$\boldsymbol{u} \in L^2(J; \boldsymbol{L}^\infty(\Omega)) \cap H^1(J; \boldsymbol{H}^{l_1}(\Omega))$, $p \in H^1(J; H^{l_2}(\Omega))$.

(H8) *For the partial true solutions $(\boldsymbol{j}^{\pm}, c^{\pm})$ it additionally holds that*
$\boldsymbol{j}^{\pm} \in H^1(J; \boldsymbol{H}^{l_3}(\Omega))$, $c^{\pm} \in H^2(J; L^2(\Omega)) \cap H^1(J; H^{l_4}(\Omega))$.

(H9) *For the partial true solution $(\boldsymbol{E}, \phi)$ it additionally holds that*
$\boldsymbol{E} \in L^2(J; \boldsymbol{L}^\infty(\Omega)) \cap H^1(J; \boldsymbol{H}^{l_5,\mathrm{div}}(\Omega))$, $\phi \in H^1(J; H^{l_6}(\Omega))$.

(H10) *For the initial data $c^{\pm,0}$ it additionally holds that $c^{\pm,0} \in H^{l_4}(\Omega)$.*

Proposition 3.23. *Let $(\boldsymbol{E}, \phi, c^+, c^-)$ and $(\boldsymbol{E}_h^n, \phi_h^n, c_h^+, c_h^-)$ be partial solutions of Problem 3.14 and Problem 3.21, respectively. Then, if in addition the regularity requirements of* (H9) *are satisfied, there exist constants $C > 0$ independent of h such that for $n \in \{1, \dots, N\}$,*

$$\|\boldsymbol{\nabla} \cdot (\boldsymbol{E}_h^n - \boldsymbol{E}(t_n))\|_{L^2(\Omega)}^2 \;\le\; C\left(h^{2l_5}\,|\boldsymbol{\nabla} \cdot \boldsymbol{E}(t_n)|_{H^{l_5}(\Omega)}^2 + \sum_{i\in\{+,-\}} \|c_h^{i,n} - c^i(t_n)\|_{L^2(\Omega)}^2\right), \tag{3.23a}$$

$$\begin{aligned}\|\boldsymbol{E}_h^n - \boldsymbol{E}(t_n)\|_{\boldsymbol{L}^2(\Omega)}^2 + \|\phi_h^n - \phi(t_n)\|_{L^2(\Omega)}^2 \;\le\; C\Big(&h^{2l_5}|\boldsymbol{E}(t_n)|_{\boldsymbol{H}^{l_5,\mathrm{div}}(\Omega)}^2 + h^{2l_6}|\phi(t_n)|_{H^{l_6}(\Omega)}^2 \\ &+ \sum_{i\in\{+,-\}} \|c_h^{i,n} - c^i(t_n)\|_{L^2(\Omega)}^2 + \|\phi_{\mathrm{D},h}^n - \phi_{\mathrm{D}}(t_n)\|_{H^{1/2}(\partial\Omega)}^2\Big).\end{aligned} \tag{3.23b}$$

Proof. Since we deal with a fixed time level here, we suppress the time index n and the argument for the evaluation at t_n. We write $\boldsymbol{E}_h$ instead of $\boldsymbol{E}_h^n$, and $\boldsymbol{E}$ instead of $\boldsymbol{E}(t_n)$ etc. for the sake of presentation.

We start with the proof of (3.23a). Subtraction of {(3.14e), (3.14f)} from {(3.22e), (3.22f)} yields the error equations

$$-\left(\mathbf{D}^{-1}(\boldsymbol{E}_h - \boldsymbol{E})\,,\,\boldsymbol{v}_h\right) + (\boldsymbol{\nabla}\cdot\boldsymbol{v}_h\,,\,\phi_h - \phi) \;=\; \langle \boldsymbol{v}_h\cdot\boldsymbol{\nu}\,,\,\phi_{\mathrm{D},h} - \phi_{\mathrm{D}}\rangle_{H^{-1/2}(\partial\Omega),H^{1/2}(\partial\Omega)}\,, \tag{3.24a}$$

$$(\boldsymbol{\nabla}\cdot(\boldsymbol{E}_h - \boldsymbol{E})\,,\,w_h) \;=\; (c_h^+ - c^+\,,\,w_h) - (c_h^- - c^-\,,\,w_h) \tag{3.24b}$$

for all $\boldsymbol{v}_h \in \mathbb{RT}_k(\mathcal{T}_h)$ and for all $w_h \in \mathbb{P}_k(\mathcal{T}_h)$. We choose $w_h = P_h^k(\boldsymbol{\nabla}\cdot(\boldsymbol{E}_h - \boldsymbol{E})) \overset{\text{Lem. 3.8}}{=} \boldsymbol{\nabla}\cdot\boldsymbol{\Pi}_h^k(\boldsymbol{E}_h - \boldsymbol{E}) \in \mathbb{P}_k(\mathcal{T}_h)$ in (3.24b) and use the identity $\boldsymbol{\nabla}\cdot(\boldsymbol{E}_h - \boldsymbol{E}) = \boldsymbol{\nabla}\cdot\boldsymbol{\Pi}_h^k(\boldsymbol{E}_h - \boldsymbol{E}) + \boldsymbol{\nabla}\cdot(\boldsymbol{\Pi}_h^k - \boldsymbol{I})\boldsymbol{E}$ to see that

$$\begin{aligned}&\left(\boldsymbol{\nabla}\cdot(\boldsymbol{E}_h - \boldsymbol{E})\,,\,\boldsymbol{\nabla}\cdot\boldsymbol{\Pi}_h^k(\boldsymbol{E}_h - \boldsymbol{E})\right) \;=\; \left(c_h^+ - c^+\,,\,\boldsymbol{\nabla}\cdot\boldsymbol{\Pi}_h^k(\boldsymbol{E}_h - \boldsymbol{E})\right) - \left(c_h^- - c^-\,,\,\boldsymbol{\nabla}\cdot\boldsymbol{\Pi}_h^k(\boldsymbol{E}_h - \boldsymbol{E})\right) \\ &\Leftrightarrow\; \|\boldsymbol{\nabla}\cdot(\boldsymbol{E}_h - \boldsymbol{E})\|^2 \;=\; \left(\boldsymbol{\nabla}\cdot(\boldsymbol{E}_h - \boldsymbol{E})\,,\,\boldsymbol{\nabla}\cdot(\boldsymbol{\Pi}_h^k - \boldsymbol{I})\boldsymbol{E}\right) + (\boldsymbol{\nabla}\cdot(\boldsymbol{E}_h - \boldsymbol{E})\,,\,c_h^+ - c^+) \\ &\qquad - (\boldsymbol{\nabla}\cdot(\boldsymbol{E}_h - \boldsymbol{E})\,,\,c_h^- - c^-) - \left(\boldsymbol{\nabla}\cdot(\boldsymbol{\Pi}_h^k - \boldsymbol{I})\boldsymbol{E}\,,\,c_h^+ - c^+\right) + \left(\boldsymbol{\nabla}\cdot(\boldsymbol{\Pi}_h^k - \boldsymbol{I})\boldsymbol{E}\,,\,c_h^- - c^-\right).\end{aligned}$$

Denoting the terms by I to V, we infer from the inequalities of Cauchy–Schwarz and of Young that

$$\begin{aligned}&I \le \frac{\delta}{2}\|\boldsymbol{\nabla}\cdot(\boldsymbol{E}_h - \boldsymbol{E})\|^2 + \frac{1}{2\delta}\|\boldsymbol{\nabla}\cdot(\boldsymbol{\Pi}_h^k - \boldsymbol{I})\boldsymbol{E}\|^2\,, \quad II \le \frac{\delta}{2}\|\boldsymbol{\nabla}\cdot(\boldsymbol{E}_h - \boldsymbol{E})\|^2 + \frac{1}{2\delta}\|c_h^+ - c^+\|^2\,, \\ &|III| \le \frac{\delta}{2}\|\boldsymbol{\nabla}\cdot(\boldsymbol{E}_h - \boldsymbol{E})\|^2 + \frac{1}{2\delta}\|c_h^- - c^-\|^2\,, \qquad |IV| \le \frac{\delta'}{2}\|\boldsymbol{\nabla}\cdot(\boldsymbol{\Pi}_h^k - \boldsymbol{I})\boldsymbol{E}\|^2 + \frac{1}{2\delta'}\|c_h^+ - c^+\|^2\,, \\ &V \le \frac{\delta'}{2}\|\boldsymbol{\nabla}\cdot(\boldsymbol{\Pi}_h^k - \boldsymbol{I})\boldsymbol{E}\|^2 + \frac{1}{2\delta'}\|c_h^- - c^-\|^2\end{aligned}$$

for all $\delta, \delta' > 0$. Hence, we obtain the estimate

$$\left(1 - \frac{3}{2}\delta\right)\|\boldsymbol{\nabla} \cdot (\boldsymbol{E}_h - \boldsymbol{E})\|^2 \;\leq\; \left(\frac{1}{2\delta} + \delta'\right)\|\boldsymbol{\nabla} \cdot (\boldsymbol{\Pi}_h^k - \boldsymbol{I})\boldsymbol{E}\|^2 + \left(\frac{1}{2\delta} + \frac{1}{2\delta'}\right)\sum_{i\in\{+,-\}} \|c_h^i - c^i\|^2$$

with the constraint that $0 < \delta < 2/3$. Using the projection error estimate of Lemma 3.10 it follows (3.23a).

We continue with the proof of (3.23b). With the projector properties (3.9) and (3.11), the error equations (3.24) can be written as

$$\begin{aligned} -\left(\mathbf{D}^{-1}(\boldsymbol{E}_h - \boldsymbol{E})\,,\, \boldsymbol{v}_h\right) + \left(\boldsymbol{\nabla} \cdot \boldsymbol{v}_h\,,\, P_h^k(\phi_h - \phi)\right) \;&=\; \langle \boldsymbol{v}_h \cdot \boldsymbol{\nu}\,,\, \phi_{\mathrm{D},h} - \phi_{\mathrm{D}}\rangle_{H^{-1/2}(\partial\Omega),H^{1/2}(\partial\Omega)}\,, \\ \left(\boldsymbol{\nabla} \cdot \boldsymbol{\Pi}_h^k(\boldsymbol{E}_h - \boldsymbol{E})\,,\, w_h\right) \;&=\; (c_h^+ - c^+\,,\, w_h) - (c_h^- - c^-\,,\, w_h) \end{aligned}$$

for all $\boldsymbol{v}_h \in \mathbb{RT}_k(\mathcal{T}_h)$ and for all $w_h \in \mathbb{P}_k(\mathcal{T}_h)$. Choose $\boldsymbol{v}_h = \boldsymbol{\Pi}_h^k(\boldsymbol{E}_h - \boldsymbol{E}) \in \mathbb{RT}_k(\mathcal{T}_h)$ and $w_h = P_h^k(\phi_h - \phi) \in \mathbb{P}_k(\mathcal{T}_h)$ and subtract the resulting equations to obtain

$$\begin{aligned} \left(\mathbf{D}^{-1}(\boldsymbol{E}_h - \boldsymbol{E})\,,\, \boldsymbol{\Pi}_h^k(\boldsymbol{E}_h - \boldsymbol{E})\right) \;=\; &\left(c_h^+ - c^+\,,\, P_h^k(\phi_h - \phi)\right) - \left(c_h^- - c^-\,,\, P_h^k(\phi_h - \phi)\right) \\ &- \left\langle \boldsymbol{\Pi}_h^k(\boldsymbol{E}_h - \boldsymbol{E}) \cdot \boldsymbol{\nu}\,,\, \phi_{\mathrm{D},h} - \phi_{\mathrm{D}}\right\rangle_{H^{-1/2}(\partial\Omega),H^{1/2}(\partial\Omega)}. \end{aligned}$$

The use of the identities $\boldsymbol{E}_h - \boldsymbol{E} = \boldsymbol{\Pi}_h^k(\boldsymbol{E}_h - \boldsymbol{E}) + (\boldsymbol{\Pi}_h^k - \boldsymbol{I})\boldsymbol{E}$ and $\phi_h - \phi = P_h^k(\phi_h - \phi) + (P_h^k - I)\phi$, the ellipticity of $\mathbf{D}^{-1}$ (cf. (H1)) yields

$$\begin{aligned} D_\alpha\|\boldsymbol{E}_h - \boldsymbol{E}\|^2 \;\leq\; &\left(\mathbf{D}^{-1}(\boldsymbol{E}_h - \boldsymbol{E})\,,\, (\boldsymbol{\Pi}_h^k - \boldsymbol{I})\boldsymbol{E}\right) + (\phi_h - \phi\,,\, c_h^+ - c^+) \\ &- \left((P_h^k - I)\phi\,,\, c_h^+ - c^+\right) - (\phi_h - \phi\,,\, c_h^- - c^-) + \left((P_h^k - I)\phi\,,\, c_h^- - c^-\right) \\ &- \langle(\boldsymbol{E}_h - \boldsymbol{E}) \cdot \boldsymbol{\nu}\,,\, \phi_{\mathrm{D},h} - \phi_{\mathrm{D}}\rangle_{H^{-1/2}(\partial\Omega),H^{1/2}(\partial\Omega)} + \left\langle(\boldsymbol{\Pi}_h^k - \boldsymbol{I})\boldsymbol{E} \cdot \boldsymbol{\nu}\,,\, \phi_{\mathrm{D},h} - \phi_{\mathrm{D}}\right\rangle_{H^{-1/2}(\partial\Omega),H^{1/2}(\partial\Omega)}. \end{aligned}$$

We estimate the terms on the right side, which are denoted by *I* to *VII*. Due to the boundedness of $\mathbf{D}^{-1}$ in $\mathbf{L}^\infty(\Omega)$ (cf. (H1)), it follows by the Hölder inequality that

$$\begin{aligned} I \;&\leq\; \frac{\delta}{2}D_\infty\|\boldsymbol{E}_h - \boldsymbol{E}\|^2 + \frac{1}{2\delta}D_\infty\|(\boldsymbol{\Pi}_h^k - \boldsymbol{I})\boldsymbol{E}\|^2\,, & \mathit{II} \;&\leq\; \frac{\delta}{2}\|\phi_h - \phi\|^2 + \frac{1}{2\delta}\|c_h^+ - c^+\|^2\,, \\ |\mathit{III}| \;&\leq\; \frac{\delta'}{2}\|(P_h^k - I)\phi\|^2 + \frac{1}{2\delta'}\|c_h^+ - c^+\|^2\,, & |\mathit{IV}| \;&\leq\; \frac{\delta}{2}\|\phi_h - \phi\|^2 + \frac{1}{2\delta}\|c_h^- - c^-\|^2\,, \\ V \;&\leq\; \frac{\delta'}{2}\|(P_h^k - I)\phi\|^2 + \frac{1}{2\delta'}\|c_h^- - c^-\|^2 \end{aligned}$$

for all $\delta, \delta' > 0$. We estimate the terms *VI* and *VII* by

$$\begin{aligned} |VI| &\leq \|(\boldsymbol{E}_h - \boldsymbol{E}) \cdot \boldsymbol{\nu}\|_{H^{-1/2}(\partial\Omega)} \|\phi_{\mathrm{D},h} - \phi_{\mathrm{D}}\|_{H^{1/2}(\partial\Omega)} \overset{(3.3)}{\leq} \|\boldsymbol{E}_h - \boldsymbol{E}\|_{\boldsymbol{H}^{\mathrm{div}}(\Omega)} \|\phi_{\mathrm{D},h} - \phi_{\mathrm{D}}\|_{H^{1/2}(\partial\Omega)} \\ &\leq \frac{\delta}{2} \|\boldsymbol{E}_h - \boldsymbol{E}\|^2_{\boldsymbol{H}^{\mathrm{div}}(\Omega)} + \frac{1}{2\delta} \|\phi_{\mathrm{D},h} - \phi_{\mathrm{D}}\|^2_{H^{1/2}(\partial\Omega)} \\ &= \frac{\delta}{2} \|\boldsymbol{E}_h - \boldsymbol{E}\|^2 + \frac{\delta}{2} \|\boldsymbol{\nabla} \cdot (\boldsymbol{E}_h - \boldsymbol{E})\|^2 + \frac{1}{2\delta} \|\phi_{\mathrm{D},h} - \phi_{\mathrm{D}}\|^2_{H^{1/2}(\partial\Omega)} , \end{aligned} \tag{3.25}$$

where the last identity holds due to the definition of the $\boldsymbol{H}^{\mathrm{div}}(\Omega)$ norm. Analogously,

$$VII \leq \frac{\delta'}{2} \|(\boldsymbol{\Pi}_h^k - \boldsymbol{I})\boldsymbol{E}\|^2 + \frac{\delta'}{2} \|\boldsymbol{\nabla} \cdot (\boldsymbol{\Pi}_h^k - \boldsymbol{I})\boldsymbol{E}\|^2 + \frac{1}{2\delta'} \|\phi_{\mathrm{D},h} - \phi_{\mathrm{D}}\|^2_{H^{1/2}(\partial\Omega)} .$$

Setting $\delta' := 1$ we recapitulatory obtain

$$\begin{aligned} 2D_\alpha \|\boldsymbol{E}_h - \boldsymbol{E}\|^2 \leq\ & \delta \|\boldsymbol{\nabla} \cdot (\boldsymbol{E}_h - \boldsymbol{E})\|^2 + \|\boldsymbol{\nabla} \cdot (\boldsymbol{\Pi}_h^k - \boldsymbol{I})\boldsymbol{E}\|^2 + \delta(D_\infty + 1) \|\boldsymbol{E}_h - \boldsymbol{E}\|^2 \\ &+ \left(\frac{1}{\delta} D_\infty + 1\right) \|(\boldsymbol{\Pi}_h^k - \boldsymbol{I})\boldsymbol{E}\|^2 + 2\delta \|\phi_h - \phi\|^2 + 2\|(P_h^k - I)\phi\|^2 \\ &+ \left(\frac{1}{\delta} + 1\right) \sum_{i \in \{+,-\}} \|c_h^i - c^i\|^2 + \left(\frac{1}{\delta} + 1\right) \|\phi_{\mathrm{D},h} - \phi_{\mathrm{D}}\|^2_{H^{1/2}(\partial\Omega)} \end{aligned} \tag{3.26}$$

with the constraint $0 < \delta < 2D_\alpha/(D_\infty + 1)$. Having the estimate (3.26) for $\|\boldsymbol{E}_h - \boldsymbol{E}\|$ at hand, an estimate for $\|\phi_h - \phi\|$ needs to be derived: according to Lemma 3.9, we may choose $\boldsymbol{v}_h \in \mathbb{RT}_k(\mathcal{T}_h)$ in (3.24a) such that $\boldsymbol{\nabla} \cdot \boldsymbol{v}_h = P_h^k(\phi_h - \phi) \in \mathbb{P}_k(\mathcal{T}_h)$:

$$\begin{aligned} \left(P_h^k(\phi_h - \phi)\,,\, \phi_h - \phi\right) &= (\boldsymbol{\nabla} \cdot \boldsymbol{v}_h\,,\, \phi_h - \phi) \\ &\overset{(3.24a)}{=} \left(\mathbf{D}^{-1}(\boldsymbol{E}_h - \boldsymbol{E})\,,\, \boldsymbol{v}_h\right) + \langle \boldsymbol{v}_h \cdot \boldsymbol{\nu}\,,\, \phi_{\mathrm{D},h} - \phi_{\mathrm{D}} \rangle_{H^{-1/2}(\partial\Omega), H^{1/2}(\partial\Omega)} . \end{aligned}$$

Using the identity $\phi_h - \phi = P_h^k(\phi_h - \phi) + (P_h^k - I)\phi$, we obtain

$$\|\phi_h - \phi\|^2 = \left(\mathbf{D}^{-1}(\boldsymbol{E}_h - \boldsymbol{E})\,,\, \boldsymbol{v}_h\right) + \langle \boldsymbol{v}_h \cdot \boldsymbol{\nu}\,,\, \phi_{\mathrm{D},h} - \phi_{\mathrm{D}} \rangle_{H^{-1/2}(\partial\Omega), H^{1/2}(\partial\Omega)} + \left((P_h^k - I)\phi\,,\, \phi_h - \phi\right)$$

and estimate the terms on the right side, which are denoted by *VIII*, *IX*, *X*. Since $\mathbf{D}^{-1}$ is bounded due to (H1),

$$VIII \leq \frac{1}{2\delta''} D_\infty \|\boldsymbol{E}_h - \boldsymbol{E}\|^2 + \frac{\delta''}{2} D_\infty \|\boldsymbol{v}_h\|^2$$

holds. Using $\|\boldsymbol{v}_h\| \leq \|\boldsymbol{v}_h\|_{\boldsymbol{H}^{\mathrm{div}}(\Omega)} \overset{\text{Lem. 3.9}}{\leq} C_\Omega \|P_h^k(\phi_h - \phi)\|$ and the Minkowski inequality together with $(a+b)^2 \leq 2a^2 + 2b^2$ (discrete Jensen), we arrive at

$$VIII \;\leq\; \frac{1}{2\delta''} D_\infty \|\boldsymbol{E}_h - \boldsymbol{E}\|^2 + \delta'' C_\Omega^2 D_\infty \|\phi_h - \phi\|^2 + \delta'' C_\Omega^2 D_\infty \|(P_h^k - I)\phi\|^2 \,.$$

We can treat the boundary term in IX as in (3.25):

$$IX \;\leq\; \frac{\delta''}{2} \|\boldsymbol{v}_h\|^2_{\boldsymbol{H}^{\mathrm{div}}(\Omega)} + \frac{1}{2\delta''} \|\phi_{\mathrm{D},h} - \phi_{\mathrm{D}}\|^2_{H^{1/2}(\partial\Omega)} \,.$$

Analogously to $VIII$, by estimating $\|\boldsymbol{v}_h\|^2_{\boldsymbol{H}^{\mathrm{div}}(\Omega)}$,

$$IX \;\leq\; \delta'' C_\Omega^2 \|\phi_h - \phi\|^2 + \delta'' C_\Omega^2 \|(P_h^k - I)\phi\|^2 + \frac{1}{2\delta''} \|\phi_{\mathrm{D},h} - \phi_{\mathrm{D}}\|^2_{H^{1/2}(\partial\Omega)}$$

holds. Eventually, we estimate X by

$$|X| \;\leq\; \frac{\delta''}{2} \|\phi_h - \phi\|^2 + \frac{1}{2\delta''} \|(P_h^k - I)\phi\|^2$$

and obtain in total

$$\begin{aligned}\Big(2 - \left(2C_\Omega^2(D_\infty + 1) + 1\right)\delta''\Big)\|\phi_h - \phi\|^2 \;\leq\; & \frac{1}{\delta''} D_\infty \|\boldsymbol{E}_h - \boldsymbol{E}\|^2 + \frac{1}{\delta''} \|\phi_{\mathrm{D},h} - \phi_{\mathrm{D}}\|^2_{H^{1/2}(\partial\Omega)} \\ & + \left(2\delta'' C_\Omega^2 (D_\infty + 1) + \frac{1}{\delta''}\right) \|(P_h^k - I)\phi\|^2 \end{aligned} \tag{3.27}$$

with the constraint $0 < \delta'' < 1/(C_\Omega^2(D_\infty + 1) + 1/2)$. By setting $\delta'' \coloneqq 1/C_1 \coloneqq 1/(2C_\Omega^2(D_\infty + 1) + 1)$ and substituting $\|\phi_h - \phi\|^2$ into (3.26), we obtain

$$\begin{aligned}&\Big(2D_\alpha - \delta(3D_\infty + 1 + 4C_\Omega^2 D_\infty (D_\infty + 1))\Big)\|\boldsymbol{E}_h - \boldsymbol{E}\|^2 \;\leq\; \delta \|\boldsymbol{\nabla} \cdot (\boldsymbol{E}_h - \boldsymbol{E})\|^2 \\ &\quad + \|\boldsymbol{\nabla} \cdot (\boldsymbol{\Pi}_h^k - \boldsymbol{I})\boldsymbol{E}\|^2 + \left(\frac{1}{\delta} D_\infty + 1\right) \|(\boldsymbol{\Pi}_h^k - \boldsymbol{I})\boldsymbol{E}\|^2 + 2\left(1 + \delta\Big(1 - \frac{1}{C_1} + C_1\Big)\right) \|(P_h^k - I)\phi\|^2 \\ &\qquad + \left(\frac{1}{\delta} + 1\right) \sum_{i \in \{+,-\}} \|c_h^i - c^i\|^2 + \left(\frac{1}{\delta} + 1 + 2\delta C_1\right) \|\phi_{\mathrm{D},h} - \phi_{\mathrm{D}}\|^2_{H^{1/2}(\partial\Omega)} \end{aligned} \tag{3.28}$$

with the constraint $0 < \delta < 2D_\alpha/(3D_\infty + 1 + 4C_\Omega^2 D_\infty(D_\infty + 1))$. Fixing δ, inserting the estimate (3.28) into (3.27), and summing up the resulting equation with (3.28) yields

$$\|\boldsymbol{E}_h - \boldsymbol{E}\|^2 + \|\phi_h - \phi\|^2 \;\leq\; C\Big(\|\boldsymbol{\nabla} \cdot (\boldsymbol{E}_h - \boldsymbol{E})\|^2 + \|\boldsymbol{\nabla} \cdot (\boldsymbol{\Pi}_h^k - \boldsymbol{I})\boldsymbol{E}\|^2 + \|(\boldsymbol{\Pi}_h^k - \boldsymbol{I})\boldsymbol{E}\|^2$$

$$+ \|(P_h^k - I)\phi\|^2 + \sum_{i\in\{+,-\}} \|c_h^i - c^i\|^2 + \|\phi_{\mathrm{D},h} - \phi_{\mathrm{D}}\|^2_{H^{1/2}(\partial\Omega)}\Big)$$

with a constant C depending on D_α, D_∞, and C_Ω. We conclude the inequality (3.23b) by using (3.23a), the projection error estimate of Lemma 3.10, and the definition of the $\boldsymbol{H}^{\mathrm{div}}(\Omega)$ seminorm. □

Although the estimate (3.23a) is no longer used in the analysis that follows, it was required in the proof for (3.23b), which will enter the proof for Theorem 3.26.

Proposition 3.24. *Let $(\boldsymbol{u}, p, \boldsymbol{j}^+, c^+, \boldsymbol{j}^-, c^-, \boldsymbol{E}, \phi)$ and $(\boldsymbol{u}_h^n, p_h^n, \boldsymbol{j}_h^{+,n}, c_h^{+,n}, \boldsymbol{j}_h^{-,n}, c_h^{-,n}, \boldsymbol{E}_h^n, \phi_h^n)$ be solutions of Problem 3.14 and Problem 3.21, respectively. Then, if in addition the regularity requirements of* (H8) *and* (H10) *are satisfied, there exists a constant $C > 0$ independent of h and τ such that for sufficiently small τ, for $n \in \{1, \dots, N\}$,*

$$\begin{aligned}
\|c_h^{\pm,n} - c^\pm(t_n)\|^2_{L^2(\Omega)} + \tau \sum_{m=1}^n \|\boldsymbol{j}_h^{\pm,m} - \boldsymbol{j}^\pm(t_m)\|^2_{\boldsymbol{L}^2(\Omega)} \;\le\; C\Bigg(&\tau^2 \|\partial_{tt} c^\pm\|^2_{L^2(]0,t_n[\times\Omega)} \\
&+ h^{2l_3}\tau \sum_{m=1}^n |\boldsymbol{j}^\pm(t_m)|^2_{\boldsymbol{H}^{l_3}(\Omega)} + h^{2l_4}\Big(|c^{\pm,0}|^2_{H^{l_4}(\Omega)} + \int_0^{t_n} |\partial_t c^\pm(s)|^2_{H^{l_4}(\Omega)}\,\mathrm{d}s + \tau \sum_{m=1}^n |c^\pm(t_m)|^2_{H^{l_4}(\Omega)}\Big) \\
&+ \tau \sum_{m=1}^n \Big(\|\boldsymbol{E}_h^m - \boldsymbol{E}(t_m)\|^2_{\boldsymbol{L}^2(\Omega)} + \|\boldsymbol{u}_h^m - \boldsymbol{u}(t_m)\|^2_{\boldsymbol{L}^2(\Omega)} + \|c_h^{\mp,m} - c^\mp(t_m)\|^2_{L^2(\Omega)}\Big)\Bigg). \quad (3.29)
\end{aligned}$$

Some ideas of the proof that follows stem from the work of F. A. Radu (Radu 2004; Radu & Wang 2011; Radu et al. 2010).

Proof (of Proposition 3.24). In this proof we abbreviate $c^\pm(t_n)$ by $c^{\pm,n}$ (and also analogously further quantities) keeping in mind that $c^\pm$ is a function existing everywhere in J. Subtraction of {(3.14c), (3.14d)} from {(3.22c), (3.22d)} yields the following error equations for $n \in \{1, \dots, N\}$:

$$\begin{aligned}
-\Big(\mathbf{D}^{-1}(\boldsymbol{j}_h^{\pm,n} - \boldsymbol{j}^{\pm,n})\,,\, \boldsymbol{v}_h\Big) + \Big(\boldsymbol{\nabla}\cdot\boldsymbol{v}_h\,,\, c_h^{\pm,n} - c^{\pm,n}\Big) \\
+ \Big(\mathbf{D}^{-1}((\boldsymbol{u}_h^n \pm \boldsymbol{E}_h^n)\mathcal{M}(c_h^{\pm,n}) - (\boldsymbol{u}^n \pm \boldsymbol{E}^n)c^{\pm,n})\,,\, \boldsymbol{v}_h\Big) \;=\; 0\,, \\
\Big(\overline{\partial} c_h^{\pm,n} - \partial_t c^{\pm,n}\,,\, w_h\Big) + \Big(\boldsymbol{\nabla}\cdot(\boldsymbol{j}_h^{\pm,n} - \boldsymbol{j}^{\pm,n})\,,\, w_h\Big) \;=\; \Big(r^\pm(c_h^{+,n}, c_h^{-,n}) - r^\pm(c^{+,n}, c^{-,n})\,,\, w_h\Big)
\end{aligned}$$

for all $\boldsymbol{v}_h \in \mathbb{RT}_k(\mathcal{T}_h)$ and for all $w_h \in \mathbb{P}_k(\mathcal{T}_h)$. We proceed analogously to the proof of (3.23b) in order to eliminate the divergence terms by using the projector properties {(3.9), (3.11)} and

choosing $\boldsymbol{v}_h = \boldsymbol{\Pi}_h^k(\boldsymbol{j}_h^{\pm,n} - \boldsymbol{j}^{\pm,n}) \in \mathbb{RT}_k(\mathcal{T}_h)$ and $w_h = P_h^k(c_h^{\pm,n} - c^{\pm,n}) \in \mathbb{P}_k(\mathcal{T}_h)$. The resulting equation reads

$$\begin{aligned}\left(\overline{\partial} c_h^{\pm,n} - \partial_t c^{\pm,n}\,,\, P_h^k(c_h^{\pm,n} - c^{\pm,n})\right) + \left(\mathbf{D}^{-1}(\boldsymbol{j}_h^{\pm,n} - \boldsymbol{j}^{\pm,n})\,,\, \boldsymbol{\Pi}_h^k(\boldsymbol{j}_h^{\pm,n} - \boldsymbol{j}^{\pm,n})\right)\\ = \left(\mathbf{D}^{-1}((\boldsymbol{u}_h^n \pm \boldsymbol{E}_h^n)\mathcal{M}(c_h^{\pm,n}) - (\boldsymbol{u}^n \pm \boldsymbol{E}^n)c^{\pm,n})\,,\, \boldsymbol{\Pi}_h^k(\boldsymbol{j}_h^{\pm,n} - \boldsymbol{j}^{\pm,n})\right)\\ + \left(r^{\pm}(c_h^{+,n}, c_h^{-,n}) - r^{\pm}(c^{+,n}, c^{-,n})\,,\, P_h^k(c_h^{\pm,n} - c^{\pm,n})\right). \quad (3.30)\end{aligned}$$

In the following, we make a frequent use of the identities

$$\boldsymbol{j}_h^{\pm,n} - \boldsymbol{j}^{\pm,n} = \boldsymbol{\Pi}_h^k(\boldsymbol{j}_h^{\pm,n} - \boldsymbol{j}^{\pm,n}) + (\boldsymbol{\Pi}_h^k - \boldsymbol{I})\boldsymbol{j}^{\pm,n}\,, \quad (3.31a)$$

$$c_h^{\pm,n} - c^{\pm,n} = P_h^k(c_h^{\pm,n} - c^{\pm,n}) + (P_h^k - I)c^{\pm,n}\,. \quad (3.31b)$$

Following the idea of Arbogast et al. (1996), we use the identity (3.31b), the projector property (3.8), and the fact that $\overline{\partial}$ commutes with P_h^k to decompose the time derivative term as follows:

$$\begin{aligned}\left(\overline{\partial} c_h^{\pm,n} - \partial_t c^{\pm,n}\,,\, P_h^k(c_h^{\pm,n} - c^{\pm,n})\right) &= \left(\overline{\partial}(c_h^{\pm,n} - c^{\pm,n})\,,\, c_h^{\pm,n} - c^{\pm,n}\right)\\ &\quad - \left(\overline{\partial}(P_h^k - I)c^{\pm,n}\,,\, c_h^{\pm,n} - c^{\pm,n}\right) + \left((\overline{\partial} - \partial_t)c^{\pm,n}\,,\, P_h^k(c_h^{\pm,n} - c^{\pm,n})\right).\end{aligned}$$

With this decomposition the combined error equation (3.30) becomes

$$\begin{aligned}&\left(\overline{\partial}(c_h^{\pm,n} - c^{\pm,n})\,,\, c_h^{\pm,n} - c^{\pm,n}\right) + D_\alpha\|\boldsymbol{j}_h^{\pm,n} - \boldsymbol{j}^{\pm,n}\|^2\\ &\quad\le \left(\overline{\partial}(P_h^k - I)c^{\pm,n}\,,\, c_h^{\pm,n} - c^{\pm,n}\right) - \left((\overline{\partial} - \partial_t)c^{\pm,n}\,,\, P_h^k(c_h^{\pm,n} - c^{\pm,n})\right)\\ &+\left(\mathbf{D}^{-1}(\boldsymbol{j}_h^{\pm,n} - \boldsymbol{j}^{\pm,n})\,,\, (\boldsymbol{\Pi}_h^k - \boldsymbol{I})\boldsymbol{j}^{\pm,n}\right) + \left(\mathbf{D}^{-1}((\boldsymbol{u}_h^n \pm \boldsymbol{E}_h^n)\mathcal{M}(c_h^{\pm,n}) - (\boldsymbol{u}^n \pm \boldsymbol{E}^n)c^{\pm,n})\,,\, \boldsymbol{\Pi}_h^k(\boldsymbol{j}_h^{\pm,n} - \boldsymbol{j}^{\pm,n})\right)\\ &\quad + \left(r^{\pm}(c_h^{+,n}, c_h^{-,n}) - r^{\pm}(c^{+,n}, c^{-,n})\,,\, P_h^k(c_h^{\pm,n} - c^{\pm,n})\right), \quad (3.32)\end{aligned}$$

where the identity (3.31a) and the ellipticity of $\mathbf{D}^{-1}$ due to (H1) was used. Next, consider the term $(\overline{\partial}(c_h^{\pm,n} - c^{\pm,n})\,,\, c_h^{\pm,n} - c^{\pm,n})$. Using the definition of $\overline{\partial}$ and the identity $2(a-b)a = a^2 - b^2 + (a-b)^2$, we see that if we replace n by m, for the sum from one to n multiplied by 2τ, there holds

$$2\tau\sum_{m=1}^{n}\left(\overline{\partial}(c_h^{\pm,m} - c^{\pm,m})\,,\, c_h^{\pm,m} - c^{\pm,m}\right) = 2\sum_{m=1}^{n}\left((c_h^{\pm,m} - c^{\pm,m}) - (c_h^{\pm,m-1} - c^{\pm,m-1})\,,\, c_h^{\pm,m} - c^{\pm,m}\right)$$

$$= \sum_{m=1}^{n} \left(\|c_h^{\pm,m} - c^{\pm,m}\|^2 - \|c_h^{\pm,m-1} - c^{\pm,m-1}\|^2 \right) + \sum_{m=1}^{n} \|(c_h^{\pm,m} - c^{\pm,m}) - (c_h^{\pm,m-1} - c^{\pm,m-1})\|^2$$

$$= \|c_h^{\pm,n} - c^{\pm,n}\|^2 - \|c_h^{\pm,0} - c^{\pm,0}\|^2 + \sum_{m=1}^{n} \|(c_h^{\pm,m} - c^{\pm,m}) - (c_h^{\pm,m-1} - c^{\pm,m-1})\|^2 \ .$$

We multiply (3.32) by 2τ, replace n by m, sum from one to n, and use the last result with the last term dropped, to obtain

$$\begin{aligned}
\|c_h^{\pm,n} - c^{\pm,n}\|^2 + 2D_\alpha \tau \sum_{m=1}^{n} \|\boldsymbol{j}_h^{\pm,m} - \boldsymbol{j}^{\pm,m}\|^2 \ \leq \ & \|c_h^{\pm,0} - c^{\pm,0}\|^2 \\
& + 2\tau \sum_{m=1}^{n} \left(\overline{\partial}(P_h^k - I)c^{\pm,m} \, , \, c_h^{\pm,m} - c^{\pm,m} \right) \\
& - 2\tau \sum_{m=1}^{n} \left((\overline{\partial} - \partial_t)c^{\pm,m} \, , \, P_h^k(c_h^{\pm,m} - c^{\pm,m}) \right) \\
& + 2\tau \sum_{m=1}^{n} \left(\mathbf{D}^{-1}(\boldsymbol{j}_h^{\pm,m} - \boldsymbol{j}^{\pm,m}) \, , \, (\boldsymbol{\Pi}_h^k - \boldsymbol{I})\boldsymbol{j}^{\pm,m} \right) \\
& + 2\tau \sum_{m=1}^{n} \left(\mathbf{D}^{-1}((\boldsymbol{u}_h^m \pm \boldsymbol{E}_h^m)\mathcal{M}(c_h^{\pm,m}) - (\boldsymbol{u}^m \pm \boldsymbol{E}^m)c^{\pm,m}) \, , \, \boldsymbol{\Pi}_h^k(\boldsymbol{j}_h^{\pm,m} - \boldsymbol{j}^{\pm,m}) \right) \\
& + 2\tau \sum_{m=1}^{n} \left(r^{\pm}(c_h^{+,m}, c_h^{-,m}) - r^{\pm}(c^{+,m}, c^{-,m}) \, , \, P_h^k(c_h^{\pm,m} - c^{\pm,m}) \right) . \qquad (3.33)
\end{aligned}$$

We denote the terms on the right side of (3.33) by *I* to *VI*. By definition of $c_h^{\pm,0}$ (cf. Prob. 3.21) we immediately obtain

$$I \ = \ \|(P_h^k - I)c^{\pm,0}\|^2 \ .$$

We continue by estimating *II* to *VI* in terms of time truncation and projection errors. With the Cauchy–Schwarz and the Young inequality we estimate the second term:

$$II \ \leq \ \delta_2 \tau \sum_{m=1}^{n} \|c_h^{\pm,m} - c^{\pm,m}\|^2 + \frac{1}{\delta_2} \tau \sum_{m=1}^{n} \|\overline{\partial}(P_h^k - I)c^{\pm,m}\|^2 \ .$$

We apply the Taylor identity (3.13a) and the Jensen inequality and use the fact that P_h^k commutes with time derivative and time integration:

$$\tau \sum_{m=1}^{n} \|\overline{\partial}(P_h^k - I)c^{\pm,m}\|^2 \ = \ \tau \sum_{m=1}^{n} \left\| \frac{1}{\tau} \int_{t_{m-1}}^{t_m} (P_h^k - I) \, \partial_t c^{\pm}(s) \, \mathrm{d}s \right\|^2$$

$$\leq \sum_{m=1}^{n} \int_{t_{m-1}}^{t_m} \|(P_h^k - I)\,\partial_t c^{\pm}(s)\|^2 \,\mathrm{d}s \;=\; \int_0^{t_n} \|(P_h^k - I)\,\partial_t c^{\pm}(s)\|^2 \,\mathrm{d}s$$

and thus, collectively,

$$I\!I \;\leq\; \delta_2 \tau \sum_{m=1}^{n} \|c_h^{\pm,m} - c^{\pm,m}\|^2 + \frac{1}{\delta_2} \|(P_h^k - I)\,\partial_t c^{\pm}\|^2_{L^2(]0,t_n[\times\Omega)} \,.$$

Analogously, for the third term we obtain

$$|I\!I\!I| \;\leq\; \delta_3 \tau \sum_{m=1}^{n} \|P_h^k(c_h^{\pm,m} - c^{\pm,m})\|^2 + \frac{1}{\delta_3} \tau \sum_{m=1}^{n} \|(\overline{\partial} - \partial_t) c^{\pm,m}\|^2 \,.$$

We apply the Taylor identity (3.13b) and the Jensen inequality to estimate the time truncation error term:

$$\begin{aligned}
\tau \sum_{m=1}^{n} \|(\overline{\partial} - \partial_t) c^{\pm,m}\|^2 \;&=\; \tau \sum_{m=1}^{n} \left\| \frac{1}{\tau} \int_{t_{m-1}}^{t_m} (s - t_{m-1})\,\partial_{tt} c^{\pm}(s) \,\mathrm{d}s \right\|^2 \\
&\leq \sum_{m=1}^{n} \int_{t_{m-1}}^{t_m} \|(s - t_{m-1})\,\partial_{tt} c^{\pm}(s)\|^2 \,\mathrm{d}s \\
&\leq\; \tau^2 \sum_{m=1}^{n} \int_{t_{m-1}}^{t_m} \|\partial_{tt} c^{\pm}(s)\|^2 \,\mathrm{d}s \;=\; \tau^2 \|\partial_{tt} c^{\pm}\|^2_{L^2(]0,t_n[\times\Omega)} \,.
\end{aligned}$$

With the Minkowski inequality together with $(a+b)^2 \leq 2a^2 + 2b^2$ (discrete Jensen) we eventually obtain

$$|I\!I\!I| \;\leq\; 2\delta_3 \tau \sum_{m=1}^{n} \|c_h^{\pm,m} - c^{\pm,m}\|^2 + 2\delta_3 \tau \sum_{m=1}^{n} \|(P_h^k - I) c^{\pm,m}\|^2 + \frac{1}{\delta_3} \tau^2 \|\partial_{tt} c^{\pm}\|^2_{L^2(]0,t_n[\times\Omega)} \,.$$

Proceeding as usual, the boundedness of $\mathbf{D}^{-1}$ due to (H1) immediately reveals

$$I\!V \;\leq\; \delta_4 D_\infty \tau \sum_{m=1}^{n} \|\boldsymbol{j}_h^{\pm,m} - \boldsymbol{j}^{\pm,m}\|^2 + \frac{1}{\delta_4} D_\infty \tau \sum_{m=1}^{n} \|(\boldsymbol{\Pi}_h^k - \boldsymbol{I})\boldsymbol{j}^{\pm,m}\|^2 \,.$$

We continue estimating the term V. We derive the following estimate using (H1), the boundedness of $\boldsymbol{u}^m$ and $\boldsymbol{E}^m$ in $\boldsymbol{L}^\infty(\Omega)$ due to (H7) and (H9), and Lem. 3.16:

$$\left\| \mathbf{D}^{-1}\big((\boldsymbol{u}_h^m \pm \boldsymbol{E}_h^m)\,\mathcal{M}(c_h^{\pm,m}) - (\boldsymbol{u}^m \pm \boldsymbol{E}^m) c^{\pm,m}\big) \right\|$$

$$\leq D_\infty\Big(\|(\boldsymbol{u}_h^m - \boldsymbol{u}^m)\mathcal{M}(c_h^{\pm,m}) \pm (\boldsymbol{E}_h^m - \boldsymbol{E}^m)\mathcal{M}(c_h^{\pm,m})\| + \|(\boldsymbol{u}^m \pm \boldsymbol{E}^m)(\mathcal{M}(c_h^{\pm,m}) - \mathcal{M}(c^{\pm,m}))\|\Big)$$
$$\leq D_\infty\Big(M\|\boldsymbol{u}_h^m - \boldsymbol{u}^m\| + M\|\boldsymbol{E}_h^m - \boldsymbol{E}^m\| + C_5\|c_h^{\pm,m} - c^{\pm,m}\|\Big)$$

with $C_5 \coloneqq \|\boldsymbol{u}^m \pm \boldsymbol{E}^m\|_{\boldsymbol{L}^\infty(\Omega)}$. The above estimate yields the estimate for the fifth term:

$$V \leq 2D_\infty\,\tau \sum_{m=1}^{n}\Bigg(\delta_5\Big(\|\boldsymbol{j}_h^{\pm,m} - \boldsymbol{j}^{\pm,m}\|^2 + \|(\boldsymbol{\Pi}_h^k - \boldsymbol{I})\boldsymbol{j}^{\pm,m}\|^2\Big)$$
$$+ \frac{1}{\delta_5}\Big(M^2\|\boldsymbol{u}_h^m - \boldsymbol{u}^m\|^2 + M^2\|\boldsymbol{E}_h^m - \boldsymbol{E}^m\|^2 + C_5^2\|c_h^{\pm,m} - c^{\pm,m}\|^2\Big)\Bigg).$$

Lastly, we estimate the sixth term *VI*. Due to the Lipschitz continuity of $r^\pm$ (cf. (H3)) the inequality

$$\|r^\pm(c_h^{+,m}, c_h^{-,m}) - r^\pm(c^{+,m}, c^{-,m})\| \leq r_\mathrm{L}\left\|\begin{pmatrix} c_h^{+,m} \\ c_h^{-,m}\end{pmatrix} - \begin{pmatrix} c^{+,m} \\ c^{-,m}\end{pmatrix}\right\| \leq r_\mathrm{L}\|c_h^{+,m} - c^{+,m}\| + r_\mathrm{L}\|c_h^{-,m} - c^{-,m}\|$$

holds, where r_L denotes the Lipschitz constant. The latter inequality holds due to the definition of the $\boldsymbol{L}^2(\Omega)$ norm (3.2). With the identity (3.31b) and the Cauchy–Schwarz inequality then follows

$$\Big(r^\pm(c_h^{+,m}, c_h^{-,m}) - r^\pm(c^{+,m}, c^{-,m}),\, P_h^k(c_h^{\pm,m} - c^{\pm,m})\Big)$$
$$\leq r_\mathrm{L}\Big(\|c_h^{+,m} - c^{+,m}\| + \|c_h^{-,m} - c^{-,m}\|\Big)\Big(\|(P_h^k - I)c^{\pm,m}\| + \|c_h^{\pm,m} - c^{\pm,m}\|\Big)$$
$$= r_\mathrm{L}\Big(\|c_h^{+,m} - c^{+,m}\|\,\|(P_h^k - I)c^{\pm,m}\| + \|c_h^{+,m} - c^{+,m}\|\,\|c_h^{\pm,m} - c^{\pm,m}\|$$
$$+ \|c_h^{-,m} - c^{-,m}\|\,\|(P_h^k - I)c^{\pm,m}\| + \|c_h^{-,m} - c^{-,m}\|\,\|c_h^{\pm,m} - c^{\pm,m}\|\Big).$$

Application of the Young inequality yields

$$VI \leq \Big(\frac{1}{\delta_6} + \delta_6\Big)2r_\mathrm{L}\,\tau\sum_{m=1}^{n}\|c_h^{\pm,m} - c^{\pm,m}\|^2 + \delta_6 2r_\mathrm{L}\,\tau\sum_{m=1}^{n}\|c_h^{\mp,m} - c^{\mp,m}\|^2$$
$$+ \frac{1}{\delta_6}2r_\mathrm{L}\,\tau\sum_{m=1}^{n}\|(P_h^k - I)c^{\pm,m}\|^2.$$

With the estimates of *II* to *VI*, it follows from (3.33) that

$$\|c_h^{\pm,n} - c^{\pm,n}\|^2 + \Big(2D_\alpha - \delta_4 D_\infty - 2\delta_5 D_\infty\Big)\tau\sum_{m=1}^{n}\|\boldsymbol{j}_h^{\pm,m} - \boldsymbol{j}^{\pm,m}\|^2$$

$$
\begin{aligned}
&\leq \|(P_h^k - I)c^{\pm,0}\|^2 + \frac{1}{\delta_2}\|(P_h^k - I)\,\partial_t c^{\pm}\|^2_{L^2(]0,t_n[\times\Omega)} + \frac{1}{\delta_3}\tau^2\|\partial_{tt}c^{\pm}\|^2_{L^2(]0,t_n[\times\Omega)} \\
&+ 2\Big(\frac{\delta_2}{2}+\delta_3+\frac{C_5^2}{\delta_5}D_\infty+r_{\mathrm{L}}(\delta_6+\frac{1}{\delta_6})\Big)\tau\sum_{m=1}^{n}\|c_h^{\pm,m} - c^{\pm,m}\|^2 + D_\infty\Big(\frac{1}{\delta_4}+2\delta_5\Big)\tau\sum_{m=1}^{n}\|(\boldsymbol{\Pi}_h^k - \boldsymbol{I})\boldsymbol{j}^{\pm,m}\|^2 \\
&+ 2(\delta_3 + \frac{r_{\mathrm{L}}}{\delta_6})\tau\sum_{m=1}^{n}\|(P_h^k - I)c^{\pm,m}\|^2 + \frac{2}{\delta_5}D_\infty M^2\,\tau\sum_{m=1}^{n}\|\boldsymbol{E}_h^m - \boldsymbol{E}^m\|^2 \\
&+ \frac{2}{\delta_5}D_\infty M^2\,\tau\sum_{m=1}^{n}\|\boldsymbol{u}_h^m - \boldsymbol{u}^m\|^2 + 2\delta_6 r_{\mathrm{L}}\tau\sum_{m=1}^{n}\|c_h^{\mp,m} - c^{\mp,m}\|^2
\end{aligned}
$$

with the constraint that $\delta_4, \delta_5 > 0$ have to be chosen small enough. The discretization error in $c^{\pm}$ at time level t_n on the right side can be absorbed for sufficiently small τ. In doing so, application of Lemma 3.3 (discrete Gronwall) yields

$$
\begin{aligned}
\|c_h^{\pm,n} - c^{\pm,n}\|^2 + \tau\sum_{m=1}^{n}\|\boldsymbol{j}_h^{\pm,m} - \boldsymbol{j}^{\pm,m}\|^2 \;\leq\; C\Bigg(&\|(P_h^k - I)c^{\pm,0}\|^2 + \|(P_h^k - I)\,\partial_t c^{\pm}\|^2_{L^2(]0,t_n[\times\Omega)} \\
&+ \tau^2\|\partial_{tt}c^{\pm}\|^2_{L^2(]0,t_n[\times\Omega)} + \tau\sum_{m=1}^{n}\|(\boldsymbol{\Pi}_h^k - \boldsymbol{I})\boldsymbol{j}^{\pm,m}\|^2 + \tau\sum_{m=1}^{n}\|(P_h^k - I)c^{\pm,m}\|^2 \\
&+ \tau\sum_{m=1}^{n}\|\boldsymbol{E}_h^m - \boldsymbol{E}^m\|^2 + \tau\sum_{m=1}^{n}\|\boldsymbol{u}_h^m - \boldsymbol{u}^m\|^2 + \tau\sum_{m=1}^{n}\|c_h^{\mp,m} - c^{\mp,m}\|^2\Bigg).
\end{aligned}
$$

Conclude by accounting for the initial conditions (3.1j) and by using the projection error estimates of Lemma 3.10. □

Proposition 3.25. *Let* $(\boldsymbol{u}, p, \boldsymbol{j}^+, c^+, \boldsymbol{j}^-, c^-, \boldsymbol{E}, \phi)$ *and* $(\boldsymbol{u}_h^n, p_h^n, \boldsymbol{j}_h^{+,n}, c_h^{+,n}, \boldsymbol{j}_h^{-,n}, c_h^{-,n}, \boldsymbol{E}_h^n, \phi_h^n)$ *be solutions of Problem 3.14 and Problem 3.21, respectively. Then, if in addition the regularity requirements of* (H7) *and* (H9) *are satisfied, there exist constants* $C > 0$ *independent of* h *such that for* $n \in \{1, \dots, N\}$,

$$
\begin{aligned}
\|\boldsymbol{u}_h^n - \boldsymbol{u}(t_n)\|^2_{\boldsymbol{L}^2(\Omega)} \;\leq\; C\Big(&h^{2l_1}|\boldsymbol{u}(t_n)|^2_{\boldsymbol{H}^{l_1}(\Omega)} + h^{2l_5}|\boldsymbol{E}(t_n)|^2_{\boldsymbol{H}^{l_5,\mathrm{div}}(\Omega)} + h^{2l_6}|\phi(t_n)|^2_{H^{l_6}(\Omega)} \\
&+ \sum_{i\in\{+,-\}}\|c_h^{i,n} - c^i(t_n)\|^2_{L^2(\Omega)} + \|\phi_{\mathrm{D},h}^n - \phi_{\mathrm{D}}(t_n)\|^2_{H^{1/2}(\partial\Omega)}\Big), \qquad (3.34a) \\
\|p_h^n - p(t_n)\|^2_{L^2(\Omega)} \;\leq\; C\Big(&h^{2l_1}|\boldsymbol{u}(t_n)|^2_{\boldsymbol{H}^{l_1}(\Omega)} + h^{2l_2}|p(t_n)|^2_{H^{l_2}(\Omega)} + h^{2l_5}|\boldsymbol{E}(t_n)|^2_{\boldsymbol{H}^{l_5,\mathrm{div}}(\Omega)} \\
&+ h^{2l_6}|\phi(t_n)|^2_{H^{l_6}(\Omega)} + \sum_{i\in\{+,-\}}\|c_h^{i,n} - c^i(t_n)\|^2_{L^2(\Omega)} + \|\phi_{\mathrm{D},h}^n - \phi_{\mathrm{D}}(t_n)\|^2_{H^{1/2}(\partial\Omega)}\Big). \qquad (3.34b)
\end{aligned}
$$

Proof. The proof can be accomplished analogously to that of Proposition 3.23 with minor modifications. Once again, we suppress the time index n and the argument for the evaluation at the time level t_n. Due to {(3.14a), (3.14b)}, {(3.22a), (3.22b)} the error equations read

$$-\Big(\mathbf{K}^{-1}(\boldsymbol{u}_h - \boldsymbol{u})\,,\,\boldsymbol{v}_h\Big) + (\boldsymbol{\nabla}\cdot\boldsymbol{v}_h\,,\,p_h - p) = -\Big(\mathbf{D}^{-1}(\boldsymbol{E}_h\mathcal{M}(c_h^+ - c_h^-) - \boldsymbol{E}(c^+ - c^-))\,,\,\boldsymbol{v}_h\Big)\,, \quad (3.35a)$$

$$(\boldsymbol{\nabla}\cdot(\boldsymbol{u}_h - \boldsymbol{u})\,,\,w_h) \;=\; 0 \quad (3.35b)$$

for all $\boldsymbol{v}_h \in \mathbb{RT}_k(\mathcal{T}_h)$ and for all $w_h \in \mathbb{P}_k(\mathcal{T}_h)$. The arising force term in (3.35a) requires a special treatment. Recalling the chosen cut-off level M for the cut-off operator $\mathcal{M}$ (cf. Prob. 3.21), Lemma 3.16, and (H9), we see that

$$\|\boldsymbol{E}_h\mathcal{M}(c_h^+ - c_h^-) - \boldsymbol{E}(c^+ - c^-)\| \;\le\; M\,\|\boldsymbol{E}_h - \boldsymbol{E}\| + \|\boldsymbol{E}\|_{\boldsymbol{L}^\infty(\Omega)}\sum_{i\in\{+,-\}}\|c_h^i - c^i\|\,. \quad (3.36)$$

The choice of $w_h = P_h^k(p_h - p) \in \mathbb{P}_k(\mathcal{T}_h)$ in (3.35b) and the projector property (3.9) yields

$$\Big(\boldsymbol{\nabla}\cdot\boldsymbol{\Pi}_h^k(\boldsymbol{u}_h - \boldsymbol{u})\,,\,P_h^k(p_h - p)\Big) \;=\; 0\,. \quad (3.37)$$

Choosing the test function $\boldsymbol{v}_h = \boldsymbol{\Pi}_h^k(\boldsymbol{u}_h - \boldsymbol{u}) \in \mathbb{RT}_k(\mathcal{T}_h)$ in (3.35a), using (3.11) and (3.37), we obtain

$$\Big(\mathbf{K}^{-1}(\boldsymbol{u}_h - \boldsymbol{u})\,,\,\boldsymbol{\Pi}_h^k(\boldsymbol{u}_h - \boldsymbol{u})\Big) \;=\; \Big(\mathbf{D}^{-1}(\boldsymbol{E}_h\mathcal{M}(c_h^+ - c_h^-) - \boldsymbol{E}(c^+ - c^-))\,,\,\boldsymbol{\Pi}_h^k(\boldsymbol{u}_h - \boldsymbol{u})\Big)\,.$$

With the identity $\boldsymbol{u}_h - \boldsymbol{u} = \boldsymbol{\Pi}_h^k(\boldsymbol{u}_h - \boldsymbol{u}) + (\boldsymbol{\Pi}_h^k - \boldsymbol{I})\boldsymbol{u}$, (H1), (H2), (3.36), and the Hölder inequality, we arrive at the estimate

$$\begin{aligned} K_\alpha\|\boldsymbol{u}_h - \boldsymbol{u}\|^2 \;\le\; & K_\infty\|\boldsymbol{u}_h - \boldsymbol{u}\|\,\|(\boldsymbol{\Pi}_h^k - \boldsymbol{I})\boldsymbol{u}\| \\ & + D_\infty\Big(M\,\|\boldsymbol{E}_h - \boldsymbol{E}\| + \|\boldsymbol{E}\|_{\boldsymbol{L}^\infty(\Omega)}\sum_{i\in\{+,-\}}\|c_h^i - c^i\|\Big)\Big(\|\boldsymbol{u}_h - \boldsymbol{u}\| + \|(\boldsymbol{\Pi}_h^k - \boldsymbol{I})\boldsymbol{u}\|\Big)\,. \end{aligned}$$

Application of Young's inequality, (3.23b), and the projection error estimates of Lemma 3.10 yields (3.34a).

With a similar treatment of the additional force term, the error estimate (3.34b) is obtained analogously to the second part of the proof of (3.23b). □

Theorem 3.26 (A priori error estimate). *Let* $(\boldsymbol{u}, p, \boldsymbol{j}^+, c^+, \boldsymbol{j}^-, c^-, \boldsymbol{E}, \phi)$ *and* $(\boldsymbol{u}_h^n, p_h^n, \boldsymbol{j}_h^{+,n}, c_h^{+,n}, \boldsymbol{j}_h^{-,n}, c_h^{-,n}, \boldsymbol{E}_h^n, \phi_h^n)$ *be solutions of Problem 3.14 and Problem 3.21, respectively. Then, if in addition the regularity requirements of* (H7)–(H10) *are satisfied, there exists a constant* $C > 0$ *independent of* h *and* τ *such that for sufficiently small* τ*,*

$$
\begin{aligned}
&\max_{m\in\{1,\dots,N\}} \|\boldsymbol{u}_h^m - \boldsymbol{u}(t_m)\|^2 + \max_{m\in\{1,\dots,N\}} \|p_h^m - p(t_m)\|^2 + \sum_{i\in\{+,-\}} \tau \sum_{m=1}^{N} \|\boldsymbol{j}_h^{i,m} - \boldsymbol{j}^i(t_m)\|^2 \\
&\quad + \sum_{i\in\{+,-\}} \max_{m\in\{1,\dots,N\}} \|c_h^{i,m} - c^i(t_n)\|^2 + \max_{m\in\{1,\dots,N\}} \|\boldsymbol{E}_h^m - \boldsymbol{E}(t_m)\|^2 + \max_{m\in\{1,\dots,N\}} \|\phi_h^m - \phi(t_m)\|^2 \\
&\le C\Bigg(\sum_{i\in\{+,-\}} \tau^2 \|\partial_{tt} c^i\|^2_{L^2(J\times\Omega)} + h^{2l_1} |\boldsymbol{u}(t_n)|^2_{\boldsymbol{H}^{l_1}(\Omega)} + h^{2l_2} |p(t_n)|^2_{H^{l_2}(\Omega)} \\
&\quad + h^{2l_3} \sum_{i\in\{+,-\}} |\boldsymbol{j}^i(t_m)|^2_{\boldsymbol{H}^{l_3}(\Omega)} + h^{2l_4} \sum_{i\in\{+,-\}} \Big(|c^{i,0}|^2_{H^{l_4}(\Omega)} + \int_J |\partial_t c^i(s)|^2_{H^{l_4}(\Omega)} \,\mathrm{d}s + |c^i(t_m)|^2_{H^{l_4}(\Omega)} \Big) \\
&\quad + h^{2l_5} |\boldsymbol{E}(t_n)|^2_{\boldsymbol{H}^{l_5,\mathrm{div}}(\Omega)} + h^{2l_6} |\phi(t_n)|^2_{H^{l_6}(\Omega)} + \max_{m\in\{1,\dots,N\}} \|\phi_{\mathrm{D},h}^m - \phi_{\mathrm{D}}(t_m)\|^2_{H^{1/2}(\partial\Omega)} \Bigg). \qquad (3.38)
\end{aligned}
$$

Proof. We sum up (3.29) for both signs, eliminate the discretization errors of $c^\pm$ on the right-hand side as performed at the end of the proof of Proposition 3.24, and call the resulting inequality (3.39). Substitution of $\sum_{i\in\{+,-\}} \|c_h^{i,n} - c^i(t_n)\|^2_{L^2(\Omega)}$ from (3.39) into {(3.23b), (3.34a), (3.34b)} and summation yields

$$
\begin{aligned}
&\|\boldsymbol{u}_h^n - \boldsymbol{u}(t_n)\|^2 + \|p_h^n - p(t_n)\|^2 + \|\boldsymbol{E}_h^n - \boldsymbol{E}(t_n)\|^2 + \|\phi_h^n - \phi(t_n)\|^2 \\
&\le C\Bigg(\tau^2 \sum_{i\in\{+,-\}} \|\partial_{tt} c^i\|^2_{L^2(]0,t_n[\times\Omega)} + h^{2l_1} |\boldsymbol{u}(t_n)|^2_{\boldsymbol{H}^{l_1}(\Omega)} + h^{2l_2} |p(t_n)|^2_{H^{l_2}(\Omega)} + h^{2l_3} \sum_{i\in\{+,-\}} \tau \sum_{m=1}^{n} |\boldsymbol{j}^i(t_m)|^2_{\boldsymbol{H}^{l_3}(\Omega)} \\
&\quad + h^{2l_4} \sum_{i\in\{+,-\}} \Big(|c^{i,0}|^2_{H^{l_4}(\Omega)} + \int_0^{t_n} |\partial_t c^i(s)|^2_{H^{l_4}(\Omega)} \,\mathrm{d}s + \tau \sum_{m=1}^{n} |c^i(t_m)|^2_{H^{l_4}(\Omega)} \Big) + h^{2l_5} |\boldsymbol{E}(t_n)|^2_{\boldsymbol{H}^{l_5,\mathrm{div}}(\Omega)} \\
&\quad + h^{2l_6} |\phi(t_n)|^2_{H^{l_6}(\Omega)} + \tau \sum_{m=1}^{n} \Big(\|\boldsymbol{u}_h^m - \boldsymbol{u}(t_m)\|^2 + \|\boldsymbol{E}_h^m - \boldsymbol{E}(t_m)\|^2 \Big) + \|\phi_{\mathrm{D},h}^n - \phi_{\mathrm{D}}(t_n)\|^2_{H^{1/2}(\partial\Omega)} \Bigg). \qquad (3.40)
\end{aligned}
$$

Adding (3.39) to (3.40) and eliminating the discretization errors of $\boldsymbol{u}$ and $\boldsymbol{E}$ on the right-hand side bounds the discretization errors of all partial unknowns in terms of the true solution and the data. We conclude by bounding the right-hand side by the respective maximum on J (admissible due to (H7)–(H10)) yielding a right-hand side that is independent of n such that the estimate holds for every $n \in \{1, \dots, N\}$. □

Chapter 4

Numerical Solution of the SNPP System and the DNPP Systems

This chapter presents a fully discrete numerical scheme capable of approximating the solutions of the SNPP system (cf. Prob. 2.1, p. 19) and its homogenization results—the DNPP systems (cf. Thms. 2.5 and 2.8, pages 23 and 25)—in two space dimensions.

In Section 4.1, we apply Rothe's method to the SNPP system, using the implicit Euler method to obtain a sequence of time-discrete, yet still coupled / nonlinear systems. The couplings between the subsystems for liquid flow, transport, and electric field are resolved by means of linearization schemes: either an iterative splitting approach or the Newton scheme. The application to the time-discrete SNPP system is demonstrated and their usability discussed. We proceed with an iterative splitting approach that is also applicable for the homogenized systems in an analogous way. At the end of this paragraph, publications that appeared in the last decade dealing with the numerical approximation of the SNPP system and related systems are reviewed.

The spatial discretization of the decoupled subsystems is performed in two space dimensions on unstructured grids. In particular, lowest order mixed finite elements according to Raviart and Thomas are used for the discretization of convection–diffusion equations in Section 4.2 and Taylor–Hood elements are used for the discretization of the Stokes equations in Section 4.3. Hereby, the flux unknowns, which are meaningful physical magnitudes, are computed directly and therefore numerical differentiation is avoided. These unknowns couple the SNPP system and also the associated homogenization results and are further required for the computation of the effective macroscopic tensors (2.2a), (2.3a).

In addition to the advantages mentioned above, the use of lowest order Raviart–Thomas elements has approved for discretization schemes for mass transport: besides local mass conservation, less numerical diffusion is produced, and more robustness is gained in the

case of large element Péclet numbers (cf. Rem. 4.12) or non-smooth coefficients (Brunner et al. 2011) in comparison to non-mixed discretizations.

4.1 Linearization Schemes

In this section, we exemplify two basic iterative linearization schemes applied to the time-discrete nonlinear SNPP system (cf. Prob. 2.1, p. 19): a *Newton scheme* and an *iterative splitting scheme* (also called iterative operator splitting, Picard iteration, and, in the context of Nernst–Planck–Poisson systems, Gummel iteration (due to Gummel 1964)). Both schemes can also be used in a straight forward way to cope with the nonlinearities of the homogenization results, i. e., the DNPP systems (cf. Thms. 2.5 and 2.8).

Let $0 =: t_0 < t_1 < \ldots < t_N := T$ be a not necessarily equidistant decomposition of the time interval J into N subintervals and let $t_n - t_{n-1} =: \tau_n$ denote the *time step size*. Furthermore, for any time-dependent function v, the notation $v^n = v^n(\boldsymbol{x}) := v(t_n, \boldsymbol{x})$ is used. Applying the implicit Euler method, i. e., approximating $\partial_t c_\varepsilon^\pm(t_n)$ by the backward difference quotient $\overline{\partial} c_\varepsilon^{\pm,n} = (c_\varepsilon^{\pm,n} - c_\varepsilon^{\pm,n-1})/\tau_n$ (cf. (3.12), p. 35), yields the following sequence of N stationary, coupled SNPP systems:

Problem 4.1 (Time-discrete family of SNPP problems). *For $n \in \{1, \ldots, N\}$, seek $(\boldsymbol{u}_\varepsilon^n, p_\varepsilon^n, \boldsymbol{j}_\varepsilon^{+,n}, c_\varepsilon^{+,n}, \boldsymbol{j}_\varepsilon^{-,n}, c_\varepsilon^{-,n}, \boldsymbol{E}_\varepsilon^n, \phi_\varepsilon^n)$ such that*

$$
\begin{aligned}
-\varepsilon^2 \Delta \boldsymbol{u}_\varepsilon^n + \boldsymbol{\nabla} p_\varepsilon^n &= \varepsilon^\beta \boldsymbol{E}_\varepsilon^n (c_\varepsilon^{+,n} - c_\varepsilon^{-,n}) && \text{in } \Omega_\varepsilon\,, && \text{(4.1a)}\\
\boldsymbol{\nabla} \cdot \boldsymbol{u}_\varepsilon^n &= 0 && \text{in } \Omega_\varepsilon\,, && \text{(4.1b)}\\
\boldsymbol{j}_\varepsilon^{\pm,n} &= -\boldsymbol{\nabla} c_\varepsilon^{\pm,n} + (\boldsymbol{u}_\varepsilon^n \pm \varepsilon^\gamma \boldsymbol{E}_\varepsilon^n)\, c_\varepsilon^{\pm,n} && \text{in } \Omega_\varepsilon\,, && \text{(4.1c)}\\
c_\varepsilon^{\pm,n} + \tau_n \boldsymbol{\nabla} \cdot \boldsymbol{j}_\varepsilon^{\pm,n} &= \mp \tau_n (c_\varepsilon^{+,n} - c_\varepsilon^{-,n}) + c^{\pm,n-1} && \text{in } \Omega_\varepsilon\,, && \text{(4.1d)}\\
\boldsymbol{E}_\varepsilon^n &= -\varepsilon^\alpha \boldsymbol{\nabla} \phi_\varepsilon^n && \text{in } \Omega_\varepsilon\,, && \text{(4.1e)}\\
\boldsymbol{\nabla} \cdot \boldsymbol{E}_\varepsilon^n &= c_\varepsilon^{+,n} - c_\varepsilon^{-,n} && \text{in } \Omega_\varepsilon && \text{(4.1f)}
\end{aligned}
$$

with given initial data $c^{\pm,0}$ and suitable boundary conditions on $\Gamma_\varepsilon \cup \partial\Omega$.

Linearization by the Newton scheme. The iterative Newton scheme copes with nonlinear problems by linearization by means of a truncated Taylor series expansion around each iterate. Considered a system of partial differential equations in residual form

$$\mathcal{R}(U) = 0$$

with solution U and an operator $\mathcal{R}$, the standard (Banach valued) Newton method consists in seeking solutions U^k such that

$$\mathrm{D}\mathcal{R}(U^{k-1})\,(U^k - U^{k-1}) \;=\; -\mathcal{R}(U^{k-1})$$

for $k = 1, 2, \ldots$, where D stands for the Fréchet derivative, until some stopping criterion is fulfilled. Note that the Jacobian $\mathrm{D}\mathcal{R}$ evaluated at a point is again a (linear) Banach operator. Referring to the system (4.1), we can exploit an additive decomposition of the operator $\mathcal{R} = \mathcal{A} + \mathcal{B} + C$ into a linear operator $\mathcal{A}$, a nonlinear operator $\mathcal{B}$, and a constant operator C. In other words, system (4.1) is equivalent to

$$(\mathcal{A} + \mathcal{B} + C)\,(\boldsymbol{u}_\varepsilon^n, p_\varepsilon^n, \boldsymbol{j}_\varepsilon^{+,n}, c_\varepsilon^{+,n}, \boldsymbol{j}_\varepsilon^{-,n}, c_\varepsilon^{-,n}, \boldsymbol{E}_\varepsilon^n, \phi_\varepsilon^n) \;=\; 0 \tag{4.2}$$

with

$$\mathcal{A}: \begin{pmatrix} \boldsymbol{u}_\varepsilon^n \\ p_\varepsilon^n \\ \boldsymbol{j}_\varepsilon^{+,n} \\ c_\varepsilon^{+,n} \\ \boldsymbol{j}_\varepsilon^{-,n} \\ c_\varepsilon^{-,n} \\ \boldsymbol{E}_\varepsilon^n \\ \phi_\varepsilon^n \end{pmatrix} \mapsto \begin{bmatrix} -\varepsilon^2\Delta & \boldsymbol{\nabla} & & & & & & \\ \boldsymbol{\nabla}\cdot & & & & & & & \\ & & \boldsymbol{I} & \boldsymbol{\nabla} & & & & \\ & & \tau_n\boldsymbol{\nabla}\cdot & (1{+}\tau_n)\,I & & -\tau_n\,I & & \\ & & & & \boldsymbol{I} & \boldsymbol{\nabla} & & \\ & & & -\tau_n\,I & \tau_n\boldsymbol{\nabla}\cdot & (1{+}\tau_n)\,I & & \\ & & & & & & \boldsymbol{I} & \varepsilon^\alpha\boldsymbol{\nabla} \\ & & & -I & & I & \boldsymbol{\nabla}\cdot & \end{bmatrix} \begin{pmatrix} \boldsymbol{u}_\varepsilon^n \\ p_\varepsilon^n \\ \boldsymbol{j}_\varepsilon^{+,n} \\ c_\varepsilon^{+,n} \\ \boldsymbol{j}_\varepsilon^{-,n} \\ c_\varepsilon^{-,n} \\ \boldsymbol{E}_\varepsilon^n \\ \phi_\varepsilon^n \end{pmatrix},$$

$$\mathcal{B}: \begin{pmatrix} \boldsymbol{u}_\varepsilon^n \\ p_\varepsilon^n \\ \boldsymbol{j}_\varepsilon^{+,n} \\ c_\varepsilon^{+,n} \\ \boldsymbol{j}_\varepsilon^{-,n} \\ c_\varepsilon^{-,n} \\ \boldsymbol{E}_\varepsilon^n \\ \phi_\varepsilon^n \end{pmatrix} \mapsto \begin{pmatrix} -\varepsilon^\beta\,\boldsymbol{E}_\varepsilon^n\,(c_\varepsilon^{+,n} - c_\varepsilon^{-,n}) \\ 0 \\ -(\boldsymbol{u}_\varepsilon^n + \varepsilon^\gamma\,\boldsymbol{E}_\varepsilon^n)\,c_\varepsilon^{+,n} \\ 0 \\ -(\boldsymbol{u}_\varepsilon^n - \varepsilon^\gamma\,\boldsymbol{E}_\varepsilon^n)\,c_\varepsilon^{-,n} \\ 0 \\ \boldsymbol{0} \\ 0 \end{pmatrix}, \qquad \text{and} \qquad C :\equiv \begin{pmatrix} \boldsymbol{0} \\ 0 \\ \boldsymbol{0} \\ -c_\varepsilon^{+,n-1} \\ \boldsymbol{0} \\ -c_\varepsilon^{-,n-1} \\ \boldsymbol{0} \\ 0 \end{pmatrix}.$$

Now let the column vector

$$U^k \;:=\; (\boldsymbol{u}_\varepsilon^{n,k}, p_\varepsilon^{n,k}, \boldsymbol{j}_\varepsilon^{+,n,k}, c_\varepsilon^{+,n,k}, \boldsymbol{j}_\varepsilon^{-,n,k}, c_\varepsilon^{-,n,k}, \boldsymbol{E}_\varepsilon^{n,k}, \phi_\varepsilon^{n,k})^{\mathrm{T}}$$

abbreviate the vector of unknowns. Here, the index n is still associated with the (fixed) time level and k with the iteration index. Using the fact that $\mathrm{D}(\mathcal{A}U^k + \mathcal{B}(U^k)) = \mathcal{A} + \mathrm{D}\mathcal{B}(U^k)$ (we may omit the argument braces for linear operators), the Newton scheme for the approximation of the solution U of (4.2) reads:

Algorithm 4.2 (Newton scheme 1). *Iteratively, for $k = 1, 2, \ldots$, seek U^k such that*

$$(\mathcal{A} + \mathrm{D}\mathcal{B}(U^{k-1}))\, U^k \;=\; (\mathrm{D}\mathcal{B}(U^{k-1}) - \mathcal{B})\,(U^{k-1}) - C$$

as long as the residual of the system does not fall below a given tolerance (cf. (4.2)).

An equivalent scheme is obtained when Algorithm 4.2 is written in *correction form / update form*, in which the system's residual appears as right-hand side:

Algorithm 4.3 (Newton scheme 2). *Iteratively, for $k = 1, 2, \ldots$, seek Δ^k such that*

$$(\mathcal{A} + \mathrm{D}\mathcal{B}(U^{k-1}))\,\Delta^k \;=\; -(\mathcal{A} + \mathcal{B} + C)\,(U^{k-1}) \quad \text{and set} \quad U^k \;:=\; U^{k-1} + \Delta^k$$

as long as the residual of the system does not fall below a given tolerance (cf. (4.2)).

Note that both schemes are in fact linear in U^k and Δ^k, respectively. The Jacobian $\mathrm{D}\mathcal{B}(U^{k-1})$ in Algorithms 4.2 and 4.3 takes the explicit form

$$\begin{bmatrix}
0 & 0 & 0 & -\varepsilon^\beta \boldsymbol{E}_\varepsilon^{n,k-1} & 0 & \varepsilon^\beta \boldsymbol{E}_\varepsilon^{n,k-1} & -\varepsilon^\beta (c_\varepsilon^{+,n,k-1} - c_\varepsilon^{-,n,k-1}) & 0 \\
0 & 0 & 0 & 0 & 0 & 0 & 0 & 0 \\
-c_\varepsilon^{+,n,k-1} & 0 & 0 & -\boldsymbol{u}_\varepsilon^{n,k-1} - \varepsilon^\gamma \boldsymbol{E}_\varepsilon^{n,k-1} & 0 & 0 & \varepsilon^\gamma\, c_\varepsilon^{+,n,k-1} & 0 \\
0 & 0 & 0 & 0 & 0 & 0 & 0 & 0 \\
-c_\varepsilon^{-,n,k-1} & 0 & 0 & 0 & 0 & -\boldsymbol{u}_\varepsilon^{n,k-1} + \varepsilon^\gamma \boldsymbol{E}_\varepsilon^{n,k-1} & -\varepsilon^\gamma\, c_\varepsilon^{-,n,k-1} & 0 \\
0 & 0 & 0 & 0 & 0 & 0 & 0 & 0 \\
0 & 0 & 0 & 0 & 0 & 0 & 0 & 0 \\
0 & 0 & 0 & 0 & 0 & 0 & 0 & 0
\end{bmatrix}.$$

The iterates U^k are expected to converge *quadratically* for a sufficiently well chosen starting iterate (cf. Deuflhard 2004; Kelley 1995, 2003). The most obvious choice for this initial guess is the solution of the previous time step, i. e.,

$$\begin{aligned} U^0 &= (\boldsymbol{u}_\varepsilon^{n,0}, p_\varepsilon^{n,0}, \boldsymbol{j}_\varepsilon^{+,n,0}, c_\varepsilon^{+,n,0}, \boldsymbol{j}_\varepsilon^{-,n,0}, c_\varepsilon^{-,n,0}, \boldsymbol{E}_\varepsilon^{n,0}, \phi_\varepsilon^{n,0}) \\ &:= (\boldsymbol{u}_\varepsilon^{n-1}, p_\varepsilon^{n-1}, \boldsymbol{j}_\varepsilon^{+,n-1}, c_\varepsilon^{+,n-1}, \boldsymbol{j}_\varepsilon^{-,n-1}, c_\varepsilon^{-,n-1}, \boldsymbol{E}_\varepsilon^{n-1}, \phi_\varepsilon^{n-1}) \,, \end{aligned}$$

which means that the question whether the schemes converge or not only depends on the time step sizes τ_n. In other words, there exist sufficiently small step sizes τ_n such that Algorithms 4.2 and 4.3 converge. However, these step sizes may be very small in practice. One remedy to circumvent this issue is to expand the range of convergence, e. g., by using a damped version of the Newton scheme, e. g., according to the Armijo rule (Armijo 1966; cf. Deuflhard 2004; Kelley 1995, 2003). Another remedy is to choose the starting iterates for each time step equal to the last iterate of a Picard iteration, which was performed previously. The latter scheme is the object of the next paragraph.

Linearization by an iterative splitting scheme. Considering the fully coupled system (4.1) again, the basic idea of an iterative splitting approach is to decouple the system (4.1) by consecutively solving the subsystems {(4.1a), (4.1b)}, {(4.1c), (4.1d)}, {(4.1e), (4.1f)}, all of which are linear. This procedure is repeated until the iterates converge toward a fixed-point. In our situation, the hierarchical structure of Problem 4.1 suggests to solve the Poisson subsystem at first by taking the concentrations from the last time step, using the result to solve the Stokes subsystem, and finally inserting all computed solutions into the coupled system for the mass transport. This approach is similar to the one that Herz et al. (2012) used in the analysis of the homogenized system as given in Theorem 2.5 for $\beta = \gamma = 0$. For further fixed-point schemes with respect to similar systems, we refer to Roubíček (2006) and Prohl & Schmuck (2010).

Consider a fixed-point operator $\mathcal{F} = \mathcal{F}_3 \circ \mathcal{F}_2 \circ \mathcal{F}_1$, where $\mathcal{F} : (c_\varepsilon^{+,n}, c_\varepsilon^{-,n}) \mapsto \mathcal{F}(c_\varepsilon^{+,n}, c_\varepsilon^{-,n})$ with the suboperators $\mathcal{F}_1, \mathcal{F}_2, \mathcal{F}_3$ defined as follows:

(i) $\mathcal{F}_1 : (c_\varepsilon^{+,n}, c_\varepsilon^{-,n}) \mapsto (c_\varepsilon^{+,n}, c_\varepsilon^{-,n}, \boldsymbol{E}_\varepsilon^n)$ such that $(\boldsymbol{E}_\varepsilon^n, \phi_\varepsilon^n)$ is the weak solution of the subsystem {(4.1e), (4.1f)},

(ii) $\mathcal{F}_2 : (c_\varepsilon^{+,n}, c_\varepsilon^{-,n}, \boldsymbol{E}_\varepsilon^n) \mapsto (\boldsymbol{u}_\varepsilon^n, c_\varepsilon^{+,n}, c_\varepsilon^{-,n}, \boldsymbol{E}_\varepsilon^n)$ such that $(\boldsymbol{u}_\varepsilon^n, p_\varepsilon^n)$ is the weak solution of the subsystem {(4.1a), (4.1b)},

(iii) $\mathcal{F}_3 : (\boldsymbol{u}_\varepsilon^n, c_\varepsilon^{+,n}, c_\varepsilon^{-,n}, \boldsymbol{E}_\varepsilon^n) \mapsto (c_\varepsilon^{+,n}, c_\varepsilon^{-,n})$ such that $(\boldsymbol{j}_\varepsilon^{+,n}, c_\varepsilon^{+,n}, \boldsymbol{j}_\varepsilon^{-,n}, c_\varepsilon^{-,n})$ is the weak solution of the subsystem {(4.1c), (4.1d)}.

Then the partial solution $(c_\varepsilon^{+,n}, c_\varepsilon^{-,n})$ of the system (4.1) is the same as the fixed-point of the operator $\mathcal{F}$.

We abbreviate the iterates of the iteration scheme that follows by

$$X^k \;:=\; (c_\varepsilon^{+,n,k}, c_\varepsilon^{-,n,k})$$

with index n associated with the (fixed) time level t_n and with k denoting the iteration index. We take the starting iterate from the previous time level, i. e.,

$$X^0 \;=\; (c_\varepsilon^{+,n,0}, c_\varepsilon^{-,n,0}) \;:=\; (c_\varepsilon^{+,n-1}, c_\varepsilon^{-,n-1})$$

and define the iterative splitting scheme as follows:

Algorithm 4.4 (Iterative splitting scheme). *Iteratively, for* $k = 1, 2, \ldots,$

(i) *seek* Y^k *such that* $\quad Y^k \;=\; \mathcal{F}_1(X^{k-1})\,,$

(ii) *seek* Z^k *such that* $\quad Z^k \;=\; \mathcal{F}_2(Y^k)\,,$

(iii) *seek* X^k *such that* $\quad X^k \;=\; \mathcal{F}_3(Z^k)$

until the stopping criterion

$$\|X^k - X^{k-1}\|_{\boldsymbol{L}^2(\Omega_\varepsilon)} \;<\; \mathrm{tol}$$

is fulfilled, where $\mathrm{tol} > 0$ *is a given small tolerance.*

The system's residual (cf. (4.2)) is controlled by the value tol. Note that seeking solutions of the subsystems of Algorithm 4.4 are linear problems due to the performed splitting. As usual for an iterative splitting, the iterates X^k are expected to converge *linearly*. Simulations show that the magnitude of the error decreases fairly fast and that the range of convergence is huge making large time steps possible.

Despite the fact that the fixed-point operator $\mathcal{F}$ is a function only of the concentrations, all remaining unknowns are well-defined and can be evaluated by means of the subopera-tors $\mathcal{F}_1$ and $\mathcal{F}_2$ in a postprocessing procedure (cf., e. g., Herz et al. 2012).

Remark 4.5 (Comparison of the linearization schemes' structures). One iteration step of the iterative splitting scheme according to Algorithm 4.4 has the following explicit form:

$$\text{(i)} \quad \left\{ \begin{aligned} \boldsymbol{E}_\varepsilon^{n,k} + \varepsilon^\alpha \nabla \phi_\varepsilon^{n,k} &= \mathbf{0} \\ \nabla \cdot \boldsymbol{E}_\varepsilon^{n,k} - c_\varepsilon^{+,n,k-1} + c_\varepsilon^{-,n,k-1} &= 0 \end{aligned} \right\},$$

$$\text{(ii)} \quad \left\{ \begin{aligned} -\varepsilon^2 \Delta \boldsymbol{u}_\varepsilon^{n,k} + \nabla p_\varepsilon^{n,k} - \varepsilon^\beta \boldsymbol{E}_\varepsilon^{n,k} (c_\varepsilon^{+,n,k-1} - c_\varepsilon^{-,n,k-1}) &= \mathbf{0} \\ \nabla \cdot \boldsymbol{u}_\varepsilon^{n,k} &= 0 \end{aligned} \right\},$$

$$\text{(iii)} \quad \left\{ \begin{aligned} \boldsymbol{j}_\varepsilon^{+,n,k} + \nabla c_\varepsilon^{+,n,k} - (\boldsymbol{u}_\varepsilon^{n,k} + \varepsilon^\gamma \boldsymbol{E}_\varepsilon^{n,k}) c_\varepsilon^{+,n,k} &= \mathbf{0} \\ \tau_n \nabla \cdot \boldsymbol{j}_\varepsilon^{+,n,k} + (1+\tau_n) c_\varepsilon^{+,n,k} - \tau_n c_\varepsilon^{-,n,k} - c_\varepsilon^{+,n-1} &= 0 \\ \boldsymbol{j}_\varepsilon^{-,n,k} + \nabla c_\varepsilon^{-,n,k} - (\boldsymbol{u}_\varepsilon^{n,k} - \varepsilon^\gamma \boldsymbol{E}_\varepsilon^{n,k}) c_\varepsilon^{-,n,k} &= \mathbf{0} \\ \tau_n \nabla \cdot \boldsymbol{j}_\varepsilon^{-,n,k} + (1+\tau_n) c_\varepsilon^{-,n,k} - \tau_n c_\varepsilon^{+,n,k} - c_\varepsilon^{-,n-1} &= 0 \end{aligned} \right\}.$$

Here, the braces are associated with a simultaneous solving. As opposed to this, the structure of one iteration step of the Newton scheme from Algorithms 4.2 and 4.3 is

$$\begin{aligned}
\boldsymbol{E}_\varepsilon^{n,k} + \varepsilon^\alpha \nabla \phi_\varepsilon^{n,k} &= \mathbf{0}\,, \\
\nabla \cdot \boldsymbol{E}_\varepsilon^{n,k} - c_\varepsilon^{+,n,k} + c_\varepsilon^{-,n,k} &= 0\,, \\
-\varepsilon^2 \Delta \boldsymbol{u}_\varepsilon^{n,k} + \nabla p_\varepsilon^{n,k} - \varepsilon^\beta \boldsymbol{E}_\varepsilon^{n,k-1} (c_\varepsilon^{+,n,k} - c_\varepsilon^{-,n,k}) - \varepsilon^\beta (\boldsymbol{E}_\varepsilon^{n,k} - \boldsymbol{E}_\varepsilon^{n,k-1}) (c_\varepsilon^{+,n,k-1} - c_\varepsilon^{-,n,k-1}) &= \mathbf{0}\,, \\
\nabla \cdot \boldsymbol{u}_\varepsilon^{n,k} &= 0\,, \\
\boldsymbol{j}_\varepsilon^{+,n,k} + \nabla c_\varepsilon^{+,n,k} - (\boldsymbol{u}_\varepsilon^{n,k-1} + \varepsilon^\gamma \boldsymbol{E}_\varepsilon^{n,k-1}) c_\varepsilon^{+,n,k} - ((\boldsymbol{u}_\varepsilon^{n,k} - \boldsymbol{u}_\varepsilon^{n,k-1}) + \varepsilon^\gamma (\boldsymbol{E}_\varepsilon^{n,k} - \boldsymbol{E}_\varepsilon^{n,k-1})) c_\varepsilon^{+,n,k-1} &= \mathbf{0}\,, \\
\tau_n \nabla \cdot \boldsymbol{j}_\varepsilon^{+,n,k} + (1+\tau_n) c_\varepsilon^{+,n,k} - \tau_n c_\varepsilon^{-,n,k} - c_\varepsilon^{+,n-1} &= 0\,, \\
\boldsymbol{j}_\varepsilon^{-,n,k} + \nabla c_\varepsilon^{-,n,k} - (\boldsymbol{u}_\varepsilon^{n,k-1} - \varepsilon^\gamma \boldsymbol{E}_\varepsilon^{n,k-1}) c_\varepsilon^{-,n,k} - ((\boldsymbol{u}_\varepsilon^{n,k} - \boldsymbol{u}_\varepsilon^{n,k-1}) + \varepsilon^\gamma (\boldsymbol{E}_\varepsilon^{n,k} - \boldsymbol{E}_\varepsilon^{n,k-1})) c_\varepsilon^{-,n,k-1} &= \mathbf{0}\,, \\
\tau_n \nabla \cdot \boldsymbol{j}_\varepsilon^{-,n,k} + (1+\tau_n) c_\varepsilon^{-,n,k} - \tau_n c_\varepsilon^{+,n,k} - c_\varepsilon^{-,n-1} &= 0\,.
\end{aligned}$$

Comparing the terms for each equation of the representations above reveals that the used fixed-point approach can be derived from the Newton scheme by some minor modifications. Hence, it can be interpreted as an approximation of the Newton scheme. △

Concluding remarks. Provided that the two different linearization schemes converge, they produce the same solution. In particular, a globally implicit discretization in time is obtained. Thus, the assessment of the schemes toward the computation time and the amount of consumed memory remains: despite the fact that the quadratic order of convergence of the Newton scheme (cf. Algs. 4.2 and 4.3) is superior to that of the iterative

splitting (cf. Alg. 4.4), which is linear only, the first has several disadvantages: the treatment of a system as whole in each iteration step involves the assembly of a very large system of equations, which consumes far more memory than the iterative splitting approach (cf. Saaltink et al. 2000; Yeh & Tripathi 1989). The iterative splitting scheme in turn reduces the problem to small-sized linear subproblems, which are to be solved consecutively. In our case, these linear subproblems are either of the Stokes type (cf. {(4.1a), (4.1b)}) or of convection–diffusion type (cf. {(4.1c), (4.1d)}, {(4.1e), (4.1f)}, and all (decoupled) subproblems of the time discretized DNPP systems (2.5) and (2.7)).

Because of all these reasons and due to the hierarchical structure of the SNPP system and of its homogenized equivalences, the iterative splitting scheme according to Algorithm 4.4 is the linearization scheme of choice. Hence, we proceed with the spatial discretization of convection–diffusion type problems in Section 4.2 and of Stokes type problems in Section 4.3. Moreover, this is an asset as the spatial discretization schemes of the following sections can also be applied to the cell problems (2.2b) and (2.3b), which flux solutions are required in order to compute the effective coefficients appearing in the DNPP systems (2.5) and (2.7) (and also to further cell problems defined in Chapter 7). However, note that the argumentation above is only admissible due to the fact that the reaction rates we consider are linear.

However, when nonlinear reaction rates are taken into account, in particular, when the nonlinearities are of dominant nature, an iterative splitting approach may lead to very small time step sizes and thus to an unfeasible number of time steps—as opposed to the Newton scheme (Saaltink et al. 2000). Especially for the case of large reactive multicomponent transport systems, the Newton scheme has proven itself to be advantageous in the last decade (Carrayrou et al. 2010).

A short bibliographical review. Here, we briefly review publications that appeared in the last decade dealing with finite element approximations of the SNPP system and related systems. For a historical overview on numerical models for solving the Nernst–Planck–Poisson system, the reader is referred to, for instance, Samson et al. (1999, Sec. 3.1).

Prohl & Schmuck (2009, 2010) investigated analytically a finite element discretization of an incompressible, non-dimensionalized Navier–Stokes–Nernst–Planck–Poisson system for a binary electrolyte. The system is fully coupled since electrophoretic and electroosmotic phenomena are taken into account. However, only homogeneous boundary conditions are considered. The discretization in time is fully implicit, using the backward Euler method and iterative operator splitting. The spatial discretization is carried out using $\mathbb{P}_1^c$-bubble ele-

ments for the velocity (mini element, cf. Arnold et al. 1984), and $\mathbb{P}_1^c$ elements for all other unknowns on triangular (two-dimensional) uniform grids.

An electrochemical system in three space dimensions including liquid flow, multi-ion transport due to advection, diffusion, and electric drift is considered in Bauer et al. (2011). An arbitrary number of ionic species, represented by their molar concentrations, obey the following system of equations:

$$\partial_t c_i + \boldsymbol{u} \cdot \boldsymbol{\nabla} c_i + \boldsymbol{\nabla} \cdot \Big(- D_i \, \boldsymbol{\nabla} c_i - z_i \, v_i \, F \, c_i \, \boldsymbol{\nabla} \phi \Big) \;=\; 0 \quad \text{in } J \times \Omega \,, \tag{4.3}$$

together with the electroneutrality condition (1.10), with quantities as listed in Tables B.2 and B.5 (p. 142f.). Provided that no reactions take place, Equation (4.3) is an equivalent formulation of $\{(1.4), (1.6)\}$, since $\boldsymbol{u}$ is divergence-free. The electroneutrality condition is an algebraic constraint, which is a simplification of the Poisson equation. The system $\{(4.3), (1.10)\}$ has the unknowns c_i and ϕ and is completed with initial conditions and linear boundary conditions for c_i and / or conditions prescribing the mass / molar flux across the boundary due to diffusion and electromigration. A nonlinear boundary condition depending on all concentrations and on ϕ is allowed for one single species. Due to the fact that electroosmosis is not considered, the coupling to the liquid velocity $\boldsymbol{u}$ is only one-sided. The nonlinear system $\{(4.3), (1.10)\}$ is linearized by a Newton scheme incorporating a Jacobian with saddle point structure owing to the electroneutrality condition. The discretization in space is performed by (non-mixed) Lagrange finite elements of equal order for c_i and ϕ ($\mathbb{P}_1^c$ elements on hexahedrals are used in the simulations) and a Crank–Nicolson scheme is used for time discretization. Due to the one-sided coupling, the velocity $\boldsymbol{u}$ can be precomputed in each time step. Altogether, a globally implicit scheme is presented that is formally accurate of second order in time and space. In Bauer et al. (2012), the same authors introduce a stabilization scheme capable of preventing oscillations arising in the convection–dominated case (see also Bauer 2012).

Paz-García et al. (2011) consider the transport due to diffusion and electromigration of an arbitrary number of charged chemical species between an anode and a cathode in a liquid medium. The model consists of a Poisson–Nernst–Planck system similar to the SNPP system in Section 1.1 with $\boldsymbol{u} \equiv \boldsymbol{0}$ on a one-dimensional domain, equipped with flux boundary conditions for the transport and also for the Poisson equation. The implicit Euler method is used to integrate in time, while (non-mixed) Lagrange $\mathbb{P}_1^c$ finite elements are used for the space discretization. The nonlinearity in the drift term is treated by Gummel's iteration (cf. Sec. 4.1).

4.2 Discretization of Equations of Convection–Diffusion Type

In this section, we present the discretization of a general convection–diffusion equation equipped with three types of different boundary conditions. By choosing specific coefficients, boundary data, and optionally constraints, the discretization scheme covers all subproblems of the SNPP system, DNPP systems, and cell problems in this work that are not of Stokes type.

4.2.1 Formulation of the Weak Problems

Model equations. Consider a time interval $J =]0, T[$ and a domain $\Omega \subset \mathbb{R}^2$ as described in Section 3.1, except that Ω is also allowed to contain interior boundaries. Furthermore, let the boundary $\partial\Omega$ be split into not necessarily connected flux, Neumann, and closed Dirichlet boundaries $\partial\Omega_{\text{flux}}$, $\partial\Omega_{\text{N}}$, and $\partial\Omega_{\text{D}}$, respectively, such that $\partial\Omega = \overline{\partial\Omega_{\text{flux}}} \cup \overline{\partial\Omega_{\text{N}}} \cup \partial\Omega_{\text{D}}$.

Given the coefficient functions $\mathsf{A}, \mathsf{F} : J \times \Omega \to \mathbb{R}$, $\boldsymbol{C}, \boldsymbol{E} : J \times \Omega \to \mathbb{R}^2$, $\mathbf{D} : J \times \Omega \to \mathbb{R}^{2,2}$, the boundary data $q_{\text{flux}} : J \times \partial\Omega_{\text{flux}} \to \mathbb{R}$, $u_{\text{D}} : J \times \partial\Omega_{\text{D}} \to \mathbb{R}$, and the initial data $u^0 : \Omega \to \mathbb{R}$, we consider the following initial boundary value problem in seeking two functions $\boldsymbol{q} : J \times \Omega \to \mathbb{R}^2$ and $u : J \times \Omega \to \mathbb{R}$ such that

$$\begin{aligned}
\boldsymbol{q} &= -\mathbf{D}\boldsymbol{\nabla} u + \boldsymbol{C}u + \boldsymbol{E} && \text{in } J \times \Omega\,, && \text{(4.4a)}\\
\partial_t(\mathsf{A}u) + \boldsymbol{\nabla}\cdot\boldsymbol{q} &= \mathsf{F} && \text{in } J \times \Omega\,, && \text{(4.4b)}\\
\boldsymbol{q}\cdot\boldsymbol{\nu} &= q_{\text{flux}} && \text{on } J \times \partial\Omega_{\text{flux}}\,, && \text{(4.4c)}\\
-(\mathbf{D}\boldsymbol{\nabla} u)\cdot\boldsymbol{\nu} &= 0 && \text{on } J \times \partial\Omega_{\text{N}}\,, && \text{(4.4d)}\\
u &= u_{\text{D}} && \text{on } J \times \partial\Omega_{\text{D}}\,, && \text{(4.4e)}\\
u &= u^0 && \text{on } \{0\} \times \Omega\,. && \text{(4.4f)}
\end{aligned}$$

In contrast to the previous chapters, we consider a time and space dependent coefficient $\mathbf{D} = \mathbf{D}(t, \boldsymbol{x})$ here and assume tacitly that for a. e. $(t, \boldsymbol{x}) \in J \times \Omega$ the hypothesis (H1) on p. 36 holds. Even though we do not need this generalization for the numerical investigation of the SNPP system or of the DNPP systems in Chapter 6, we do require it in Chapter 7. Furthermore, we assume that $\partial\Omega_{\text{N}}$ is an *outflow boundary*, i. e.,

$$\boldsymbol{q}\cdot\boldsymbol{\nu} > 0 \quad \overset{(4.4\text{d})}{\Longleftrightarrow} \quad (\boldsymbol{C}u + \boldsymbol{E})\cdot\boldsymbol{\nu} > 0 \qquad \text{on } J \times \partial\Omega_{\text{N}}\,. \tag{4.5}$$

The Neumann boundary condition (4.4d) is discussed in Remark 4.7. If the flux boundary $\partial\Omega_{\text{flux}}$ is non-empty and is used as *inflow boundary* for instance, it has to be assured that the mass that enters the domain has to be equal to the mass that is transported away from the boundary into the inside of Ω by the advective flux.

Example 4.6 (Choice of the coefficient functions). By choosing specific coefficient functions and boundary data, the discretization scheme for (4.4) presented hereinafter can be applied directly to the (linearized) model problems appearing in this work: the *cell problems* (2.2b) are obtained, e. g., by choosing $\mathsf{A}, \boldsymbol{C}, \mathsf{F}$ equal to zero, $\mathbf{D} = \mathbf{I}$, where $\mathbf{I}$ denotes the unit matrix, and $\boldsymbol{E} = -\boldsymbol{e}_j$ together with $g = 0$ on the interior boundary Γ, while choosing periodic boundary conditions on the exterior boundary ∂Y. The *transport problem* for the positively charged particles in Algorithm 4.4 is obtained by choosing A equal to one, $\boldsymbol{C} = \boldsymbol{u}_\varepsilon^{n,k} + \varepsilon^\gamma \boldsymbol{E}_\varepsilon^{n,k}$, $\mathbf{D} = \mathbf{I}$, $\boldsymbol{E}$ equal to zero, and $\mathsf{F} = -(c_\varepsilon^{+,n,k-1} - c_\varepsilon^{-,n,k-1})$ at a fixed time level t_n, and so on. △

Remark 4.7 (Neumann boundary condition for the transport problem). The use of Neumann boundary conditions as given in (4.4d)—also called *zero-gradient condition* or *outflow condition*—is a common way to model outflow boundaries (cf. Kinzelbach (1992, Sec. 2.2), Knabner & Angermann (2003, Sec. 3.2, p. 108f.), Logan (2001, Sec. 2.7.2), and Spitz & Moreno (1996, p. 84)). Here, only the diffusive flux is prescribed to be zero at the boundary, whereas the convective flux "adjusts" itself automatically. By assumption, the convective flux is nonvanishing on the boundary $\partial\Omega_{\text{N}}$ and points outside the domain (cf. (4.5)). Indeed, the fact that the diffusive flux through the boundary $\partial\Omega_{\text{N}}$ is prescribed to be zero in (4.4d) yields a detention of mass and thus a local increase of the amount of concentration at this boundary—a "blow up" is expected. However, this increase implies also an increase of mass that is transported outside of the domain by advection, and thus no critical situation occurs. △

Weak continuous formulation. Next, the weak formulation of (4.4) is derived. Recall the space $\boldsymbol{H}^{\text{div}}(\Omega) := \{\boldsymbol{v} \in \boldsymbol{L}^2(\Omega);\ \nabla \cdot \boldsymbol{v} \in L^2(\Omega)\} \supset \boldsymbol{H}^1(\Omega)$ (cf. Sec. 3.1). For $\Gamma \subset \partial\Omega$, we define the constrained ansatz space

$$\boldsymbol{H}^{\text{div}}_{a,\Gamma}(\Omega) \ := \ \left\{ \boldsymbol{v} \in \boldsymbol{H}^{\text{div}}(\Omega);\ \boldsymbol{v} \cdot \boldsymbol{\nu} = a \text{ on } \Gamma \right\},$$

with a being an element of $H^{-1/2}(\Gamma)$ according to Theorem 3.1. We take the flux boundary condition as the *essential boundary condition* by imposing it explicitly in the solution

space. That of Dirichlet type is taken as *natural boundary condition* imposed by the weak formulation itself. Regarding the Neumann boundary, we take the equivalence

$$-(\mathbf{D}\nabla u)\cdot\boldsymbol{\nu} \;=\; 0 \quad \overset{(4.4d)}{\Leftrightarrow} \quad \boldsymbol{q}\cdot\boldsymbol{\nu} \;=\; (u\boldsymbol{C}+\boldsymbol{E})\cdot\boldsymbol{\nu} \qquad \text{on } J\times\partial\Omega_{\mathrm{N}} \tag{4.6}$$

into account and claim it weakly in the continuous variational problem. This linear constraint will later be used to substitute the Neumann degrees of freedom in the linear algebra system (4.13) that results from the discretization below with terms that depend on the scalar solution u (*static condensation*). It is also possible to treat the Neumann boundary condition as a natural one entailing certain disadvantages. For a discussion in this regard, see Remark 4.9.

For the sake of presentation, the coefficients A, $\mathbf{D}$, and F are assumed to exist componentwise in $L^\infty(J\times\Omega)$ and $\boldsymbol{C}$, $\boldsymbol{E}\in L^2(J,\boldsymbol{H}^{\mathrm{div}}(\Omega))$ in this section. Multiplication of (4.4a) by the inverse of $\mathbf{D}$ and using the Green's formula (3.4), we define the following *continuous variational problem*:

Problem 4.8 (Weak continuous convection–diffusion problem). *Let the data $u^0 \in L^2(\Omega)$, $q_{\mathrm{flux}}\in L^2(J;H^{-1/2}(\partial\Omega_{\mathrm{flux}}))$, $u_{\mathrm{D}}\in L^2(J;H^{1/2}(\partial\Omega_{\mathrm{D}}))$ and the coefficients A to F be given. Seek $(\boldsymbol{q},u)\in L^2(J;\boldsymbol{H}^{\mathrm{div}}_{q_{\mathrm{flux}},\partial\Omega_{\mathrm{flux}}}(\Omega))\times(H^1(J;L^2(\Omega))\cap L^2(J;L^\infty(\Omega)))$ such that for a. e. $t\in J$,*

$$\begin{aligned}
\forall\boldsymbol{v}\in\boldsymbol{H}^{\mathrm{div}}_{0,\partial\Omega_{\mathrm{flux}}\cup\partial\Omega_{\mathrm{N}}}(\Omega),\quad & -\left(\mathbf{D}(t)^{-1}\boldsymbol{q}(t)\,,\,\boldsymbol{v}\right)_{\boldsymbol{L}^2(\Omega)}+(\nabla\cdot\boldsymbol{v}\,,\,u(t))_{L^2(\Omega)}+\left(\mathbf{D}(t)^{-1}\boldsymbol{C}(t)\,u(t)\,,\,\boldsymbol{v}\right)_{\boldsymbol{L}^2(\Omega)}\\
&\qquad=\langle\boldsymbol{v}\cdot\boldsymbol{\nu}\,,\,u_{\mathrm{D}}\rangle_{H^{-1/2}(\partial\Omega_{\mathrm{D}}),H^{1/2}(\partial\Omega_{\mathrm{D}})}-\left(\mathbf{D}(t)^{-1}\boldsymbol{E}(t)\,,\,\boldsymbol{v}\right)_{\boldsymbol{L}^2(\Omega)},\\
\forall w\in L^2(\Omega),\quad & (\partial_t(\mathsf{A}(t)\,u(t))\,,\,w)_{L^2(\Omega)}+(\nabla\cdot\boldsymbol{q}(t)\,,\,w)_{L^2(\Omega)}\;=\;(\mathsf{F}(t)\,,\,w)_{L^2(\Omega)}\,,\\
\forall z\in H^{1/2}(\partial\Omega_{\mathrm{N}}),\quad & \langle\boldsymbol{q}(t)\cdot\boldsymbol{\nu}\,,\,z\rangle_{H^{-1/2}(\partial\Omega_{\mathrm{N}}),H^{1/2}(\partial\Omega_{\mathrm{N}})}\;=\;\langle(u\,\boldsymbol{C}+\boldsymbol{E})(t)\cdot\boldsymbol{\nu}\,,\,z\rangle_{H^{-1/2}(\partial\Omega_{\mathrm{N}}),H^{1/2}(\partial\Omega_{\mathrm{N}})}
\end{aligned}$$

with $u(0,\cdot)=u^0$ in Ω and $u(0,\cdot)=u_{\mathrm{D}}(0)$ on $\partial\Omega_{\mathrm{D}}$.

The boundary term in the first equation vanished on $\partial\Omega_{\mathrm{flux}}\cup\partial\Omega_{\mathrm{N}}$ due to the chosen space of test functions. Note that the regularity assumptions are sufficient here. For instance, regarding the last equation, we have by Hölder's inequality and Theorem 3.1 (ii) that $\|u(t)\boldsymbol{C}(t)\cdot\boldsymbol{\nu}\|_{H^{-1/2}(\partial\Omega_{\mathrm{N}})}\le\|u(t)\|_{L^\infty(\Omega)}\|\boldsymbol{C}(t)\|_{\boldsymbol{H}^{\mathrm{div}}(\Omega)}<\infty$.

Remark 4.9 (Natural Neumann boundary condition). An alternative weak continuous formulation is obtained by treating the Neumann boundary condition (4.4d) as a natural

condition. Then the corresponding problem to Problem 4.8 consists in seeking $(\boldsymbol{q}, u) \in L^2(J; \boldsymbol{H}^{\mathrm{div}}_{q_{\mathrm{flux}},\partial\Omega_{\mathrm{flux}}}(\Omega)) \times H^1(J; L^2(\Omega))$ such that for a. e. $t \in J$,

$$\begin{aligned}\forall \boldsymbol{v} \in \boldsymbol{H}^{\mathrm{div}}_{0,\partial\Omega_{\mathrm{flux}}}(\Omega), \quad & -\left(\mathbf{D}(t)^{-1}\boldsymbol{q}(t)\,,\,\boldsymbol{v}\right)_{\boldsymbol{L}^2(\Omega)} + (\boldsymbol{\nabla}\cdot\boldsymbol{v}\,,\,u(t))_{L^2(\Omega)} \\ & + \left(\mathbf{D}(t)^{-1}\boldsymbol{C}(t)\,u(t)\,,\,\boldsymbol{v}\right)_{\boldsymbol{L}^2(\Omega)} \;=\; \text{“}\int_{\partial\Omega_{\mathrm{N}}} \boldsymbol{q}(t)\cdot\boldsymbol{\nu}\,(\boldsymbol{C}(t)\cdot\boldsymbol{\nu})^{-1}\,\boldsymbol{v}\cdot\boldsymbol{\nu}\text{”} \\ & \qquad + \langle \boldsymbol{v}\cdot\boldsymbol{\nu}\,,\,u_{\mathrm{D}}\rangle_{H^{-1/2}(\partial\Omega_{\mathrm{D}}),H^{1/2}(\partial\Omega_{\mathrm{D}})} - \left(\mathbf{D}(t)^{-1}\boldsymbol{E}(t)\,,\,\boldsymbol{v}\right)_{\boldsymbol{L}^2(\Omega)}\,, \qquad (4.7a)\\ \forall w \in L^2(\Omega), \quad & (\partial_t(\mathsf{A}(t)\,u(t))\,,\,w)_{L^2(\Omega)} + (\boldsymbol{\nabla}\cdot\boldsymbol{q}(t)\,,\,w)_{L^2(\Omega)} \;=\; (\mathsf{F}(t)\,,\,w)_{L^2(\Omega)}\,. \qquad (4.7b)\end{aligned}$$

The boundary integral on $\partial\Omega_{\mathrm{N}}$ in (4.7a) is set in quotes here, since at this point, the regularity assumptions are not enough so that this term is meaningful. Notwithstanding this, the discretization of the system (4.7) yields a larger system of equations (cf. (4.13)) than that of Problem 4.8. This is due to the fact that in the latter case the degrees of freedom are eliminated not only on $\partial\Omega_{\mathrm{flux}}$ but also on $\partial\Omega_{\mathrm{N}}$ by static condensation. The main disadvantage of the strategy of treating the Neumann condition as natural one is certainly the involving constraint of $\boldsymbol{C}\cdot\boldsymbol{\nu} \neq 0$ a. e. on $J \times \partial\Omega_{\mathrm{N}}$. This cannot be guaranteed in our applications, considered that $\boldsymbol{C}$ stems from the solution of the Stokes subsystem or Darcy subsystem in the SNPP system or DNPP systems, respectively (cf. Prob. 2.1 and Thms. 2.5 and 2.8). △

Weak discrete formulation. We continue with the formulation of the fully discrete problem using the backward Euler scheme in time and the Galerkin method with Raviart–Thomas elements of lowest order in space. Recall the spaces $\mathbb{RT}_k(\mathcal{T}_h)$ and $\mathbb{P}_k(\mathcal{T}_h)$, defined in (3.7) and (3.6), respectively. Also recall the symbols $\mathcal{E}_\Omega$ and $\mathcal{E}_{\partial\Omega}$ that denote the sets of interior edges and exterior edges of the triangular grid $\mathcal{T}_h$, respectively, such that $\mathcal{E}_\Omega \cup \mathcal{E}_{\partial\Omega} = \mathcal{E} = \{E\}$. In addition, we refer to $\mathcal{E}_{\mathrm{flux}}$, $\mathcal{E}_{\mathrm{N}}$, and $\mathcal{E}_{\mathrm{D}}$ as the set of edges that lie on $\partial\Omega_{\mathrm{flux}}$, $\partial\Omega_{\mathrm{N}}$, and $\partial\Omega_{\mathrm{D}}$, respectively. For a list of symbols regarding the triangulation and grid related symbols, see Table B.6.

Problem 4.8 is discretized in time as described in Section 4.1. For a set of edges $\mathcal{E}'$ covering some part of the boundary $\Gamma \subset \partial\Omega$, we define the finite-dimensional affine space

$$\boldsymbol{V}_h^{a_h,\mathcal{E}'} \;:=\; \left\{\boldsymbol{v}_h \in \mathbb{RT}_0(\mathcal{T}_h);\, \boldsymbol{v}_h\cdot\boldsymbol{\nu}_E = a_h|_E \text{ for } E \in \mathcal{E}'\right\} \;=\; \boldsymbol{H}^{\mathrm{div}}_{a_h,\Gamma}(\Omega) \cap \mathbb{RT}_0(\mathcal{T}_h)$$

with $a_h \in \mathbb{P}_0(\mathcal{E}')$ being an edgewise constant function according to Lemma 3.4 (iii). We choose a *conformal* approximation setting (cf. Ern & Guermond 2004, Def. 2.13) by taking the solution space $\boldsymbol{V}_h^{q^n_{\mathrm{flux},h},\mathcal{E}_{\mathrm{flux}}} \times \mathbb{P}_0(\mathcal{T}_h) \subset \boldsymbol{H}^{\mathrm{div}}_{q^n_{\mathrm{flux},h},\partial\Omega_{\mathrm{flux}}}(\Omega) \times L^2(\Omega)$ for $n \in \{1,\dots,N\}$ and the

test space $\boldsymbol{V}_h^{0,\mathcal{E}_{\mathrm{flux}}\cup\mathcal{E}_{\mathrm{N}}} \times \mathbb{P}_0(\mathcal{T}_h) \subset \boldsymbol{H}^{\mathrm{div}}_{0,\partial\Omega_{\mathrm{flux}}\cup\partial\Omega_{\mathrm{N}}}(\Omega) \times L^2(\Omega)$. The data and the coefficients are assumed to be given in the following discrete spaces (for each time level t_n):

$$\mathsf{A}_h^n,\ \mathsf{F}_h^n \in \mathbb{P}_0(\mathcal{T}_h)\,, \qquad \boldsymbol{C}_h^n,\ \boldsymbol{E}_h^n \in \mathbb{RT}_0(\mathcal{T}_h)\,, \qquad \mathbf{D}_h^n \in \mathbb{P}_0(\mathcal{T}_h)^{2,2}\,, \tag{4.8a}$$

$$u_h^0 \in \mathbb{P}_0(\mathcal{T}_h)\,, \qquad q_{\mathrm{flux},h}^n \in \mathbb{P}_0(\mathcal{E}_{\mathrm{flux}})\,, \qquad u_{\mathrm{D},h}^n \in \mathbb{P}_0(\mathcal{E}_{\mathrm{D}})\,. \tag{4.8b}$$

For the initial and boundary data, this can be realized by using a projection of the associated data of Problem 4.8. One possibility to do this is to take the respective mean values (e. g., $q_{\mathrm{flux},h}^n|_E := \fint_E q_{\mathrm{flux}}^n$).

Remark 4.10 (Discrete coefficients). The demand that the coefficients are elements of the discrete spaces as described in (4.8a) can be justified as follows: admittedly, accuracy is lost—in particular, when the coefficients are the discrete solutions of previously solved problems. For instance, in the fixed-point iteration for the SNPP system (cf. Alg. 4.4), the water flux $\boldsymbol{u}$ (indices suppressed), which is determined in the space $\mathbb{P}_2^{\mathrm{c}}(\mathcal{T}_h)^2$, must be mapped into the space $\mathbb{RT}_0(\mathcal{T}_h)$ in order to fit in the discretization scheme presented in this section. However, this treatment is admissible as long as the resulting *consistence error* vanishes at least with the same order as the *approximation error* of the underlying discretization (in our case, this is first order in h, cf. Prop. 3.24). The numerical investigation in Section 5.3 shows that this is indeed the case.

Certainly, the use of discrete coefficients as described above bears several major advantages: the case of non-fitting coupling terms as just described only appears once in all the systems that are solved in this thesis (this is the convection term in the SNPP system, cf. Prob. 4.1). All further coupling terms are already derived in the demanded discrete spaces $\mathbb{RT}_0(\mathcal{T}_h)$ and $\mathbb{P}_0(\mathcal{T}_h)$. This holds especially for the discretizations of all homogenization results (cf. Thms. 2.5 and 2.8, p. 23f.). The most crucial advantage is the exploitation of the basis representation of these coefficients (cf. (4.10)) in the assembly of the large system of equations (4.13). More precisely, the respective integrals appearing in the variational formulation can be computed *exactly*. Using instead a quadrature rule of high order to approximate these integrals would result in high computation times that are not acceptable here. △

With the above preliminary considerations, the *fully discrete variational problem* is defined as follows:

Problem 4.11 (Weak discrete convection–diffusion problem). *Let the data* u_h^0, $q_{\mathrm{flux},h}^n$, $u_{\mathrm{D},h}^n$ *and the discrete coefficients* A_h^n *to* F_h^n *be given according to* (4.8). *For* $n \in \{1, \dots, N\}$, *seek* $(\boldsymbol{q}_h^n, u_h^n) \in \boldsymbol{V}_h^{q_{\mathrm{flux},h}^n, \mathcal{E}_{\mathrm{flux}}} \times \mathbb{P}_0(\mathcal{T}_h)$ *such that*

$$
\begin{aligned}
\forall \boldsymbol{v}_h \in \boldsymbol{V}_h^{0,\mathcal{E}_{\mathrm{flux}} \cup \mathcal{E}_{\mathrm{N}}}, \quad & -\left((\mathbf{D}_h^n)^{-1} \boldsymbol{q}_h^n \,,\, \boldsymbol{v}_h\right)_{\boldsymbol{L}^2(\Omega)} + (\boldsymbol{\nabla} \cdot \boldsymbol{v}_h \,,\, u_h^n)_{L^2(\Omega)} + \left((\mathbf{D}_h^n)^{-1} \boldsymbol{C}_h^n u_h^n \,,\, \boldsymbol{v}_h\right)_{\boldsymbol{L}^2(\Omega)} \\
& \qquad = \left(\boldsymbol{v}_h \cdot \boldsymbol{\nu} \,,\, u_{\mathrm{D},h}^n\right)_{L^2(\partial\Omega_{\mathrm{D}})} - \left((\mathbf{D}_h^n)^{-1} \boldsymbol{E}_h^n \,,\, \boldsymbol{v}_h\right)_{\boldsymbol{L}^2(\Omega)} , \\
\forall w_h \in \mathbb{P}_0(\mathcal{T}_h), \quad & (\mathsf{A}_h^n u_h^n \,,\, w_h)_{L^2(\Omega)} + \tau_n \left(\boldsymbol{\nabla} \cdot \boldsymbol{q}_h^n \,,\, w_h\right)_{L^2(\Omega)} \\
& \qquad = (\tau_n \mathsf{F}_h^n \,,\, w_h)_{L^2(\Omega)} + \left(\mathsf{A}_h^{n-1} u_h^{n-1} \,,\, w_h\right)_{L^2(\Omega)} , \\
\forall z_h \in \mathbb{P}_0(\mathcal{E}_{\mathrm{N}}), \quad & \left(\boldsymbol{q}_h^n \cdot \boldsymbol{\nu} \,,\, z_h\right)_{L^2(\partial\Omega_{\mathrm{N}})} = \left((u_h^n \boldsymbol{C}_h^n + \boldsymbol{E}_h^n) \cdot \boldsymbol{\nu} \,,\, z_h\right)_{L^2(\partial\Omega_{\mathrm{N}})} .
\end{aligned}
$$

In the first and in the last equation we write the $L^2(\Omega)$ scalar products instead of the duality pairings as in Problem 4.8, since the respective left-hand sides are clearly element of $L^2(\Omega)$.

Remark 4.12 (Local Péclet number). Characteristic quantities as derived in Section 1.1 may serve as error indicator due to a loss of stability. Such a quantity is the *local* or *element Péclet number* Pe_T (Hughes 1987; Knabner & Angermann 2003, p. 372), which is defined by

$$
\mathrm{Pe}_T := \frac{\|\boldsymbol{C}\|_{L^\infty(T)} \, h_T}{2 \, \|\mathbf{D}\|_{L^\infty(T)}} \quad \text{for } T \in \mathcal{T}_h .
$$

This dimensionless number describes the ratio of the advective to the diffusive transport rate. If $\mathrm{Pe}_T > 1$, the convective part dominates the diffusive one and the flux is said to be (locally) *convection dominated* (and vice versa for $\mathrm{Pe}_T \leq 1$). If Pe_T becomes too high, the discretization may become unstable and unphysical oscillations appear. This is due to the fact that the constant C in the respective a priori estimate for the discretization error of the gradient depends on Pe_T (cf. Hughes 1987).

Stabilization methods such as *streamline-upwinding* can handle the aforementioned situation, but have the disadvantage of causing additional numerical diffusion (cf. Radu et al. 2011). See, for instance, Hughes et al. (2004, Chap. 5) or Kuzmin (2010, Sec. 2.2) for overviews of stabilization methods in this context. *Local grid refinement* can also reduce the local Péclet number, however, to the expense of an increased computation cost. △

In the next section, we derive the linear system of equations that is the analog of Problem 4.11.

4.2.2 Matrix Formulation

Basis representation. We first choose bases for the discrete ansatz spaces in order to be able to represent the unknowns $(\boldsymbol{q}_h^n, u_h^n)$ and also the coefficients of Problem 4.11 in their associated coordinates. An explicit formulation of the basis functions or *form functions* is given below (cf. Sec. 4.2.3). In this sense, let

$$\begin{aligned} \boldsymbol{V}_h^{q^n_{\mathrm{flux},h},\mathcal{E}_{\mathrm{flux}}} &:= \operatorname{span}\{\boldsymbol{\varphi}_E\}_{E\in\mathcal{E}} \cap \boldsymbol{H}^{\mathrm{div}}_{q^n_{\mathrm{flux},h},\partial\Omega_{\mathrm{flux}}}(\Omega)\,, \quad \boldsymbol{V}_h^{0,\mathcal{E}_{\mathrm{flux}}\cup\mathcal{E}_{\mathrm{N}}} := \operatorname{span}\{\boldsymbol{\varphi}_E\}_{E\in\mathcal{E}_\Omega\cup\mathcal{E}_{\mathrm{D}}}\,, \\ \mathbb{P}_0(\mathcal{T}_h) &:= \operatorname{span}\{\chi_T\}_{T\in\mathcal{T}_h} \end{aligned}$$

with $\{\boldsymbol{\varphi}_E\}_{E\in\mathcal{E}}$ being the basis of $\mathbb{RT}_0(\mathcal{T}_h)$ and with χ_T denoting the characteristic function on T. The basis functions $\boldsymbol{\varphi}_E$ are extended by zero outside their local support, i. e., $\boldsymbol{\varphi}_E : \Omega \to \mathbb{R}^2$ (cf. Def. 4.14) and therefore, the definition of the space $\boldsymbol{V}_h^{0,\mathcal{E}_{\mathrm{flux}}\cup\mathcal{E}_{\mathrm{N}}}$ is meaningful. With respect to these spaces, we obtain the following representation of the solution $(\boldsymbol{q}_h^n, u_h^n)$:

$$\boldsymbol{V}_h^{q^n_{\mathrm{flux},h},\mathcal{E}_{\mathrm{flux}}} \ni \boldsymbol{q}_h^n(\boldsymbol{x}) = \sum_{E\in\mathcal{E}} q_E^n\,\boldsymbol{\varphi}_E(\boldsymbol{x})\,, \qquad \mathbb{P}_0(\mathcal{T}_h) \ni u_h^n(\boldsymbol{x}) = \sum_{T\in\mathcal{T}_h} u_T^n\,\chi_T(\boldsymbol{x}) \tag{4.9a}$$

with the degrees of freedom q_E^n and u_T^n and the constraint that $q_E^n = q^n_{\mathrm{flux},h}|_E$ for $E \in \mathcal{E}_{\mathrm{flux}}$. As test functions $(\boldsymbol{v}_h, w_h)$, we choose

$$\begin{aligned} \boldsymbol{V}_h^{0,\mathcal{E}_{\mathrm{flux}}\cup\mathcal{E}_{\mathrm{N}}} \ni \boldsymbol{v}_h(\boldsymbol{x}) &= \boldsymbol{\varphi}_{E'}(\boldsymbol{x}) && \text{for } E' \in \mathcal{E}_\Omega \cup \mathcal{E}_{\mathrm{D}}\,, \\ \mathbb{P}_0(\mathcal{T}_h) \ni w_h(\boldsymbol{x}) &= \chi_{T'}(\boldsymbol{x}) && \text{for } T' \in \mathcal{T}_h\,. \end{aligned} \tag{4.9b}$$

Similarly, we obtain the following representation for the coefficients in $\mathbb{RT}_0(\mathcal{T}_h)$:

$$\boldsymbol{C}_h^n(\boldsymbol{x}) = \sum_{E\in\mathcal{E}} \boldsymbol{c}_E^n\,\boldsymbol{\varphi}_E(\boldsymbol{x})\,, \qquad \boldsymbol{E}_h^n(\boldsymbol{x}) = \sum_{E\in\mathcal{E}} \boldsymbol{e}_E^n\,\boldsymbol{\varphi}_E(\boldsymbol{x})\,. \tag{4.10}$$

We denote the $\mathbb{P}_0(\mathcal{T}_h)$ coordinates of the time-discrete coefficients A_h^n, $\mathbf{D}_h^n$, and F_h^n associated with a fixed $T \in \mathcal{T}_h$ by a_T^n, $\mathbf{d}_T^n$, and f_T^n, respectively.

Linear algebra system. In this paragraph, we abbreviate the $L^2(\Omega)$ and the $\boldsymbol{L}^2(\Omega)$ scalar product by $(\cdot\,,\,\cdot)$. With the representation (4.9), the system of equations for the nth time step reads

$$\begin{aligned}
-\sum_{E\in\mathcal{E}} q_E^n \left((\mathbf{D}_h^n)^{-1}\boldsymbol{\varphi}_E\,,\,\boldsymbol{\varphi}_{E'}\right) + \sum_{T\in\mathcal{T}_h} u_T^n\Big((\chi_T\,,\,\boldsymbol{\nabla}\cdot\boldsymbol{\varphi}_{E'}) + \left((\mathbf{D}_h^n)^{-1}\boldsymbol{C}_h^n\chi_T\,,\,\boldsymbol{\varphi}_{E'}\right)\Big) \\
= \left(u_{\mathrm{D},h}^n\,,\,\boldsymbol{\varphi}_{E'}\cdot\boldsymbol{\nu}\right)_{L^2(\partial\Omega_\mathrm{D})} - \left((\mathbf{D}_h^n)^{-1}\boldsymbol{E}_h^n\,,\,\boldsymbol{\varphi}_{E'}\right), \\
\sum_{T\in\mathcal{T}_h} u_T^n\,(\mathsf{A}_h^n\chi_T\,,\,\chi_{T'}) + \tau_n\sum_{E\in\mathcal{E}} q_E^n(\boldsymbol{\nabla}\cdot\boldsymbol{\varphi}_E\,,\,\chi_{T'}) \;=\; (\tau_n\mathsf{F}_h^n\,,\,\chi_{T'}) + \sum_{T\in\mathcal{T}_h} u_T^{n-1}\Big(\mathsf{A}_h^{n-1}\chi_T\,,\,\chi_{T'}\Big), \\
\sum_{E\in\mathcal{E}_\mathrm{N}} q_E^n(\boldsymbol{\varphi}_E\cdot\boldsymbol{\nu}\,,\,\chi_{E''})_{L^2(\partial\Omega_\mathrm{N})} \;=\; \sum_{E\in\mathcal{E}_\mathrm{N}} (u_{T\supset E}^n\boldsymbol{c}_E^n + \boldsymbol{e}_E^n)(\boldsymbol{\varphi}_E\cdot\boldsymbol{\nu}\,,\,\chi_{E''})_{L^2(\partial\Omega_\mathrm{N})}
\end{aligned}$$

for $E'\in\mathcal{E}_\Omega\cup\mathcal{E}_\mathrm{D}$, $T'\in\mathcal{T}_h$, and $E''\in\mathcal{E}_\mathrm{N}$. Using $(\boldsymbol{\varphi}_E\cdot\boldsymbol{\nu}\,,\,\chi_{E''})_{L^2(\partial\Omega_\mathrm{N})} = \delta_{EE''}|E|$ (cf. Def. 4.14 and Thm. 4.15 (iii)), the last equation yields the (edgewise valid) relation

$$q_E^n \;=\; u_{T\supset E}^n\,\boldsymbol{c}_E^n + \boldsymbol{e}_E^n \quad \text{for } E\in\mathcal{E}_\mathrm{N}\,. \tag{4.11}$$

We eliminate the degrees of freedom on Neumann edges in the first two equations by (4.11) and account for the constraint of $\boldsymbol{V}_h^{q_{\mathrm{flux},h}^n,\mathcal{E}_\mathrm{flux}}$ by setting $q_E^n = q_{\mathrm{flux},h}^n|_E$ on flux edges. Hence,

$$\begin{aligned}
&-\sum_{E\in\mathcal{E}_\Omega\cup\mathcal{E}_\mathrm{D}} q_E^n\int_\Omega (\mathbf{D}_h^n)^{-1}\boldsymbol{\varphi}_E\cdot\boldsymbol{\varphi}_{E'} \\
&\quad + \sum_{T\in\mathcal{T}_h} u_T^n\left(\int_T \boldsymbol{\nabla}\cdot\boldsymbol{\varphi}_{E'} + \int_T (\mathbf{d}_T^n)^{-1}\boldsymbol{C}_h^n\cdot\boldsymbol{\varphi}_{E'} - \sum_{\{E\subset T\,|\,E\in\mathcal{E}_\mathrm{N}\}}\boldsymbol{c}_E\int_T (\mathbf{d}_T^n)^{-1}\,\boldsymbol{\varphi}_E\cdot\boldsymbol{\varphi}_{E'}\right) \\
&\quad = \int_{\partial\Omega_\mathrm{D}} u_{\mathrm{D},h}^n\,\boldsymbol{\varphi}_{E'}\cdot\boldsymbol{\nu} - \int_\Omega (\mathbf{D}_h^n)^{-1}\boldsymbol{E}_h^n\cdot\boldsymbol{\varphi}_{E'} + \sum_{E\in\mathcal{E}_\mathrm{N}}\boldsymbol{e}_E^n\int_\Omega (\mathbf{D}_h^n)^{-1}\boldsymbol{\varphi}_E\cdot\boldsymbol{\varphi}_{E'} \\
&\qquad\qquad + \sum_{E\in\mathcal{E}_\mathrm{flux}} q_{\mathrm{flux},h}^n\big|_E\int_\Omega (\mathbf{D}_h^n)^{-1}\boldsymbol{\varphi}_E\cdot\boldsymbol{\varphi}_{E'}\,, \qquad (4.12a)
\end{aligned}$$

$$\begin{aligned}
&\tau_n\sum_{E\in\mathcal{E}_\Omega\cup\mathcal{E}_\mathrm{D}} q_E^n\int_{T'}\boldsymbol{\nabla}\cdot\boldsymbol{\varphi}_E + u_{T'}^n\left(|T'|\,\mathsf{a}_{T'}^n + \tau_n\sum_{\{E\subset T\,|\,E\in\mathcal{E}_\mathrm{N}\}}\boldsymbol{c}_E^n\int_{T'}\boldsymbol{\nabla}\cdot\boldsymbol{\varphi}_E\right) \\
&\quad = |T'|\left(\tau_n\,\mathsf{f}_{T'}^n + u_{T'}^{n-1}\mathsf{a}_{T'}^{n-1}\right) - \tau_n\sum_{E\in\mathcal{E}_\mathrm{N}}\boldsymbol{e}_E^n\int_{T'}\boldsymbol{\nabla}\cdot\boldsymbol{\varphi}_E - \tau_n\sum_{E\in\mathcal{E}_\mathrm{flux}} q_{\mathrm{flux},h}^n\big|_E\int_{T'}\boldsymbol{\nabla}\cdot\boldsymbol{\varphi}_E \qquad (4.12b)
\end{aligned}$$

for $E'\in\mathcal{E}_\Omega\cup\mathcal{E}_\mathrm{D}$ and $T'\in\mathcal{T}_h$. Since $\mathbb{RT}_0(\mathcal{T}_h)\ni\boldsymbol{C}_h^n(\boldsymbol{x}) = \sum_{E\in\mathcal{E}}\boldsymbol{c}_E^n\boldsymbol{\varphi}_E(\boldsymbol{x})$, it locally holds that

$$\int_T\left((\mathbf{d}_T^n)^{-1}\,\boldsymbol{C}_h^n\right)\cdot\boldsymbol{\varphi}_{E'}\,\mathrm{d}\boldsymbol{x} \;=\; \sum_{E\subset T}\boldsymbol{c}_E^n\int_T (\mathbf{d}_T^n)^{-1}\,\boldsymbol{\varphi}_E\cdot\boldsymbol{\varphi}_{E'}$$

and thus the associated two terms can be summarized in (4.12a). This works analogously for the terms containing the coefficient $\boldsymbol{E}_h^n$. The system (4.12) is thus equivalent to the following *system of equations*:

$$\begin{bmatrix} \mathbf{B}^n & \mathbf{C}^n + \mathbf{D}^{\mathrm{T}} \\ \tau_n \mathbf{D} & \mathbf{E}^n \end{bmatrix} \begin{pmatrix} \boldsymbol{Q}^n \\ \boldsymbol{U}^n \end{pmatrix} = \begin{pmatrix} \boldsymbol{b}^{q,n} \\ \boldsymbol{b}^{u,n} \end{pmatrix} \tag{4.13}$$

with submatrices

$$\mathbf{B}^n = \left[B^n_{E'E}\right]_{E',E\in\mathcal{E}_\Omega\cup\mathcal{E}_\mathrm{D}}, \qquad \mathbf{C}^n = \left[C^n_{E'T}\right]_{E'\in\mathcal{E}_\Omega\cup\mathcal{E}_\mathrm{D},T\in\mathcal{T}_h}, \qquad \mathbf{D} = \left[D_{T'E}\right]_{T'\in\mathcal{T}_h,E\in\mathcal{E}_\Omega\cup\mathcal{E}_\mathrm{D}},$$
$$\mathbf{E}^n = \left[E^n_{T'T}\right]_{T',T\in\mathcal{T}_h}, \qquad \boldsymbol{b}^{q,n} = \left(b^{q,n}_{E'}\right)_{E'\in\mathcal{E}_\Omega\cup\mathcal{E}_\mathrm{D}}, \qquad \boldsymbol{b}^{u,n} = \left(b^{u,n}_{T'}\right)_{T'\in\mathcal{T}_h}$$

and the *representation vectors* of the solution $(\boldsymbol{q}_h^n, u_h^n) \in \mathbb{RT}_0(\mathcal{T}_h) \times \mathbb{P}_0(\mathcal{T}_h)$ of Problem 4.11

$$\boldsymbol{Q}^n = \left(q_E^n\right)_{E\in\mathcal{E}_\Omega\cup\mathcal{E}_\mathrm{D}}, \quad \boldsymbol{U}^n = \left(u_T^n\right)_{T\in\mathcal{T}_h}.$$

Here, the data is given by

$$\mathbf{B}^n := -\mathop{\mathbin{\Large\mathbf{A}}}_{T\in\mathcal{T}_h} \mathbf{H}_T^n, \tag{4.14a}$$

$$C^n_{E'T} := \sum_{\{E\subset T | E\notin\mathcal{E}_\mathrm{N}\}} \boldsymbol{c}_E^n \int_T \left((\mathbf{d}_T^n)^{-1}\,\boldsymbol{\varphi}_E\right)\cdot\boldsymbol{\varphi}_{E'} \quad \text{for } E'\in\mathcal{E}_\Omega\cup\mathcal{E}_\mathrm{D}, T\in\mathcal{T}_h, \tag{4.14b}$$

$$D_{T'E} := \int_{T'} \boldsymbol{\nabla}\cdot\boldsymbol{\varphi}_E \quad \text{for } T'\in\mathcal{T}_h, E\in\mathcal{E}_\Omega\cup\mathcal{E}_\mathrm{D}, \tag{4.14c}$$

$$E^n_{TT} := |T|\,\mathsf{a}_T^n + \tau_n \sum_{\{E\subset T | E\in\mathcal{E}_\mathrm{N}\}} \boldsymbol{c}_E^n\, D_{TE} \quad \text{for } T\in\mathcal{T}_h, \tag{4.14d}$$

$$b^{q,n}_{E'} := \delta_{E'\in\mathcal{E}_\mathrm{D}}\,|E'|\,u^n_{\mathrm{D},h}\big|_E - \sum_{T\in\mathcal{T}_h}\sum_{E\subset T} \boldsymbol{e}_E^n\, H^n_{T,E',E} - \sum_{E\in\mathcal{E}_\mathrm{N}} \boldsymbol{e}_E^n\, B_{E'E} - \sum_{E\in\mathcal{E}_\mathrm{flux}} q^n_{\mathrm{flux},h}\big|_E\, B_{E'E} \tag{4.14e}$$
$$\text{for } E'\in\mathcal{E}_\Omega\cup\mathcal{E}_\mathrm{D},$$

$$b^{u,n}_{T'} := |T'|\left(\tau_n\,\mathsf{f}^n_{T'} + u^{n-1}_{T'}\mathsf{a}^{n-1}_{T'}\right) - \sum_{E\in\mathcal{E}_\mathrm{N}} \boldsymbol{e}_E^n\,\tau_n\,D_{T'E} - \sum_{E\in\mathcal{E}_\mathrm{flux}} q^n_{\mathrm{flux},h}\big|_E\,\tau_n\,D_{T'E} \tag{4.14f}$$
$$\text{for } T'\in\mathcal{T}_h.$$

The auxiliary local assembly matrix variable $\mathbf{H}_T^n \in \mathbb{R}^{3,3}$ is given by

$$\mathbf{H}_T^n \;:=\; \Bigg[\underbrace{\int_T \Big((\mathbf{d}_T^n)^{-1}\, \boldsymbol{\varphi}_E \Big) \cdot \boldsymbol{\varphi}_{E'}}_{=:\, H_{T,E,E'}^n} \Bigg]_{E',E \subset T} . \tag{4.14g}$$

The operator A denotes the *assembly operator*, which maps the element contribution $\mathbf{H}_T^n$ to the global matrix $\mathbf{B}^n$ (cf. Bathe 2007; Hughes 2000). In particular, this is done by a loop over all elements $T \in \mathcal{T}_h$, calculating only the nine non-zero entries of the local assembly matrix $\mathbf{H}_T^n$ per element, i. e., where $\boldsymbol{\varphi}_E$ and $\boldsymbol{\varphi}_{E'}$ have a common support. A representative structure of the large sparse matrix in (4.13) is illustrated in Figure 4.4 (a) on p. 85.

Remark 4.13 (Degrees of freedom and postprocessing). Even though the degrees of freedom for the flux unknowns $\boldsymbol{q}^n$ are located on the sets edges $\mathcal{E}_\Omega \cup \mathcal{E}_\mathrm{D}$, the block matrices in (4.13) are assembled with respect to *all* edges. Subsequently, a subindexing technique is used to solve (4.13) for the degrees of freedom only (Alberty et al. 1999, Sec. 8). The flux unknown on flux edges, i. e. $(q_E)_{E \in \mathcal{E}_\mathrm{flux}}$, is directly determined according to the boundary data q_flux. The flux unknown on Neumann edges, i. e., $(q_E)_{E \in \mathcal{E}_\mathrm{N}}$, has to be computed in a postprocessing step according to (4.6), since it depends on the scalar solution u^n. Note that this linear constraint appearing in the flux ansatz space was taken into account implicitly. △

Balance constraint of the scalar unknown. If we consider the stationary case, i. e., the coefficient A in (4.4) is chosen equal to zero, $\tau_n = 1$, and at the same time $\partial\Omega_\mathrm{D} = \emptyset$, the scalar solution is given only up to a constant and the system of equations (4.13) has a rank deficiency of one. To introduce a constraint in order to reobtain uniqueness of the scalar solution, we define a *balance constraint* by demanding the mean scalar solution to be equal to a constant b^λ, i. e., $\fint_\Omega u_h \overset{!}{=} b^\lambda$. This relation is reformulated by means of the basis representation (4.9b) of u_h to

$$\sum_{T \in \mathcal{T}_h} |T|\, u_T \;=\; \boldsymbol{F} \cdot \boldsymbol{U} \;=\; |\Omega|\, b^\lambda$$

with $\boldsymbol{F} = (|T|)_{T\in\mathcal{T}_h}$. The constraint is incorporated into system (4.13) by appending an additional column as follows:

$$\begin{bmatrix} \mathbf{B} & \mathbf{C}+\mathbf{D}^{\mathrm{T}} \\ \mathbf{D} & \mathbf{E} \\ & \boldsymbol{F}^{\mathrm{T}} \end{bmatrix} \begin{pmatrix} \boldsymbol{Q} \\ \boldsymbol{U} \end{pmatrix} = \begin{pmatrix} \boldsymbol{b}^q \\ \boldsymbol{b}^u \\ b^\lambda \end{pmatrix}, \tag{4.15}$$

which omits again a unique solution.

4.2.3 Assembly

We have derived the large system of equations (4.13), which solution is equivalent to that of Problem 4.11. This system contains terms depending on the basis functions $\boldsymbol{\varphi}_E$, which are yet of abstract nature. In this section, we define an *explicit* (global) basis of $\mathbb{RT}_0(\mathcal{T}_h)$. In contrast to Section 4.3, where only a basis on the reference triangle $\hat{T}$ is defined and the Piola transformation is used, it is demonstrated that there is no disadvantage in not using Piola mapping. Eventually, it is shown how the explicit choice of form functions leads to simplifications of the integral terms in (4.14). Furthermore, we comment on the solving of the system of equations (4.13).

Form functions. Recall that each edge $E \in \mathcal{E} = \mathcal{E}_\Omega \cup \mathcal{E}_{\partial\Omega}$ is equipped with a (globally defined) unique normal unit vector $\boldsymbol{\nu}_E$, such that $\boldsymbol{\nu}_E$ is exterior to Ω for $E \in \mathcal{E}_{\partial\Omega}$. In the following, $\boldsymbol{x}_{ET}^{\mathrm{opp}}$ denotes the node of T opposite to E, $\boldsymbol{x}_E^{\mathrm{bary}}$ the barycenter of E, and σ_{ET} the sign of E according to the local orientation, i. e.,

$$\sigma_{ET} \coloneqq \left\{ \begin{matrix} 1\,, & \boldsymbol{\nu}_{ET} = \boldsymbol{\nu}_E \\ -1\,, & \boldsymbol{\nu}_{ET} = -\boldsymbol{\nu}_E \end{matrix} \right\},$$

where $\boldsymbol{\nu}_{ET}$ is the unit edge normal under *local* orientation (cf. Fig. 4.1; Tab. B.6, p. 145). Thus,

$$\boldsymbol{\nu}_E = \sigma_{ET}\boldsymbol{\nu}_{ET} \quad \text{for } E \subset T \in \mathcal{T}_h \tag{4.16}$$

holds by definition.

We define the *global* form functions and linear forms as follows and show later on in Theorem 4.15 that these define a global finite element space:

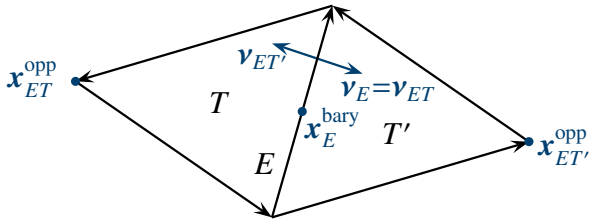

Figure 4.1. Illustration of the local edge orientation and the notation for a grid consisting of two triangles, i. e., $\mathcal{T}_h = \{T, T'\}$. Here, $\sigma_{ET} = 1$ and $\sigma_{ET'} = -1$. Note that the boundary edge orientation is always chosen in a way that the local edge normals point outward of the domain.

Definition 4.14 (Global form functions and global linear forms). *Let the* global form functions $\boldsymbol{\varphi}_E$ *be defined by*

$$\boldsymbol{\varphi}_E : \quad \Omega \ni \boldsymbol{x} \mapsto \boldsymbol{\varphi}_E|_T(\boldsymbol{x}) := \left\{ \begin{array}{cc} \sigma_{ET}\dfrac{|E|}{2\,|T|}(\boldsymbol{x} - \boldsymbol{x}_{ET}^{\text{opp}}), & E \subset T \\ 0\,, & E \not\subset T \end{array} \right\} \in \mathbb{R}^2 \quad \text{for } T \in \mathcal{T}_h \tag{4.17a}$$

and the global degrees of freedom ϱ_E *be defined by*

$$\varrho_E : \quad \mathbb{RT}_0(\mathcal{T}_h) \ni \boldsymbol{v}_h \mapsto \varrho_E(\boldsymbol{v}_h) := \int_E \boldsymbol{v}_h \cdot \boldsymbol{\nu}_E \in \mathbb{R} \quad \text{for } E \in \mathcal{E}\,. \tag{4.17b}$$

Obviously, the domain of ϱ_E can be extended to $\boldsymbol{H}^{\text{div}}(\Omega)$. Clearly, $\boldsymbol{\varphi}_E \in \mathbb{RT}_0(\mathcal{T}_h) \subset \boldsymbol{H}^{\text{div}}(\Omega)$ for $E \in \mathcal{E}$ (cf. (3.5), p. 32; (3.7), p. 33) noting that $[\![\boldsymbol{\varphi}_E]\!]_E$, i. e., the jump of $\boldsymbol{\varphi}_E$ across the edge E, vanishes.

A (local) finite element is a quadruplet $\{T, P_T, \Sigma_T, V_T\}$, satisfying the following properties (e. g. Ern & Guermond 2004):

(i) $T \subset \mathbb{R}^2$ non-empty, compact, and connected, ∂T Lipschitz.

(ii) P_T is a vector space of functions $p : T \to \mathbb{R}^2$.

(iii) $\Sigma_T = \{\varrho_k\}$ is a basis for P_T'.

In this spirit, we show that the explicit global form function and linear forms according to Definition 4.14 define the global lowest-order Raviart–Thomas finite element space:

Theorem 4.15 (Global finite element property). *Consider* $\boldsymbol{\varphi}_E \in \mathbb{RT}_0(\mathcal{T}_h)$ *and* $\varrho_E \in \mathcal{L}(\mathbb{RT}_0(\mathcal{T}_h); \mathbb{R})$ *due to Definition 4.14. Then*

(i) $\mathbb{RT}_0(\mathcal{T}_h) = \operatorname{span}\{\boldsymbol{\varphi}_E\}_{E\in\mathcal{E}}$.

(ii) $\mathcal{L}\big(\mathbb{RT}_0(\mathcal{T}_h);\mathbb{R}\big) = \operatorname{span}\{\varrho_E\}_{E\in\mathcal{E}}$.

(iii) $\varrho_{E'}(\boldsymbol{\varphi}_E) = \delta_{E'E}$, *with* δ *denoting the Kronecker delta.*

Proof. See Bahriawati & Carstensen (2005, Lem. 4.1). In addition, we give an alternative / adapted proof of (iii). Consider $T \in \mathcal{T}_h$ fixed. Then there holds

$$\varrho_{E'}(\boldsymbol{\varphi}_E) \overset{(4.17b)}{=} \fint_{E'} \boldsymbol{\varphi}_E \cdot \boldsymbol{\nu}_{E'}\,\mathrm{d}\boldsymbol{x} \overset{(4.17a)}{=} \sigma_{ET}\frac{|E|}{2|T|}\fint_{E'}(\boldsymbol{x}-\boldsymbol{x}_{ET}^{\mathrm{opp}})\cdot\boldsymbol{\nu}_{E'}\,\mathrm{d}\boldsymbol{x}\,.$$

For $E \neq E' \subset T$, the vector $(\boldsymbol{x}-\boldsymbol{x}_{ET}^{\mathrm{opp}})$ is orthogonal to $\boldsymbol{\nu}_{E'}$. Otherwise, considering $E' = E$,

$$\varrho_E(\boldsymbol{\varphi}_E) = \sigma_{ET}\frac{|E|}{2|T|}\fint_E(\boldsymbol{x}-\boldsymbol{x}_{ET}^{\mathrm{opp}})\cdot\boldsymbol{\nu}_E\,\mathrm{d}\boldsymbol{x} \overset{(4.16)}{=} \frac{1}{2|T|}\int_E(\boldsymbol{x}-\boldsymbol{x}_{ET}^{\mathrm{opp}})\cdot\boldsymbol{\nu}_{ET}\,\mathrm{d}\boldsymbol{x} = 1\,. \qquad \square$$

The linear forms $\{\varrho_E\}$ are called *global degrees of freedom*. If those are the evaluations of functions at certain points (often on grid vertices or barycenters), the elements are called *Lagrangian* and the evaluation points are called *nodes*. Since the normal trace on edges of elements of $\mathbb{RT}_0(\mathcal{T}_h)$ are constant (cf. Lem. 3.4, (iii)), we can write

$$\varrho_{E'}(\boldsymbol{\varphi}_E) = \fint_{E'}\boldsymbol{\varphi}_E\cdot\boldsymbol{\nu}_{E'}\,\mathrm{d}\boldsymbol{x} = \boldsymbol{\varphi}_E(\boldsymbol{x})\cdot\boldsymbol{\nu}_{E'} \quad \text{for (arbitrary) } \boldsymbol{x}\in E\,.$$

Consequently, if we choose nodes by $\boldsymbol{x} \coloneqq \boldsymbol{x}_E^{\mathrm{bary}}$, the degrees of freedom are simply the normal components of fluxes at the edge barycenters.

Evaluation of the integrals. This paragraph is dedicated to the simplification of the integral terms in (4.14), inter alia, by the exploitation of the special structure of the explicit $\mathbb{RT}_0(\mathcal{T}_h)$ basis in Definition 4.14. Using (4.14g), the term (4.14b) can be written as

$$C_{E'T}^n = \sum_{\{E\subset T\,|\,E\notin\mathcal{E}_{\mathrm{N}}\}} \boldsymbol{c}_E^n\, H_{T,E,E'}^n\,.$$

With the divergence theorem, (4.16), and the definition of the degrees of freedom (4.17b), the term (4.14c) is reformulated to

$$D_{T'E} = \int_{T'}\boldsymbol{\nabla}\cdot\boldsymbol{\varphi}_E = \sum_{E'\subset T'}\fint_{E'}\boldsymbol{\varphi}_E\cdot\boldsymbol{\nu}_{E'T'} = \sigma_{ET'}\,|E|\,.$$

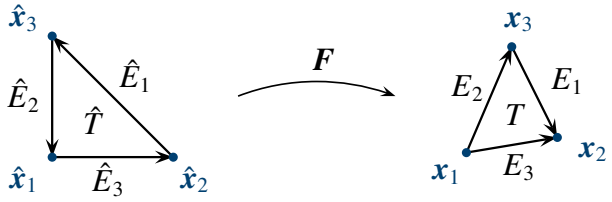

Figure 4.2. The affine mapping $\boldsymbol{F}$ transforms the reference triangle $\hat{T}$ with $\hat{\boldsymbol{x}}_1 = \mathbf{0}$, $\hat{\boldsymbol{x}}_2 = (1,\, 0)^{\mathrm{T}}$, $\hat{\boldsymbol{x}}_3 = (0,\, 1)^{\mathrm{T}}$ to some triangle T with *local* vertices $\boldsymbol{x}_k$. The edge orientation for $\hat{T}$ is defined such that $\sigma_{\hat{E}_k T} = 1$. The edge orientation and thus the orientation of the edge normals may *not* be maintained under $\boldsymbol{F}$.

Note that the matrix $\mathbf{D} = [D_{T'E}]_{T' \in \mathcal{T}_h, E \in \mathcal{E}_\Omega \cup \mathcal{E}_\mathrm{D}}$ in (4.13) is invariant in time and thus has to be assembled only once for all time steps.

Now consider a component of the local assembly matrix $\mathbf{H}_T^n$ as defined in (4.14g). The use of the explicit definition of the basis functions (4.17a) yields

$$\begin{aligned} H_{T,E,E'}^n &= \int_T \left((\mathbf{d}_T^n)^{-1} \boldsymbol{\varphi}_E \right) \cdot \boldsymbol{\varphi}_{E'} \\ &= \sigma_{ET} \sigma_{E'T} \frac{|E||E'|}{4\,|T|^2} \int_T \left((\mathbf{d}_T^n)^{-1} (\boldsymbol{x} - \boldsymbol{x}_{ET}^{\mathrm{opp}}) \right) \cdot (\boldsymbol{x} - \boldsymbol{x}_{E'T}^{\mathrm{opp}})\, \mathrm{d}\boldsymbol{x} \,. \end{aligned}$$

The integrand belongs to $\mathbb{P}_2(T)$ and thus the integral can be evaluated exactly by sampling at the barycenters of each edge (cf. Ern & Guermond 2004, Tab. 8.2, p. 360):

$$H_{T,E,E'}^n = \sigma_{ET} \sigma_{E'T} \frac{|E||E'|}{12\,|T|} \sum_{E'' \subset T} \left((\mathbf{d}_T^n)^{-1} (\boldsymbol{x}_{E''}^{\mathrm{bary}} - \boldsymbol{x}_{ET}^{\mathrm{opp}}) \right) \cdot (\boldsymbol{x}_{E''}^{\mathrm{bary}} - \boldsymbol{x}_{E'T}^{\mathrm{opp}}) \,.$$

An alternative to the quadrature above is the use of the Piola transformation as described in Section 4.3.3. For vector-valued functions, we have the transformation rule (cf. Durán 2008, (22), p. 12)

$$\boldsymbol{v}(\boldsymbol{x}) = \boldsymbol{v}(\boldsymbol{F}(\hat{\boldsymbol{x}})) = \frac{\boldsymbol{\nabla}\mathbf{F}}{\det \boldsymbol{\nabla}\mathbf{F}} \hat{\boldsymbol{v}}(\hat{\boldsymbol{x}}) \,. \tag{4.18a}$$

The form functions as given in Definition 4.14 simplify to

$$\hat{\boldsymbol{\varphi}}_1(\hat{\boldsymbol{x}}) = \sqrt{2}\hat{\boldsymbol{x}} \,, \quad \hat{\boldsymbol{\varphi}}_2(\hat{\boldsymbol{x}}) = \hat{\boldsymbol{x}} - \begin{pmatrix} 1 \\ 0 \end{pmatrix} , \quad \hat{\boldsymbol{\varphi}}_3(\hat{\boldsymbol{x}}) = \hat{\boldsymbol{x}} - \begin{pmatrix} 0 \\ 1 \end{pmatrix} \tag{4.18b}$$

on the reference triangle $\hat{T}$ (cf. Fig. 4.2) with $\hat{\varphi}_k := \hat{\varphi}_{\hat{E}_k}$. Equation (4.18) can be used to integrate $H^n_{\hat{T},E,E'}$ *exactly* on $\hat{T}$ in the manner of Section 4.3.3. However, when transforming T to $\hat{T}$, attention has to be paid to the edge signs $\sigma_{E_k T}$.

Remark 4.16 (Solving the linear algebra system). The linear algebra system (4.13), which has to be solved for each time step $n \in \{1, \dots, N\}$, has a *saddle point* structure. The paper of Benzi et al. (2005) provides an extensive review of iterative methods for large sparse systems of this type. We succeeded both with direct solvers from the package UMFPACK (Davis 2004) and with the iterative solver provided by ILUPACK (Bollhöfer & Saad 2006; Bollhöfer et al. 2011, and further publications of M. Bollhöfer) that uses preconditioned Krylov subspace methods. In the case of balance constraints (cf. (4.15)), we obtain a rectangular system of equations with a rank deficiency of one. This system admits a unique solution that is computed by a sparse QR decomposition (SPQR), also contained in the package UMFPACK (Davis 2011). The algorithm SPQR is rank-revealing, i. e., it effectively results in a pseudo-quadratic upper triangular system of full rank. △

4.3 Discretization of Equations of Stokes Type

This section presents the discretization of the stationary Stokes equations (cf. {(1.1), (1.3)}) equipped with two different types of boundary conditions using mixed finite elements of Taylor–Hood type.

4.3.1 Formulation of the Weak Problems

Model equations. Consider the following model problem in a domain $\Omega \subset \mathbb{R}^2$ with boundary $\partial\Omega = \partial\Omega_D \cup \partial\Omega_N$ that decomposes into a non-empty and closed Dirichlet part $\partial\Omega_D$ and a Neumann part $\partial\Omega_N$:

$$-\mu\Delta \boldsymbol{u} + \boldsymbol{\nabla} p = \boldsymbol{f} \quad \text{in } \Omega\,, \tag{4.19a}$$

$$\boldsymbol{\nabla} \cdot \boldsymbol{u} = 0 \quad \text{in } \Omega\,, \tag{4.19b}$$

$$\boldsymbol{u} = \boldsymbol{u}_D \quad \text{on } \partial\Omega_D\,, \tag{4.19c}$$

$$(\mu \boldsymbol{\nabla} \boldsymbol{u} - p\,\mathbf{I})\,\boldsymbol{\nu} = \mathbf{0} \quad \text{on } \partial\Omega_N \tag{4.19d}$$

with the unknowns $\boldsymbol{u} = (u, v)^{\mathrm{T}} : \Omega \to \mathbb{R}^2$, the *liquid velocity*, and $p : \Omega \to \mathbb{R}$, the *liquid pressure*, and the following given data: $\mu \in \mathbb{R}^+$, $\boldsymbol{f} = (f^x, f^y)^{\mathrm{T}} : \Omega \to \mathbb{R}^2$, $\boldsymbol{u}_{\mathrm{D}} = (u_{\mathrm{D}}, v_{\mathrm{D}})^{\mathrm{T}} : \partial\Omega_{\mathrm{D}} \to \mathbb{R}^2$. Moreover, let $\mathbf{I}$ denote the identity matrix. If $\partial\Omega_{\mathrm{N}} = \emptyset$, the pressure p is defined only up to a constant. Hence, in this case, we additionally demand that $\fint_\Omega p = 0$ holds.

Remark 4.17 (Boundary conditions for the Stokes problem). In applications the Dirichlet boundary condition (4.19c) prescribes the velocity at inflow boundaries or the condition at the solid–liquid interface. The latter case is termed *no-slip condition* for which $\boldsymbol{u}_{\mathrm{D}} = \mathbf{0}$ is demanded. The Neumann condition (4.19d) realizes a "free" boundary that serves as inflow and / or outflow boundary in the sense that the normal velocity on $\partial\Omega_{\mathrm{N}}$ automatically adjusts itself such that mass is conserved globally, i. e., $\int_{\partial\Omega} \boldsymbol{u} \cdot \boldsymbol{\nu} \, \mathrm{d}s_{\boldsymbol{x}} = 0$ holds. For a more detailed discussion we refer to the books of Elman et al. (2005, Chap. 5) and Gross & Reusken (2011, Sec. 1.2). △

Weak continuous formulation. We define the constrained ansatz space

$$\boldsymbol{H}^1_{\boldsymbol{a},\partial\Omega_{\mathrm{D}}}(\Omega) \coloneqq \left\{ \boldsymbol{s} \in \boldsymbol{H}^1(\Omega);\ \boldsymbol{s}|_{\partial\Omega_{\mathrm{D}}} = \boldsymbol{a} \right\}$$

with $\boldsymbol{a} \in \boldsymbol{H}^{1/2}(\partial\Omega_{\mathrm{D}})$, i. e., the Dirichlet boundary condition is the *essential boundary condition* here. By choosing the test functions $(\boldsymbol{s}, w) \in \boldsymbol{H}^1_{\mathbf{0},\partial\Omega_{\mathrm{D}}}(\Omega) \times L^2(\Omega)$, integrating over Ω, and integrating by parts we obtain the *continuous variational problem* with respect to (4.19):

Problem 4.18 (Weak continuous Stokes problem). *Let $\boldsymbol{f} \in \boldsymbol{L}^2(\Omega)$, $\mu \in \mathbb{R}^+$ be given. Seek $(\boldsymbol{u}, p) \in \boldsymbol{H}^1_{\boldsymbol{u}_{\mathrm{D}},\partial\Omega_{\mathrm{D}}}(\Omega) \times L^2(\Omega)$ such that*

$$\begin{aligned} \forall \boldsymbol{s} \in \boldsymbol{H}^1_{\mathbf{0},\partial\Omega_{\mathrm{D}}}(\Omega), \qquad & \mu(\boldsymbol{\nabla u}\,,\, \boldsymbol{\nabla s})_{\mathbf{L}^2(\Omega)} - (p\,,\, \boldsymbol{\nabla}\cdot\boldsymbol{s})_{L^2(\Omega)} = (\boldsymbol{f}\,,\, \boldsymbol{s})_{\boldsymbol{L}^2(\Omega)}\,, \\ \forall w \in L^2(\Omega), \qquad & (\boldsymbol{\nabla}\cdot\boldsymbol{u}\,,\, w)_{L^2(\Omega)} = 0\,. \end{aligned}$$

Recall that the $\mathbf{L}^2(\Omega)$ scalar product is defined by $(\boldsymbol{\nabla u}\,,\, \boldsymbol{\nabla s})_{\mathbf{L}^2(\Omega)} \coloneqq \sum_{i,j=1}^2 \int_\Omega [\boldsymbol{\nabla u}]_{i,j} [\boldsymbol{\nabla s}]_{i,j} \, \mathrm{d}\boldsymbol{x}$. Note that in the first equation of Problem 4.18 the term $\int_{\partial\Omega_{\mathrm{N}}} (\mu \boldsymbol{\nabla u} - p\boldsymbol{I})\boldsymbol{\nu} \cdot \boldsymbol{s} \, \mathrm{d}s_{\boldsymbol{x}}$ appeared after integrating by parts. However, this boundary integral vanishes due to the homogeneous natural boundary condition (4.19d). Problem 4.18 admits a unique solution $(\boldsymbol{u}, p) \in \boldsymbol{H}^1_0(\Omega) \times L^2(\Omega)$, at least for the case of $\partial\Omega_{\mathrm{N}} = \emptyset$ together with a homogeneous Dirichlet boundary condition (cf. Ern & Guermond 2004, Thm. 4.3, p. 178).

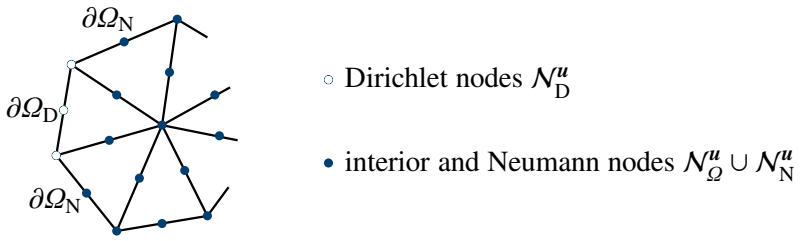

Figure 4.3. Definition of the set of nodes $\mathcal{N}_{\Omega}^{\boldsymbol{u}}$, $\mathcal{N}_{\mathrm{D}}^{\boldsymbol{u}}$, $\mathcal{N}_{\mathrm{N}}^{\boldsymbol{u}}$ for the velocity $\boldsymbol{u}_h$. A vertex $\boldsymbol{x}_N$ with $\boldsymbol{x}_N = \overline{\partial\Omega}_{\mathrm{D}} \cap \overline{\partial\Omega}_{\mathrm{N}}$ is declared as a Dirichlet node $N \in \mathcal{N}_{\mathrm{D}}^{\boldsymbol{u}}$. The degrees of freedom are located on $\mathcal{N}_{\Omega}^{\boldsymbol{u}} \cup \mathcal{N}_{\mathrm{N}}^{\boldsymbol{u}}$.

Weak discrete formulation. For $k \in \mathbb{N}$, let

$$\mathbb{P}_k^{\mathrm{c}}(\mathcal{T}_h) \;\coloneqq\; \mathbb{P}_k(\mathcal{T}_h) \cap C^0(\overline{\Omega}) \;\subset\; H^1(\Omega) \tag{4.20}$$

denote the global polynomial space on the triangulation $\mathcal{T}_h$ that is piecewise polynomial of order k (cf. (3.6)) and globally continuous. Analogously, let $\mathbb{P}_k^{\mathrm{c}}(\mathcal{E})$ be the edgewise polynomial, globally continuous space. We define the finite-dimensional subspace $\boldsymbol{S}_h^{\boldsymbol{a},\partial\Omega_{\mathrm{D}}} \subset \boldsymbol{H}^1_{\boldsymbol{a},\partial\Omega_{\mathrm{D}}}(\Omega)$ by

$$\boldsymbol{S}_h^{\boldsymbol{a}_h,\partial\Omega_{\mathrm{D}}} \;\coloneqq\; \boldsymbol{H}^1_{\boldsymbol{a}_h,\partial\Omega_{\mathrm{D}}}(\Omega) \cap \mathbb{P}_2^{\mathrm{c}}(\mathcal{T}_h)^2$$

with $\boldsymbol{a}_h \in \mathbb{P}_2^{\mathrm{c}}(\mathcal{E}_{\mathrm{D}})^2$. Thus, the discrete velocity space consists of globally continuous, piecewise quadratic functions and the discrete pressure space of globally continuous, piecewise linear functions. The associated finite element is referred to as Taylor–Hood element (cf. Hood & Taylor 1973; Girault & Raviart 1986, Sec. 4.2). For the analysis of Taylor–Hood schemes see, e. g., Bercovier & Pironneau (1979) and Brezzi & Falk (1991).

We are now able to formulate the discrete version of Problem 4.18, the *fully discrete variational problem*:

Problem 4.19 (Weak discrete Stokes problem). *Let $\boldsymbol{f} \in \boldsymbol{L}^2(\Omega)$, $\mu \in \mathbb{R}^+$ be given. Seek $(\boldsymbol{u}_h, p_h) \in \boldsymbol{S}_h^{0,\partial\Omega_{\mathrm{D}}} \times \mathbb{P}_1^{\mathrm{c}}(\mathcal{T}_h)$ such that*

$$\begin{aligned} \forall \boldsymbol{s}_h \in \boldsymbol{S}_h^{\boldsymbol{a}_h,\partial\Omega_{\mathrm{D}}}, \qquad & \mu(\boldsymbol{\nabla}\boldsymbol{u}_h\,,\,\boldsymbol{\nabla}\boldsymbol{s}_h)_{\mathbf{L}^2(\Omega)} - (p_h\,,\,\boldsymbol{\nabla}\cdot\boldsymbol{s}_h)_{L^2(\Omega)} \;=\; (\boldsymbol{f}\,,\,\boldsymbol{s}_h)_{\boldsymbol{L}^2(\Omega)}\,, \\ \forall w_h \in \mathbb{P}_1^{\mathrm{c}}(\mathcal{T}_h), \qquad & (\boldsymbol{\nabla}\cdot\boldsymbol{u}_h\,,\,w_h)_{L^2(\Omega)} \;=\; 0\,. \end{aligned}$$

4.3.2 Matrix Formulation

Following the idea of Elman et al. (2005, Sec. 5.3), we derive the linear system of equations that is equivalent to Problem 4.19.

Basis representation. Let $\mathcal{N}^{\boldsymbol{u}} := \mathcal{N}^{\boldsymbol{u}}_{\Omega} \cup \mathcal{N}^{\boldsymbol{u}}_{\mathrm{D}} \cup \mathcal{N}^{\boldsymbol{u}}_{\mathrm{N}}$ be the set of velocity nodes consisting of the union of vertices $\mathcal{V}$ and edge barycenters $\{\boldsymbol{x}_E^{\mathrm{bary}}\}_E$ as described in Figure 4.3, and let $\mathcal{N}^p := \mathcal{V}$ denote the set of pressure nodes. Thus, the solution for the vector-valued unknown $\boldsymbol{u}_h$ can be expressed by

$$\boldsymbol{S}_h^{\boldsymbol{a}_h,\partial\Omega_{\mathrm{D}}} \ni \boldsymbol{u}_h(\boldsymbol{x}) \;=\; \sum_{N\in\mathcal{N}^{\boldsymbol{u}}} u_N \begin{pmatrix} \phi_N(\boldsymbol{x}) \\ 0 \end{pmatrix} + \sum_{N\in\mathcal{N}^{\boldsymbol{u}}} v_N \begin{pmatrix} 0 \\ \phi_N(\boldsymbol{x}) \end{pmatrix}, \tag{4.21}$$

keeping in mind that u_N and v_N are prescribed by the Dirichlet data $\boldsymbol{u}_{\mathrm{D}}$ on $\partial\Omega_{\mathrm{D}}$, where $\{\phi_N\}_N$ is the nodal basis of $\mathbb{P}^{\mathrm{c}}_2(\mathcal{T}_h)$. Clearly, $\phi_N(\boldsymbol{x}_{N'}) = \delta_{NN'}$ holds for $N, N' \in \mathcal{N}^{\boldsymbol{u}}$. Hence, u_N and v_N are the coordinates of the components of u_h with respect to $\{\phi_N\}$ and

$$\mathbb{P}^{\mathrm{c}}_2(\mathcal{T}_h)^2 \;=\; \operatorname{span}\left\{(\phi_N, 0)^{\mathrm{T}}, (0, \phi_N)^{\mathrm{T}}\right\}_N .$$

The pressure solution is represented by

$$W_h \ni p_h(\boldsymbol{x}) \;=\; \sum_{N\in\mathcal{N}^p} p_N \psi_N(\boldsymbol{x}) \tag{4.22}$$

with $\{\psi_N\}_N$ being the basis of $\mathbb{P}^{\mathrm{c}}_1(\mathcal{T}_h)$. Similarly, $\psi_N(\boldsymbol{x}_{N'}) = \delta_{NN'}$ for $N, N' \in \mathcal{N}^p$. We assume for the discrete coefficients that $\boldsymbol{u}_{\mathrm{D},h} \in \mathbb{P}^{\mathrm{c}}_2(\mathcal{E}_{\mathrm{D}})^2$ and $\boldsymbol{f}_h \in \mathbb{P}^{\mathrm{c}}_2(\mathcal{T})^2$ holds using a similar coordinate notation as in (4.21). For the sake of presentation, we suppress the index h in the following.

Linear algebra system. In this paragraph, we abbreviate the $L^2(\Omega)$ and the $\boldsymbol{L}^2(\Omega)$ scalar product by $(\cdot\,,\cdot)$. With

$$\boldsymbol{s}_h \;=\; \begin{pmatrix} \phi_{N'} \\ 0 \end{pmatrix}, \begin{pmatrix} 0 \\ \phi_{N'} \end{pmatrix} \text{ for } N' \in \mathcal{N}^{\boldsymbol{u}}_{\Omega} \cup \mathcal{N}^{\boldsymbol{u}}_{\mathrm{N}} \qquad \text{and} \qquad w_h \;=\; \psi_{N'} \text{ for } N' \in \mathcal{N}^p$$

and taking into account that there are no degrees of freedom on Dirichlet nodes, we obtain the following system of equations, which has saddle-point structure:

$$\mu \sum_{N \in \mathcal{N}_\Omega^{\boldsymbol{u}} \cup \mathcal{N}_\mathrm{N}^{\boldsymbol{u}}} u_N \, (\boldsymbol{\nabla} \phi_N \, , \, \boldsymbol{\nabla} \phi_{N'}) - \sum_{N \in \mathcal{N}^p} p_N \, (\psi_N \, , \, \partial_x \phi_{N'}) \;=\; (f^x \, , \, \phi_{N'}) - \mu \sum_{N \in \mathcal{N}_\mathrm{D}^{\boldsymbol{u}}} u_\mathrm{D}|_N \, (\boldsymbol{\nabla} \phi_N \, , \, \boldsymbol{\nabla} \phi_{N'}) \, ,$$
$$\text{for } N' \in \mathcal{N}_\Omega^{\boldsymbol{u}} \cup \mathcal{N}_\mathrm{N}^{\boldsymbol{u}} \, ,$$

$$\mu \sum_{N \in \mathcal{N}_\Omega^{\boldsymbol{u}} \cup \mathcal{N}_\mathrm{N}^{\boldsymbol{u}}} v_N \, (\boldsymbol{\nabla} \phi_N \, , \, \boldsymbol{\nabla} \phi_{N'}) - \sum_{N \in \mathcal{N}^p} p_N \, (\psi_N \, , \, \partial_y \phi_{N'}) \;=\; (f^y \, , \, \phi_{N'}) - \mu \sum_{N \in \mathcal{N}_\mathrm{D}^{\boldsymbol{u}}} v_\mathrm{D}|_N \, (\boldsymbol{\nabla} \phi_N \, , \, \boldsymbol{\nabla} \phi_{N'})$$
$$\text{for } N' \in \mathcal{N}_\Omega^{\boldsymbol{u}} \cup \mathcal{N}_\mathrm{N}^{\boldsymbol{u}} \, ,$$

$$\sum_{N \in \mathcal{N}_\Omega^{\boldsymbol{u}} \cup \mathcal{N}_\mathrm{N}^{\boldsymbol{u}}} \Big(u_N(\psi_{N'} \, , \, \partial_x \phi_N) + v_N(\psi_{N'} \, , \, \partial_y \phi_N) \Big) \;=\; - \sum_{N \in \mathcal{N}_\mathrm{D}^{\boldsymbol{u}}} \Big(u_\mathrm{D}|_N(\psi_{N'} \, , \, \partial_x \phi_N) + v_\mathrm{D}|_N(\psi_{N'} \, , \, \partial_y \phi_N) \Big)$$
$$\text{for } N' \in \mathcal{N}^p \, ,$$

or equivalently,

$$\begin{bmatrix} \mu \mathbf{A} & & \mathbf{B}^\mathrm{T} \\ & \mu \mathbf{A} & \mathbf{C}^\mathrm{T} \\ \mathbf{B} & \mathbf{C} & \end{bmatrix} \begin{pmatrix} \boldsymbol{U} \\ \boldsymbol{V} \\ \boldsymbol{P} \end{pmatrix} = \begin{pmatrix} \boldsymbol{b}^u \\ \boldsymbol{b}^v \\ \boldsymbol{b}^p \end{pmatrix} , \tag{4.23}$$

where

$$\mathbf{A} \;=\; \Big[A_{N'N} \Big]_{N', N \in \mathcal{N}_\Omega^{\boldsymbol{u}} \cup \mathcal{N}_\mathrm{N}^{\boldsymbol{u}}} \, , \qquad \mathbf{B} \;=\; \Big[B_{N'N} \Big]_{N' \in \mathcal{N}^p, N \in \mathcal{N}_\Omega^{\boldsymbol{u}} \cup \mathcal{N}_\mathrm{N}^{\boldsymbol{u}}} \, , \qquad \mathbf{C} \;=\; \Big[C_{N'N} \Big]_{N' \in \mathcal{N}^p, N \in \mathcal{N}_\Omega^{\boldsymbol{u}} \cup \mathcal{N}_\mathrm{N}^{\boldsymbol{u}}} \, ,$$
$$\boldsymbol{b}^u \;=\; \Big(b^u_{N'} \Big)_{N' \in \mathcal{N}_\Omega^{\boldsymbol{u}} \cup \mathcal{N}_\mathrm{N}^{\boldsymbol{u}}} \, , \qquad \boldsymbol{b}^v \;=\; \Big(b^v_{N'} \Big)_{N' \in \mathcal{N}_\Omega^{\boldsymbol{u}} \cup \mathcal{N}_\mathrm{N}^{\boldsymbol{u}}} \, , \qquad \boldsymbol{b}^p \;=\; \Big(b^p_{N'} \Big)_{N' \in \mathcal{N}^p}$$

with

$$A_{N'N} = (\boldsymbol{\nabla} \phi_N \, , \, \boldsymbol{\nabla} \phi_{N'}) \, , \qquad B_{N'N} = (\psi_{N'} \, , \, \partial_x \phi_N) \, , \qquad C_{N'N} = (\psi_{N'} \, , \, \partial_y \phi_N) \, ,$$
$$b^u_{N'} = (f^x \, , \, \phi_{N'}) - \mu \sum_{N \in \mathcal{N}_\mathrm{D}^{\boldsymbol{u}}} A_{N'N} \, u_\mathrm{D}|_N \, , \qquad b^v_{N'} = (f^y \, , \, \phi_{N'}) - \mu \sum_{N \in \mathcal{N}_\mathrm{D}^{\boldsymbol{u}}} A_{N'N} \, v_\mathrm{D}|_N \, ,$$
$$b^p_{N'} = - \sum_{N \in \mathcal{N}_\mathrm{D}^{\boldsymbol{u}}} \Big(B_{N'N} \, u_\mathrm{D}|_N + C_{N'N} \, v_\mathrm{D}|_N \Big)$$

and the following *representation vectors* of the solution of Problem 4.19 with respect to the bases of $\mathbb{P}_2^\mathrm{c}(\mathcal{T}_h)$, $\mathbb{P}_2^\mathrm{c}(\mathcal{T}_h)$, and $\mathbb{P}_1^\mathrm{c}(\mathcal{T}_h)$, respectively:

$$\boldsymbol{U} \;=\; \Big(u_N \Big)_{N \in \mathcal{N}_\Omega^{\boldsymbol{u}} \cup \mathcal{N}_\mathrm{N}^{\boldsymbol{u}}} \, , \qquad \boldsymbol{V} \;=\; \Big(v_N \Big)_{N \in \mathcal{N}_\Omega^{\boldsymbol{u}} \cup \mathcal{N}_\mathrm{N}^{\boldsymbol{u}}} \, , \qquad \boldsymbol{P} \;=\; \Big(p_N \Big)_{N \in \mathcal{N}^p} \, .$$

A representative structure of the large sparse matrix in (4.23) is illustrated in Figure 4.4 (b).

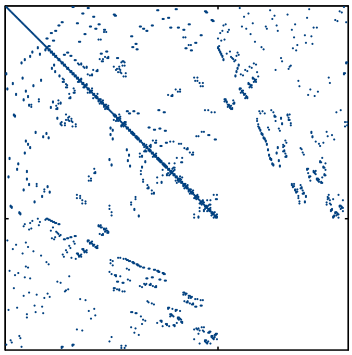

DOF = 315, NNZ = 1 635 (a)

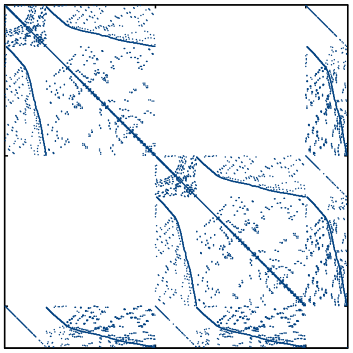

DOF = 612, NNZ = 7 475 (b)

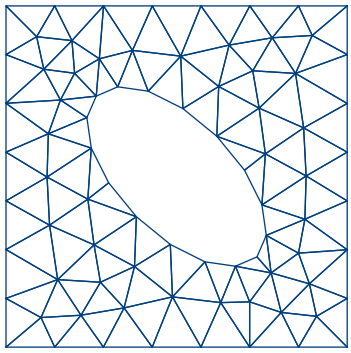

$\#\mathcal{T}$ =120, $\#\mathcal{E}$=195, $\#V$=74 (c)

Figure 4.4. Representative sparse matrix structure of the system of equations for (a) convection–diffusion type problems (cf. (4.13), p. 74), and for (b) Stokes type problems (cf. (4.23), p. 84) on (c) a grid (DOF: degrees of freedom; NNZ: number of non-zero entries).

Pressure-balance constraint. If $\partial\Omega_{\mathrm{N}} = \emptyset$ then the pressure solution is defined only up to a constant and the system of equations (4.23) has a rank deficiency of one. To introduce a constraint in order to reobtain uniqueness of the pressure, we define a *pressure-balance constraint* by demanding the mean pressure to be equal to a constant b^λ, i. e., $\fint_\Omega p_h \overset{!}{=} b^\lambda$, which can be reformulated by means of the basis representation (4.22) of p_h to

$$\sum_{N\in\mathcal{N}^p} p_N \,(\psi_N\,,\,1)_{L^2(\Omega)} \;=\; |\Omega|\, b^\lambda \;.$$

With

$$\boldsymbol{D} \;=\; \big(D_N\big)_{N\in\mathcal{N}^p}\,, \qquad \text{where} \qquad D_N \;\coloneqq\; (\psi_N\,,\,1)_{L^2(\Omega)}$$

the pressure balance can be written as $\boldsymbol{D}\cdot\boldsymbol{P} = |\Omega|\, b^\lambda$ and be appended to (4.23). As a few linear algebra solvers require quadratic or even more symmetric systems, we further append a column as follows:

$$\begin{bmatrix} \mu\mathbf{A} & & \mathbf{B}^{\mathrm{T}} & \\ & \mu\mathbf{A} & \mathbf{C}^{\mathrm{T}} & \\ \mathbf{B} & \mathbf{C} & & \boldsymbol{D} \\ & & \boldsymbol{D}^{\mathrm{T}} & 1 \end{bmatrix} \begin{pmatrix} \boldsymbol{U} \\ \boldsymbol{V} \\ \boldsymbol{P} \\ \lambda \end{pmatrix} = \begin{pmatrix} \boldsymbol{b}^u \\ \boldsymbol{b}^v \\ \boldsymbol{b}^p \\ |\Omega|\, b^\lambda \end{pmatrix}. \tag{4.24}$$

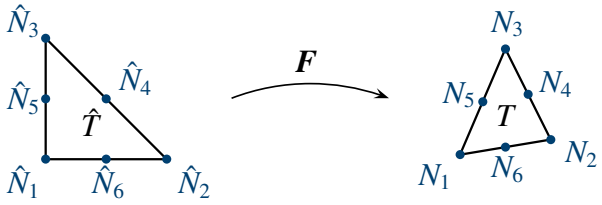

Figure 4.5. The affine mapping $\boldsymbol{F}$ transforms the reference triangle $\hat{T}$ to some triangle T with *local* nodes N_k. The orientation is maintained under $\boldsymbol{F}$.

The vector $\boldsymbol{D}$ is assembled elementwise, similar to the term $(f^x, \phi_{N'})_{L^2(\Omega)}$ in (4.23). Note that the solution of (4.24) must satisfy $\lambda = 0$ and that the symmetry of the system of equations (4.24) is preserved.

4.3.3 Assembly

The integration of the terms appearing in (4.23) is performed *exactly* after transformation to the reference triangle $\hat{T}$ by the Piola transformation (cf. Chen (2005), Durán (2008), and Knabner & Angermann (2003), and Fig. 4.5). We therefore define the affine one-to-one mapping $\boldsymbol{F} : \hat{T} \ni \hat{\boldsymbol{x}} \mapsto \boldsymbol{x} \in T$ and further the function $\hat{w} : \hat{T} \to \mathbb{R}$ for a $w : T \to \mathbb{R}$ by $\hat{w} = w \circ \boldsymbol{F}$, i. e., $w(\boldsymbol{x}) = \hat{w}(\hat{\boldsymbol{x}})$. Application of the chain rule yields

$$\hat{\boldsymbol{\nabla}} u(\boldsymbol{x}) = \hat{\boldsymbol{\nabla}} u(\boldsymbol{F}(\hat{\boldsymbol{x}})) = \begin{pmatrix} \partial_x u(\boldsymbol{x})\, \partial_{\hat{x}} F^x(\hat{\boldsymbol{x}}) + \partial_y u(\boldsymbol{x})\, \partial_{\hat{x}} F^y(\hat{\boldsymbol{x}}) \\ \partial_x u(\boldsymbol{x})\, \partial_{\hat{y}} F^x(\hat{\boldsymbol{x}}) + \partial_y u(\boldsymbol{x})\, \partial_{\hat{y}} F^y(\hat{\boldsymbol{x}}) \end{pmatrix} = \left(\hat{\boldsymbol{\nabla}} \mathbf{F}(\hat{\boldsymbol{x}})\right)^{\mathrm{T}} \boldsymbol{\nabla} u(\boldsymbol{x}) = \left(\boldsymbol{\nabla} \mathbf{F}\right)^{\mathrm{T}} \boldsymbol{\nabla} u(\boldsymbol{x}),$$

with the notations $\hat{\boldsymbol{\nabla}} = (\partial_{\hat{x}}, \partial_{\hat{y}})^{\mathrm{T}}$, $\boldsymbol{F} = (F^x, F^y)^{\mathrm{T}}$ used. In short terms,

$$\boldsymbol{\nabla} \;=\; \left(\boldsymbol{\nabla} \mathbf{F}\right)^{-\mathrm{T}} \hat{\boldsymbol{\nabla}} \,. \tag{4.25}$$

The affine mapping can be expressed explicitly in terms of the vertices $\boldsymbol{x}_k$ of T by

$$\boldsymbol{F} : \quad \hat{\boldsymbol{x}} \mapsto \underbrace{\left[\boldsymbol{x}_2 - \boldsymbol{x}_1 \middle| \boldsymbol{x}_3 - \boldsymbol{x}_1\right]}_{=\boldsymbol{\nabla}\mathbf{F}} \hat{\boldsymbol{x}} + \boldsymbol{x}_1 \,. \tag{4.26}$$

Eventually, we need an explicit representation of the local spaces $\mathbb{P}_1^{\mathrm{c}}(T) = \mathrm{span}\{\psi_{N_k}\}_{k\in\{1,2,3\}}$ and $\mathbb{P}_2^{\mathrm{c}}(T) = \mathrm{span}\{\phi_{N_k}\}_{k\in\{1,\ldots,6\}}$. Here, $N_k = \boldsymbol{x}_k$ denote the local nodes on a considered tri-

angle T (cf. Fig. 4.3). With the abbreviations $\psi_k := \psi_{N_k}$, the linear basis functions ψ_k are simply the barycentric coordinates on T:

$$\psi_1(\boldsymbol{x}) = \frac{1}{2|T|}\det\begin{bmatrix} x & y & 1 \\ x_2 & y_2 & 1 \\ x_3 & y_3 & 1 \end{bmatrix},\ \psi_2(\boldsymbol{x}) = \frac{1}{2|T|}\det\begin{bmatrix} x_1 & y_1 & 1 \\ x & y & 1 \\ x_3 & y_3 & 1 \end{bmatrix},\ \psi_3(\boldsymbol{x}) = \frac{1}{2|T|}\det\begin{bmatrix} x_1 & y_2 & 1 \\ x_2 & y_2 & 1 \\ x & y & 1 \end{bmatrix}$$

with derivatives

$$\begin{aligned} \frac{\partial\psi_1}{\partial x} &= \frac{y_2 - y_3}{2\,|T|}\,, & \frac{\partial\psi_2}{\partial x} &= \frac{y_3 - y_1}{2\,|T|}\,, & \frac{\partial\psi_3}{\partial x} &= \frac{y_1 - y_2}{2\,|T|}\,, \\ \frac{\partial\psi_1}{\partial y} &= \frac{x_3 - x_2}{2\,|T|}\,, & \frac{\partial\psi_2}{\partial y} &= \frac{x_1 - x_3}{2\,|T|}\,, & \frac{\partial\psi_3}{\partial y} &= \frac{x_2 - x_1}{2\,|T|}\,. \end{aligned}$$

Moreover, the quadratic functions ϕ_i are expressed in terms of ψ_k via

$$\phi_i = \psi_i(2\psi_i - 1)\,, \qquad \phi_{ij} = 4\psi_i\psi_j\,, \quad i \neq j \quad \text{for} \quad i, j \in \{1, 2, 3\}$$

with derivatives

$$\begin{aligned} \frac{\partial\phi_i}{\partial x} &= \frac{\partial\psi_i}{\partial x}\Big(4\psi_i - 1\Big), & \frac{\partial\phi_i}{\partial y} &= \frac{\partial\psi_i}{\partial y}\Big(4\psi_i - 1\Big), \\ \frac{\partial\phi_{ij}}{\partial x} &= 4\left(\psi_i\frac{\partial\psi_j}{\partial x} + \psi_j\frac{\partial\psi_i}{\partial x}\right), & \frac{\partial\phi_{ij}}{\partial y} &= 4\left(\psi_i\frac{\partial\psi_j}{\partial y} + \psi_j\frac{\partial\psi_i}{\partial y}\right), \end{aligned}$$

where $\phi_{23} := \phi_4$, $\phi_{13} := \phi_5$, $\phi_{12} := \phi_6$. On the reference triangle $\hat{T}$, the linear basis functions simplify to

$$\hat{\psi}_1(\hat{\boldsymbol{x}}) = 1 - \hat{x} - \hat{y}\,, \qquad \hat{\psi}_2(\hat{\boldsymbol{x}}) = \hat{x}\,, \qquad \hat{\psi}_3(\hat{\boldsymbol{x}}) = \hat{y}$$

with the following derivatives:

$$\frac{\partial\hat{\psi}_1}{\partial\hat{x}} = -1\,, \quad \frac{\partial\hat{\psi}_2}{\partial\hat{x}} = 1\,, \quad \frac{\partial\hat{\psi}_3}{\partial\hat{x}} = 0\,, \quad \frac{\partial\hat{\psi}_1}{\partial\hat{y}} = -1\,, \quad \frac{\partial\hat{\psi}_2}{\partial\hat{y}} = 0\,, \quad \frac{\partial\hat{\psi}_3}{\partial\hat{y}} = 1\,.$$

With these preparations we continue with the description of the assembly of the sparse matrices $\mathbf{A}$, $\mathbf{B}$, $\mathbf{C}$ and of the vectors $\boldsymbol{b}^u$, $\boldsymbol{b}^v$ in the large system of equations (4.23).

Assembly of A. Decomposition of the integral yields

$$A_{N'N} \;=\; \sum_{T\in\mathcal{T}_h} \int_T \boldsymbol{\nabla}\phi_N \cdot \boldsymbol{\nabla}\phi_{N'} \;,$$

where $N,\, N' \in \mathcal{N}_\Omega^{\boldsymbol{u}} \cup \mathcal{N}_{\mathrm{N}}^{\boldsymbol{u}}$ denote the (global) nodes. Let again $N_k,\, k \in \{1,\dots,6\}$ denote the local nodes on a considered triangle T. We define the local assembly matrix $\mathbf{A}_T \in \mathbb{R}^{6,6}$ by

$$\left[\mathbf{A}_T\right]_{l,k} \;=\; \int_T \boldsymbol{\nabla}\phi_{N_k} \cdot \boldsymbol{\nabla}\phi_{N_l} \quad \text{such that} \quad \mathbf{A} \;=\; \mathop{\mathrm{A}}_{T\in\mathcal{T}_h} \mathbf{A}_T \;,$$

with A denoting the *assembly operator* that maps the element contribution to the global matrix (cf. Bathe 2007; Hughes 2000). Using the abbreviations $\phi_k \coloneqq \phi_{N_k}$, $\hat{\phi}_k \coloneqq \hat{\phi}_{\hat{N}_k}$, there holds

$$\begin{aligned}
\int_T \boldsymbol{\nabla}\phi_k(\boldsymbol{x}) \cdot \boldsymbol{\nabla}\phi_l(\boldsymbol{x})\,\mathrm{d}\boldsymbol{x} \;&=\; \int_{\hat{T}} \boldsymbol{\nabla}\phi_k(\boldsymbol{F}(\hat{\boldsymbol{x}})) \cdot \boldsymbol{\nabla}\phi_l(\boldsymbol{F}(\hat{\boldsymbol{x}}))\,\det\boldsymbol{\nabla}\mathbf{F}\,\mathrm{d}\hat{\boldsymbol{x}} \\
&\overset{(4.25)}{=} \int_{\hat{T}} (\boldsymbol{\nabla}\mathbf{F})^{-\mathrm{T}}\hat{\boldsymbol{\nabla}}\phi_k(\boldsymbol{F}(\hat{\boldsymbol{x}})) \cdot (\boldsymbol{\nabla}\mathbf{F})^{-\mathrm{T}}\hat{\boldsymbol{\nabla}}\phi_l(\boldsymbol{F}(\hat{\boldsymbol{x}}))\,\det\boldsymbol{\nabla}\mathbf{F}\,\mathrm{d}\hat{\boldsymbol{x}} \\
&=\; \int_{\hat{T}} (\boldsymbol{\nabla}\mathbf{F})^{-\mathrm{T}}\hat{\boldsymbol{\nabla}}\hat{\phi}_k(\hat{\boldsymbol{x}}) \cdot (\boldsymbol{\nabla}\mathbf{F})^{-\mathrm{T}}\hat{\boldsymbol{\nabla}}\hat{\phi}_l(\hat{\boldsymbol{x}})\,\det\boldsymbol{\nabla}\mathbf{F}\,\mathrm{d}\hat{\boldsymbol{x}} \\
&=\; \int_{\hat{T}} \mathbf{G}\,\hat{\boldsymbol{\nabla}}\hat{\phi}_k(\hat{\boldsymbol{x}}) \cdot \hat{\boldsymbol{\nabla}}\hat{\phi}_l(\hat{\boldsymbol{x}})\,\mathrm{d}\hat{\boldsymbol{x}}
\end{aligned} \tag{4.27a}$$

with

$$\begin{aligned}
\mathbf{G} \;=\; \left[G_{ij}\right]_{i,j=1,2} \;&=\; (\boldsymbol{\nabla}\mathbf{F})^{-1}(\boldsymbol{\nabla}\mathbf{F})^{-\mathrm{T}}\det\boldsymbol{\nabla}\mathbf{F} \;=\; \left((\boldsymbol{\nabla}\mathbf{F})^{\mathrm{T}}\,\boldsymbol{\nabla}\mathbf{F}\right)^{-1}\det\boldsymbol{\nabla}\mathbf{F} \\
&\overset{(4.26)}{=} \frac{1}{2\,|T|}\begin{bmatrix} [\boldsymbol{\nabla}\mathbf{F}]_2 \cdot [\boldsymbol{\nabla}\mathbf{F}]_2 & -[\boldsymbol{\nabla}\mathbf{F}]_1 \cdot [\boldsymbol{\nabla}\mathbf{F}]_2 \\ \mathrm{sym} & [\boldsymbol{\nabla}\mathbf{F}]_1 \cdot [\boldsymbol{\nabla}\mathbf{F}]_1 \end{bmatrix},
\end{aligned} \tag{4.27b}$$

where $[\boldsymbol{\nabla}\mathbf{F}]_i$ refers to the ith column of $\boldsymbol{\nabla}\mathbf{F}$. Due to the vertex orientation it holds that $0 < \det\boldsymbol{\nabla}\mathbf{F} = 2\,|T|$ for every $T \in \mathcal{T}_h$. Consequently, we are able to express the local assembly matrix $\mathbf{A}_T$ as linear combination of constant matrices:

$$\mathbf{A}_T \;=\; \int_T \begin{bmatrix} \boldsymbol{\nabla}\phi_1 \cdot \boldsymbol{\nabla}\phi_1 & \cdots & \boldsymbol{\nabla}\phi_6 \cdot \boldsymbol{\nabla}\phi_1 \\ \vdots & & \vdots \\ \mathrm{sym} & \cdots & \boldsymbol{\nabla}\phi_6 \cdot \boldsymbol{\nabla}\phi_6 \end{bmatrix} \mathrm{d}\boldsymbol{x} \overset{(4.27)}{=} G_{11} \int_{\hat{T}} \begin{bmatrix} \partial_{\hat{x}}\hat{\phi}_1\partial_{\hat{x}}\hat{\phi}_1 & \cdots & \partial_{\hat{x}}\hat{\phi}_6\partial_{\hat{x}}\hat{\phi}_1 \\ \vdots & & \vdots \\ \mathrm{sym} & \cdots & \partial_{\hat{x}}\hat{\phi}_6\partial_{\hat{x}}\hat{\phi}_6 \end{bmatrix} \mathrm{d}\hat{\boldsymbol{x}}$$

$$+ G_{12} \int_{\hat{T}} \left(\begin{bmatrix} \partial_{\hat{x}}\hat{\phi}_1 \partial_{\hat{y}}\hat{\phi}_1 & \cdots & \partial_{\hat{x}}\hat{\phi}_6 \partial_{\hat{y}}\hat{\phi}_1 \\ \vdots & & \vdots \\ \partial_{\hat{x}}\hat{\phi}_1 \partial_{\hat{y}}\hat{\phi}_6 & \cdots & \partial_{\hat{x}}\hat{\phi}_6 \partial_{\hat{y}}\hat{\phi}_6 \end{bmatrix} + \begin{bmatrix} \partial_{\hat{y}}\hat{\phi}_1 \partial_{\hat{x}}\hat{\phi}_1 & \cdots & \partial_{\hat{y}}\hat{\phi}_6 \partial_{\hat{x}}\hat{\phi}_1 \\ \vdots & & \vdots \\ \partial_{\hat{y}}\hat{\phi}_1 \partial_{\hat{x}}\hat{\phi}_6 & \cdots & \partial_{\hat{y}}\hat{\phi}_6 \partial_{\hat{x}}\hat{\phi}_6 \end{bmatrix} \right) \mathrm{d}\hat{\boldsymbol{x}}$$

$$+ G_{22} \int_{\hat{T}} \begin{bmatrix} \partial_{\hat{y}}\hat{\phi}_1 \partial_{\hat{y}}\hat{\phi}_1 & \cdots & \partial_{\hat{y}}\hat{\phi}_6 \partial_{\hat{y}}\hat{\phi}_1 \\ \vdots & & \vdots \\ \text{sym} & \cdots & \partial_{\hat{y}}\hat{\phi}_6 \partial_{\hat{y}}\hat{\phi}_6 \end{bmatrix} \mathrm{d}\hat{\boldsymbol{x}} \,,$$

which can be integrated exactly.

Assembly of B and C. We decompose the term $B_{N'N}$ as follows:

$$B_{N'N} \;=\; \sum_{T \in \mathcal{T}_h} \int_T \psi_{N'}\, \partial_x \phi_N \quad \text{for} \quad N \in \mathcal{N}_\Omega^{\boldsymbol{u}} \cup \mathcal{N}_{\mathrm{N}}^{\boldsymbol{u}},\; N' \in \mathcal{N}^p.$$

Let again, the indices k, l refer to the local nodes on a considered triangle T (cf. Fig. 4.5). We define the local assembly matrix $\mathbf{B}_T \in \mathbb{R}^{3,6}$ by

$$\left[\mathbf{B}_T\right]_{l,k} \;=\; \int_T \psi_l\, \partial_x \phi_k \quad \text{such that} \quad \mathbf{B} \;=\; \mathop{\mathbf{A}}_{T \in \mathcal{T}_h} \mathbf{B}_T \;.$$

With (4.25), we derive $\partial_x = \left([\boldsymbol{\nabla}\mathbf{F}]_{22}\, \partial_{\hat{x}} - [\boldsymbol{\nabla}\mathbf{F}]_{12}\, \partial_{\hat{y}} \right) \big/ \det \boldsymbol{\nabla}\mathbf{F}$ and thus

$$\left[\mathbf{B}_T\right]_{l,k} \;=\; [\boldsymbol{\nabla}\mathbf{F}]_{22} \int_{\hat{T}} \hat{\psi}_l\, \partial_{\hat{x}} \hat{\phi}_k \,\mathrm{d}\hat{\boldsymbol{x}} - [\boldsymbol{\nabla}\mathbf{F}]_{21} \int_{\hat{T}} \hat{\psi}_l\, \partial_{\hat{y}} \hat{\phi}_k \,\mathrm{d}\hat{\boldsymbol{x}} \;.$$

Analogously, we obtain

$$\left[\mathbf{C}_T\right]_{l,k} \;=\; \int_T \psi_l\, \partial_y \phi_k \,\mathrm{d}\boldsymbol{x} \;=\; -\,[\boldsymbol{\nabla}\mathbf{F}]_{12} \int_{\hat{T}} \hat{\psi}_l\, \partial_{\hat{x}} \hat{\phi}_k \,\mathrm{d}\hat{\boldsymbol{x}} + [\boldsymbol{\nabla}\mathbf{F}]_{11} \int_{\hat{T}} \hat{\psi}_l\, \partial_{\hat{y}} \hat{\phi}_k \,\mathrm{d}\hat{\boldsymbol{x}} \;.$$

Assembly of b^u and b^v. At first, we consider only the first term of $b^u_{N'}$ as given in (4.23). For a homogeneous Dirichlet boundary condition, we have

$$b^u_{N'} \;=\; (f^x,\, \phi_{N'}) \;=\; \sum_{T \in \mathcal{T}_h} \int_T f^x \phi_{N'} \quad \text{for} \quad N' \in \mathcal{N}_\Omega^{\boldsymbol{u}} \cup \mathcal{N}_{\mathrm{N}}^{\boldsymbol{u}} \;.$$

Since $f^x|_T \in \mathbb{P}_2^c(T)$, there is the local basis representation $f^x(\boldsymbol{x})|_T = \sum_{k=1}^6 f_k^x \phi_k(\boldsymbol{x})$ and thus we obtain by transformation to the reference triangle $\hat{T}$

$$\int_T f^x \phi_l \,\mathrm{d}\boldsymbol{x} \;=\; \sum_{k=1}^6 f_k^x \int_T \phi_k \phi_l \,\mathrm{d}\boldsymbol{x} \;=\; 2\,|T| \sum_{k=1}^6 f_k^x \int_{\hat{T}} \hat{\phi}_k \hat{\phi}_l \,\mathrm{d}\hat{\boldsymbol{x}} \quad \text{for} \quad l \in \{1,\ldots,6\}\,.$$

Let $\boldsymbol{f}_T^{x,\mathrm{loc}} \in \mathbb{R}^6$ denote the vector of the first component of $\boldsymbol{f}$ evaluated at the six nodes of T. Furthermore, let $\mathbf{E}_T \in \mathbb{R}^{6,6}$ be the local assembly matrix defined by

$$\left[\mathbf{E}_T\right]_{l,k} \;:=\; \int_T \phi_k\, \phi_l \;,$$

where after transformation to the reference triangle $\hat{T}$

$$\mathbf{E}_T \;=\; 2\,|T| \int_{\hat{T}} \begin{bmatrix} \hat{\phi}_1\hat{\phi}_1 & \cdots & \hat{\phi}_1\hat{\phi}_6 \\ \vdots & & \vdots \\ \mathrm{sym} & \cdots & \hat{\phi}_6\hat{\phi}_6 \end{bmatrix} \mathrm{d}\hat{\boldsymbol{x}}\,. \tag{4.28}$$

Then, the local assembly vector $\boldsymbol{b}_T^u$ with $\boldsymbol{b}^u = \mathrm{A}_{T\in\mathcal{T}_h} \boldsymbol{b}_T^u$ is expressed by a matrix vector product with the local assembly matrix $\mathbf{E}_T$ (cf. (4.28)):

$$\mathbb{R}^6 \ni \boldsymbol{b}_T^u \;=\; \mathbf{E}_T\, \boldsymbol{f}_T^{x,\mathrm{loc}}\,.$$

The vector $\boldsymbol{b}_T^v$ is assembled analogously. Remark that the matrix $\mathbf{E} := \mathrm{A}_{T\in\mathcal{T}_h} \mathbf{E}_T$ appeared in the large system of equations (4.23) if the non-stationary case of the Stokes equations is considered.

Chapter 5

Verification of the Discretization Schemes

In this chapter, we apply the *method of manufactured solutions* (*MMS*—cf. Roache 1998a,b, 2002; Salari & Knupp 2000) to the implemented discretization schemes in order to validate numerically the implemented solver and thus to verify the underlying discretization schemes of Chapters 3 and 4. In particular, the tests implicitly demonstrate the convergence of the incorporated iterative splitting algorithm (cf. Alg. 4.4). Furthermore, the numerically estimated orders of convergence in Section 5.4 show that the a priori error estimates for the DNPP system in Section 3.2 are valid for lowest order discretization spaces. The verification of the discretization schemes for all systems under consideration is the basis for the numerical investigations that follow in Chapter 6.

Preliminaries. We make use of the following lemma to numerically estimate the orders of convergence in the discretization parameter h:

Lemma 5.1 (Estimates for the convergence order). *Assume an a priori error estimate of the form*

$$\forall h > 0\,, \qquad \|z_h - z\|_{L^2(\Omega)} \;\leq\; C(z)\, h^k \tag{5.1}$$

to hold, using the usual notation. Here, $C = C(z) > 0$ depends only of the domain Ω and of the true solution z. Let $(h_j)_{j\in\mathbb{N}}$ be a positive decreasing sequence. Then the convergence order k of the underlying discretization scheme satisfies

$$k \;\geq\; \ln\left(\frac{\|z_{h_{j-1}} - z\|_{L^2(\Omega)}}{\|z_{h_j} - z\|_{L^2(\Omega)}}\right) \Big/ \ln\left(\frac{h_{j-1}}{h_j}\right), \tag{5.2a}$$

and also

$$k \;\geq\; \ln\left(\frac{\|z_{h_{j-1}} - z_{h_{j-2}}\|_{L^2(\Omega)}}{\|z_{h_j} - z_{h_{j-1}}\|_{L^2(\Omega)}}\right) \Big/ \ln\left(\frac{h_{j-1} + h_{j-2}}{h_j + h_{j-1}}\right). \tag{5.2b}$$

Proof. Inequality (5.2a) immediately follows by the quotient of (5.1) with $h = h_{j-1}, h_j$ and taking the logarithm. Further, by $\|z_{h_j} - z_{h_{j-1}}\| \leq \|z - z_{h_j}\| + \|z - z_{h_{j-1}}\|$, (5.1), and $h_j^k + h_{j-1}^k \leq (h_j + h_{j-1})^k$ analogously (5.2b) is obtained. □

Inequalities (5.2) provide bounds for the *minimum* convergence order. In the following, the minimum experimental convergence order is frequently denoted by co and is set equal to the right-hand side of (5.2a) or (5.2b). If $h_j = h_{j-1}/2$—as done in this thesis—the denominators of (5.2a) and (5.2b) simplify to $\ln 2$. The estimate (5.2a) is only meaningful if the true solution z is known—this is the case for scenarios according to the MMS. Otherwise, if the true solution is missing (cf. Par. "Upscaled Tensors" of Sec. 6.2), the estimate (5.2b) is used.

5.1 Verification of the Convection–Diffusion Discretization

5.1.1 Scenario: Reactive Transport

The following test scenario was taken from Bause & Knabner (2004) and Radu et al. (2008).

Model problem. In this scenario, two chemical species—an electron acceptor A and an electron donor D—represented by their molar concentrations c^{A} and c^{D}, respectively, are transported through a saturated porous medium. The transport mechanisms are diffusion and advection due to a prescribed water flux $\boldsymbol{u}$. If both species are available in any area of the considered domain Ω, they degrade according to the stoichiometry

$$2\mathrm{A} + \mathrm{D} \;\rightarrow\; \emptyset \tag{5.3}$$

with a rate constant equal to one. Let $J :=]0,\ 1[\,, \Omega :=]0,\ 2[\times]0,\ 3[\,, \boldsymbol{u} := (0,\ -1)^{\mathrm{T}}, \theta := 1.0$, $\mathbf{D} := 0.1\,\mathbf{I}$, $\nu^{\mathrm{A}} := 2$, $\nu^{\mathrm{D}} := 1$, where θ denotes the water saturation, $\mathbf{D}$ the diffusion–dispersion coefficient, and ν^i the stoichiometric coefficients due to (5.3). Then, the considered system of equations reads

$$\begin{aligned} \boldsymbol{j}^i &= -\mathbf{D}\,\boldsymbol{\nabla} c^i + \boldsymbol{u}\, c^i && \text{in } J \times \Omega\,, \\ \partial_t(\theta\, c^i) + \boldsymbol{\nabla} \cdot \boldsymbol{j}^i &= f^i - \theta\, \nu^i\, (c^{\mathrm{A}})^2\, c^{\mathrm{D}} && \text{in } J \times \Omega\,, \end{aligned}$$

$$
\begin{aligned}
c^i &= c^i_{\mathrm{D}} && \text{on } J \times \partial\Omega \,, \\
c^i &= c^{i,0} && \text{on } \{0\} \times \Omega \quad \text{for } i \in \{\mathrm{A}, \mathrm{D}\} \,.
\end{aligned} \tag{5.4}
$$

Numerical setting. For numerical studies the true solution is prescribed by

$$c^{\mathrm{A}}(t, \boldsymbol{x}) := (x-1)^2\, y \exp(-0.1t)/9 \,, \tag{5.5a}$$

$$c^{\mathrm{D}}(t, \boldsymbol{x}) := x(2-x)\, y^3 \exp(-0.1t)/27 \,. \tag{5.5b}$$

The coefficient f^i is determined by (5.4) and the initial conditions and the boundary conditions are obtained by the evaluation of (5.5) on $\{0\}\times\Omega$ and $J\times\partial\Omega$, respectively. The problem is solved with the discretization scheme of Section 4.2 setting $\mathsf{A}^i := 1$, $\boldsymbol{C}^i := \boldsymbol{u}$, $\mathbf{D}^i := \mathbf{D}$, and $\mathsf{F}^i := f^i$. As linearization scheme the Newton method was used (cf. Algs. 4.2 and 4.3).

The discretization errors $\|\boldsymbol{j}^i_h - \boldsymbol{j}^i\|_{\boldsymbol{L}^2(\Omega)}$ and $\|c^i_h - c^i\|_{L^2(\Omega)}$ at end time $T = 1$ are estimated for different mesh sizes h and the minimum experimental convergence orders are computed according to (5.2a). The temporal step size is set to $\tau = 0.1$ and the maximum residual for the Newton stepper to 1E−10.

Results. The discretization errors and estimated bounds for the minimum convergence orders due to (5.2a) at end time $T = 1$ are listed in Table 5.1. Here, we used the following discrete norms for $\boldsymbol{q}_h, \boldsymbol{q} \in \mathbb{RT}_0(\mathcal{T}_h)$ and $u_h, u \in \mathbb{P}_0(\mathcal{T}_h)$:

$$\|\boldsymbol{q}_h - \boldsymbol{q}\|^2_{\mathbb{RT}_0(\mathcal{T}_h)} := \sum_{T\in\mathcal{T}_h} \sum_{E\subset\mathcal{E}} \frac{|T|}{3} \big(\boldsymbol{q}(\boldsymbol{x}^{\mathrm{bary}}_E) \cdot \boldsymbol{\nu}_E - q_E\big)^2 \,, \tag{5.6a}$$

$$\|u_h - u\|^2_{\mathbb{P}_0(\mathcal{T}_h)} := \sum_{T\in\mathcal{T}_h} |T| \,\big(u(\boldsymbol{x}^{\mathrm{bary}}_T) - u_T\big)^2 \,, \tag{5.6b}$$

where the time index was suppressed. The $L^2(\Omega)$ norms are approximated by a quadrature rule of high order on $\mathcal{T}_h$ (e. g. Ern & Guermond 2004, p. 360).

The expected linear grid convergence order in $L^2(\Omega)$ (cf. Douglas & Roberts 1985) is obtained for both molar flux and concentration and superconvergence is observed for the concentration in the discrete norm as defined in (5.6b). The results are listed in Table 5.1. The slightly varying convergence orders in the $L^2(\Omega)$ norms are due to the non-regular grid refinements. The rapidly decreasing convergence orders in the discrete norms toward $h = 1.25\mathrm{E}{-2}$ result from the time discretization error, which begins to dominate over the spatial one. Smaller time stepping re-establishes the optimal order.

h	$\#\mathcal{T}$	$\#\mathcal{E}$	$\|\boldsymbol{j}_h^{\mathrm{A}} - \boldsymbol{j}^{\mathrm{A}}\|_{\boldsymbol{L}^2(\Omega)}$	co	$\|\boldsymbol{j}_h^{\mathrm{D}} - \boldsymbol{j}^{\mathrm{D}}\|_{\boldsymbol{L}^2(\Omega)}$	co	$\|\boldsymbol{j}_h^{\mathrm{A}} - \boldsymbol{j}^{\mathrm{A}}\|_{\mathbb{RT}_0(\mathcal{T}_h)}$	co	$\|\boldsymbol{j}_h^{\mathrm{D}} - \boldsymbol{j}^{\mathrm{D}}\|_{\mathbb{RT}_0(\mathcal{T}_h)}$	co
4.00E−1	64	108	1.762E−1	—	2.228E−1	—	3.229E−2	—	1.099E−1	—
2.00E−1	316	498	7.473E−2	1.24	7.904E−2	1.50	1.203E−2	1.42	1.948E−2	2.50
1.00E−1	1 272	1 956	3.778E−2	0.98	3.959E−2	1.00	4.734E−3	1.35	6.547E−3	1.57
5.00E−2	5 356	8 130	1.727E−2	1.13	1.824E−2	1.12	1.848E−3	1.36	1.997E−3	1.71
2.50E−2	21 452	32 370	8.645E−3	1.00	9.036E−3	1.01	9.151E−4	1.01	8.406E−4	1.25
1.25E−2	86 936	130 788	4.219E−3	1.04	4.438E−3	1.03	3.804E−4	1.27	3.598E−4	1.22
6.25E−3	347 872	522 576	2.103E−3	1.00	2.219E−3	1.00	1.997E−4	0.93	2.161E−4	0.74

h	$\#\mathcal{T}$	$\#\mathcal{E}$	$\|c_h^{\mathrm{A}} - c^{\mathrm{A}}\|_{L^2(\Omega)}$	co	$\|c_h^{\mathrm{D}} - c^{\mathrm{D}}\|_{L^2(\Omega)}$	co	$\|c_h^{\mathrm{A}} - c^{\mathrm{A}}\|_{\mathbb{P}_0(\mathcal{T}_h)}$	co	$\|c_h^{\mathrm{D}} - c^{\mathrm{D}}\|_{\mathbb{P}_0(\mathcal{T}_h)}$	co
4.00E−1	64	108	1.385E−1	—	1.916E−1	—	4.873E−2	—	1.436E−1	—
2.00E−1	316	498	5.824E−2	1.25	5.904E−2	1.70	7.451E−3	2.71	2.277E−2	2.66
1.00E−1	1 272	1 956	2.842E−2	1.04	2.862E−2	1.04	1.744E−3	2.10	6.561E−3	1.80
5.00E−2	5 356	8 130	1.319E−2	1.11	1.325E−2	1.11	3.869E−4	2.17	1.432E−3	2.20
2.50E−2	21 452	32 370	6.578E−3	1.00	6.511E−3	1.03	1.261E−4	1.62	2.524E−4	2.50
1.25E−2	86 936	130 788	3.210E−3	1.04	3.202E−3	1.02	7.277E−5	0.79	1.339E−4	0.91
6.25E−3	347 872	522 576	1.602E−3	1.00	1.606E−3	1.00	6.754E−5	0.11	1.716E−4	0.36

Table 5.1. Discretization errors at end time $T = 1$ (time index suppressed) and estimated convergence orders for the scenario according to Section 5.1.1. The total degress of freedom for one species per time step is equal to $\#\mathcal{T} + \#\mathcal{E}$.

5.1.2 Scenario: Water Flow with Flux Boundaries

The following test scenario was taken from Bahriawati & Carstensen (2005).

Model problem. The stationary Darcy-type problem

$$\begin{aligned} \boldsymbol{u} &= -\boldsymbol{\nabla} p && \text{in } \Omega\,, \\ \boldsymbol{\nabla}\cdot\boldsymbol{u} &= 0 && \text{in } \Omega\,, \\ p &= 0 && \text{on } \partial\Omega_{\mathrm{D}}\,, \\ \boldsymbol{u}\cdot\boldsymbol{\nu} &= u_{\mathrm{N}} && \text{on } \partial\Omega_{\mathrm{N}} \end{aligned} \tag{5.7}$$

is considered on the L-shaped domain $\Omega =]-1,\,1[^2 \setminus [0,\,1]\times[-1,\,0]$ (cf. Fig. 5.1). The pressure p is set equal to zero on the Dirichlet boundary $\partial\Omega_{\mathrm{D}} := \{0\}\times[-1,\,0]\cap[0,\,1]\times\{0\}$, while the water flux $\boldsymbol{u}$ over the Neumann boundary $\partial\Omega_{\mathrm{N}} = \partial\Omega \setminus \partial\Omega_{\mathrm{D}}$ is prescribed by

$$u_{\mathrm{N}}(r,\,\varphi) \;:=\; 2/3\, r^{-1/3} \begin{pmatrix} -\sin(1/3\,\varphi) \\ \cos(1/3\varphi) \end{pmatrix} \cdot \boldsymbol{\nu}$$

in the polar coordinates (r, φ).

Numerical setting. The true pressure solution of (5.7) is given by

$$p(r,\,\varphi) \;=\; r^{2/3}\sin(2/3\,\varphi)\,.$$

Transformation of the gradient into polar coordinates

$$\boldsymbol{\nabla} p \;=\; \left[\boldsymbol{\nu}_r \,\middle|\, \tfrac{1}{r}\,\boldsymbol{\nu}_\varphi\right] \boldsymbol{\nabla}_{(r,\varphi)} p\,, \qquad \boldsymbol{\nu}_r \;:=\; \frac{\boldsymbol{x}}{|\boldsymbol{x}|}\,, \qquad \boldsymbol{\nu}_\varphi \;:=\; \begin{bmatrix} 0 & -1 \\ 1 & 0 \end{bmatrix} \boldsymbol{\nu}_r$$

yields the true flux solution

$$\boldsymbol{u} \;=\; -\frac{2}{3}\, r^{-1/3} \Big(\sin(2/3\,\varphi)\,\boldsymbol{\nu}_r + \cos(2/3\varphi)\,\boldsymbol{\nu}_\varphi \Big)\,.$$

The problem (5.7) is solved with the discretization scheme presented in Section 4.2. The discretization errors $\|\boldsymbol{u}_h - \boldsymbol{u}\|_{\boldsymbol{L}^2(\Omega)}$ and $\|p_h - p\|_{L^2(\Omega)}$, where $(\boldsymbol{u}_h,\, p_h)$ denotes the discrete

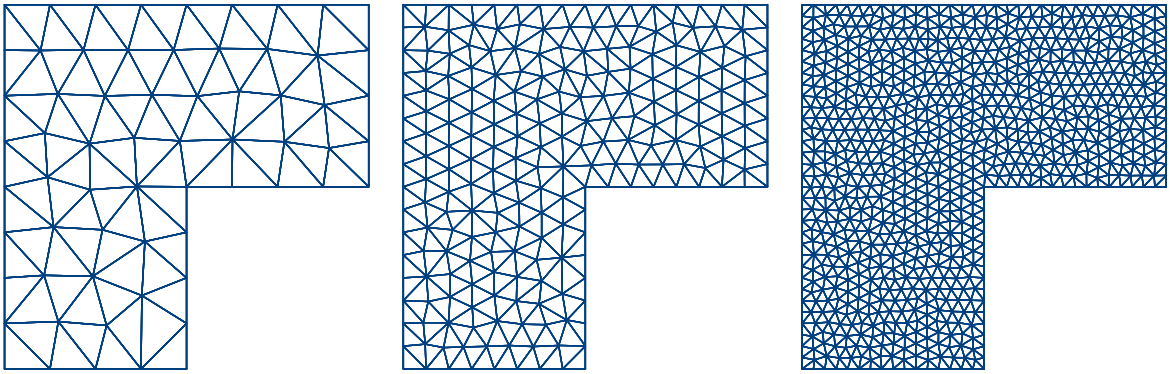

Figure 5.1. Unstructured grids on the domain $\Omega =]-1, 1[^2 \setminus [0, 1] \times [-1, 0]$ with $h = 1/4, 1/8, 1/16$.

h	$\#\mathcal{E}$	$\#\mathcal{T}$	$\|\boldsymbol{u}_h - \boldsymbol{u}\|_{\boldsymbol{L}^2(\Omega)}$	co	$\|\boldsymbol{u}_h - \boldsymbol{u}\|_{\mathbb{RT}_0(\mathcal{T}_h)}$	co	$\|p_h - p\|_{L^2(\Omega)}$	co	$\|p_h - p\|_{\mathbb{P}_0(\mathcal{T}_h)}$	co
1/2	44	24	3.025E−1	—	1.089E−1	—	1.770E−1	—	9.392E−2	—
1/4	157	94	2.010E−1	0.59	6.928E−2	0.65	8.473E−2	1.06	2.991E−2	1.65
1/8	602	380	1.249E−1	0.69	4.465E−2	0.63	4.070E−2	1.06	1.330E−2	1.17
1/16	2 362	1 532	7.828E−2	0.67	2.452E−2	0.86	1.990E−2	1.03	5.588E−3	1.25
1/32	9 320	6 128	4.863E−2	0.69	1.581E−2	0.63	9.731E−3	1.03	2.016E−3	1.47
1/64	37 036	24 520	3.245E−2	0.58	1.149E−2	0.46	4.835E−3	1.01	9.147E−4	1.14
1/128	147 812	98 200	2.068E−2	0.65	7.656E−3	0.59	2.398E−3	1.01	3.624E−4	1.34
1/156	689 047	458 682	1.284E−2	0.68	4.989E−3	0.62	1.133E−3	1.08	1.172E−4	1.63

Table 5.2. Discretization errors and estimated convergence orders for the scenario according to Section 5.1.2.

solution, are subsequently estimated for different mesh sizes and the minimum experimental convergence orders are computed due to (5.2a).

Results. The discretization errors and estimated convergence orders are listed in Table 5.2. We observe the expected linear convergence order in the $L^2(\Omega)$ norm (cf. Prop. 3.23 with vanishing errors for $\boldsymbol{E}$ and $\boldsymbol{u}$; and Brezzi & Fortin 1991, Prop. 1.2, p. 139) for the pressure and a convergence order of about $2/3$ for the water flux. This suboptimal order is obtained due to a loss of regularity of the solution originating from the reentrant corner of the domain (cf. Fig. 5.1).

5.2 Verification of the Stokes Discretization

The discretization scheme for Stokes-type problems as described in Section 4.3 on p. 80 is applied to several test scenarios in order to verify the theoretically predicted orders of convergence. The a priori error estimates for the Taylor–Hood discretization of the Stokes equations read as follows:

Theorem 5.2 (Order of grid convergence). *Let $(\boldsymbol{u}, p) \in \boldsymbol{H}^1(\Omega) \times L^2(\Omega)$ and $(\boldsymbol{u}_h, p_h) \in \mathbb{P}_2^c(\mathcal{T}_h)^2 \times \mathbb{P}_1^c(\mathcal{T}_h)$ be the solutions of Problem 4.18 and Problem 4.19, respectively. Then, if $\boldsymbol{u} \in \boldsymbol{H}^3(\Omega)$ and $p \in H^2(\Omega)$, there exists a constant C independent of h such that*

$$\forall h, \qquad \|\boldsymbol{u}_h - \boldsymbol{u}\|_{\boldsymbol{L}^2(\Omega)} \leq Ch^3(\|\boldsymbol{u}\|_{\boldsymbol{H}^3(\Omega)} + \|p\|_{H^2(\Omega)}) , \tag{5.8a}$$

$$\forall h, \qquad \|p_h - p\|_{L^2(\Omega)} \leq Ch^2(\|\boldsymbol{u}\|_{\boldsymbol{H}^3(\Omega)} + \|p\|_{H^2(\Omega)}) . \tag{5.8b}$$

Proof. See Ern & Guermond (2004) and references cited therein. □

As in the previous section, (5.2a) is used to estimate the minimum convergence order in h, again denoted by co.

5.2.1 Scenario: Colliding Flow

In the scenario "colliding flow" (cf. Elman et al. 2005) the true solution $\boldsymbol{u} = (20xy^3, 5x^4 - 5y^4)^{\mathrm{T}}$ and $p = 60x^2y - 20y^3$ is prescribed on a domain $\Omega =]-1, 1[^2$ and the constraint $\int_\Omega p = 0$ is claimed.

The discretization errors and the estimated convergence orders according to (5.2a) are listed in Table 5.3. We receive the expected cubic convergence order in $L^2(\Omega)$ for both velocity components and a quadratic order of convergence for the pressure.

h	DOF	$\|u - u_h\|_{L^2(\Omega)}$	co	$\|v - v_h\|_{L^2(\Omega)}$	co	$\|p - p_h\|_{L^2(\Omega)}$	co
1	95	1.038E+0	—	7.131E−1	—	9.877E+0	—
1/2	259	1.027E−1	3.34	8.765E−2	3.02	2.143E+0	2.20
1/4	1 019	1.116E−2	3.20	1.054E−2	3.06	4.961E−1	2.11
1/8	4 087	1.468E−3	2.93	1.235E−3	3.09	1.230E−1	2.01
1/16	15 704	1.734E−4	3.08	1.536E−4	3.01	2.987E−2	2.04
1/32	63 796	2.118E−5	3.03	1.843E−5	3.06	7.276E−3	2.04
1/64	255 974	2.600E−6	3.03	2.282E−6	3.01	1.807E−3	2.01

Table 5.3. Mesh sizes, degrees of freedom (DOF), discretization errors, and convergence orders for the test scenario "colliding flow" according to Elman et al. (2005). The total DOF are given by $2\,(\#\mathcal{V} + \#\mathcal{E}) + \#\mathcal{V}$.

5.2.2 Scenario: Force Term

To verify the discretization of the force term $\boldsymbol{f}$ in (4.19) a true solution $(\boldsymbol{u}, p)$ is again prescribed and balanced by the right-hand side $\boldsymbol{f}$. We choose $\Omega :=]0, 1[^2$, $\boldsymbol{u} := (-\cos(\pi x)\,\sin(\pi y),\, \sin(\pi x)\,\cos(\pi y))^{\mathrm{T}}$, $p := 0$, and the constraint $\int_\Omega p = 0$. Hence, $\boldsymbol{f} = 2\pi\boldsymbol{u}$ holds. The discretization errors together with the estimated convergence orders are shown in Table 5.4.

h	DOF	$\|u - u_h\|_{L^2(\Omega)}$	co	$\|v - v_h\|_{L^2(\Omega)}$	co	$\|p - p_h\|_{L^2(\Omega)}$	co
1	31	2.431E−2	—	2.431E−2	—	3.995E−16	—
1/2	95	1.082E−2	1.17	1.082E−2	1.17	3.778E−2	—
1/4	259	1.702E−3	2.67	1.702E−3	2.67	7.548E−3	2.32
1/8	1 019	2.239E−4	2.93	2.240E−4	2.93	1.512E−3	2.32
1/16	4 087	2.724E−5	3.04	2.755E−5	3.02	3.955E−4	1.94
1/32	15 731	3.413E−6	3.00	3.405E−6	3.02	5.817E−5	2.77
1/64	63 670	4.257E−7	3.00	4.261E−7	3.00	1.609E−5	1.85
1/128	255 659	5.279E−8	3.01	5.282E−8	3.01	3.956E−6	2.02

Table 5.4. Mesh sizes, degrees of freedom (DOF), discretization errors, and convergence orders for the test scenario "force term". The total DOF are given by $5\,(\#\mathcal{V}) + 2\,(\#\mathcal{E})$.

5.3 Verification of the SNPP Discretization

As a representative system we choose the SNPP equations with essential boundary conditions:

$$
\begin{aligned}
-\Delta \boldsymbol{u} + \boldsymbol{\nabla} p &= \boldsymbol{E}\,(c^+ - c^-) + \boldsymbol{f} && \text{in } J \times \Omega\,, && \text{(5.9a)}\\
\boldsymbol{\nabla} \cdot \boldsymbol{u} &= 0 && \text{in } J \times \Omega\,, && \text{(5.9b)}\\
\boldsymbol{u} &= \boldsymbol{u}_{\mathrm{D}} && \text{on } J \times \partial\Omega\,, && \text{(5.9c)}\\
\boldsymbol{j}^{\pm} &= -\boldsymbol{\nabla} c^{\pm} + (\boldsymbol{u} \pm \boldsymbol{E})\, c^{\pm} && \text{in } J \times \Omega\,, && \text{(5.9d)}\\
\partial_t c^{\pm} + \boldsymbol{\nabla} \cdot \boldsymbol{j}^{\pm} &= s^{\pm} && \text{in } J \times \Omega\,, && \text{(5.9e)}\\
\boldsymbol{j}^{\pm} \cdot \boldsymbol{\nu} &= j^{\pm}_{\mathrm{flux}} && \text{on } J \times \partial\Omega\,, && \text{(5.9f)}\\
c^{\pm} &= c^{\pm,0} && \text{on } \{0\} \times \Omega\,, && \text{(5.9g)}\\
\boldsymbol{E} &= -\boldsymbol{\nabla}\phi && \text{in } J \times \Omega\,, && \text{(5.9h)}\\
\boldsymbol{\nabla} \cdot \boldsymbol{E} &= c^+ - c^- && \text{in } J \times \Omega\,, && \text{(5.9i)}\\
\boldsymbol{E} \cdot \boldsymbol{\nu} &= E_{\mathrm{N}} && \text{on } J \times \partial\Omega\,. && \text{(5.9j)}
\end{aligned}
$$

Natural and mixed boundary conditions are also considered for verification (cf. Rem. 5.3). The artificial force and source / sink terms $\boldsymbol{f}$ and s^+, s^-, respectively, are required as balancing terms for the application of the MMS.

Reference solution and data. The following scenario is based on Prohl & Schmuck (2010). We choose the time interval $J =]0,1[$, the unit square domain $\Omega :=]0,1[^2$, and the prescribed solution ansatz

$$
\begin{aligned}
&\boldsymbol{u}(t,\boldsymbol{x}) := t \begin{pmatrix} -\mathrm{cx}\,\mathrm{sy} \\ \mathrm{sx}\,\mathrm{cy} \end{pmatrix}, \qquad p(t,\boldsymbol{x}) := -\tfrac{1}{4}\Big(\cos(2\pi x) + \cos(2\pi y)\Big)\,,\\
&c^+(t,\boldsymbol{x}) := t\,\mathrm{cx}\,, \qquad c^-(t,\boldsymbol{x}) := t\,\mathrm{sy}\,, \qquad \phi(t,\boldsymbol{x}) := \tfrac{t}{\pi^2}(\mathrm{cx} - \mathrm{sy}) \qquad \text{(5.10a)}
\end{aligned}
$$

using the abbreviations $\mathrm{sx} \coloneqq \sin(\pi x)$, $\mathrm{sy} \coloneqq \sin(\pi y)$, $\mathrm{cx} \coloneqq \cos(\pi x)$, $\mathrm{cy} \coloneqq \cos(\pi y)$. Since we use mixed finite elements, we are further interested in the discretization errors of the fluxes. Computing the derivatives analytically, we obtain the following expressions:

$$\begin{aligned} \boldsymbol{E}(t,\boldsymbol{x}) &= \frac{t}{\pi}\begin{pmatrix}\mathrm{sx}\\ \mathrm{cy}\end{pmatrix}, \quad \boldsymbol{j}^{+}(t,\boldsymbol{x}) = t\begin{pmatrix}\pi\,\mathrm{sx} + \frac{t}{\pi}\mathrm{sx}\,\mathrm{cx} - t\,\mathrm{cx}\,\mathrm{cx}\,\mathrm{sy}\\ \frac{t}{\pi}\mathrm{cx}\,\mathrm{cy} + t\,\mathrm{sx}\,\mathrm{cx}\,\mathrm{cy}\end{pmatrix}, \\ \boldsymbol{j}^{-}(t,\boldsymbol{x}) &= -t\begin{pmatrix}\frac{t}{\pi}\mathrm{sx}\,\mathrm{sy} + t\,\mathrm{cx}\,\mathrm{sy}\,\mathrm{sy}\\ \pi\,\mathrm{cy} + \frac{t}{\pi}\mathrm{sy}\,\mathrm{cy} - t\,\mathrm{sx}\,\mathrm{sy}\,\mathrm{cy}\end{pmatrix}. \end{aligned} \tag{5.10b}$$

Substituting (5.10) into (5.9) produces the following balancing source terms:

$$\begin{aligned} \boldsymbol{f}(t,\boldsymbol{x}) &= 2t\pi^2\begin{pmatrix}-\mathrm{cx}\,\mathrm{sy}\\ \mathrm{sx}\,\mathrm{cy}\end{pmatrix} + \frac{\pi}{2}\begin{pmatrix}\sin(2\pi x)\\ \sin(2\pi y)\end{pmatrix} + \frac{t^2}{\pi}(\mathrm{sy}-\mathrm{cx})\begin{pmatrix}\mathrm{sx}\\ \mathrm{cy}\end{pmatrix}, \\ s^{+}(t,\boldsymbol{x}) &= (1+\pi^2 t)\,\mathrm{cx} + t^2\Big(\mathrm{cx}^2 - \mathrm{sx}^2 - \mathrm{cx}\,\mathrm{sy} + \pi\,\mathrm{sx}\,\mathrm{cx}\,\mathrm{sy}\Big), \\ s^{-}(t,\boldsymbol{x}) &= (1+\pi^2 t)\,\mathrm{sy} + t^2\Big(\mathrm{sy}^2 - \mathrm{cy}^2 - \mathrm{cx}\,\mathrm{sy} + \pi\,\mathrm{sx}\,\mathrm{cy}\,\mathrm{cy}\Big). \end{aligned} \tag{5.11a}$$

The boundary data and the initial data are obtained by sampling the reference solution (5.10) on the boundary $\partial\Omega$ and at $t = 0$, respectively. Thus, we obtain

$$\begin{aligned} j^{+}_{\mathrm{flux}}(t,\boldsymbol{x}) &= \left\{\begin{array}{ll} -t^2\,\mathrm{sx}\,\mathrm{cx} - \frac{t^2}{\pi}\mathrm{cx} & \text{on } J\times\{\partial\Omega_1\cup\partial\Omega_3\}\\ -t^2\,\mathrm{sy} & \text{on } J\times\partial\Omega_2\\ t^2\,\mathrm{sy} & \text{on } J\times\partial\Omega_4\end{array}\right\}, \\ j^{-}_{\mathrm{flux}}(t,\boldsymbol{x}) &= \left\{\begin{array}{ll} \pi\,t & \text{on } J\times\{\partial\Omega_1\cup\partial\Omega_3\}\\ t^2\,\mathrm{sy}^2 & \text{on } J\times\{\partial\Omega_2\cup\partial\Omega_4\}\end{array}\right\}, \\ E_{\mathrm{N}}(t,\boldsymbol{x}) &= \left\{\begin{array}{ll} -\frac{t}{\pi} & \text{on } J\times\{\partial\Omega_1\cup\partial\Omega_3\}\\ 0 & \text{on } J\times\{\partial\Omega_2\cup\partial\Omega_4\}\end{array}\right\} \end{aligned} \tag{5.11b}$$

with $\partial\Omega_j$ as given in Figure 5.2. and obvious formulations for $\boldsymbol{u}_{\mathrm{D}}$ and $c^{\pm,0}$. In order to ensure uniqueness we prescribe

$$\fint_{\Omega} p \equiv 0 \qquad \text{and} \qquad \fint_{\Omega} \phi = -\frac{2}{\pi^3}t \tag{5.12}$$

in (5.9).

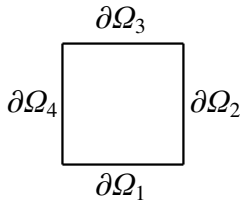

Figure 5.2. Boundary notation for the assignment of different boundary conditions.

Results. Solving system (5.9) with the data and constraints as defined above yields discretization errors as shown in Figure 5.3 and Table 5.5. We verify the predicted convergence orders in h, namely three for $\boldsymbol{u}$, two for p (cf. (5.8)), and one for the other unknowns (cf. Douglas & Roberts 1985; Ern & Guermond 2004). As expected, we further observe a linear grid convergence order for the overall unknown $(\boldsymbol{u}, p, \boldsymbol{j}^+, c^+, \boldsymbol{j}^-, c^-, \boldsymbol{E}, \phi)$.

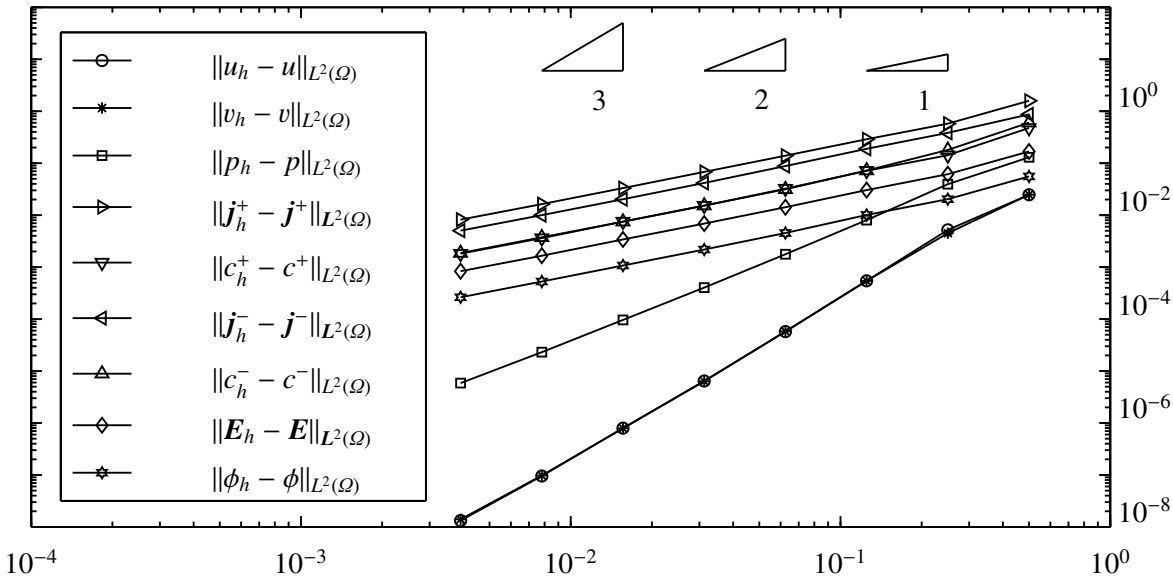

Figure 5.3. Discretization errors vs. grid sizes. The slope of each graph represents the convergence order in h. Here, u and v denote the components of $\boldsymbol{u}$.

Remark 5.3 (Further boundary conditions). The experimental orders of convergence are as in Figure 5.3 if using the conditions $c^\pm = c_\mathrm{D}^\pm$ on $J \times \partial\Omega$ in (5.9f) and/or $\phi = \phi_\mathrm{D}$ on $J \times \partial\Omega$ in (5.9j) or if taking any decomposition of $\partial\Omega$ into the considered boundary types (for each subproblem chosen independently from the partition of the others). Hereby, the data $c_\mathrm{D}^\pm$, ϕ_D are obtained in the fashion demonstrated above. In all cases, both balance constraints (5.12) must be disregarded again.

The different boundary conditions must satisfy certain *transition conditions* at points on the boundary at which two boundary types meet. With the aforementioned procedure, those are naturally fulfilled and smooth transitions are expected, which do not perturb the convergence behavior. △

5.4 Verification of the DNPP Discretization

As a representative system we choose the DNPP equations associated with the homogenization result for the parameters $(\alpha, \beta, \gamma) = (0, 0, 0)$ (cf. Thm. 2.5) with essential boundary conditions:

$$\begin{aligned}
\boldsymbol{u} &= -\boldsymbol{\nabla} p + \boldsymbol{E}\,(c^+ - c^-) + \boldsymbol{f} && \text{in } J \times \Omega\,, && (5.13a)\\
\boldsymbol{\nabla} \cdot \boldsymbol{u} &= 0 && \text{in } J \times \Omega\,, && (5.13b)\\
\boldsymbol{u} \cdot \boldsymbol{\nu} &= u_{\mathrm{N}} && \text{on } J \times \partial\Omega\,, && (5.13c)\\
\boldsymbol{j}^{\pm} &= -\boldsymbol{\nabla} c^{\pm} + (\boldsymbol{u} \pm \boldsymbol{E})\, c^{\pm} && \text{in } J \times \Omega\,, && (5.13d)\\
\partial_t c^{\pm} + \boldsymbol{\nabla} \cdot \boldsymbol{j}^{\pm} &= s^{\pm} && \text{in } J \times \Omega\,, && (5.13e)\\
\boldsymbol{j}^{\pm} \cdot \boldsymbol{\nu} &= j^{\pm}_{\mathrm{flux}} && \text{on } J \times \partial\Omega\,, && (5.13f)\\
c^{\pm} &= c^{\pm,0} && \text{on } \{0\} \times \Omega\,, && (5.13g)\\
\boldsymbol{E} &= -\boldsymbol{\nabla} \phi && \text{in } J \times \Omega\,, && (5.13h)\\
\boldsymbol{\nabla} \cdot \boldsymbol{E} &= c^+ - c^- && \text{in } J \times \Omega\,, && (5.13i)\\
\boldsymbol{E} \cdot \boldsymbol{\nu} &= E_{\mathrm{N}} && \text{on } J \times \partial\Omega\,. && (5.13j)
\end{aligned}$$

Natural and mixed boundary conditions are also considered for verification (cf. Rem. 5.4). Similar to the setting of Section 5.3, the artificial force and source / sink terms $\boldsymbol{f}$ and s^+, s^-, respectively, are required as balancing terms for the application of the MMS.

Reference solution and data. We choose the same prescribed solution ansatz as in Section 5.3, i. e., $(\boldsymbol{u}, p, \boldsymbol{j}^+, c^+, \boldsymbol{j}^-, c^-, \boldsymbol{E}, \phi)$ is defined as in (5.10) on the time interval $J =]0, 1[$ and the unit square domain $\Omega \coloneqq]0, 1[^2$. If we substitute this solution vector into (5.13), we obtain the same data as given in (5.11) except that

$$\boldsymbol{f}(t, \boldsymbol{x}) = t \begin{pmatrix} -\mathrm{cx}\,\mathrm{sy} \\ \mathrm{sx}\,\mathrm{cy} \end{pmatrix} + \frac{\pi}{2} \begin{pmatrix} \sin(2\pi x) \\ \sin(2\pi y) \end{pmatrix} + \frac{t^2}{\pi} (\mathrm{sy} - \mathrm{cx}) \begin{pmatrix} \mathrm{sx} \\ \mathrm{cy} \end{pmatrix},$$

h	1/2	1/4	1/8	1/16	1/32	1/64	1/128	1/256
$\#\mathcal{T}$	4	26	112	516	2 224	9 166	37 928	151 038
$\#\mathcal{E}$	8	45	182	804	3 398	13 875	57 148	227 069
$\#\mathcal{V}$	5	20	71	289	1175	4 710	19 221	76 032
$\|u_h - u\|_{L^2(\Omega)}$	2.472E−2	5.204E−3	5.450E−4	5.737E−5	6.436E−6	7.967E−7	9.552E−8	1.323E−8
$\|v_h - v\|_{L^2(\Omega)}$	2.474E−2	4.494E−3	5.420E−4	5.793E−5	6.360E−6	7.909E−7	9.760E−8	1.400E−8
$\|p_h - p\|_{L^2(\Omega)}$	1.299E−1	3.944E−2	8.028E−3	1.769E−3	4.032E−4	9.624E−5	2.310E−5	5.863E−6
$\|\boldsymbol{j}_h^+ - \boldsymbol{j}^+\|_{\boldsymbol{L}^2(\Omega)}$	1.589E−0	5.761E−1	2.889E−1	1.394E−1	6.793E−2	3.314E−2	1.630E−2	8.197E−3
$\|c_h^+ - c^+\|_{L^2(\Omega)}$	4.762E−1	1.424E−1	7.134E−2	3.236E−2	1.521E−2	7.514E−3	3.609E−3	1.811E−3
$\|\boldsymbol{j}_h^- - \boldsymbol{j}^-\|_{\boldsymbol{L}^2(\Omega)}$	8.692E−1	3.842E−1	1.890E−1	8.806E−2	4.164E−2	2.026E−2	9.993E−3	5.029E−3
$\|c_h^- - c^-\|_{L^2(\Omega)}$	6.022E−1	1.797E−1	7.224E−2	3.150E−2	1.529E−2	7.489E−3	3.751E−3	1.865E−3
$\|\boldsymbol{E}_h - \boldsymbol{E}\|_{\boldsymbol{L}^2(\Omega)}$	1.678E−1	6.157E−2	3.036E−2	1.422E−2	6.887E−3	3.403E−3	1.657E−3	8.344E−4
$\|\phi_h - \phi\|_{L^2(\Omega)}$	5.567E−2	2.028E−2	1.009E−2	4.534E−3	2.178E−3	1.073E−3	5.277E−4	2.629E−4
$\mathrm{co}_h\, u$	—	2.25	3.26	3.25	3.16	3.01	3.06	2.85
$\mathrm{co}_h\, v$	—	2.46	3.05	3.23	3.19	3.01	3.02	2.80
$\mathrm{co}_h\, p$	—	1.72	2.30	2.18	2.13	2.07	2.06	1.98
$\mathrm{co}_h\, \boldsymbol{j}^+$	—	1.46	1.00	1.05	1.04	1.04	1.02	0.99
$\mathrm{co}_h\, c^+$	—	1.74	1.00	1.14	1.09	1.02	1.06	0.99
$\mathrm{co}_h\, \boldsymbol{j}^-$	—	1.18	1.02	1.10	1.08	1.04	1.02	0.99
$\mathrm{co}_h\, c^-$	—	1.74	1.31	1.20	1.04	1.03	1.00	1.01
$\mathrm{co}_h\, \boldsymbol{E}$	—	1.45	1.02	1.09	1.05	1.02	1.04	0.99
$\mathrm{co}_h\, \phi$	—	1.46	1.01	1.15	1.06	1.02	1.02	1.00

Table 5.5. Discretization errors and minimum convergence orders for decreasing mesh size h for tol = 1E−6 at end time $T = 1$ (time index suppressed). The total number of degrees of freedoms is $3\,(\#\mathcal{T}) + 5\,(\#\mathcal{E}) + 3\,(\#\mathcal{V})$ per fixed-point iteration.

and

$$u_{\mathrm{N}}(t,\boldsymbol{x}) \;=\; \left\{ \begin{array}{ll} -t\,\mathrm{sx} & \text{on } J\times\partial\Omega_1 \\ t\,\mathrm{sy} & \text{on } J\times\partial\Omega_2 \\ -t\,\mathrm{sx} & \text{on } J\times\partial\Omega_3 \\ t\,\mathrm{sy} & \text{on } J\times\partial\Omega_4 \end{array} \right\}$$

with $\partial\Omega_j$ as given in Figure 5.2. In order to ensure uniqueness, again, we have to prescribe the constraints (5.12) in (5.13).

Results. Solving system (5.13) with the data and constraints as defined above yields discretization errors as shown in Figure 5.4 and Table 5.6. We verify the predicted linear convergence order in h for all unknowns $\boldsymbol{u}$, p, $\boldsymbol{j}^+$, c^+, $\boldsymbol{j}^-$, c^-, $\boldsymbol{E}$, ϕ (cf. Thm. 3.26).

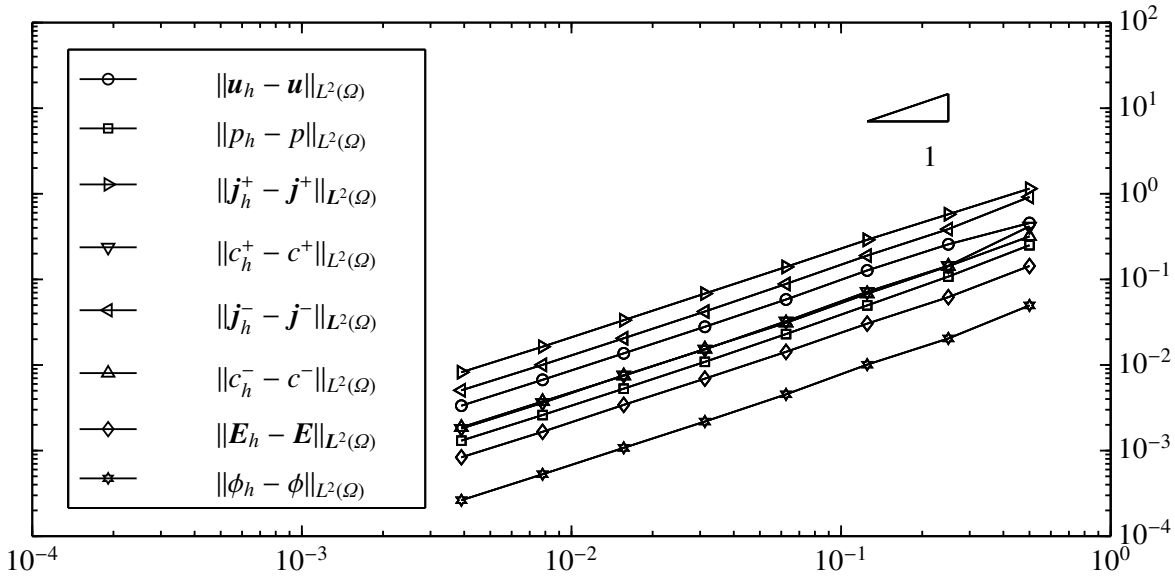

Figure 5.4. Discretization errors vs. grid sizes. The slope of each graph represents the convergence order in h.

Remark 5.4 (Further boundary conditions). The experimental orders of convergence are the same if using the conditions $p = p_{\mathrm{D}}$ on $J\times\partial\Omega$ in (5.13c) and/or $c^{\pm} = c^{\pm}_{\mathrm{D}}$ on $J\times\partial\Omega$ in (5.13f) and/or $\phi = \phi_{\mathrm{D}}$ on $J\times\partial\Omega$ in (5.13j) or if taking any decomposition of $\partial\Omega$ into the considered boundary types (for each subproblem chosen independently from the partition of the others). Hereby, the data p_{D}, $c^{\pm}_{\mathrm{D}}$, and ϕ_{D} are obtained in a fashion demonstrated above. In all cases, both balance constraints (5.12) must be neglected again. See Remark 5.3 regarding transition conditions. △

h	1/2	1/4	1/8	1/16	1/32	1/64	1/128	1/256	1/512
$\#\mathcal{T}$	4	26	112	516	2 224	9 166	37 928	151 038	603 960
$\#\mathcal{E}$	8	45	182	804	3 398	13 875	57 148	227 069	906 964
$\|\boldsymbol{u}_h - \boldsymbol{u}\|_{L^2(\Omega)}$	4.553E−1	2.567E−1	1.271E−1	5.815E−2	2.794E−2	1.366E−2	6.703E−3	3.343E−3	1.653E−3
$\|p_h - p\|_{L^2(\Omega)}$	2.505E−1	1.078E−1	4.965E−2	2.296E−2	1.087E−2	5.284E−3	2.599E−3	1.307E−3	6.517E−4
$\|\boldsymbol{j}_h^+ - \boldsymbol{j}^+\|_{\boldsymbol{L}^2(\Omega)}$	1.147E−0	5.758E−1	2.896E−1	1.397E−1	6.826E−2	3.335E−2	1.634E−2	8.219E−3	4.086E−3
$\|c_h^+ - c^+\|_{L^2(\Omega)}$	4.160E−1	1.441E−1	7.150E−2	3.237E−2	1.522E−2	7.577E−3	3.614E−3	1.811E−3	9.389E−4
$\|\boldsymbol{j}_h^- - \boldsymbol{j}^-\|_{\boldsymbol{L}^2(\Omega)}$	9.174E−1	3.867E−1	1.897E−1	8.841E−2	4.209E−2	2.049E−2	1.005E−2	5.061E−3	2.512E−3
$\|c_h^- - c^-\|_{L^2(\Omega)}$	3.174E−1	1.426E−1	6.809E−2	3.108E−2	1.538E−2	7.481E−3	3.744E−3	1.866E−3	9.211E−4
$\|\boldsymbol{E}_h - \boldsymbol{E}\|_{\boldsymbol{L}^2(\Omega)}$	1.432E−1	6.193E−2	3.039E−2	1.422E−2	6.919E−3	3.419E−3	1.657E−3	8.349E−4	4.188E−4
$\|\phi_h - \phi\|_{L^2(\Omega)}$	4.961E−2	2.041E−2	1.010E−2	4.536E−3	2.184E−3	1.077E−3	5.285E−4	2.629E−4	1.327E−4
$\mathrm{co}_h\,\boldsymbol{u}$	—	0.83	1.01	1.13	1.06	1.03	1.03	1.00	1.02
$\mathrm{co}_h\,p$	—	1.22	1.12	1.11	1.08	1.04	1.02	0.99	1.00
$\mathrm{co}_h\,\boldsymbol{j}^+$	—	0.99	0.99	1.05	1.03	1.03	1.03	0.99	1.01
$\mathrm{co}_h\,c^+$	—	1.53	1.01	1.14	1.09	1.01	1.07	1.00	0.95
$\mathrm{co}_h\,\boldsymbol{j}^-$	—	1.25	1.03	1.10	1.07	1.04	1.03	0.99	1.01
$\mathrm{co}_h\,c^-$	—	1.15	1.07	1.13	1.02	1.04	1.00	1.00	1.02
$\mathrm{co}_h\,\boldsymbol{E}$	—	1.21	1.03	1.10	1.04	1.02	1.05	0.99	1.00
$\mathrm{co}_h\,\phi$	—	1.28	1.01	1.15	1.05	1.02	1.03	1.01	0.99

Table 5.6. Discretization errors and minimum convergence orders for decreasing mesh size h for tol = 1E−6 at end time $T = 1$ (time index suppressed). The total number of degrees of freedoms is $4\,(\#\mathcal{T}) + 4\,(\#\mathcal{E})$ per fixed-point iteration.

Chapter 6

Numerical Investigation of the Homogenization Process

The main issue of this chapter is the comparison of solutions of the scaled SNPP systems introduced in Chapter 2 with that of its associated homogenized systems in two space dimensions. Since a choice of fixed scaling parameters (α, β, γ) adjusts a weighting between the different electrokinetic processes modeled by the SNPP system, the types of the corresponding upscaled DNPP system varies and especially also the couplings within. This chapter presents qualitative and also quantitative studies of the convergence rates in ε according to which the pore-scale solutions converge toward their upscaled equivalents.

Even though, periodic homogenization is a popular averaging technique, publications dealing with the numerical approximation of its homogenization results as well as investigations based on those are scarce. Most of the publications focusing on the numerical aspect are dealing with the computation of effective coefficients by solving cell problems (e. g., Allaire et al. 2013; Chavarria-Krauser & Ptashnyk 2010; Griebel & Klitz 2010; Smith et al. 2004). An even smaller number of publications have numerically investigated the quality of homogenized systems (e. g., Bourgat 1979; Mahato 2013; Sarkis & Versieux 2008; van Noorden 2009).

The outline of this chapter is as follows: in Section 6.1 an appropriate test scenario is constructed based on which the subsequent numerical simulations for both the SNPP systems and DNPP systems, are performed. This contains, inter alia, the definition of appropriate initial conditions and boundary conditions including the respective data. Additional boundary conditions on the solid surfaces have to be defined for the SNPP systems due to the resolving of the pore scale. Section 6.2 outlines the three different DNPP systems obtained by three choices of fixed sets of scaling parameters. These upscaled systems incorporate effective tensors, which are pre-computed for the simulations that follow. Here, we examine the grid convergence rate and illustrate different possible choices of pore ge-

ometries represented by unit cells. We proceed in Section 6.3 with the investigation of the simulation results by interpreting the different behaviors of physical meaningful quantities with regard to the different choices of scalings. In Section 6.4 we study qualitatively the rate of convergence in the scale parameter ε by comparing outflow curves. Section 6.5, which is the main part of this chapter, deals with quantitative studies of the approximation quality with respect to ε of the three SNPP systems under consideration. The computation of the distance between SNPP solutions and DNPP solutions—that we call the *scale error*—requires the application of a *grid-to-grid projection algorithm* including a *stencil jumping algorithm* as a subroutine. We show the numerically estimated orders of convergence in the scale parameter ε and present explicit visualizations of the scale errors.

All simulations in this chapter were performed with the numerical toolbox *HyPHM* (cf. Appx. A). Most of the simulation results were published in Frank et al. (2011).

Notation. For fixed values of scaling parameters α, β, γ the corresponding SNPP system due to Problem 2.1 on p. 19 is abbreviated by $P_\varepsilon^{\alpha,\beta,\gamma}$, while the corresponding DNPP system as stated in Theorems 2.5 and 2.8 on pages 23 and 25 is abbreviated by $P_0^{\alpha,\beta,\gamma}$.

6.1 Formulation of a Test Scenario

This section deals with the construction of an expedient test scenario in order to show the convergence $P_{\varepsilon,h}^{\alpha,\beta,\gamma} \to P_{0,h}^{\alpha,\beta,\gamma}$ numerically as $\varepsilon \to 0$ for three considered sets of parameters (α,β,γ), where $P_0^{\alpha,\beta,\gamma}$ denote the limit systems stated in Theorems 2.5 and 2.8. The symbols $P_{\varepsilon,h}^{\alpha,\beta,\gamma}$ and $P_{0,h}^{\alpha,\beta,\gamma}$ stand for the associated discretized versions of $P_\varepsilon^{\alpha,\beta,\gamma}$ and $P_0^{\alpha,\beta,\gamma}$, respectively.

Domains and general setting. Recall the periodic two-scale framework as illustrated in Figure 2.1 on p. 18. We consider a square domain $\Omega =]0,1[^2$ and its perforated version Ω_ε with solid inclusions as described later in this section. On both scales, we choose boundary and initial conditions such that a horizontal flow field arises in which two oppositely charged species are transported through the domain.

Boundary conditions, initial conditions, and constraints. To complete $P_\varepsilon^{\alpha,\beta,\gamma}$ and $P_0^{\alpha,\beta,\gamma}$ boundary conditions on the exterior boundary $\partial\Omega$ for both systems have to be defined. We choose periodic conditions on $]0,1[\times\{0,1\}$, an inflow boundary condition on $\{0\}\times]0,1[$,

and an outflow boundary condition on $\{1\}\times\,]0,1[$. The corresponding boundaries are denoted by $\partial\Omega^{\text{in}}$ and $\partial\Omega^{\text{out}}$, respectively, and write $\partial\Omega := \partial\Omega^{\text{in}} \cup \partial\Omega^{\text{out}}$ in this section.

The pore velocity $\boldsymbol{u}_\varepsilon$ in $P_\varepsilon^{\alpha,\beta,\gamma}$ is given by Stokes equations and the averaged velocity $\bar{\boldsymbol{u}}_0$ in $P_0^{\alpha,\beta,\gamma}$ by an extended Darcy's law. According to Section 2.2.1, the exterior boundary conditions for the homogenized system coincide with that of the pore scale system, for which we choose inflow boundary conditions of Dirichlet type:

$$\boldsymbol{u}_\varepsilon \;=\; \boldsymbol{u}_{\text{D}} \qquad \text{on } J\times\partial\Omega^{\text{in}}\,.$$

This boundary condition is not feasible for the averaged velocity $\boldsymbol{u}_0$, since $\boldsymbol{u}_0 \in L^2(J;\boldsymbol{H}^{\text{div}}(\Omega)) \not\subset L^2(J;\boldsymbol{H}^1(\Omega))$ lacks on regularity. As a remedy, we choose flux inflow conditions, i. e.,

$$\bar{\boldsymbol{u}}_0\cdot\boldsymbol{\nu} \;=\; u_{\text{flux}} \qquad \text{on } J\times\partial\Omega^{\text{in}}\,.$$

In order to obtain a coincident normal inflow, let

$$\boldsymbol{u}_{\text{D}} \;:=\; \begin{pmatrix} u^{\text{in}} \\ 0 \end{pmatrix} \qquad \text{and} \qquad u_{\text{flux}} \;:=\; -u^{\text{in}}\,,$$

where $u^{\text{in}} : J\times\partial\Omega^{\text{in}} \to \mathbb{R}$ is a given inflow rate. For both problems, outflow boundary conditions are chosen on $\partial\Omega^{\text{out}}$ (cf. (6.1b) and (6.2b)).

For the transport problems on both scales, we take $\partial\Omega^{\text{in}}$ to be a boundary through which the molar fluxes $\boldsymbol{j}^{\pm,\text{in}} : J\times\partial\Omega^{\text{in}} \to \mathbb{R}^2$ are prescribed and $\partial\Omega^{\text{out}}$ to be of homogeneous Neumann type (cf. (6.1d) and (6.2d)).

By choosing a homogeneous Neumann boundary condition $\boldsymbol{E}_\varepsilon\cdot\boldsymbol{\nu} = 0$ on the exterior boundary $\partial\Omega$ in the case of $\alpha = 0$, we would have to satisfy a *global electro-neutrality condition* as a compatibility condition, which is obtained by testing (2.1h) with one and applying the divergence theorem:

$$\int_{\Omega_\varepsilon} c_\varepsilon^+ - c_\varepsilon^-\,\mathrm{d}\boldsymbol{x} \overset{(2.1\text{h})}{=} \int_{\Omega_\varepsilon} \boldsymbol{\nabla}\cdot\boldsymbol{E}_\varepsilon\,\mathrm{d}\boldsymbol{x} \;=\; \int_{\Gamma_\varepsilon} \boldsymbol{E}_\varepsilon\cdot\boldsymbol{\nu}\,\mathrm{d}s_{\boldsymbol{x}} + \int_{\partial\Omega} \boldsymbol{E}_\varepsilon\cdot\boldsymbol{\nu}\,\mathrm{d}s_{\boldsymbol{x}} \overset{(2.1\text{i})}{=} \varepsilon\int_{\Gamma_\varepsilon}\sigma\,\mathrm{d}s_{\boldsymbol{x}}$$

for a. e. $t\in J$. An analogous condition is obtained for (2.5f). In order to avoid this situation—which is not feasible for a general setting—we choose homogeneous Dirichlet boundary data in the case of $\alpha = 0$ (cf. (6.1f)). For $\alpha = 2$, a homogeneous Dirichlet condition is not reasonable since in general $\bar{\phi}_0$ is non-zero on $\partial\Omega$ (cf. Rem. 2.9). Therefore, we apply homogeneous Neumann boundary data in the case $\alpha = 2$ (cf. (6.1f)).

Recapitulating, the pore scale problem $P_\varepsilon^{\alpha,\beta,\gamma}$ as given in (2.1) is completed with the boundary and initial conditions

$$\begin{aligned}
\boldsymbol{u}_\varepsilon &= \begin{pmatrix} u^{\mathrm{in}} \\ 0 \end{pmatrix}, && \text{on } J \times \partial\Omega^{\mathrm{in}}, && (6.1a)\\
(\boldsymbol{\nabla} \boldsymbol{u}_\varepsilon - p_\varepsilon \mathbf{I})\, \boldsymbol{\nu} &= \mathbf{0}, && \text{on } J \times \partial\Omega^{\mathrm{out}}, && (6.1b)\\
\boldsymbol{j}_\varepsilon^{\pm} \cdot \boldsymbol{\nu} &= -j^{\pm,\mathrm{in}}, && \text{on } J \times \partial\Omega^{\mathrm{in}}, && (6.1c)\\
-\boldsymbol{\nabla} c_\varepsilon^{\pm} \cdot \boldsymbol{\nu} &= 0, && \text{on } J \times \partial\Omega^{\mathrm{out}}, && (6.1d)\\
c_\varepsilon^{\pm} &= 0, && \text{on } \{0\} \times \Omega_\varepsilon, && (6.1e)\\
\begin{Bmatrix} \phi_\varepsilon = 0, & \alpha = 0 \\ \boldsymbol{E}_\varepsilon \cdot \boldsymbol{\nu} = 0, & \alpha = 2 \end{Bmatrix}, && \text{on } J \times \partial\Omega. && (6.1f)
\end{aligned}$$

The upscaled problem $P_0^{\alpha,\beta,\gamma}$, as stated in Theorems 2.5 and 2.8, is completed with

$$\begin{aligned}
\bar{\boldsymbol{u}}_0 \cdot \boldsymbol{\nu} &= -u^{\mathrm{in}}, && \text{on } J \times \partial\Omega^{\mathrm{in}}, && (6.2a)\\
p_0 &= 0, && \text{on } J \times \partial\Omega^{\mathrm{out}}, && (6.2b)\\
\boldsymbol{j}_0^{\pm} \cdot \boldsymbol{\nu} &= -j^{\pm,\mathrm{in}}, && \text{on } J \times \partial\Omega^{\mathrm{in}}, && (6.2c)\\
-\boldsymbol{\nabla} c_0^{\pm} \cdot \boldsymbol{\nu} &= 0, && \text{on } J \times \partial\Omega^{\mathrm{out}}, && (6.2d)\\
c_0^{\pm} &= 0, && \text{on } \{0\} \times \Omega, && (6.2e)\\
\begin{Bmatrix} \phi_0 = 0, & \alpha = 0 \\ \text{—}, & \alpha = 2 \end{Bmatrix}, && \text{on } J \times \partial\Omega. && (6.2f)
\end{aligned}$$

The boundary data u^{in}, $j^{\pm,\mathrm{in}}$ on $\partial\Omega^{\mathrm{in}}$ and also the boundary data ϕ_{D}, σ on the interior boundary Γ_ε (cf. (2.1i)) are defined below.

Boundary data. We choose a stationary inflow $u^{\mathrm{in}} := 1$ and molar fluxes across the boundary

$$j^{+,\mathrm{in}} := \begin{Bmatrix} 1, & t \in]0,1] \\ 0, & \text{otherwise} \end{Bmatrix}, \qquad j^{-,\mathrm{in}} := \begin{Bmatrix} 1, & t \in]1/2,3/2] \\ 0, & \text{otherwise} \end{Bmatrix}.$$

These fluxes realize a “pulse” of each concentration entering the domain of duration one. Since both pulses exist for $t \in]1/2, 1]$, it is ensured that a reaction between both species

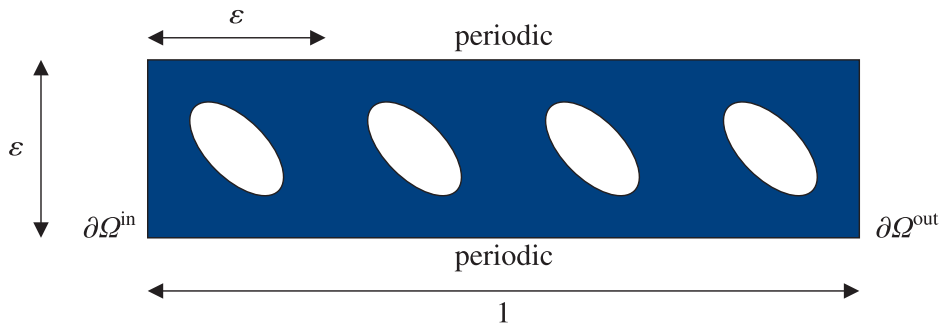

Figure 6.1. Stripes with a vertical length of ε used as computational domain Ω_ε.

takes place (cf. (2.1e) and associated homogenization results). The surface charge density σ and the surface potential ϕ_D appear in the (interior) boundary condition of (2.1i) and also as effective magnitudes in (2.5f) and (2.8). We choose the data $\sigma := 1$ and $\phi_D := 1$. Even though the latter value has no impact on the electric field, since it was assumed to be a constant, the correct reference state with regard to the averaged potential $\bar{\phi}_0$ has to be chosen.

Simplifications. The boundary conditions defined above allow the computation of $P_{\varepsilon,h}^{\alpha,\beta,\gamma}$ on stripes of vertical length ε as illustrated in Figure 6.1 with periodic boundary conditions on $]0,1[\times\{0,\varepsilon\}$ as performed, e. g., by van Noorden (2009), and Efendiev & Hou (2009). This reduces the computation cost from quadratic to linear order in $1/\varepsilon$.

6.2 Preliminary Remarks

By applying the test scenario defined in Section 6.1, we numerically investigate the theoretically predicted convergence in the small-scale parameter $\varepsilon \to 0$. Therefore, we consider the following conceptually different types of limit problems $P_0^{\alpha,\beta,\gamma}$ (cf. Thms. 2.5 and 2.8): the first model corresponds to the parameter set $(\alpha,\beta,\gamma) = (0,0,0)$, the second to the set $(0,1,0)$ and the third to the set $(2,1,1)$ (cf. Sec. 2.2; Tab. 2.1).

In the first case, we deal with a fully coupled system of partial differential equations similar to the pore scale-model $P_\varepsilon^{0,0,0}$. Here, the liquid flow is directly coupled to both the electric and the concentration fields by means of an extended Darcy's law. The transport of the concentrations is given by Nernst–Planck equations with effective coefficients. Moreover, the extended Darcy velocity enters the convective term and the electric field occurs in the drift term. Eventually, the electric field is given by an elliptic second-order partial differential equation with effective coefficients and charge densities of the concentrations as source term.

In the second case, the macroscopic velocity is determined by a standard Darcy's law. Consequently, the Darcy velocity serves as a convective term in the transport of the concentrations, but there is no back coupling of the electric field or the concentrations on the velocity field. However, since the transport is given by a Nernst–Planck system, the upscaling procedure yields a (partially) coupled system of partial differential equations. On the one hand the concentration distribution influences the electric field, which on the other hand determines the concentrations.

The third choice of parameter set results in a decoupled limit system. The liquid flow is determined by a standard Darcy's law and the transport is determined by a standard convection–diffusion equation with Darcy velocity in the convective term. The electric term vanishes completely in the limit description for the velocity and the concentrations. Even though there is no averaged presentation of the pore-scale electric field, the averaged electric potential can be reconstructed from the concentration fields (cf. (2.8)). Note that in this case the volume additivity constraint (cf. (2.6), p. 25 and Sec. 2.2.2) is not required from the numerical point of view and thus is released in what follows.

For the numerical validation of the convergence, the pore-scale problems $P^{\alpha,\beta,\gamma}_{\varepsilon,h}$ as well as the averaged problems $P^{\alpha,\beta,\gamma}_{0,h}$ are solved for the three parameter sets $(\alpha,\beta,\gamma) = (0,0,0)$, $(0,1,0)$, and $(2,1,1)$ according to the setting described in Section 6.1. In all cases, it is reasonable to precompute the upscaled tensors, since they decouple from the upscaled systems. In order to obtain a sufficiently good approximation, we proceed as follows.

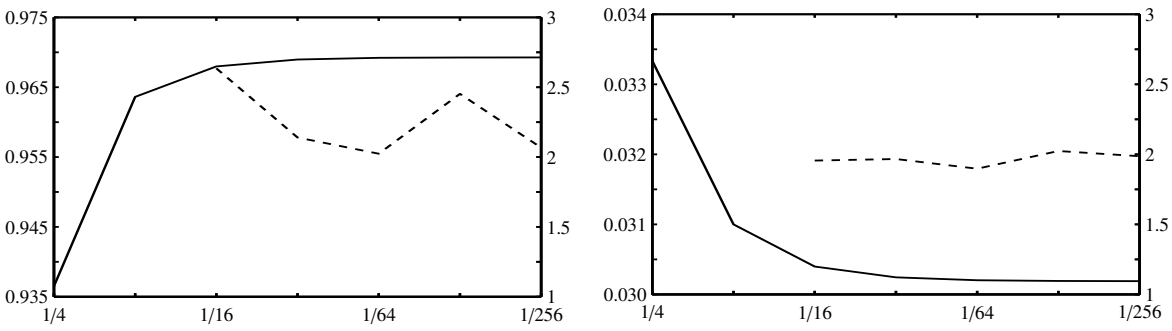

Figure 6.2. The graphs show the convergence behavior of the computed upscaled tensors $\mathbf{D}_h$ (a) and $\mathbf{K}_h$ (b) for vanishing mesh size h. The Frobenius norms of the tensors (*solid*) and the minimum convergence orders according to (5.2b) (*dashed*) are plotted against h.

Geometry of the representative cell. The solid inclusion Y_s of the representative unit cell $Y =]0,1[^2$ (cf. Fig. 2.1) may be replaced by more general geometries. Thereby the

h	1/4	1/8	1/16	1/32	1/64	1/128	1/256
triangles	24	120	505	2 126	9 336	37 438	155 108
edges	40	188	774	3 222	14 071	56 291	232 930
vertices	15	67	268	1 095	4 734	18 852	77 821
permeability tensor							
$(\mathbf{K}_h)_{1,1}$	2.301E−2	2.145E−2	2.103E−2	2.092E−2	2.090E−2	2.089E−2	2.089E−2
$(\mathbf{K}_h)_{2,1}$	−5.096E−3	−4.531E−3	−4.436E−3	−4.415E−3	−4.409E−3	−4.408E−3	−4.407E−3
$(\mathbf{K}_h)_{1,2}$	−5.096E−3	−4.531E−3	−4.436E−3	−4.415E−3	−4.409E−3	−4.408E−3	−4.407E−3
$(\mathbf{K}_h)_{2,2}$	2.301E−2	2.145E−2	2.103E−2	2.092E−2	2.090E−2	2.089E−2	2.089E−2
$\|\mathbf{K}_h\|_{\mathrm{F}}$	3.334E−2	3.100E−2	3.040E−2	3.024E−2	3.020E−2	3.019E−2	3.019E−2
diffusion / permittivity tensor							
$(\mathbf{D}_h)_{1,1}$	6.532E−1	6.755E−1	6.790E−1	6.798E−1	6.800E−1	6.801E−1	6.801E−1
$(\mathbf{D}_h)_{2,1}$	−1.087E−1	−8.890E−2	−8.608E−2	−8.538E−2	−8.519E−2	−8.515E−2	−8.514E−2
$(\mathbf{D}_h)_{1,2}$	−1.087E−1	−8.890E−2	−8.608E−2	−8.538E−2	−8.519E−2	−8.515E−2	−8.514E−2
$(\mathbf{D}_h)_{2,2}$	6.532E−1	6.756E−1	6.790E−1	6.798E−1	6.800E−1	6.801E−1	6.801E−1
$\|\mathbf{D}_h\|_{\mathrm{F}}$	9.365E−1	9.636E−1	9.680E−1	9.690E−1	9.692E−1	9.693E−1	9.693E−1

Table 6.1. Approximated upscaled tensors $\mathbf{D}_h$ and $\mathbf{K}_h$ computed on a periodically bounded grid for decreasing mesh size h.

statements of Theorems 2.5 and 2.8 remain true. Even though our numerical scheme can deal with such geometric settings, we consider a solid part with an elliptic shape in this thesis (cf. Fig. 6.3 (a) to (d)). The reason is that on the one hand, angular geometries as depicted in Figure 6.3 (e), (f) reduce the convergence order co_h in h (cf. Sec. 5.1.2) and on the other hand the simplest geometry—a circle—would yield isotropic upscaled tensors $\mathbf{D}_h$ and $\mathbf{K}_h$ (cf. Def. 2.3 and Expl. 1.1).

Upscaled tensors. The upscaled tensors $\mathbf{D}_h$ and $\mathbf{K}_h$ are computed by integration of the flux solution of the (discretized) cell problems (2.2b) and (2.3b) according to (2.2a) and (2.3a), respectively, for a sequence of decreasing mesh sizes $(h_j)_j$. Owing to the regularity of the chosen geometry (cf. Fig. 6.3), we observe a superconvergence of second order in h (cf. Tab. 6.1 and Fig. 6.2). For the computation of the homogenized problems $P_{0,h}^{\alpha,\beta,\gamma}$, for every h, we use the best approximation of $\mathbf{D}$ and $\mathbf{K}$. Also note that the computed tensors are symmetric and positive definite as expected (cf. Def. 2.3).

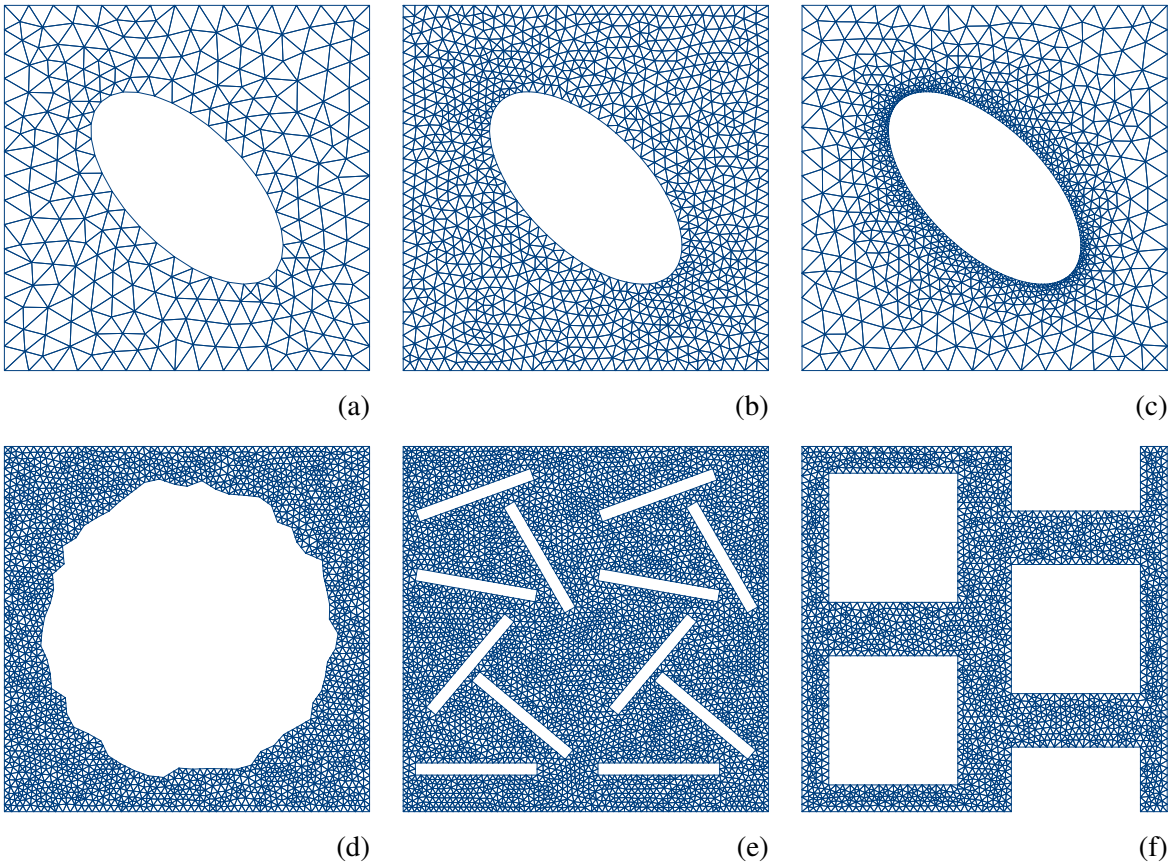

Figure 6.3. The considered solid part is bounded by a centered ellipsis of diameters 1/3 and 2/3 with a rotation angle of $\pi/4$. The triangulated unit cell as used in this chapter is shown for $h = 1/16$ in (a) and for $h = 1/32$ in (b). Pre-adaptation is also feasible for practical computations (c). More complex geometries as illustrated in (d) or as used by Smith et al. (2004) (e) or by Allaire et al. (2013) (f) are also valid choices for our numerical scheme.

Since we focus on the scale error in ε (cf. Sec. 6.5), for the remainder of this thesis, the discretization parameters (τ, h) as well as the iteration tolerance tol are chosen sufficiently small to exclude discretization and splitting errors.

6.3 Comparison of Different Scalings and Investigation of Physical Quantities

We qualitatively investigate the convergence of different physically meaningful variables and compare the different choices of scalings with regard to their physical behavior.

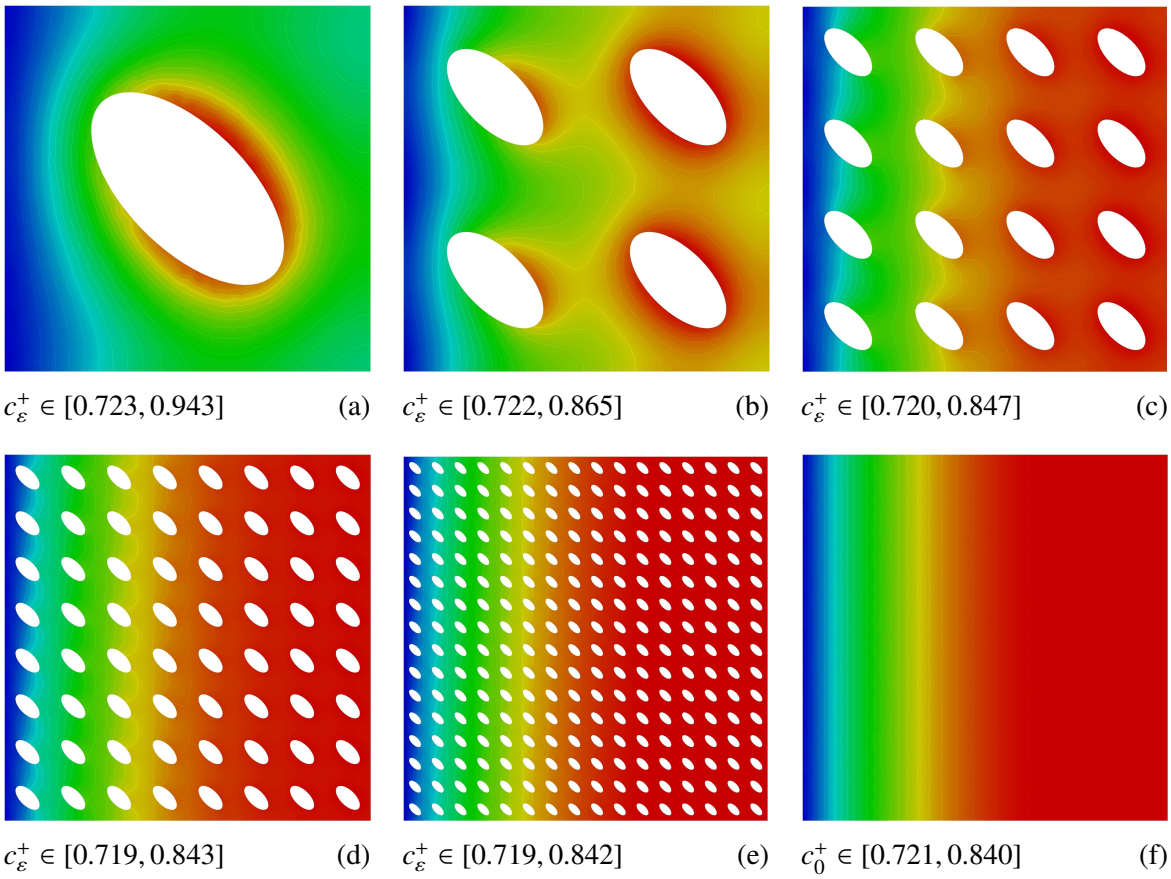

Figure 6.4. Concentration profiles (*blue* / low to *red* / high) for the parameters $(\alpha, \beta, \gamma) = (0, 0, 0)$ at time $t = 1$ for $\varepsilon = 1, 1/2, \ldots, 1/16$ (a)–(e) and the limit (f).

Velocity and pressure. In Figure 6.7, the velocity fields are compared and the convergence in the scale parameter ε is demonstrated. The Stokes flow $\boldsymbol{u}_\varepsilon$ as a solution of the pore-scale model shows the physically expected flow around the obstacles. The Darcy flow $\boldsymbol{u}_0$ is directed diagonally to the lower right corner of the computational domain due to the geometry of the underlying perforated domain that determines the permeability tensor $\mathbf{K}$ (cf. (2.3)).

We observe very similar flow fields for the cases of $(\alpha, \beta, \gamma) = (0, 0, 0)$ and $(0, 1, 0)$, which results in similar outflow curves as depicted in Figure 6.10. In the latter case, the velocity is first slightly increased and then decreased, because the impact of the electric interaction is only of minor magnitude and the pressure field p_0 mainly balances this influence.

Concentration fields. Figure 6.4 demonstrates the convergence of the concentration fields for vanishing scale parameter ε. The concentration front that is locally varying between the

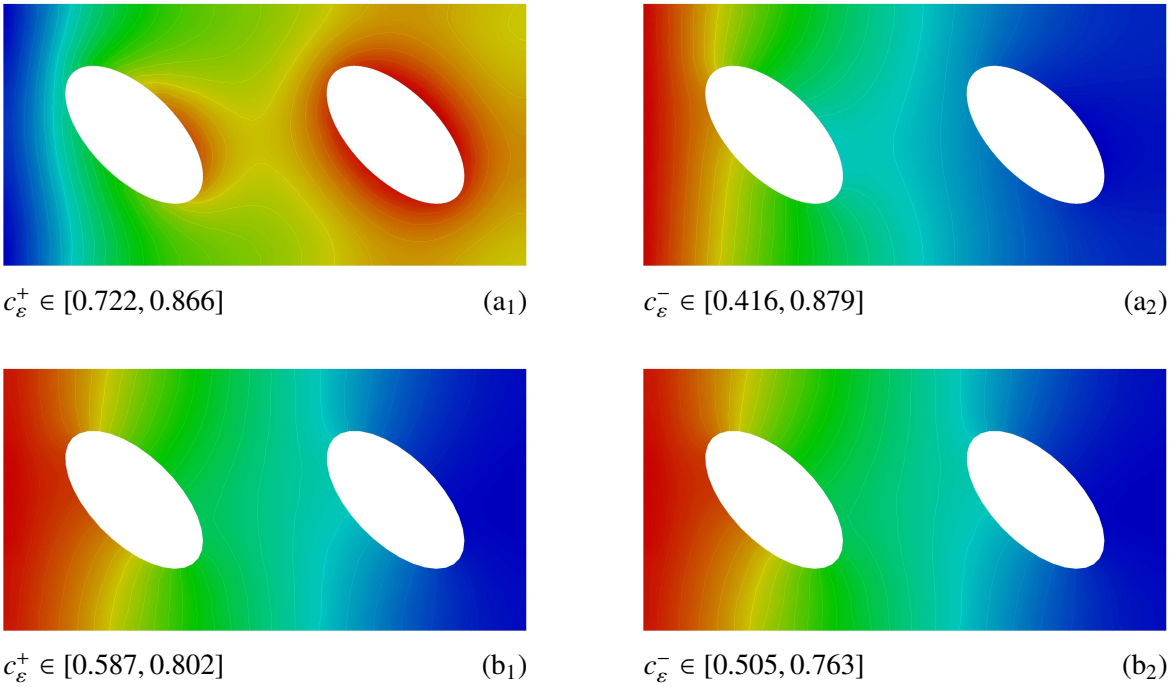

$c_\varepsilon^+ \in [0.722, 0.866]$ (a$_1$) $c_\varepsilon^- \in [0.416, 0.879]$ (a$_2$)

$c_\varepsilon^+ \in [0.587, 0.802]$ (b$_1$) $c_\varepsilon^- \in [0.505, 0.763]$ (b$_2$)

Figure 6.5. Concentration profiles (*blue* / low to *red* / high) for $\varepsilon = 1/2$, $(\alpha, \beta, \gamma) = (0, 0, 0)$ (a) and $(2, 1, 1)$ (b) at time $t = 1$.

obstacles is smeared to a uniform front more and more resembling a solution of the upscaled model.

The concentration fields c_ε^+ and c_ε^- underlie an electric drift toward and against the orientation of the electric field, respectively (cf. (2.1d)). As illustrated for $\alpha = 0$ this results in an attraction of c_ε^+ and a repulsion of c_ε^- near Γ_ε (cf. Fig. 6.5 (a)) and further causes a retention of c_ε^+ in the domain (cf. Fig. 6.10 and Fig. 6.9, charged cases). A significantly different behavior is observable for $\alpha = 2$ at which both concentrations are attracted near Γ_ε (cf. Figs. 6.5 (b) and 6.11) due to an orientation change of the electric field (see below).

Electric field and electric potential. For $\alpha = 0$ and $\alpha = 2$, two essentially different evolution behaviors for the electric field and the electric potential are observed (cf. Figs. 6.6 and 6.8). In the first case, both the Neumann condition at Γ_ε (cf. (2.1i)) and the additional force term $\bar{\sigma}$ (cf. (2.5f)) for pore and average scale, respectively, generate an electric field pointing in an 'inward direction' of the domain (Fig. 6.6). The field accounts for the transient force term (due to charge movement) appearing in (2.1h) and (2.5f) with respect to time but preserves its orientation at the boundaries. Note that the averaged electric field also

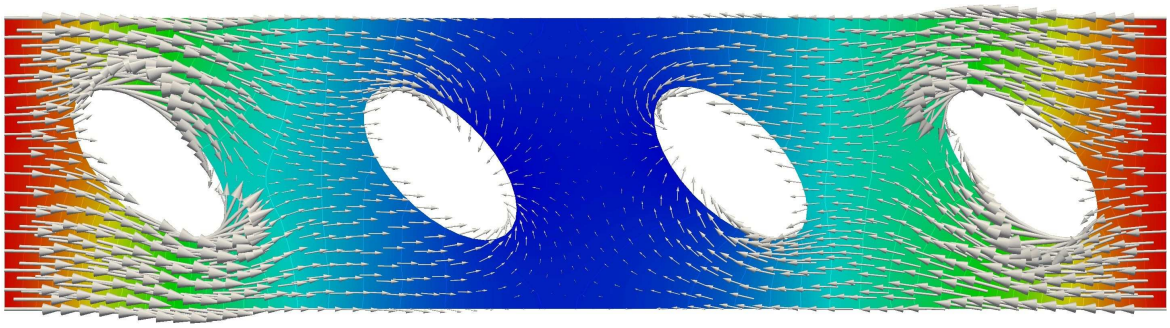

$|\boldsymbol{E}_\varepsilon| \in [0.014, 1.701]$, $\phi_\varepsilon \in [-0.307, -0.003]$

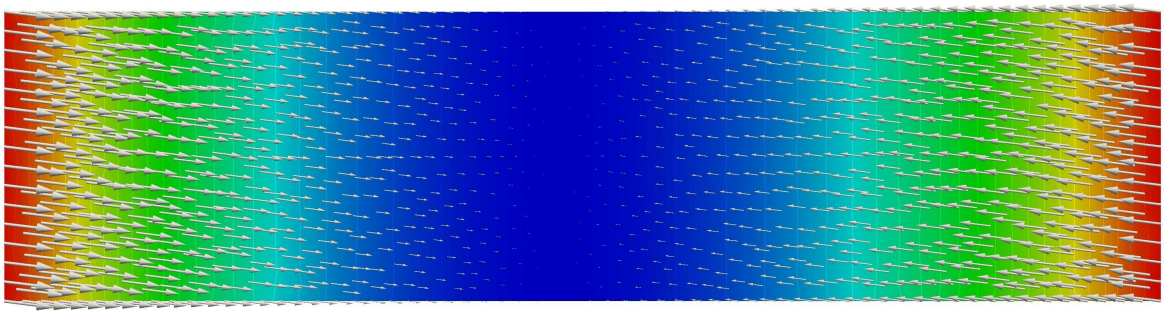

$|\boldsymbol{E}_0| \in [0, 0.898]$, $\phi_0 \in [-0.297, -0.003]$

Figure 6.6. Electric field and electric potential distribution (*blue* / low to *red* / high) for $P_\varepsilon^{0,0,0}$ (top) and $P_0^{0,0,0}$ (bottom) at time level $t = 3/2$.

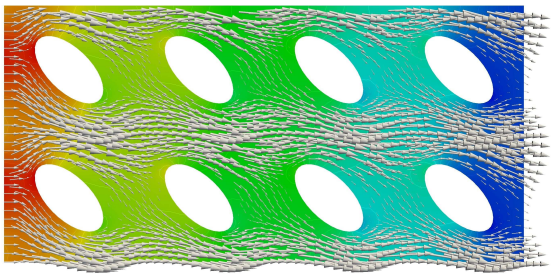

$|\boldsymbol{u}_\varepsilon| \in [0, 2.683]$, $p_\varepsilon \in [-4.549, 55.29]$ (a)

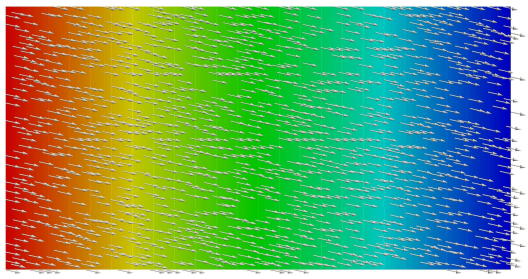

$|\boldsymbol{u}_0| \equiv 1.022$, $p_0 \in [0.150, 47.68]$ (b)

Figure 6.7. Flow and pressure profiles (*blue* / low to *red* / high) $(\boldsymbol{u}_\varepsilon, p_\varepsilon)$ (Stokes) for $\varepsilon = 1/4$ (a) and $(\boldsymbol{u}_0, p_0)$ (Darcy) (b), both for the parameters $(\alpha, \beta, \gamma) = (0, 1, 0)$.

accounts for the spatial orientation of the electric field at the pore scale, which results from the anisotropic pore geometry. The defined (constant) surface potential ϕ_D has no influence on $\boldsymbol{E}_\varepsilon$ and its orientation is solely prescribed by the presence of charged concentrations for the case of $\alpha = 2$ (cf. {(2.1g), (2.1h), (2.1i)} and Fig. 6.8). The consequence is an orientation change as soon as one species starts to dominate the other.

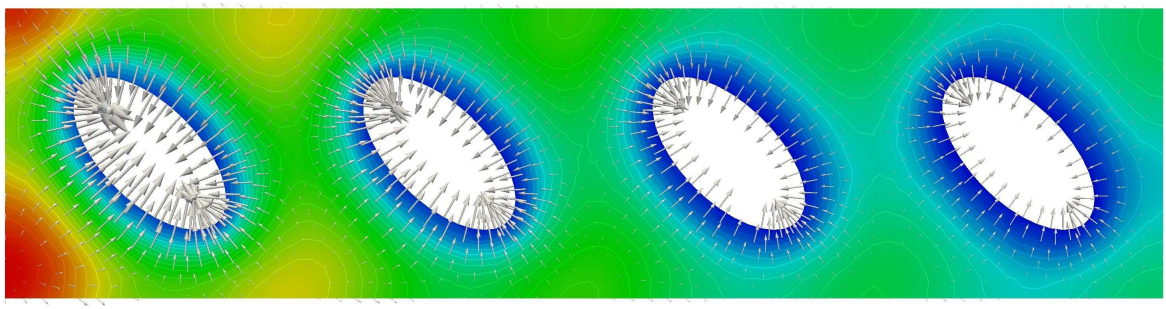

$|\boldsymbol{E}_\varepsilon| \in [0, 0.085]$, $\phi_\varepsilon \in [0.002, 0.045]$ (a_1)

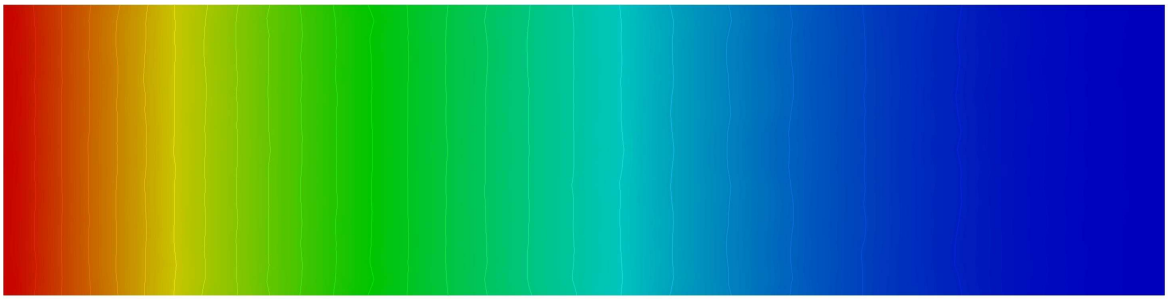

$\phi_0 \in [0.836, 0.851]$ (a_2)

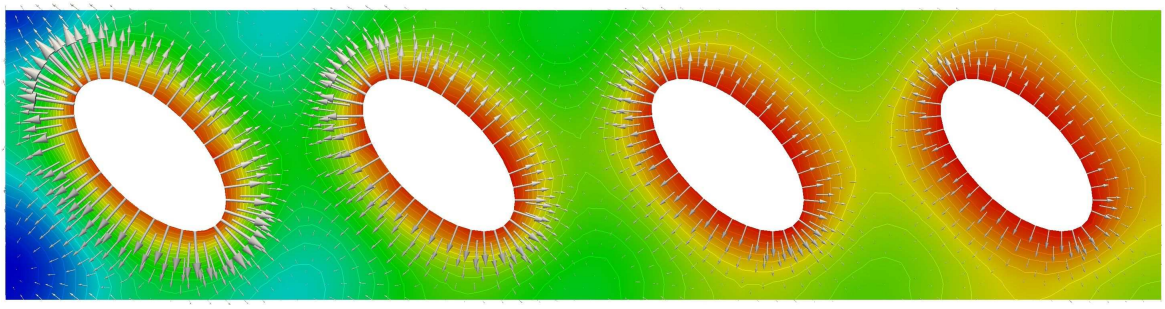

$|\boldsymbol{E}_\varepsilon| \in [0, 0.083]$, $\phi_\varepsilon \in [-0.045, -0.002]$ (b_1)

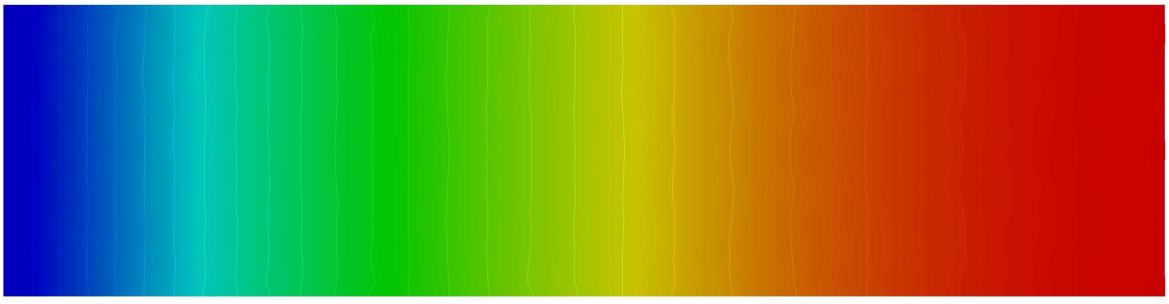

$\phi_0 \in [0.803, 0.818]$ (b_2)

Figure 6.8. Electric field and electric potential distribution (*blue* / low to *red* / high) for $P_\varepsilon^{2,1,1}$ (a_1), (b_1) and $P_0^{2,1,1}$ (a_2), (b_2) at time levels $t = 1/2$ (a) and $t = 3/2$ (b).

Remark 6.1 (Further notes). Concentrations that are attracted to the interior boundaries (cf. (2.1i)) do not create singularities in the sense that they increase to infinity near Γ_ε, since concentrations are sources in the electric field (cf. (2.1h)) or—in physical terms—the surface attraction is balanced by the interior repulsion, respectively. For $\alpha = 0$, higher absolute values of σ may cause the electric drift to dominate over the advective transport—a fact that may cause a permanent retention of concentrations in the domain or may inhibit one concentration from entering the domain. △

6.4 Qualitative Convergence Studies

In geosciences so-called column experiments are a standard way to examine flow, transport, or material properties in which substances travel through a cylinder made of either a natural soil or a synthetic porous medium. From breakthrough curves, i. e., the outflow concentrations against time, model parameters can be inferred.

Therefore, we define the *(molar) outflow curve* by

$$q_\varepsilon^{\pm,\mathrm{out}}(t) \;:=\; \int_{\partial\Omega^{\mathrm{out}}} \boldsymbol{j}_\varepsilon^{\pm}(t,\boldsymbol{x}) \cdot \boldsymbol{\nu} \,\mathrm{d}s_{\boldsymbol{x}} \,. \tag{6.3}$$

Figures 6.10 and 6.11 show that the mean outflow curves $q_\varepsilon^{\pm,\mathrm{out}}$ converge for decreasing ε to the limits $q_0^{\pm,\mathrm{out}}$ for all considered parameter sets (α,β,γ). Interestingly, the outflow curves—even of the coarsest case of $\varepsilon = 1$—are similar to that of the averaged case of $\varepsilon = 0$ and the rate of convergence is fairly fast.

In order to study the impact of electrodynamic interactions, also with respect to reactivity, we solve the most complex / fully coupled averaged problem $P_0^{0,0,0}$ additionally for uncharged concentrations and with / without reaction term. Figure 6.9 visualizes the outflow curves of these cases. First, consider the inert, uncharged case: both curves are congruent—or equivalently—both transport problems are completely decoupled. Switching to the charged setting, it is clearly realized that c_0^+ has an increased residence time in the domain, whereas c_0^- has a decreased residence time. Moreover, a transport acceleration of c_0^- is observable. Note that in all cases considered so far, mass is preserved, i. e., the integral of the curves is invariable. If the case of $(\alpha,\beta,\gamma) = (0,0,0)$ is compared with its uncharged analog, it is observed that the associated curves for each species diverge even more strongly. This indicates that electrodynamic effects have a severe impact on kinetic reactions, which clearly arises from the spatial redistribution of mass (cf. Fig. 6.5 (a)).

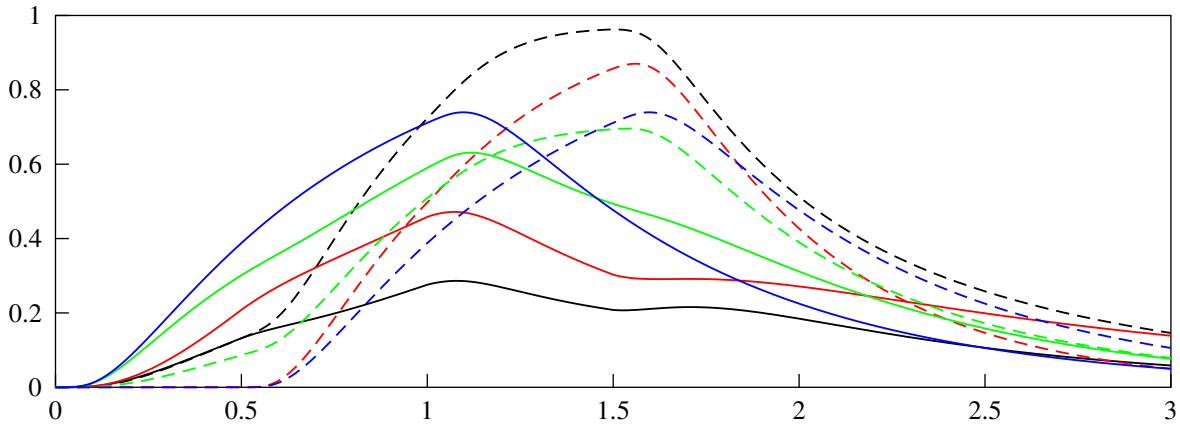

Figure 6.9. Comparison of the outflow curves $q_0^{+,\mathrm{out}}$ (*solid*) and $q_0^{-,\mathrm{out}}$ (*dashed*) defined in (6.3) of the averaged model for the parameters $(\alpha,\beta,\gamma) = (0,0,0)$ (*black*) with those of the inert case (*red*), uncharged case (*green*), and inert uncharged case (*blue*).

6.5 Quantitative Convergence Studies

In addition to the qualitative study in Section 6.4, we estimate the *order of convergence* in the scale parameter ε exemplarily for the choice of scaling $(\alpha,\beta,\gamma) = (0,0,0)$.

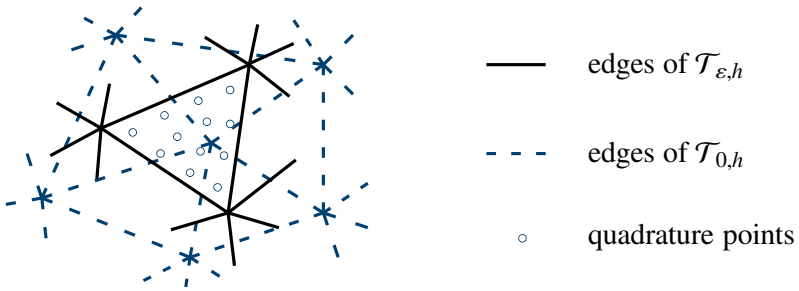

Figure 6.12. Quadrature on a triangle $T \in \mathcal{T}_{\varepsilon,h}$. The values at the quadrature points are taken on the associated underlying grid $\mathcal{T}_{\varepsilon,h}$ and $\mathcal{T}_{0,h}$, respectively.

Computation of the scale error. For a pair of discrete unknowns $(z_{\varepsilon,h}, z_{0,h})$ and a fixed scaling parameter ε, we define the L^p *scale error* on the perforated domain Ω_ε at time level t_n by

$$\|z_{\varepsilon,h}^n - z_{0,h}^n\|_{L^p(\Omega_\varepsilon)} \,. \tag{6.4}$$

Note that the area $|\Omega_\varepsilon|$ is invariant in ε (cf. Fig. 6.4). Under the assumption that the order of (6.4) is $\varepsilon^{\alpha_1} + h^{\alpha_2}/\varepsilon^{\alpha_3} + h^{\alpha_4}$ for some positive powers α_k (cf. Orive & Zuazua 2005; Sarkis

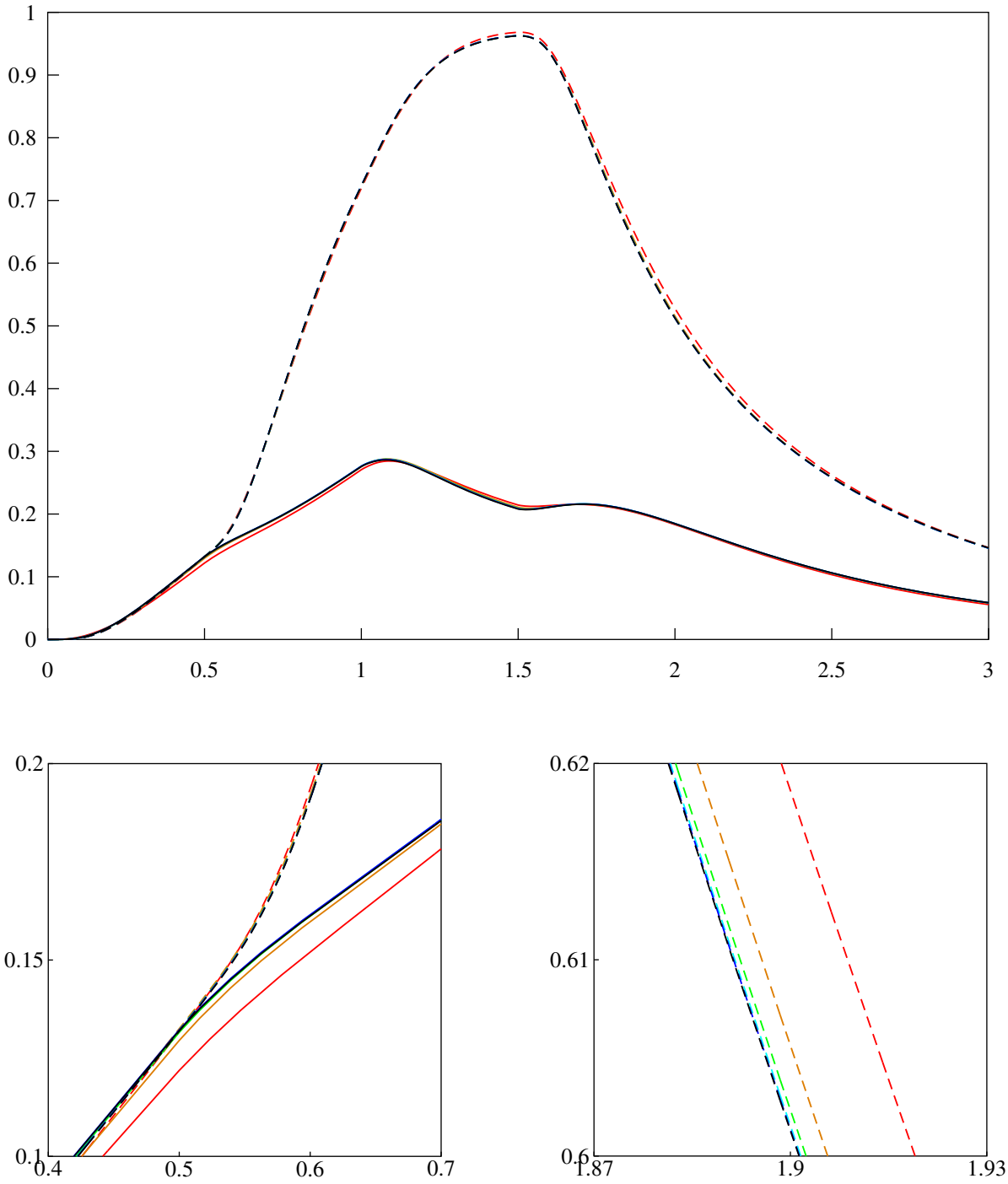

Figure 6.10. Outflow curves $q_\varepsilon^{\pm,\mathrm{out}}$ of the pore-scale model $P_\varepsilon^{\alpha,\beta,\gamma}$ and $q_0^{\pm,\mathrm{out}}$ of the averaged model $P_0^{\alpha,\beta,\gamma}$ (*solid* for +, *dashed* for −) for the parameters $(\alpha,\beta,\gamma) = (0,0,0),(0,1,0)$ (*red*, *orange*, *green*, *cyan*, *blue*, and *black* for $\varepsilon = 1, 1/2, 1/4, 1/8, 1/16$, and $\varepsilon \to 0$).

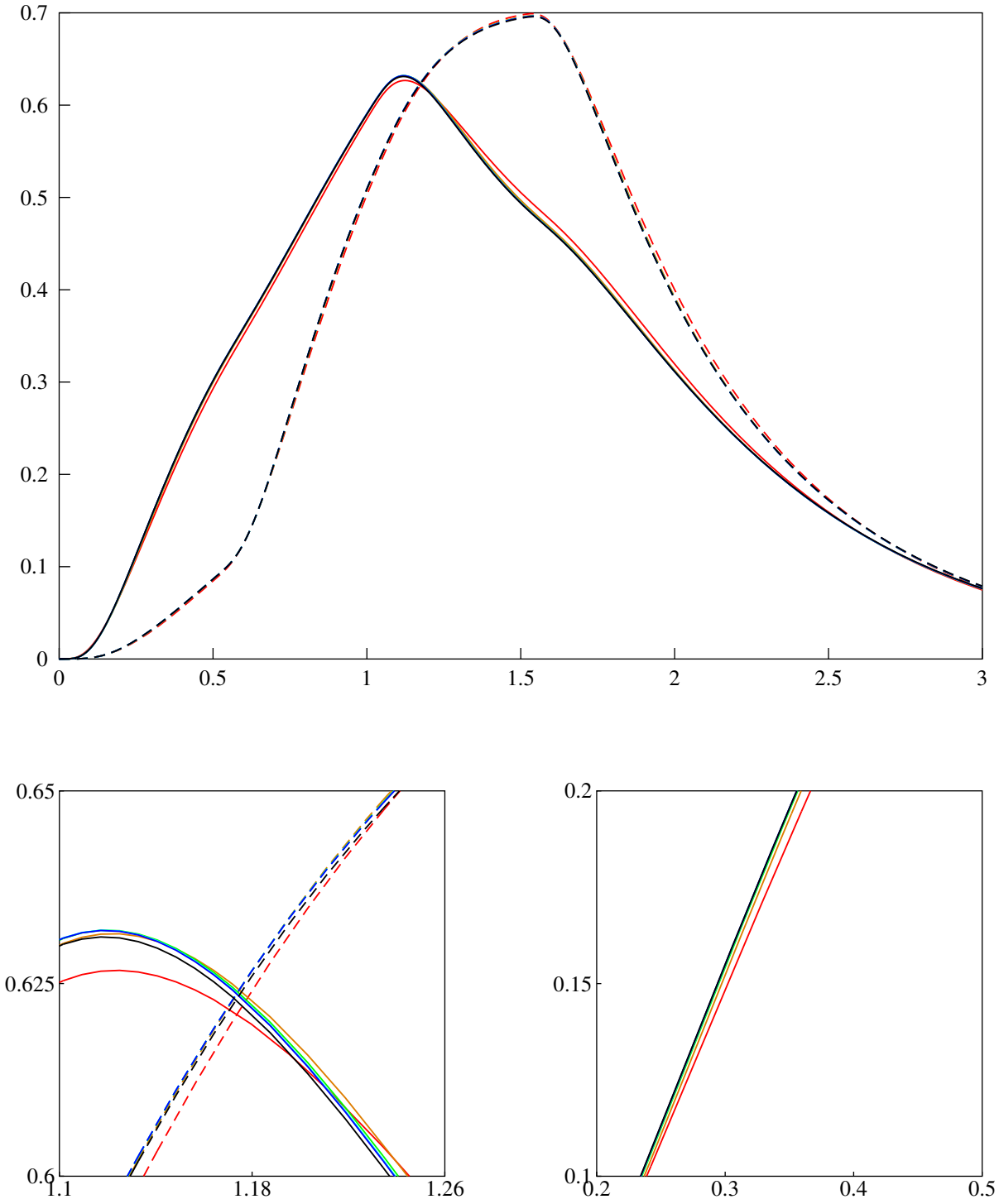

Figure 6.11. Outflow curves $q_\varepsilon^{\pm,\mathrm{out}}$ of the pore-scale model $P_\varepsilon^{2,1,1}$ and $q_0^{\pm,\mathrm{out}}$ of the averaged model $P_0^{2,1,1}$ (*solid* for +, *dashed* for −) (*red*, *orange*, *green*, *cyan*, *blue*, and *black* for $\varepsilon = 1, 1/2, 1/4, 1/8, 1/16$, and $\varepsilon \to 0$).

& Versieux 2008), the convergence order $\alpha_1 =: \mathrm{co}_\varepsilon$ in ε is estimated in the fashion of (5.2a) provided that the discretization parameters h and τ are sufficiently small.

Since $z_{\varepsilon,h}$ and $z_{0,h}$ are defined on different triangulations $\mathcal{T}_{\varepsilon,h}$ and $\mathcal{T}_{0,h}$, respectively, a direct computation of (6.4) is not possible. Therefore, the scale error is decomposed over $\mathcal{T}_{\varepsilon,h}$ and the local integrals are approximated by quadrature on each triangle $T \in \mathcal{T}_{\varepsilon,h}$ (cf. Fig. 6.12):

$$\left\| z^n_{\varepsilon,h} - z^n_{0,h} \right\|^p_{L^p(\Omega_\varepsilon)} = \sum_{T\in\mathcal{T}_{\varepsilon,h}} \int_T \left| z^n_{\varepsilon,h} - z^n_{0,h} \right|^p \approx \sum_{T\in\mathcal{T}_{\varepsilon,h}} \sum_{k=1}^{12} \omega_k \left| z^n_{\varepsilon,h}(\boldsymbol{\xi}_k) - z^n_{0,h}(\boldsymbol{\xi}_k) \right|^p$$

with *quadrature points* $\boldsymbol{\xi}_k \in T \setminus \partial T$ and *weights* $\omega_k > 0$ for each $T \in \mathcal{T}_{\varepsilon,h}$ using a sixth order quadrature rule (Stroud 1971). The values of $z^n_{\varepsilon,h}$ at the quadrature points are obtained directly by local interpolation in the underlying approximation space since $T \in \mathcal{T}_{\varepsilon,h}$. To obtain the values of $z^n_{0,h}$, for each quadrature point $\boldsymbol{\xi}_k$, the triangle $T' \in \mathcal{T}_{0,h}$ has to be determined first such that $\boldsymbol{\xi}_k \in T'$. This was realized by a *stencil jumping algorithm* (Löhner 2008, 'neighbor-to-neighbor search'), as illustrated in Figure 6.13. After the triangle T' has been identified, a local interpolation again yields the value of $z^n_{0,h}$.

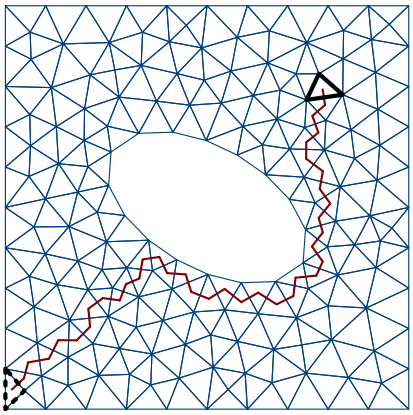

Figure 6.13. Starting on an initial triangle (*dashed bold triangle*), while aiming to identify the triangle that contains a given point (*solid bold triangle*), the *stencil jumping algorithm* successively travels the edges with the smallest possible (negative) barycentric coordinate with respect to the point searched for. The algorithm terminates when all three barycentric coordinates are nonnegative. When performed on a perforated domain—as illustrated but not used in this work—it must be ensured that no loops occur and that no boundary edge is crossed.

Computational results. The computations at time level $t = 3/2$ reveal $L^1(\Omega_\varepsilon)$ and $L^2(\Omega_\varepsilon)$ convergences of order $O(\varepsilon)$ for all scalar unknowns $p, c^\pm, \phi$ (cf. Tab. 6.2). In contrast, the scale errors of the vector-valued unknowns $\boldsymbol{u}$, $\boldsymbol{j}^\pm$, and $\boldsymbol{E}$ do not vanish but pass to a fixed value (cf. Rem. 6.2).

Figure 6.14 illustrates the *local* L^∞ scale errors of the scalar solutions for $P^{0,0,0}_\varepsilon$, $\varepsilon = 1/4$ and $P^{0,0,0}_0$ at time $t = 3/2$. The measure in L^∞ was chosen here since $\|\cdot\|_{L^p(T)}$ depend on the size of $T \in \mathcal{T}_{\varepsilon,h}$ for $p < \infty$. As expected (cf. Rem. 6.2), it is found that the highest errors

are at the interior boundaries. Analogous results are obtained for $(\alpha, \beta, \gamma) = (0, 1, 0), (2, 1, 1)$ and further time levels.

ε	$\|\boldsymbol{u}_\varepsilon - \boldsymbol{u}_0\|_{\boldsymbol{L}^1(\Omega_\varepsilon)}$	$\|\boldsymbol{u}_\varepsilon - \boldsymbol{u}_0\|_{\boldsymbol{L}^2(\Omega_\varepsilon)}$	$\|p_\varepsilon - p_0\|_{L^1(\Omega_\varepsilon)}$	co_ε	$\|p_\varepsilon - p_0\|_{L^2(\Omega_\varepsilon)}$	co_ε
1	6.033E−1	7.369E−1	7.127E+0	—	1.025E+1	—
1/2	6.112E−1	7.436E−1	3.135E+0	1.18	4.470E+0	1.20
1/4	6.153E−1	7.468E−1	1.466E+0	1.10	2.060E+0	1.11
1/8	6.178E−1	7.489E−1	7.194E−1	1.03	1.001E+0	1.04
1/16	6.188E−1	7.497E−1	3.752E−1	0.94	5.189E−1	0.95

ε	$\|\boldsymbol{j}_\varepsilon^+ - \boldsymbol{j}_0^+\|_{\boldsymbol{L}^1(\Omega_\varepsilon)}$	$\|\boldsymbol{j}_\varepsilon^+ - \boldsymbol{j}_0^+\|_{\boldsymbol{L}^2(\Omega_\varepsilon)}$	$\|c_\varepsilon^+ - c_0^+\|_{L^1(\Omega_\varepsilon)}$	co_ε	$\|c_\varepsilon^+ - c_0^+\|_{L^2(\Omega_\varepsilon)}$	co_ε
1	3.035E−1	3.982E−1	2.599E−2	—	4.113E−2	—
1/2	2.852E−1	3.744E−1	1.196E−2	1.12	1.848E−2	1.15
1/4	2.816E−1	3.691E−1	5.812E−3	1.04	8.891E−3	1.06
1/8	2.814E−1	3.681E−1	2.939E−3	0.98	4.469E−3	0.99
1/16	2.813E−1	3.677E−1	1.580E−3	0.90	2.348E−3	0.93

ε	$\|\boldsymbol{j}_\varepsilon^- - \boldsymbol{j}_0^-\|_{\boldsymbol{L}^1(\Omega_\varepsilon)}$	$\|\boldsymbol{j}_\varepsilon^- - \boldsymbol{j}_0^-\|_{\boldsymbol{L}^2(\Omega_\varepsilon)}$	$\|c_\varepsilon^- - c_0^-\|_{L^1(\Omega_\varepsilon)}$	co_ε	$\|c_\varepsilon^- - c_0^-\|_{L^2(\Omega_\varepsilon)}$	co_ε
1	4.675E−1	5.686E−1	1.664E−2	—	2.329E−2	—
1/2	4.815E−1	5.842E−1	8.008E−3	1.06	1.293E−2	0.85
1/4	4.877E−1	5.914E−1	4.033E−3	0.99	7.265E−3	0.83
1/8	4.908E−1	5.947E−1	2.082E−3	0.95	3.829E−3	0.92
1/16	4.921E−1	5.961E−1	1.136E−3	0.89	2.044E−3	0.91

ε	$\|\boldsymbol{E}_\varepsilon - \boldsymbol{E}_0\|_{\boldsymbol{L}^1(\Omega_\varepsilon)}$	$\|\boldsymbol{E}_\varepsilon - \boldsymbol{E}_0\|_{\boldsymbol{L}^2(\Omega_\varepsilon)}$	$\|\phi_\varepsilon - \phi_0\|_{L^1(\Omega_\varepsilon)}$	co_ε	$\|\phi_\varepsilon - \phi_0\|_{L^2(\Omega_\varepsilon)}$	co_ε
1	2.698E−1	3.573E−1	2.398E−2	—	3.151E−2	—
1/2	2.130E−1	2.785E−1	1.402E−2	0.77	1.924E−2	0.71
1/4	1.842E−1	2.560E−1	6.199E−3	1.18	9.639E−3	1.00
1/8	1.734E−1	2.500E−1	2.935E−3	1.08	4.826E−3	1.00
1/16	1.698E−1	2.484E−1	1.469E−3	1.00	2.421E−3	1.00

Table 6.2. Global $L^1(\Omega_\varepsilon)$ and $L^2(\Omega_\varepsilon)$ scale errors with respect to $P_\varepsilon^{0,0,0}$ and $P_0^{0,0,0}$ at time $t = 3/2$ and vanishing h (discretization indices suppressed) with associated estimated minimum convergence order in ε for scalar unknowns.

Remark 6.2 (Known error estimates). Bensoussan et al. (1978) discuss an error estimate for the diffusion problem with oscillating coefficients and a convergence order of $O(\sqrt{\varepsilon})$ is obtained. For diffusion problems in perforated domains, we refer to Cioranescu & Saint Jean Paulin (1999), Jikov et al. (1994), and Griso (2004, 2005). In the latter publications the method of periodic unfolding is used and an improvement of the error estimate to $O(\varepsilon)$ in the interior is obtained. Error estimates for subsystems of our system (Schmuck 2012) or for diffusion type problems (Fatima et al. 2012; Melnik & Sivak 2010) are still ongoing research. For the fluxes, convergence is not expected since corrector estimates are required that take into account higher order terms and corrected gradients, respectively. Including the corrected gradients of all variables, the order of convergence in ε has been determined to be $\sqrt{\varepsilon}$ for a fairly complex system by Eck (2004). Since there is no analytically proven error estimate for the complete SNPP system available in the literature, the numerically determined error estimates provided in this chapter can be seen as a first step toward evaluating the approximation quality of the pore-scale model by the homogenized model. △

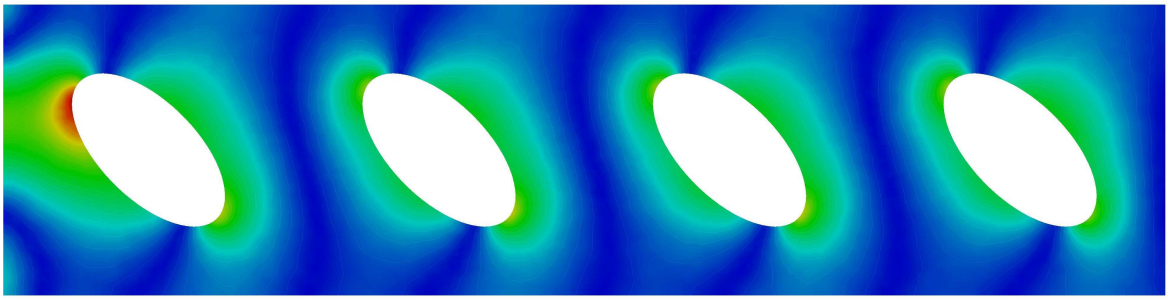

$\|p_{\varepsilon,h} - p_{0,h}\|_{L^\infty(T)} \in [2.85\text{E}{-2}, 1.01\text{E}{+1}]$

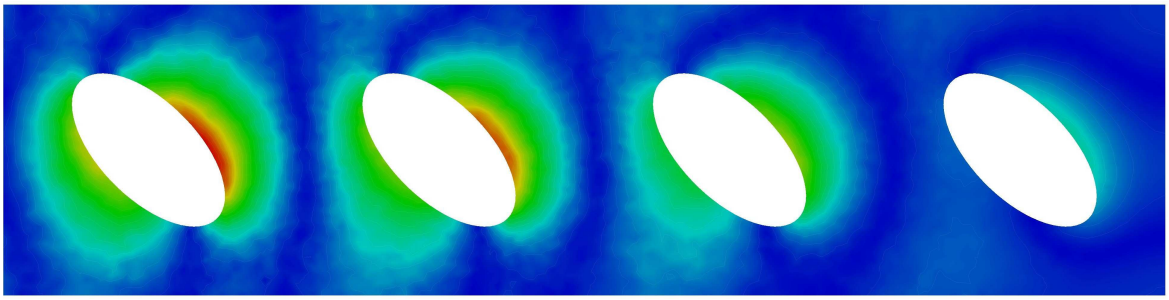

$\|c^+_{\varepsilon,h} - c^+_{0,h}\|_{L^\infty(T)} \in [7.12\text{E}{-5}, 3.99\text{E}{-2}]$

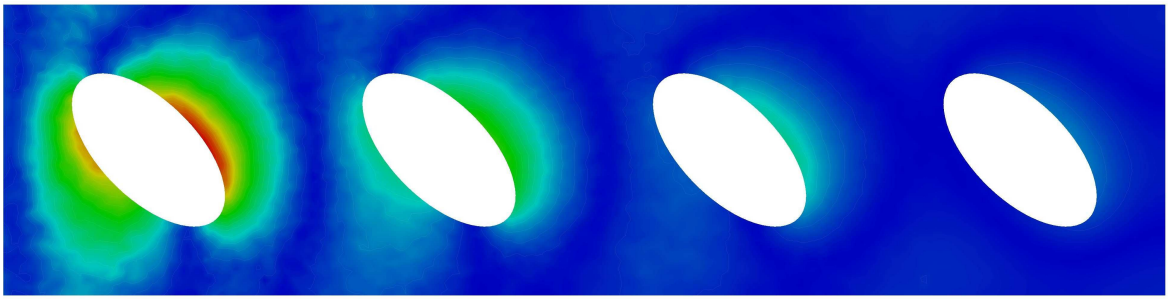

$\|c^-_{\varepsilon,h} - c^-_{0,h}\|_{L^\infty(T)} \in [5.40\text{E}{-5}, 4.18\text{E}{-2}]$

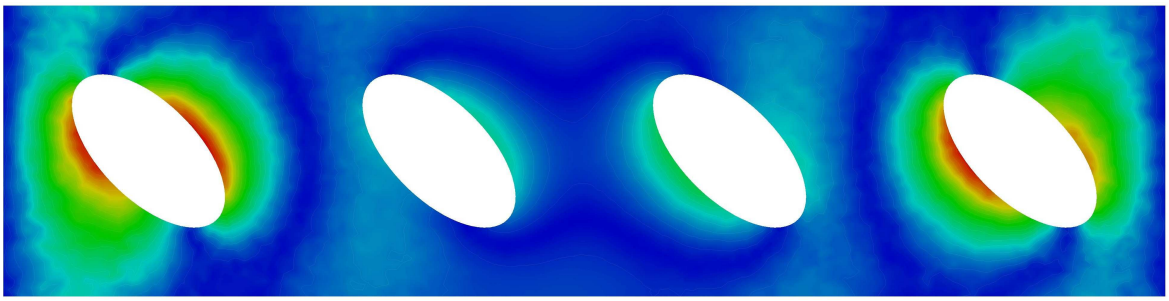

$\|\phi^-_{\varepsilon,h} - \phi^-_{0,h}\|_{L^\infty(T)} \in [9.19\text{E}{-5}, 4.01\text{E}{-2}]$

Figure 6.14. Local L^∞ scale errors for the scalar solutions p, $c^\pm$, and ϕ (*blue* / low to *red* / high) for $P^{0,0,0}_\varepsilon$, $\varepsilon = 1/4$ and $P^{0,0,0}_0$ at time $t = 3/2$ (time index suppressed).

Chapter 7

Extension to a Model with Evolving Microstructure

Ray et al. (2012c) derive a two-scale model for colloidal dynamics and single-phase liquid flow within a saturated porous medium with locally periodic pore structure. The model takes attachment and detachment processes into account, which result in an evolving microstructure of the medium. This chapter reviews the algorithmic and implementational work of that publication. The underlying pore-scale model from which the effective model under consideration is derived is an extension to the SNPP system as presented in Section 1.1. We refer with its description to the original publication and also to Ray (2013).

Following an outline of the considered two-scale problem in Section 7.1, a fully time-implicit, mass conservative numerical scheme is presented in Section 7.2 using mixed finite elements for both the macroscopic / averaged scale and the microscopic / pore scale. An academic two-scale scenario is defined, numerical simulations performed, and finally discussed in Section 7.3. Hereby, the interaction potential and the surface reaction rate are chosen such that pore clogging occurs. The simulations reveal the interplay between particle transport, evolving microstructure, and liquid flow.

7.1 The Effective Model

Ray et al. (2012c) applied an extended method of two-scale asymptotic expansion (cf. Sec. 1.2) within a level set framework according to van Noorden (2009) to a system of partial differential equations describing liquid flow and transport (by convection, diffusion, and drift) of colloidal particles within a porous medium at the pore scale in two space dimensions. Here, a model for an interaction potential and for a surface reaction may be prescribed arbitrarily. Moreover, a level set formulation was used to cope with the evolving microstructure.

We outline the system of equations for the effective model including effective coefficients, all of which are cell-averaged quantities, yet are evolving in time and are space dependent with respect to the macroscopic domain Ω. These equations are supplemented with several families of microscopic cell problems, which flux solutions are required to compute most of the effective coefficients. The coefficient functions depend explicitly on the microscopic geometry and also on the interaction potential between solid matrix and particles.

The following model description is restricted to the *radially symmetric* case, i. e., we assume a radially symmetric interaction potential between colloids and the solid matrix as well as a circular shape of the local grains during evolution (cf. Fig. 7.1). With these assumptions, the level set equation describing the surface of the solid matrix simplifies to an equation for the grain radius.

Macroscopic equations. In contrast to the remaining thesis, this chapter deals with a so-called *locally periodic* setting: associated with each point $(t, \boldsymbol{x}) \in J \times \Omega$ is a unit cell Y with *liquid phase* $Y_1(t, \boldsymbol{x})$ and *porosity* $|Y_1(t, \boldsymbol{x})|$ that evolve in time and that represent the underlying locally periodic geometry of the solid matrix in the surrounding area.

The system resulting from an averaging procedure by two-scale asymptotic expansion consists of the following equations: first, a Darcy equation {(7.1a), (7.1b)} describing the *averaged liquid velocity* $\bar{\boldsymbol{u}}_0$ [$\mathrm{m\,s^{-1}}$] and the *averaged pressure* distribution p_0 [Pa]. Second, a modified effective transport equation with the unknowns $(\tilde{\boldsymbol{j}}_0, \tilde{c}_0)$ that are auxiliary quantities from which the actual *averaged colloidal concentration* $\bar{c}_0$ [$\mathrm{kg\,m^{-3}}$] can be reconstructed (cf. (7.2)). Third, the equation (7.1e) describing the *radii distribution* R_0 [m] of the solid grains. Recapitulating, we have

$$\bar{\boldsymbol{u}}_0 = -\frac{1}{\nu \rho_1} \mathbf{K}(t, \boldsymbol{x}) \nabla_{\boldsymbol{x}} p_0 \qquad \text{in } J \times \Omega\,, \quad (7.1a)$$

$$\nabla_{\boldsymbol{x}} \cdot \bar{\boldsymbol{u}}_0 = \frac{\rho_1 - \rho_s}{\rho_1} F(t, x) \qquad \text{in } J \times \Omega\,, \quad (7.1b)$$

$$\tilde{\boldsymbol{j}}_0 = -\bar{\mathbf{D}}(t, \boldsymbol{x}) \nabla_{\boldsymbol{x}} \tilde{c}_0 + \boldsymbol{V}(t, \boldsymbol{x}) \tilde{c}_0 \qquad \text{in } J \times \Omega\,, \quad (7.1c)$$

$$\partial_t (A(t, \boldsymbol{x}) \tilde{c}_0) + \nabla_{\boldsymbol{x}} \cdot \tilde{\boldsymbol{j}}_0 = -F(t, \boldsymbol{x}) \qquad \text{in } J \times \Omega\,, \quad (7.1d)$$

$$\partial_t R_0 = f\left(\exp\Big(- \frac{\Phi_0(t, \boldsymbol{x}, \boldsymbol{y})|_{|\boldsymbol{y}|=R_0}}{k_B\, T} \Big) \tilde{c}_0(t, x) \right) \qquad \text{in } J \times \Omega\,, \quad (7.1e)$$

where the *total interaction (energy) potential* Φ_0 [J] is given in terms of R_0 and $\boldsymbol{y}$ (local distance to grain surface) due to Ray et al. (2012c, (30), p. 690). The type of the *surface*

reaction rate $f : \mathbb{R} \to \mathbb{R}$ [kg m^{-2} s^{-1}] at the solid–liquid interface can be chosen arbitrarily (e. g., Ray et al. 2012c, Sec. 2.4, p. 675). The effective coefficients A, $\bar{\mathbf{D}}$, F, $\mathbf{K}$, $\boldsymbol{V}$ are subject of the paragraph that follows, where explicit definitions are given. In system (7.1), the following physical (pseudo) constants were used (cf. Tab. B.2, p. 142): the *kinematic viscosity* of the liquid ν [m^2 s^{-1}], the *density* of the liquid / solid phase ρ_l, ρ_s [kg m^{-3}], and $k_\mathrm{B}\,T$ [kg m^2 s^{-1}], the *Boltzmann constant* times the *absolute temperature*.

The pde–ode system of macroscopic equations (7.1) is fully coupled, since—beside the liquid movement / transport coupling—all coefficients A, $\bar{\mathbf{D}}$, F, $\mathbf{K}$, $\boldsymbol{V}$ depend on the local grain radii R_0. Due to the postulated radially symmetric setting, the evolution of the underlying microstructure is completely determined by the spatial distribution of R_0. Note that in (7.1e), the variable $\boldsymbol{y}$ in the argument of Φ_0 can be expressed in terms of R_0: for fixed $\boldsymbol{x} \in \Omega$, only the set $\Gamma = \{\boldsymbol{y} \in Y;\ |\boldsymbol{y}| = R_0\}$ is a valid third argument of Φ_0, since the reaction takes place on the grain surfaces $\Gamma = \Gamma(t, \boldsymbol{x})$. Since the interaction potential Φ_0 is presumed radially symmetric, Φ_0 is constant on this set. The actual averaged (mass) concentration $\bar{c}_0$ can be recovered by

$$\bar{c}_0(t, \boldsymbol{x}) \;=\; A(t, \boldsymbol{x})\, \tilde{c}_0(t, \boldsymbol{x})\,, \tag{7.2}$$

and the *porosity* distribution $|Y_\mathrm{l}| = |Y_\mathrm{l}(t, \boldsymbol{x})|$ by $|Y_\mathrm{l}| = 1 - \pi R_0^2$.

Effective coefficients and cell problems. All effective coefficients are obtained by averaging out the microscopic part of quantities depending on $(t, \boldsymbol{x}, \boldsymbol{y})$. Some of these quantities are defined as solutions of cell problems.

The explicit formulas for the *weighted porosity* A [−] and the *effective production/consumption rate* F [kg m^{-3} s^{-1}] are

$$A(t, \boldsymbol{x}) \;\coloneqq\; \int_{Y_\mathrm{l}(t,\boldsymbol{x})} \exp\!\left(-\frac{\Phi_0(t, \boldsymbol{x}, \boldsymbol{y})}{k_\mathrm{B}\,T}\right) \mathrm{d}\boldsymbol{y}\,, \tag{7.3a}$$

$$F(t, \boldsymbol{x}) \;\coloneqq\; \frac{1}{\rho_\mathrm{s}} \int_{\Gamma(t,\boldsymbol{x})} f\!\left(\exp\!\big(-\Phi_0(t, \boldsymbol{x}, \boldsymbol{y})\big)\, \tilde{c}_0(t, \boldsymbol{x})\right) \mathrm{d}s_{\boldsymbol{y}}\,. \tag{7.3b}$$

The *effective diffusion tensor* $\bar{\mathbf{D}}$ [m^2 s^{-1}] and the *effective permeability tensor* $\mathbf{K}$ [m^2] are given by

$$\bar{\mathbf{D}}(t, \boldsymbol{x}) \;\coloneqq\; -\int_{Y_\mathrm{l}(t,\boldsymbol{x})} D\left[\boldsymbol{\xi}_1^2(t, \boldsymbol{x}, \boldsymbol{y}) \,\middle|\, \boldsymbol{\xi}_2^2(t, \boldsymbol{x}, \boldsymbol{y})\right] \mathrm{d}\boldsymbol{y}\,, \tag{7.3c}$$

$$\mathbf{K}(t,\boldsymbol{x}) \;\coloneqq\; -\int_{Y_1(t,\boldsymbol{x})} \Big[\boldsymbol{w}_1(t,\boldsymbol{x},\boldsymbol{y}) \,\Big|\, \boldsymbol{w}_2(t,\boldsymbol{x},\boldsymbol{y})\Big] \,\mathrm{d}\boldsymbol{y}\;, \tag{7.3d}$$

where the scalar D [$\mathrm{m}^2\,\mathrm{s}^{-1}$] is the *diffusivity* of the considered colloidal particles in the liquid. The notation $[\boldsymbol{a}_1|\boldsymbol{a}_2]$ denotes the matrix consisting of columns $\boldsymbol{a}_j$. In addition to the tensors defined above, we need to define the auxiliary coefficient $\hat{\mathbf{K}}$ [m^2]:

$$\hat{\mathbf{K}}(t,\boldsymbol{x}) \;\coloneqq\; -\int_{Y_1(t,\boldsymbol{x})} \Big[\boldsymbol{\xi}^1_1(t,\boldsymbol{x},\boldsymbol{y}) \,\Big|\, \boldsymbol{\xi}^1_2(t,\boldsymbol{x},\boldsymbol{y})\Big] \,\mathrm{d}\boldsymbol{y}\;. \tag{7.3e}$$

Here, the quantities $(\boldsymbol{\xi}^i_j, \zeta^i_j)$, $i, j \in \{1,2\}$ are solutions of the *cell problems*

$$\begin{aligned}
\boldsymbol{\xi}^i_j \;&=\; -\exp\Big(-\frac{\Phi_0}{k_\mathrm{B}\,T}\Big)\,\boldsymbol{\nabla}_{\boldsymbol{y}}\zeta^i_j - \exp\Big(-\frac{\Phi_0}{k_\mathrm{B}\,T}\Big)\begin{Bmatrix}\boldsymbol{w}_j(t,\boldsymbol{x},\boldsymbol{y})\,, & i=1\\ \boldsymbol{e}_j\,, & i=2\end{Bmatrix}\;,\; \boldsymbol{y}\in Y_1(t,\boldsymbol{x})\;,\\
\boldsymbol{\nabla}_{\boldsymbol{y}}\cdot\boldsymbol{\xi}^i_j \;&=\; 0\;, \qquad\qquad \boldsymbol{y}\in Y_1(t,\boldsymbol{x})\;,\\
\boldsymbol{\xi}^i_j\cdot\boldsymbol{\nu}_0 \;&=\; 0\;, \qquad\qquad \boldsymbol{y}\in \Gamma(t,\boldsymbol{x})
\end{aligned} \tag{7.4}$$

with $(\boldsymbol{\xi}^i_j, \zeta^i_j)$ componentwise periodic in Y satisfying the constraint $\int_{Y_1}\zeta^i_j(t,\boldsymbol{x},\boldsymbol{y})\,\mathrm{d}\boldsymbol{y} = 0$ for all $(t,\boldsymbol{x}) \in J\times\Omega$, where $\Phi_0 = \Phi_0(R_0(t,\boldsymbol{x}),\boldsymbol{y})$. Here and in the following, $\boldsymbol{e}_j$ denotes the jth unit vector in $\mathbb{R}^2$, and $\boldsymbol{\nu}_0$ the exterior unit normal on Γ. Similarly, the quantities $(\boldsymbol{w}_j, \pi_j)$, $j \in \{1,2\}$ are solutions of the *cell problems*

$$\begin{aligned}
-\Delta_{\boldsymbol{y}}\boldsymbol{w}_j + \boldsymbol{\nabla}_{\boldsymbol{y}}\pi_j \;&=\; \boldsymbol{e}_j\;, && \boldsymbol{y}\in Y_1(t,\boldsymbol{x})\;,\\
\boldsymbol{\nabla}_{\boldsymbol{y}}\cdot\boldsymbol{w}_j \;&=\; 0\;, && \boldsymbol{y}\in Y_1(t,\boldsymbol{x})\;,\\
\boldsymbol{w}_j \;&=\; \mathbf{0}\;, && \boldsymbol{y}\in \Gamma(t,\boldsymbol{x})\;,
\end{aligned} \tag{7.5}$$

with $(\boldsymbol{w}_j, \pi_j)$ componentwise periodic in Y. Eventually, we define the *effective transport velocity* $\boldsymbol{V}$ [$\mathrm{m}\,\mathrm{s}^{-1}$] by

$$\boldsymbol{V}(t,\boldsymbol{x}) \;\coloneqq\; \hat{\mathbf{K}}(t,\boldsymbol{x})\,\mathbf{K}^{-1}(t,\boldsymbol{x})\,\bar{\boldsymbol{u}}_0(t,\boldsymbol{x})\;,$$

where $\bar{\boldsymbol{u}}_0$ is the partial solution of (7.1). The coefficient $\mathbf{K}$ is non-singular (cf. Ray et al. 2012c, Sec. 3.8, p. 686), and thus $\boldsymbol{V}$ is well-defined.

7.2 Discretization and Solution Scheme

In what follows, a fully discrete numerical scheme is presented, capable to approximate the effective quantities of interest, i. e., in particular the concentration $\bar{c}_0$, the liquid velocity $\bar{\boldsymbol{u}}_0$, and the porosity $|Y_1|$. This incorporates the solving of the system (7.1) as well as of the cell problems (7.4) and (7.5). We apply Rothe's method to the system (7.1) using the implicit Euler method in order to obtain a sequence of time-discrete, yet still coupled systems. The couplings between the microscopic scale and the macroscopic scale and also the couplings between the subsystems for liquid flow, transport, and grain radii fields are resolved by an iterative splitting scheme. Hence, the resulting numerical scheme is fully implicit in time. Owing to the splitting between the scales, all of the emerging cell problems become uncoupled from each other. The spatial discretization is performed on unstructured triangular grids by lowest order mixed finite elements for both the macroscopic problems and the cell problems.

Time discretization. Let $0 =: t_0 < t_1 < \ldots < t_N := T$ be a not necessarily equidistant decomposition of the time interval $J =]0, T[$ and let $t_n - t_{n-1} =: \tau_n$ denote the time step size. Furthermore, for any time-dependent quantity φ, we use the notation $\varphi^n = \varphi^n(\boldsymbol{x}) := \varphi(t_n, \boldsymbol{x})$. Application of the implicit Euler method yields a sequence of N stationary coupled systems. More precisely, for $n = 1, \ldots, N$ we have to find $(\bar{\boldsymbol{u}}_0^n, p_0^n, \tilde{\boldsymbol{j}}_0^n, \tilde{c}_0^n, R_0^n)$ in terms of $A^{n-1}(\boldsymbol{x})$, $\tilde{c}_0^{n-1}(\boldsymbol{x})$, $R_0^{n-1}(\boldsymbol{x})$ with coefficients $A^n(\boldsymbol{x})$, $\bar{\mathbf{D}}^n(\boldsymbol{x})$, $F^n(\boldsymbol{x})$, $\boldsymbol{V}^n(\boldsymbol{x})$, which in turn depend in particular on $R_0^n(\boldsymbol{x})$ (cf. (7.3)).

Spatial discretization. Let $\mathcal{T}_H = \{T\}$ be a regular decomposition of the macroscopic domain Ω into closed triangles T of characteristic size H such that $\overline{\Omega} = \cup T$ (cf. Sec. 3.1). We call the associated mesh of $\mathcal{T}_H$ the *coarse-scale grid*, represented by the same symbol. In accordance with the considered locally periodic setting, each triangle $T \in \mathcal{T}_H$ is associated with a unit cell Y^T containing an evolving liquid phase $Y_1^T = Y_1^T(t)$ that is clearly time-dependent due to the evolving interface and that is denoted by $Y_1^{n,T}$ for the time level t_n (cf. Fig. 7.1). Analogously, let $\mathcal{T}_h = \mathcal{T}_h^{n,T}$ denote the family of *fine-scale grids* covering the domains $Y_1^{n,T}$, $T \in \mathcal{T}_H$.

We skip the variational formulation of the time-discrete macroscopic system and of the cell problems (7.4), (7.5) and refer instead to Chapter 4 and indicate only the major points of the discretization in the following.

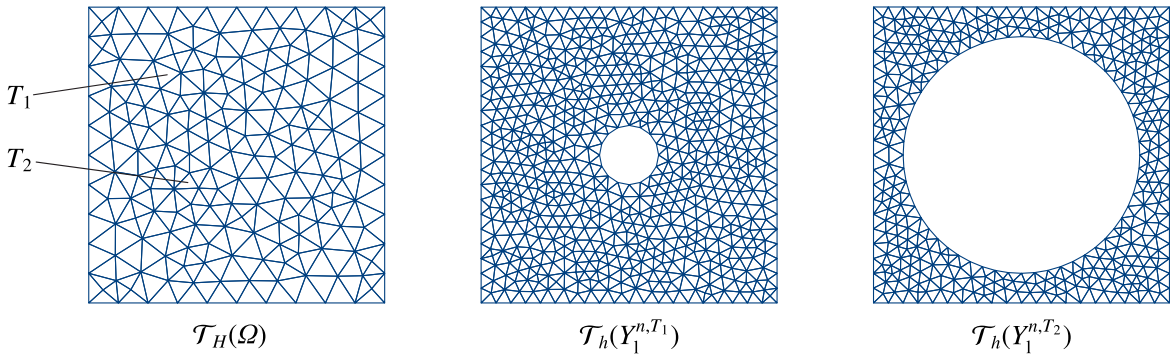

Figure 7.1. Macroscopic domain Ω covered by a coarse grid $\mathcal{T}_H$ and two cells Y_1^{n,T_k} at some time level t_n representing the local microstructure at $T_k \in \mathcal{T}_H$.

Except (7.5), all vector-valued unknowns are approximated using the approximation space due to Raviart and Thomas, $\mathbb{RT}_0(\mathcal{T}_H)$ (cf. Sec. 4.2) with associated scalar approximation space $\mathbb{P}_0(\mathcal{T}_H)$. See Table B.8 on p. 147 for a list of symbols. In order to approximate the vector and scalar unknowns of the Stokes type cell problem (7.5), we use the Taylor–Hood spaces $\mathbb{P}_2^c(\mathcal{T}_h)^2$ and $\mathbb{P}_1^c(\mathcal{T}_h)$ (cf. Sec. 4.3). The vector-valued spaces $\mathbb{RT}_0(\mathcal{T}_h)$ and $\mathbb{P}_2^c(\mathcal{T}_h)^2$ are locally and globally mass conservative, respectively. By functions indexed by H, we mean the respective spatially discretized version, i. e., $w_{0,H}^n := \sum_{T\in\mathcal{T}_H} w_0^{n,T}$ (analogously for h).

Fully discrete scheme. The solution strategy is illustrated by means of the following algorithm. Recall that we postulated an explicit local representation of Φ_0 in terms of R_0 and $\boldsymbol{y}$ (local distance to grain surface) due to Ray et al. (2012c, (30), p. 690).

Algorithm 7.1 (Two-scale approach).

Initialization

Let $n = 0$. Generate a coarse-scale grid $\mathcal{T}_H = \mathcal{T}_H(\Omega)$, initialize $R_{0,H}^n, \tilde{c}_{0,H}^n \in \mathbb{P}_0(\mathcal{T}_H)$, and choose a time step size τ_n.

Time Step

(i) *Set $n := n + 1$. If $t_n = T$ terminate.*

(ii) *For each triangle $T \in \mathcal{T}_H$, generate fine-scale grids $\mathcal{T}_h(Y_1^{n,T})$ using the coarse-scale radii distribution $R_{0,H}^{n-1}$ and appropriate mesh sizes h.*

(iii) *For each triangle* $T \in \mathcal{T}_H$*, solve the cell problems* (7.4) *and* (7.5) *for all indices* $i, j \in \{1, 2\}$ *on the fine-scale grids* $\mathcal{T}_h(Y_1^{n,T})$ *in order to compute the coarse-scale coefficients* $A_H^n, F_H^n \in \mathbb{P}_0(\mathcal{T}_H)$, $\bar{\mathbf{D}}_H^n, \mathbf{K}_H^n, \hat{\mathbf{K}}_H^n \in \mathbb{P}_0(\mathcal{T}_H)^{2,2}$.

(iv) *Solve the Darcy subproblem* {(7.1a), (7.1b)} *for* $(\bar{\boldsymbol{u}}_{0,H}^n, p_{0,H}^n)$ *using* F_H^n *and* $\mathbf{K}_H^n$.

(v) *Compute the coarse-scale transport velocity* $\boldsymbol{V}_H^n \in \mathbb{RT}_0(\mathcal{T}_H)$ *using* $\bar{\boldsymbol{u}}_{0,H}^n$, $\mathbf{K}_H^n$, *and* $\hat{\mathbf{K}}_H^n$.

(vi) *Solve the transport subproblem* {(7.1c), (7.1d)} *for* $(\tilde{\boldsymbol{j}}_{0,H}^n, \tilde{c}_{0,H}^n)$ *using* A_H^n, $\bar{\mathbf{D}}_H^n$, F_H^n, *and* $\boldsymbol{V}_H^n$.

(vii) *Solve the subproblem for the radii distribution* (7.1e) *for* $R_{0,H}^n$ *using* $\tilde{c}_{0,H}^n$.

(viii) *Proceed with* (i) .

Postprocessing

For all time levels t_n*, compute the coarse-scale porosity* $|Y_{l,H}^n| \in \mathbb{P}_0(\mathcal{T}_H)$ *using* $R_{0,H}^n$ *(satisfying* $(R_{0,H}^n)^2\pi = 1 - |Y_{l,H}^n|$ *on each* $T \in \mathcal{T}_H$*) and the actual coarse-scale concentration* $\bar{c}_{0,H}^n \in \mathbb{P}_0(\mathcal{T}_H)$ *by retransformation via* (7.2) *using* $\tilde{c}_{0,H}^n$.

The steps (ii), (iii) can be performed in parallel.

Remark 7.2 (Multiscale methods). A general concept for designing numerical multiscale methods exploiting scale separation is the *heterogeneous multiscale method (HMM)*, which was introduced by E & Engquist (2003) (see E et al. 2007, for a review). In short, overall macroscopic problems with coefficients depending on the microstructure are to be solved by estimating the missing macroscopic data from the microscopic models. This methodology was used in the context of finite elements for diffusion-type problems, see, e. g., Abdulle (2009), Abdulle & Engquist (2007/08), Du & Ming (2010), and Ming & Yue (2006), and E et al. (2005), where the *HMM finite element method* was introduced. For an comparing overview of this and other numerical multiscale methods, we refer to Ming & Yue (2006), the lecture notes of G. Allaire (Allaire 2010c), and the review in Efendiev & Hou (2009).

The aforementioned methods are designed for a large class of microstructures. For the considered model (7.1), however, we can exploit the special form of the equations stemming from the assumed locally periodic microstructure, providing the possibility of a *direct numerical approach on both scales* (e. g., as performed by Redeker & Eck 2013; Tan & Zabaras 2007). The numerical scheme defined in Algorithm 7.1 is related to the HMM in so

far that for each "node" of the coarse grid microscopic problems have to be solved in order to obtain the effective coefficients of the macroscopic problem. △

Remark 7.3 (Iterative scheme). In order to avoid splitting errors, we iterate over the steps (ii)–(vii). More precisely, after the first run, the radii distribution in (ii) is taken from (vii). The iteration is allowed to terminate and to continue with (i) as soon as the difference of two successive radii distribution iterates fall below some desired tolerance. Moreover, it is recommended to reduce the time step size τ_n in steps with a high iteration number or in time steps, where the iteration scheme diverges. △

Remark 7.4 (Look-up table). An efficient modification of Algorithm 7.1—especially for coarse grids with small mesh size H and / or a large number of time steps—is the generation of a *look-up table* for some coefficients in a preprocessing step: the effective coefficients A_H^n, $\bar{\mathbf{D}}_H^n$, $\mathbf{K}_H^n$, and $\hat{\mathbf{K}}_H^n$ (cf. (7.3)) depend only on given data and solutions of cell problems that eventually depend on the local grain geometry and thus on the local grain radius. Hence, these coefficients can be computed for a chosen number of sample radii in $]0, 1/2[$ and fine-scale grids with small mesh sizes h. These data, stored in a look-up table, can now be accessed during the run time of the main two-scale approach using polynomial interpolation between sample data. △

7.3 Numerical Results

This section presents an academic two-scale scenario that illustrates the interplay of (local) surface reaction, porosity changes, and liquid velocity. All simulations were performed with the numerical toolbox *HyPHM* (cf. Appx. A). The computation of the (local) effective coefficients on a fixed triangle $T \in \mathcal{T}_H$ in terms of the porosity for different choices of interaction potentials are shown in Ray et al. (2012c, Sec. 4.3) and Ray (2013, Sec. 5.5).

Let $J \times \Omega :=]0, 1[\times]0, 1[^2$. We use the interaction potential $\Phi_0 := (|y| - R_0 + 1)^{-6}$ (cf. Ray et al. 2012c, (30c), p. 690). In order to obtain pore clogging, we choose a linear attachment rate $f : c \mapsto c/10$ (cf. Ray et al. 2012c, Sec. 2.4, 1., p.675). Due to the considered radially symmetric setting, the effective coefficient F simplifies as follows: for a fixed $T \in \mathcal{T}_H$, R_0^n equals $|\boldsymbol{y}|$ on Γ and thus $\Phi_0^n = 1$ on Γ^n. Since $\tilde{c}_0^n$ is constant on each unit cell,

$$F^n(\boldsymbol{x}) \;=\; \int_{\Gamma^n(\boldsymbol{x})} f\Big(e^{-1}\tilde{c}_0^n(\boldsymbol{x})\Big)\,\mathrm{d}s_{\boldsymbol{y}} \;=\; f\Big(e^{-1}\tilde{c}_0^n(\boldsymbol{x})\Big)\,|\Gamma^n(\boldsymbol{x})| \;=\; 2\pi\, R_0^n(\boldsymbol{x})\, f\Big(e^{-1}\tilde{c}_0^n(\boldsymbol{x})\Big).$$

Obviously, the effective reaction term F^n is directly proportional to the local grain surface area.

The data of the simulated scenario is given as follows: we consider a macroscopic domain with heterogeneous initial porosity distribution as shown in Figure 7.2. This was generated by a random field (Suciu et al. 2012, (11)). We take the area near the lower left corner of the domain as inflow boundary for a concentration, which attaches to the solid matrix according to the reaction rate described above. At inital time, the concentration is zero everywhere. A pressure difference between the lower left corner and the upper right corner of the domain is applied. Consequently, a liquid flow evolves in which the concentration is transported.

Figure 7.2 shows transient and spatially heterogeneous porosity and liquid velocity distributions caused by a locally evolving microstructure. In particular, a local reduction of the porosity occurs, starting in the area near the lower left corner. This is due to the propagation of the concentration field and its interaction with the solid matrix in this region. This also leads to a decrease of the liquid velocity magnitude, since the pores are clogging locally.

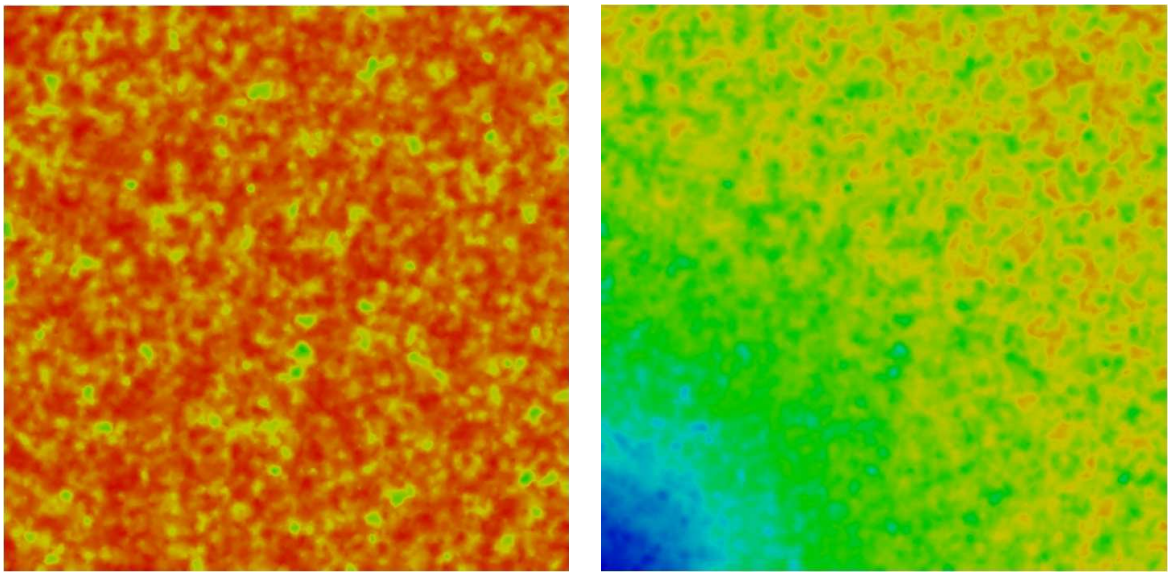

$|Y_1| \in [0.40, 0.60]$ (green / low to red / high)

$|Y_1| \in [0.23, 0.57]$ (blue / low to red / high)

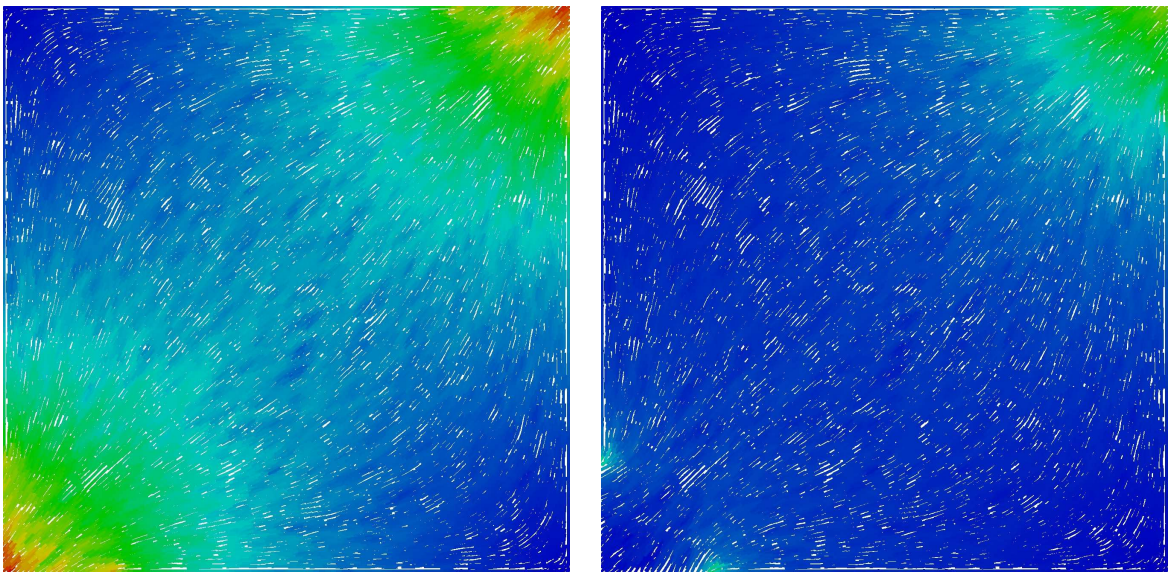

$|\bar{\boldsymbol{u}}_0| \in [0, 1.79]$ (blue / low to red / high)

$|\bar{\boldsymbol{u}}_0| \in [0, 1.35]$ (blue / low to red / high)

Figure 7.2. Distribution of the macroscopic porosity $|Y_1|$ and of the liquid velocity magnitude $|\bar{\boldsymbol{u}}_0|$ at first time level (*left*) and last time level (*right*) using a coarse-scale grid $\mathcal{T}_H$ consisting of 34 320 triangles. Each triangle $T \in \mathcal{T}_H$ is associated with an evolving unit cell (cf. Fig. 7.1). For fixed time levels $t = t_n$ the unit cells are covered by fine-scale grids $\mathcal{T}_h^{n,T}$ consisting of between 2 000 to 10 000 triangles.

Conclusion

We have presented time-implicit, mass-conservative numerical schemes using mixed finite elements that are capable of approximating accurately and efficiently the non-stationary, fully coupled SNPP system and also its homogenized systems. Solving these systems numerically is challenging, in particular, due to the resolution of the pore scale, different types of boundary conditions, especially periodic ones, and balance constraints. The schemes are based on fixed-point approaches and have been verified by numerically estimating the theoretically predicted grid convergence orders of the linear subproblems, which also hold true experimentally for the full nonlinear systems. This observation was confirmed analytically for the homogenized systems by an a priori error estimate of the overall discretization error.

Much emphasis was placed on the quality assessment of the homogenized systems: based on simulation results, the behavior of the pore-scale and field-scale solutions with regard to their physical meanings was compared and discussed for different choices of scalings. In addition, the convergence properties of the pore systems toward their upscaled limit systems were investigated qualitatively and quantitatively. For all considered choices of scalings, we found linear convergence rates in the scale parameter for each scalar unknown. This numerical estimation of convergence rates provides a first insight into the applicability of the homogenized systems, since these have not yet been accomplished analytically in a rigorous manner for the full SNPP system. From the physical point of view, it was observed that electrodynamic effects may have a severe impact on kinetic reaction rates and may furthermore cause a retardation of charged solutes in the solid matrix. Moreover, within the framework of a two-scale scenario in which an evolving microstructure and surface reactions were taken into account, the interplay between particle transport, evolving microstructure, and liquid flow were numerically revealed.

Having this validation of the derived effective models at hand, it is now possible to perform further numerical simulations regarding the identification of parameters in specific application-oriented problems based upon comparisons with experimental measurements. We consider our investigations to be an important step toward the understanding of the dynamics of dilute electrolytes and of dissolved charges particles within porous media on larger scales.

Appendix A

Implementation Issues

The implementation of the numerical schemes presented in this thesis was mainly written using the software platform / programming language *MATLAB, Release 2012b*. More precisely, a simulation toolbox *HyPHM* was newly implemented by the author, which already has been used as simulation software, inter alia, in the publications of Frank et al. (2011, 2012), Ray (2013), and Ray et al. (2012b,c) and the work of Pérez-Pardo (2012). The code is object-oriented and matrix assembly routines, the solution of cell problems, and other run in parallel on multi-core processors (*MATLAB Parallel Computing Toolbox*).

Software features. The toolbox *HyPHM* provides a framework for continuum modeling approaches by second-order partial differential equations using *mixed finite elements* in two spatial dimensions. For space discretization, *unstructured triangular grids* are used, which may contain an arbitrary number of interior holes. *HyPHM* provides besides manual grid definition the option to import grids which are generated by the *MATLAB Partial Differential Equation Toolbox* or by the mesh generator Gmsh (Geuzaine & Remacle 2009). The latter is distributed under the terms of the GNU General Public License.

Currently, a (Navier–)Stokes solver and a solver for convection–diffusion–reaction problems are available. The coefficient functions of the problems may be given either as algebraic time- and space dependent functions, or as discrete data sets. The latter option provides the possibility for realizing couplings of the different problems by using solution data as coefficient input for other problems. For instance, in our considerations, the water flux and also the electric field appear as coefficients in the Nernst–Planck equations {(2.5c), (2.5d)}. Both are explicitly given by the mixed solution of the respective problem in the Raviart–Thomas basis. This can be exploited, since the convective term in the discrete formulation of the transport problem is naturally given in this basis. Different boundary types can be chosen independently of each other for each edge of the grid, where the most established boundary types, such as Dirichlet, Neumann, or flux, were

successfully implemented. *Periodic boundary conditions* are also available for each solver, which are required at most by solving cell problems arising in periodic homogenization procedures. These boundary conditions are realized in an *implicit* way, using a grid-folding technique. Optionally, *mean value constraints* may be imposed for the scalar unknown of each problem in order to ensure well-posedness, which may otherwise be lost for some choices of boundary conditions. The time discretization follows an implicit Euler scheme allowing a variable time-step size.

By now, *MATLAB, Release 2012b* has two key ways to write parallel code: the concept of parallel "for loops" (`parfor`) and that of single-program-multiple-data (`spmd`). For the parallelization with respect to the assembly of the stiffness matrices, the latter one has approved.

The data for flux and scalar finite element solutions can be stored in the vtk file format, which subsequently can be used for the visualization using third-party software like Paraview (Squillacote 2007) or MayaVi (Ramachandran & Varoquaux 2011), which are both multi-platform and freely available.

A web link to a comprehensive documentation of *HyPHM* is found in the References.

Appendix B

Notation

The dimensionally independent *SI base units* and the *SI derived units* used in this work are listed in Table B.1 (excerpt of Probstein (2003)). Table B.2 gives an outline of *physical constants* and also of quantities, which are constant if the considered liquid is water at 20°C. A comprehensive reference for fundamental constants, data, and nomenclature in the field of chemistry and physics is Quack et al. (2007).

Physical quantities and *effective physical quantities* on an averaged scale are listed in Table B.5 and Table B.4, respectively. Symbols referring to finite element grids or to triangulations are found in Table B.6, operators and other symbols in Table B.7, subscripts and superscripts in Table B.3. Physical quantities are subscripted with the number or the symbol of the chemical species which they refer to wherever required. The subscripts are suppressed when the context is clear. Eventually, *function spaces* and *norms* are listed in Table B.8 and Table B.9, respectively.

Quantity	**Name**	**Symbol** (SI Units)	**Definition**
mass	kilogram	kg	
length	meter	m	
time	second	s	
absolute temperature	kelvin	K	
amount of substance	mole	mol	
electric current	ampere	A	
force	newton	N	$:= \mathrm{kg\,m\,s^{-2}} = \mathrm{C\,V\,m^{-1}}$
pressure	pascal	Pa	$:= \mathrm{N\,m^{-2}} = \mathrm{kg\,m^{-1}\,s^{-2}}$
energy	joule	J	$:= \mathrm{N\,m} = \mathrm{kg\,m^2\,s^{-2}} = \mathrm{C\,V}$
electric charge	coulomb	C	$:= \mathrm{A\,s}$
electric potential difference	volt	V	$:= \mathrm{J\,C^{-1}} = \mathrm{kg\,m^2\,s^{-3}\,A^{-1}}$

Table B.1. SI base units (upper list) and SI derived units (lower list).

Quantity	**Symbol**	**Value**	**SI Units**	**Relation**
Avogadro number	N_A	6.022E+23	$\mathrm{mol^{-1}}$	
Boltzmann constant	k_B	1.381E−23	$\mathrm{J\,K^{-1}}$	
elementary charge	e	1.602E−19	C	
Faraday constant	F	9.648E+4	$\mathrm{C\,mol^{-1}}$	$F = e\,N_\mathrm{A}$
gas constant	R	8.314E+0	$\mathrm{J\,K^{-1}\,mol^{-1}}$	$R = k_\mathrm{B}\,N_\mathrm{A}$
permittivity (of water)	ϵ	5.553E−8	$\mathrm{C\,V^{-1}\,m^{-1}}$	
dynamic viscosity (of water)	μ	1.002E−3	Pa s	$\mu = \rho_\mathrm{w}\,\nu$
kinematic viscosity (of water)	ν	1.004E−6	$\mathrm{m^2\,s^{-1}}$	
water density	ρ_w	9.982E+2	$\mathrm{kg\,m^{-3}}$	
temperature	T	293	K	

Table B.2. Physical constants (upper list) and physical pseudo constants (lower list). The latter quantities are constant if water at $T = 20°\mathrm{C}$ is considered.

Symbol	Definition
$\cdot^*$	dimensionless variable (cf. Sec. 1.1, p. 2)
$\overline{\cdot}$	closure of a set or $\boldsymbol{y}$-averaged quantity
$\cdot^{\mathrm{T}}$	transposition
$\cdot_{\mathrm{flux}}$	flux boundary type
$\cdot_{\mathrm{N}}$	Neumann boundary type
$\cdot_{\mathrm{D}}$	Dirichlet boundary type
$\cdot_0$	averaged physical quantity
$\cdot_\varepsilon$	physical quantity defined on the pore scale (cf. Fig. 2.1, p. 18)
$\cdot_{\mathrm{l}}$	physical quantity associated with the liquid phase
$\cdot_{\mathrm{s}}$	physical quantity associated with the solid phase
$\cdot_h^n$, $\cdot_H^n$	discrete variable on the grid $\mathcal{T}_h$ respectively $\mathcal{T}_H$ at time level t_n
$\cdot\, T^{n,T}$	quantity on a triangle $T \in \mathcal{T}_H$ at time level t_n

Table B.3. Subscripts and superscripts.

Symbol	Definition	SI Units	Relation / Comment
$\mathbf{D}$	diffusion tensor / permittivity tensor	–	
$\mathbf{K}$	permeability tensor or hydraulic conductivity tensor	–	
$\bar{\phi}_0$	background electric potential	V	
$\bar{\sigma}$	mean surface charge density	$\mathrm{C\,m^{-2}}$	$\bar{\sigma} := -\int_\Gamma \sigma \,\mathrm{d}s_{\boldsymbol{y}}$ (cf. Thm. 2.5, p. 23)
$\bar{\boldsymbol{u}}_0$	averaged water flux	$\mathrm{m\,s^{-1}}$	also called Darcy flux
$\lvert Y_{\mathrm{l}}\rvert$	porosity	–	

Table B.4. Special effective / averaged physical quantities.

Symbol	Definition	SI Units	Relation
c	molar density / concentration or number density	$\mathrm{mol\,m^{-3}}$	
D	diffusivity or diffusion coefficient	$\mathrm{m^2\,s^{-1}}$	
$\boldsymbol{E}$	electric field	$\mathrm{V\,m^{-1}}$	$\boldsymbol{E} = -\boldsymbol{\nabla}\phi$
$\boldsymbol{f}_\mathrm{E}$	electric body force density	$\mathrm{N\,m^{-3}}$	$\boldsymbol{f}_\mathrm{E} = \rho_\mathrm{E}\,\boldsymbol{E}$ (a)
h	piezometric head	m	
$\boldsymbol{j}$	molar flux	$\mathrm{mol\,m^{-2}\,s^{-1}}$	
K	hydraulic conductivity	$\mathrm{m\,s^{-1}}$	
p	hydrostatic pressure	Pa	
ϕ	electric potential / voltage	V	
Φ	interaction (energy) potential	J	
q	electric charge	C	$q = \int \rho_\mathrm{E}$
r	reaction rate	$\mathrm{mol\,m^{-3}\,s^{-1}}$	
ρ_E	charge density	$\mathrm{C\,m^{-3}}$	$\rho_\mathrm{E} = F \sum z_i\, c_i$
σ	surface charge density	$\mathrm{C\,m^{-2}}$	
t	time	s	
$\boldsymbol{u}$	pore velocity or Darcy flux of the liquid	$\mathrm{m\,s^{-1}}$	
v	mobility	$\mathrm{mol\,s\,kg^{-1}}$	$D_i = R\,T\,v_i$ (b)
$\boldsymbol{x}$	$= (x_1, \ldots, x_d)^\mathrm{T} \in \mathbb{R}^d$, point in Ω or space variable	m	
z	charge number / valence, $z \in \mathbb{Z}$	–	

Table B.5. Physical quantities. Equation (a) is termed Lorentz relation; (b) is termed Nernst–Einstein equation.

Symbol	Definition
DOF	degrees of freedom
E	edge
$\mathcal{E}$	set of edges
$\mathcal{E}_{\text{flux}}, \mathcal{E}_{\text{N}}, \mathcal{E}_{\text{D}}$	set of flux / Neumann / Dirichlet edges, $\mathcal{E}_{\partial\Omega} = \mathcal{E}_{\text{flux}} \cup \mathcal{E}_{\text{N}} \cup \mathcal{E}_{\text{D}}$
$\mathcal{E}_\Omega, \mathcal{E}_{\partial\Omega}$	set of interior edges, set of boundary edges, $\mathcal{E} = \mathcal{E}_\Omega \cup \mathcal{E}_{\partial\Omega}$
Γ	interior boundary of Y (cf. Fig. 2.1, p. 18)
Γ_ε	interior boundary of Ω_ε (cf. Fig. 2.1, p. 18)
h, H	mesh fineness of a triangulation
J	$:=]0, T[$, open time interval
$\boldsymbol{\nu}$	unit normal on a boundary pointing outward of the respective domain
$\boldsymbol{\nu}_E$	$= \sigma_{ET}\boldsymbol{\nu}_{ET}$, unit normal on E under global orientation (cf. Fig. 4.1, p. 77)
$\boldsymbol{\nu}_{ET}$	unit normal on $E \subset \partial T$ pointing outward of T
$\boldsymbol{\nu}_T$	unit normal on ∂T pointing outward of T
N	total number of time steps, $0 =: t_0 < t_1 < \ldots < t_N := T$
NNZ	number of non-zero entries of a sparse matrix
$\mathcal{N}$	set of nodes (which may be vertices, barycenters, etc.)
Ω	macroscopic domain, $\Omega = \Omega_0$
Ω_ε	periodically perforated domain representing the pore scale (cf. Fig. 2.1, p. 18)
$\partial\Omega$	boundary of Ω, exterior boundary of Ω_ε
σ_{ET}	orientation of E with respect to T (cf. Fig. 4.1, p. 77)
T	d-simplex (finite element domain) or end time
$\mathcal{T}_h$	triangulation or set of triangles associated with mesh fineness h
$\mathcal{V}$	set of vertices
$\boldsymbol{x}_{ET}^{\text{opp}}$	vertex of T opposite to E (cf. Fig. 4.1, p. 77)
$\boldsymbol{x}_E^{\text{bary}}, \boldsymbol{x}_T^{\text{bary}}$	barycenter of E, barycenter of T (cf. Fig. 4.1, p. 77)
$Y, Y_\text{l}, Y_\text{s}$	representative periodic cell, liquid part, solid part (cf. Fig. 2.1, p. 18)

Table B.6. Triangulation and grid related symbols.

Symbol	Definition
$\lvert\cdot\rvert$	absolute value of a scalar quantity or Euclidean norm in $\mathbb{R}^n$ or measure of a domain
$[\![\cdot]\!]_E$	jump across E (cf. Def. 3.5, p. 32)
$\{\ldots\}$	set or grouping or distinction of cases
$\{\cdot\}_{n\in\mathbb{N}}$	sequence
$(\cdot)_i$	component of a vector or vector buildup
$[\cdot]_{i,j}$	component of a matrix or matrix buildup
$\lfloor\cdot\rfloor$	integer part of a positive real number (floor)
$\cdot\rvert_E$	restriction to E or trace on E (cf. Thm. 3.1, p. 29)
#	cardinality of a discrete set
$\wedge$	logical AND
$\fint_Y \cdot \,\mathrm{d}\boldsymbol{y}$	average integral over Y, $\fint_Y w\,\mathrm{d}\boldsymbol{y} := \frac{1}{\lvert Y\rvert}\int_Y w\,\mathrm{d}\boldsymbol{y}$
$\boldsymbol{a}\cdot\boldsymbol{b}$	$:= \sum_{k=1}^n a_k b_k$, Euclidean scalar product in $\mathbb{R}^n$
$\boldsymbol{\nabla}$	$:= (\frac{\partial}{\partial x}, \frac{\partial}{\partial y}, \frac{\partial}{\partial z})^{\mathrm{T}}$, spatial gradient
∂_t	$:= \frac{\partial}{\partial t}$, time derivate; $\partial_{tt} := \partial_t^2$
$\overline{\partial}$	difference quotient (cf. (3.12), p. 35)
A	finite element assembly operator (cf. p. 88)
$\delta_{i,j}$	Kronecker delta
D	Fréchet derivative
$\boldsymbol{e}_j$	jth unit vector in $\mathbb{R}^n$
γ_0	$\in \mathcal{L}(H^1(\Omega); H^{1/2}(\partial\Omega))$, trace operator (cf. Thm. 3.1, p. 29)
γ_ν	$\in \mathcal{L}(\boldsymbol{H}^{\mathrm{div}}(\Omega); H^{-1/2}(\partial\Omega))$, normal trace operator (cf. Thm. 3.1, p. 29)
$\mathbf{I}$	unit matrix in $\mathbb{R}^{n,n}$ or identity operator (the latter also $\boldsymbol{I}$ (vector) and I (scalar))
$\mathcal{M}$	cut-off operator (cf. Def. 3.15, p. 37)

Table B.7. Operators, brackets, and other symbols.

Symbol	Definition
$C^k(\Omega)$	space of j times continuously differentiable functions on Ω, $k \in \mathbb{N}_0$
$C^k(\overline{J}; V)$	space of V-valued functions of class C^j with respect to t, $k \in \mathbb{N}_0$
$\mathcal{D}(\Omega)$	space of infinitely differentiable functions with compact support on Ω
$\mathcal{D}'(\Omega)$	space of distributions
$H^k(\Omega)$	k-times weakly differentiable functions in $L^2(\Omega)$ with derivatives in $L^2(\Omega)$, $k \in \mathbb{N}_0$
$\boldsymbol{H}^k(\Omega)$	$:= (H^k(\Omega))^d := H^k(\Omega; \mathbb{R}^d)$, $\mathbb{R}^d$-valued functions with components in $H^k(\Omega)$
$H_0^k(\Omega)$	closure of $\mathcal{D}(\Omega)$ in $H^k(\Omega)$
$H_a^1(\Omega)$	$:= \{w \in H^1(\Omega);\ \gamma_0 w = a \text{ on } \partial\Omega,\ a \in H^{1/2}(\partial\Omega)\}$
$H^{-k}(\Omega)$	dual of $H_0^k(\Omega)$, $k \in \mathbb{N}_0$
$\boldsymbol{H}^{k,\mathrm{div}}(\Omega)$	$:= \{\boldsymbol{v} \in \boldsymbol{H}^k(\Omega);\ \boldsymbol{\nabla} \cdot \boldsymbol{v} \in H^k(\Omega)\}$, $k \in \mathbb{N}_0$ (in particular, a Hilbert space)
$\boldsymbol{H}^{\mathrm{div}}(\Omega)$	$:= \boldsymbol{H}^{0,\mathrm{div}}(\Omega)$
$\boldsymbol{H}_a^{\mathrm{div}}(\Omega)$	$:= \{\boldsymbol{v} \in \boldsymbol{H}^{\mathrm{div}}(\Omega);\ \gamma_{\boldsymbol{\nu}}\boldsymbol{v} = a \text{ on } \partial\Omega,\ a \in H^{-1/2}(\partial\Omega)\}$
$\boldsymbol{H}^1(J \times \Omega)$	$:= H^1(J; \boldsymbol{L}^2(\Omega)) \cap L^2(J; \boldsymbol{H}^1(\Omega))$
$L^p(\Omega)$	$:= L^p(\Omega; \mathbb{R}) = \{f : \Omega \to \mathbb{R} \text{ Lebesgue-measurable};\ \|f\|_{L^p(\Omega)} < \infty\}$, $1 \le p \le \infty$
$L^p(J; V)$	space of V-valued functions, whose norm in V is in $L^p(J)$, $1 \le p \le \infty$
$L^2(\Omega)/\mathbb{R}$	quotient space in which two elements of $L^2(\Omega)$ are identified if their difference is constant
$\mathcal{L}(V; W)$	vector space of continuous, linear mappings from V to W
$\mathcal{L}(V_1 \times V_2; \mathbb{R})$	vector space of continuous, bilinear forms
$\mathbb{N}$, $\mathbb{N}_0$	set of natural numbers, set of natural numbers including zero
$\mathbb{P}_k(T)$	vector space of polynomials of maximum degree k on T
$\mathbb{P}_k(\mathcal{T}_h)$	$:= \prod_{T \in \mathcal{T}_h} \mathbb{P}_k(T)$, global approximation space (discontinuous), $k \in \mathbb{N}_0$
$\mathbb{P}_k^{\mathrm{c}}(\mathcal{T}_h)$	$:= \mathbb{P}_k(\mathcal{T}_h) \cap C^0(\overline{\Omega})$, global approximation space (continuous), $k \in \mathbb{N}$
$\mathbb{R}^+$, $\mathbb{R}_0^+$	set of (strictly) positive real numbers, set of nonnegative real numbers
$\mathbb{R}^{m,n}$	vector space of real matrices of dimension $m \times n$
$\mathbb{RT}_k(T)$	local Raviart–Thomas space of order k on triangle T
$\mathbb{RT}_k(\mathcal{T}_h)$	$:= \boldsymbol{H}^{\mathrm{div}}(\Omega) \cap \prod_{T \in \mathcal{T}_h} \mathbb{RT}_k(T)$, global Raviart–Thomas space of order k

Table B.8. Sets and function spaces.

Symbol	Definition
$\|\cdot\|_{C^j(\overline{J};V)}$	$\|v\|_{C^j(\overline{J};V)} \coloneqq \sup_{t\in\overline{J}} \sum_{l=0}^{j} \|\partial_t^l v(t,\cdot)\|_V$
$\|\cdot\|_{L^p(\Omega)}$	$\|v\|_{L^p(\Omega)} \coloneqq \begin{cases} \left(\int_\Omega \lvert v\rvert^p\right)^{1/p}, & 1 \le p < \infty \\ \operatorname{ess\,sup}_{\boldsymbol{x}\in\Omega} \lvert v(\boldsymbol{x})\rvert, & p = \infty \end{cases}$
$\|\cdot\|_{L^p(J;V)}$	$\|v\|_{L^p(J;V)} \coloneqq \begin{cases} \left(\int_J \|v(t,\cdot)\|_V^p\right)^{1/p}, & 1 \le p < \infty \\ \operatorname{ess\,sup}_{t\in J} \|v(t,\cdot)\|_V, & p = \infty \end{cases}$
$\|\cdot\|_{H^k(\Omega)}$	$\|v\|_{H^k(\Omega)}^2 \coloneqq \sum_{l=0}^{k} \lvert v\rvert_{H^l(\Omega)}^2$
$\|\cdot\|_{\boldsymbol{H}^k(\Omega)}$	$\|\boldsymbol{v}\|_{\boldsymbol{H}^k(\Omega)}^2 \coloneqq \sum_{i=1}^{d} \|v_i\|_{H^k(\Omega)}^2$
$\|\cdot\|_{\boldsymbol{H}^{k,\mathrm{div}}(\Omega)}$	$\|\boldsymbol{v}\|_{\boldsymbol{H}^{k,\mathrm{div}}(\Omega)}^2 \coloneqq \|\boldsymbol{v}\|_{\boldsymbol{H}^k(\Omega)}^2 + \|\boldsymbol{\nabla}\cdot\boldsymbol{v}\|_{H^k(\Omega)}^2$
$\lvert\cdot\rvert_{H^k(\Omega)}$	$\lvert v\rvert_{H^k(\Omega)}^2 \coloneqq \sum_{\lvert\boldsymbol{\alpha}\rvert=k} \|\partial^{\boldsymbol{\alpha}} v\|_{L^2(\Omega)}^2$, seminorm in $H^k(\Omega)$
$\|\cdot\|_{H^{1/2}(\partial\Omega)}$	$\|v\|_{H^{1/2}(\partial\Omega)}^2 \coloneqq \int_{\partial\Omega} \lvert v(\boldsymbol{x})\rvert^2 \,\mathrm{d}\boldsymbol{x} + \int_{\partial\Omega}\int_{\partial\Omega} \frac{\lvert v(\boldsymbol{x})-v(\boldsymbol{y})\rvert^2}{\lvert\boldsymbol{x}-\boldsymbol{y}\rvert^{d+1}} \,\mathrm{d}\boldsymbol{x}\,\mathrm{d}\boldsymbol{y}$
$\|\cdot\|_{V'}$	$\coloneqq \|\cdot\|_{\mathcal{L}(V;\mathbb{R})}$ (see $\|\cdot\|_{\mathcal{L}(V;W)}$)
$\|\cdot\|_{\mathcal{L}(V;W)}$	$\|A\|_{\mathcal{L}(V;W)} \coloneqq \sup_{v\in V} \frac{\|Av\|_W}{\|v\|_V} = \sup_{\|v\|_V=1} \|Av\|_W$, operator norm
$\|\cdot\|_{V_1,V_2}$	$\|a\|_{V_1,V_2} \coloneqq \sup_{v_1\in V_1, v_2\in V_2} \frac{a(v_1,v_2)}{\|v_1\|_{V_1}\|v_2\|_{V_2}}$, norm in $\mathcal{L}(V_1\times V_2;\mathbb{R})$
$(\cdot\,,\,\cdot)_V$	inner product in Hilbert space V
$(\cdot\,,\,\cdot)_{\boldsymbol{H}^{k,\mathrm{div}}(\Omega)}$	$(\boldsymbol{v}_1\,,\,\boldsymbol{v}_2)_{\boldsymbol{H}^{k,\mathrm{div}}(\Omega)} \coloneqq (\boldsymbol{v}_1\,,\,\boldsymbol{v}_2)_{\boldsymbol{H}^k(\Omega)} + (\boldsymbol{\nabla}\cdot\boldsymbol{v}_1\,,\,\boldsymbol{\nabla}\cdot\boldsymbol{v}_2)_{H^k(\Omega)}$
$\langle\cdot\,,\,\cdot\rangle_{V',V}$	duality pairing, $\langle v'\,,\,v\rangle_{V',V} = v'(v) = v'v$

Table B.9. Norms, inner products, and duality pairing.

References

Abdulle, A. (2009). "The finite element heterogeneous multiscale method: a computational strategy for multiscale PDEs." *Multiple scales problems in biomathematics, mechanics, physics and numerics* 31, pp. 133–181.

Abdulle, A. & B. Engquist (2007/08). "Finite element heterogeneous multiscale methods with near optimal computational complexity." *Multiscale Modeling & Simulation* 6.4, pp. 1059–1084. ISSN: 1540-3459. DOI: 10.1137/060676118.

Adams, R. A. (1975). *Sobolev Spaces*. Pure and Applied Mathematics Bd. 65. Academic Press.

Adams, R. A. & J. J. F. Fournier (2003). *Sobolev Spaces*. 2nd ed. Pure and Applied Mathematics Bd. 140. Elsevier Science. ISBN: 9780120441433.

Alberty, J., C. Carstensen, & S. A. Funken (1999). "Remarks around 50 lines of Matlab: short finite element implementation." *Numerical Algorithms* 20.2–3, pp. 117–137. ISSN: 1017-1398. DOI: 10.1023/A:1019155918070.

Allaire, G. (1992). "Homogenization and two-scale convergence." *SIAM Journal on Mathematical Analysis* 23.6, pp. 1482–1518.

——— (2010a). *Homogenization in Porous Media*. Accessed: Mar. 20 2013. CEA–EDF–INRIA school on homogenization. URL: http://www.cmap.polytechnique.fr/~allaire/homog/lect2.pdf.

——— (2010b). *Introduction to Homogenization Theory*. Accessed: Mar. 20 2013. CEA–EDF–INRIA school on homogenization. URL: http://www.cmap.polytechnique.fr/~allaire/homog/lect1.pdf.

——— (2010c). *Numerical Methods of Homogenization*. Accessed: Mar. 20 2013. CEA–EDF–INRIA school on homogenization. URL: http://www.cmap.polytechnique.fr/~allaire/homog/lect2.pdf.

Allaire, G., A. Mikelić, & A. Piatnitski (2010). "Homogenization of the linearized ionic transport equations in rigid periodic porous media." *Journal of Mathematical Physics* 51.12, pp. 123 103. DOI: 10.1063/1.3521555.

Allaire, G., R. Brizzi, J.-F. Dufrêche, A. Mikelić, & A. Piatnitski (2013). "Ion transport in porous media: derivation of the macroscopic equations using upscaling and properties of the effective coefficients." *Computational Geosciences*, pp. 1–17. ISSN: 1420-0597. DOI: 10.1007/s10596-013-9342-6.

Arbogast, T, M. F. Wheeler, & N. Y. Zhang (1996). "A nonlinear mixed finite element method for a degenerate parabolic equation arising in flow in porous media." *SIAM Journal on Numerical Analysis* 33.4, pp. 1669–1687. ISSN: 0036-1429. DOI: 10.1137/S0036142994266728.

Armijo, L. (1966). "Minimization of functions having Lipschitz continuous first partial derivatives." *Pacific Journal of Mathematics* 16.1, pp. 1–3.

Arnold, D. N., F. Brezzi, & M. Fortin (1984). "A stable finite element for the Stokes equations." *Calcolo* 21.4, pp. 337–344. ISSN: 0008-0624.

Bahriawati, C. & C. Carstensen (2005). "Three matlab implementations of the lowest-order Raviart–Thomas MFEM with a posteriori error control." *Computational Methods in Applied Mathematics* 5.4, pp. 333–361.

Barbeiro, S. & M. F. Wheeler (2010). "A priori error estimates for the numerical solution of a coupled geomechanics and reservoir flow model with stress-dependent permeability." *Computational Geosciences* 14 (4), pp. 755–768. ISSN: 1420-0597. DOI: 10.1007/s10596-010-9186-2.

Bathe, K.-J. (2007). *Finite Element Procedures*. London: Prentice-Hall.

Bauer, G. (2012). "A coupled finite element approach for electrochemical systems." Dissertation. Munich: Technische Universität München.

Bauer, G., V. Gravemeier, & W. A. Wall (2011). "A 3D finite element approach for the coupled numerical simulation of electrochemical systems and fluid flow." *International Journal for Numerical Methods in Engineering* 86.11, pp. 1339–1359. ISSN: 1097-0207. DOI: 10.1002/nme.3107.

——— (2012). "A stabilized finite element method for the numerical simulation of multi-ion transport in electrochemical systems." *Computer Methods in Applied Mechanics and*

Engineering 223–224.0, pp. 199–210. ISSN: 0045-7825. DOI: 10.1016/j.cma.2012.02.003.

Bause, M. & P. Knabner (2004). "Numerical simulation of contaminant biodegradation by higher order methods and adaptive time stepping." *Computing and Visualization in Science* 7 (2), pp. 61–78. ISSN: 1432-9360. DOI: 10.1007/s00791-004-0139-y.

Bear, J. (1972). *Dynamics of Fluids in Porous Media*. Dover Books on Physics and Chemistry. Dover Publications, Inc. ISBN: 9780486656755.

Bear, J. & A. H.-D. Cheng (2010). *Modeling Groundwater Flow and Contaminant Transport*. Theory and Applications of Transport in Porous Media. Springer. ISBN: 9781402066818.

Bensoussan, A., J. Lions, & G. Papanicolaou (1978). *Asymptotic Analysis for Periodic Structures*. Studies in Mathematics and Its Applications. Amsterdam: North-Holland Publishing Company. ISBN: 9780444851727.

Benzi, M., G. H. Golub, & J. Liesen (2005). "Numerical solution of saddle point problems." *Acta Numerica* 14, pp. 1–137. ISSN: 1474-0508. DOI: 10.1017/S0962492904000212.

Bercovier, M & O Pironneau (1979). "Error estimates for finite-element method solution of the Stokes problem in the primitive variables." *Numerische Mathematik* 33.2, pp. 211–224. ISSN: 0029-599X. DOI: 10.1007/BF01399555.

Berg, P. & J. Findlay (2011). "Analytical solution of the Poisson–Nernst–Planck–Stokes equations in a cylindrical channel." *Proceedings of the Royal Society A: Mathematical, Physical and Engineering Science* 467.2135, pp. 3157–3169. DOI: 10.1098/rspa.2011.0080.

Bollhöfer, M. & Y. Saad (2006). "Multilevel preconditioners constructed from inverse-based ILUs." *SIAM Journal on Scientific Computing* 27, pp. 1627–1650.

Bollhöfer, M., J. I. Aliaga, A. F. Martín, & E. S. Quintana-Ortí (2011). "ILUPACK." *Encyclopedia of Parallel Computing*. Ed. by D. Padua. Springer US, pp. 917–926. ISBN: 978-0-387-09765-7. DOI: 10.1007/978-0-387-09766-4_513.

Bourgat, J. (1979). "Numerical experiments of the homogenization method." *Computing Methods in Applied Sciences and Engineering, 1977, I*. Ed. by R. Glowinski, J. Lions, & I. Laboria. Vol. 704. Lecture Notes in Mathematics. Berlin / Heidelberg: Springer, pp. 330–356. ISBN: 978-3-540-09123-3.

Brezzi, F. & M. Fortin (1991). *Mixed and hybrid finite elements methods*. Springer series in computational mathematics. New York: Springer. ISBN: 9780387975825.

Brezzi, F. & R. S. Falk (1991). "Stability of higher-order Hood–Taylor methods." *SIAM Journal on Numerical Analysis* 28.3, pp. 581–590. ISSN: 0036-1429. DOI: 10.1137/0728032.

Brunner, F., S. Kräutle, & P. Knabner (2011). "Mixed hybrid and linear conforming finite elements for reactive multicomponent transport in porous media: a comparative numerical study." Chair of Applied Mathematics 1, University of Erlangen–Nuremberg. To appear.

Buckingham, E. (1914). "On physically similar systems; illustrations of the use of dimensional equations." *Physical Review* 4 (4), pp. 345–376. DOI: 10.1103/PhysRev.4.345.

Carrayrou, J., J. Hoffmann, P. Knabner, S. Kräutle, C. Dieuleveult, J. Erhel, J. Lee, V. Lagneau, K. U. Mayer, & K. T. B. MacQuarrie (2010). "Comparison of numerical methods for simulating strongly nonlinear and heterogeneous reactive transport problems — the MoMaS benchmark case." *Computational Geosciences* 14.3, pp. 483–502. ISSN: 1420-0597. DOI: 10.1007/s10596-010-9178-2.

Chavarria-Krauser, A. & M. Ptashnyk (2010). "Homogenization of long-range auxin transport in plant tissues." *Nonlinear Analysis: Real World Applications* 11.6, pp. 4524–4532.

Chen, Z. (2005). *Finite Element Methods and Their Applications*. Springer.

Ciarlet, P. G. (1991). "Basic Error Estimates for Elliptic Problems." *Handbook of Numerical Analysis: Finite Element Methods (Part 1)*. Ed. by P. G. Ciarlet & J. L. Lions. Vol. 2. Amsterdam: North-Holland, pp. 17–351. ISBN: 9780444703651.

Cioranescu, D. & P. Donato (1999). *An Introduction to Homogenization*. Ed. by J. Ball & D. Welsh. Vol. 17. Oxford lecture series in mathematics and its applications. Oxford University Press.

Cioranescu, D. & J. Saint Jean Paulin (1999). *Homogenization of Reticulated Structures*. Applied Mathematical Sciences 136. Springer. ISBN: 9780387986340.

Davis, T. A. (2004). "Algorithm 832: UMFPACK V4.3 — an unsymmetric-pattern multifrontal method." *ACM Trans. Math. Softw.* 30.2, pp. 196–199. ISSN: 0098-3500. DOI: 10.1145/992200.992206.

——— (2011). "Algorithm 915, SuiteSparseQR: Multifrontal multithreaded rank-revealing sparse QR factorization." *ACM Trans. Math. Softw.* 38.1, 8:1–8:22. ISSN: 0098-3500. DOI: 10.1145/2049662.2049670.

Deuflhard, P. (2004). *Newton Methods for Nonlinear Problems: Affine Invariance and Adaptive Algorithms*. Series Computational Mathematics 35. Springer.

Domenico, P. A. & F. W. Schwartz (1998). *Physical and Chemical Cydrogeology*. 2nd ed. Vol. 1. John Wiley & Sons. ISBN: 9780471597629.

Douglas Jr., J. & J. E. Roberts (1985). "Global estimates for mixed methods for second order elliptic equations." *Mathematics of Computation* 44.169, pp. 39–52. ISSN: 00255718.

Du, R. & P. Ming (2010). "Heterogeneous multiscale finite element method with novel numerical integration schemes." *Communications in Mathematical Sciences* 8.4, pp. 863–885. ISSN: 1539-6746.

Durán, R. G. (2008). "Mixed Finite Element Methods." *Mixed Finite Elements, Compatibility Conditions, and Applications: Lectures given at the C.I.M.E.* Springer. ISBN: 3540783148.

E, W. & B. Engquist (2003). "The heterogeneous multiscale methods." *Communications in Mathematical Sciences* 1.1, pp. 87–132. ISSN: 1539-6746.

E, W., P. Ming, & P. Zhang (2005). "Analysis of the heterogeneous multiscale method for elliptic homogenization problems." *Journal of the American Mathematical Society* 18.1, 121–156 (electronic). ISSN: 0894-0347. DOI: 10.1090/S0894-0347-04-00469-2.

E, W., B. Engquist, X. Li, W. Ren, & E. Vanden-Eijnden (2007). "Heterogeneous multiscale methods: a review." *Commun. Comput. Phys.* 2.3, pp. 367–450. ISSN: 1815-2406.

Eck, C. (2004). "A two-scale phase field model for liquid–solid phase transitions of binary mixtures with dendritic microstructure." Habilitation Thesis. University of Erlangen–Nuremberg.

Efendiev, Y. & T. Hou (2009). *Multiscale Finite Element Methods: Theory and Applications*. Surveys and Tutorials in the Applied Mathematical Sciences. New York: Springer. ISBN: 9780387094953.

Elman, H., D. Silvester, & A. Wathen (2005). *Finite Elements and Fast Iterative Solvers with Applications in Incompressible Fluid Dynamics*. Oxford University Press.

Ern, A. & J. L. Guermond (2004). *Theory and Practice of Finite Elements*. Applied Mathematical Sciences. Springer.

Evans, L. C. (2010). *Partial Differential Equations*. Graduate Studies in Mathematics. American Mathematical Society. ISBN: 9780821849743.

Fatima, T., A. Muntean, & M. Ptashnyk (2012). "Unfolding-based corrector estimates for a reaction–diffusion system predicting concrete corrosion." *Applicable Analysis* 91.6, pp. 1129–1154. DOI: 10.1080/00036811.2011.625016.

Frank, F., N. Ray, & P. Knabner (2011). "Numerical investigation of homogenized Stokes–Nernst–Planck–Poisson systems." *Computing and Visualization in Science* 14.8, pp. 385–400. ISSN: 1432-9360. DOI: 10.1007/s00791-013-0189-0.

——— (2012). "Numerical investigation of a homogenized Stokes–Nernst–Planck–Poisson problem." *The Preprint-Series of the Institute of Applied Mathematics* 352. University of Erlangen–Nuremberg, pp. 2–34. ISSN: 1435-5833.

Geuzaine, C. & J.-F. Remacle (2009). "Gmsh: a three-dimensional finite element mesh generator with built-in pre- and post-processing facilities." *International Journal for Numerical Methods in Engineering* 79.11, pp. 1309–1331.

Girault, V. & P. A. Raviart (1979). *Finite Element Approximation of the Navier–Stokes Equations*. Lecture Notes in Mathematics. Springer. ISBN: 9783540095576.

——— (1986). *Finite Element Methods for Navier–Stokes Equations: Theory and Algorithms*. Springer Series in Computational Mathematics. Springer. ISBN: 9783540157960.

Griebel, M. & M. Klitz (2010). "Homogenization and numerical simulation of flow in geometries with textile microstructures." *Multiscale Modeling & Simulation* 8.4, pp. 1439–1460.

Griso, G. (2004). "Error estimates and unfolding for periodic homogenization." *Asymptotic Analysis* 40, pp. 169–186.

——— (2005). "Interior error estimates for periodic homogenization." *Comptes Rendus Mathématique* 340.3, pp. 251–254.

Gross, S. & A. Reusken (2011). *Numerical Methods for Two-Phase Incompressible Flows*. Springer Series in Computational Mathematics. Springer Berlin Heidelberg. ISBN: 9783642196867.

Gummel, H. K. (1964). "A self-consistent iterative scheme for one-dimensional steady state transistor calculations." *IEEE Transactions on Electron Devices* 11, pp. 455–465.

Herz, M., N. Ray, & P. Knabner (2012). "Existence and uniqueness of a global weak solution of a Darcy–Nernst–Planck–Poisson system." *GAMM-Mitteilungen* 35.2, pp. 191–208. ISSN: 1522-2608. DOI: 10.1002/gamm.201210013.

Hood, P. & C. Taylor (1973). "A numerical solution of the Navier Stokes equations using the finite element technique." *Computers & Fluids* 1.1, pp. 73–100.

Hornung, U. (1997). *Homogenization and Porous Media*. Springer.

Hughes, T. J. R. (1987). "Recent progress in the development and understanding of SUPG methods with special reference to the compressible Euler and Navier–Stokes equation." *International Journal for Numerical Methods in Fluids* 7.11, pp. 1261–1275.

——— (2000). *The Finite Element Method: Linear Static and Dynamic Finite Element Analysis*. Dover Civil and Mechanical Engineering Series. Dover Publications. ISBN: 9780486411811.

Hughes, T. J. R., G. Scovazzi, & L. P. Franca (2004). "Multiscale and Stabilized Methods." *Encyclopedia of Computational Mechanics*. Ed. by E. Stein, R. De Borst, & T. J. R. Hughes. John Wiley & Sons, Ltd. ISBN: 9780470091357. DOI: 10.1002/0470091355.ecm051.pub2.

HyPHM. Accessed: Feb. 25 2013. Chair of Applied Mathematics 1, University of Erlangen–Nuremberg. URL: http://www1.am.uni-erlangen.de/HyPHM.

Jikov, V., S. Kozlov, & O. Oleinik (1994). *Homogenization of Differential Operators and Integral Functionals*. Berlin/Heidelberg: Springer.

Johannesson, B. (2009). "Ionic diffusion and kinetic homogeneous chemical reactions in the pore solution of porous materials with moisture transport." *Computers and Geotechnics* 36.4, pp. 577–588. ISSN: 0266-352X.

Kelley, C. T. (1995). *Iterative Methods for Linear and Nonlinear Equations*. Frontiers in Applied Mathematics 16. SIAM.

——— (2003). *Solving Nonlinear Equations with Newton's Method*. Fundamentals of Algorithms 1. SIAM.

Kinzelbach, W. (1992). *Numerische Methoden zur Modellierung des Transports von Schadstoffen im Grundwasser*. 2. Oldenbourg.

Kirby, B. (2010). *Micro- And Nanoscale Fluid Mechanics: Transport in Microfluidic Devices*. Cambridge University Press.

Knabner, P. & L. Angermann (2003). *Numerical Methods for Elliptic and Parabolic Partial Differential Equations*. Vol. 44. Texts in Applied Mathematics. New York: Springer.

Knabner, P. & W. Barth (2012). *Lineare Algebra: Grundlagen und Anwendungen*. Springer-Lehrbuch. Springer. ISBN: 978-3642321856.

Kuzmin, D. (2010). *A Guide to Numerical Methods for Transport Equations*. Accessed: Feb. 25 2013. Chair of Applied Mathematics 3, University of Erlangen–Nuremberg. URL: http://www.mathematik.uni-dortmund.de/~kuzmin/Transport.pdf.

Logan, J. D. (2001). *Transport Modeling in Hydrogeochemical Systems*. Interdisciplinary Applied Mathematics. New York: Springer. ISBN: 0-387-95276-4.

Löhner, R. (2008). *Applied Computational Fluid Dynamics Techniques: An Introduction based on Finite Element Methods. 2nd ed.* Chichester: Wiley.

Looker, J. R. & S. L. Carnie (2006). "Homogenization of the ionic transport equations in periodic porous media." *Transport in Porous Media* 65.1, pp. 107–131. ISSN: 0169-3913. DOI: 10.1007/s11242-005-6080-9.

Mahato, H. S. (2013). "Homogenization of a system of nonlinear multi-species diffusion–reaction equations in an $H^{1,p}$ setting." PhD thesis. University of Bremen.

Masliyah, J. H. & S. Bhattacharjee (2006). *Electrokinetic and Colloid Transport Phenomena*. Wiley-Interscience. ISBN: 0471788821.

MATLAB Parallel Computing Toolbox. The MathWorks, Inc., Natick, Massachusetts, United States. URL: http://www.mathworks.de/products/parallel-computing.

MATLAB Partial Differential Equation Toolbox. The MathWorks, Inc., Natick, Massachusetts, United States. URL: http://www.mathworks.de/products/pde.

MATLAB, Release 2012b. The MathWorks, Inc., Natick, Massachusetts, United States. URL: http://www.mathworks.com/products/matlab.

McNaught, A. D. & A. R. Wilkinson, eds. (1997). *Compendium of Chemical Terminology*. 2nd ed. IUPAC Chemical Nomenclature Series. Blackwell Scientific Publications. ISBN: 9780865426849.

Melnik, T. A. & O. A. Sivak (2010). "Asymptotic analysis of a parabolic semilinear problem with nonlinear boundary multiphase interactions in a perforated domain." *Journal of Mathematical Sciences* 164.3, pp. 427–453.

Ming, P. & X. Yue (2006). "Numerical methods for multiscale elliptic problems." *Journal of Computational Physics* 214.1, pp. 421–445. ISSN: 0021-9991. DOI: 10.1016/j.jcp.2005.09.024.

Moyne, C. & M. A. Murad (2002). "Electro-chemo-mechanical couplings in swelling clays derived from a micro / macro-homogenization procedure." *International Journal of Solids and Structures* 39.25, pp. 6159–6190. ISSN: 0020-7683. DOI: 10.1016/S0020-7683(02)00461-4.

——— (2006). "A two-scale model for coupled electro-chemo-mechanical phenomena and Onsager's reciprocity relations in expansive clays: I Homogenization analysis." *Transport in Porous Media* 62 (3), pp. 333–380. ISSN: 0169-3913.

Nédélec, J. (1980). "Mixed finite elements in $\mathbb{R}^3$." *Numerische Mathematik* 35 (3), pp. 315–341. ISSN: 0029-599X. DOI: 10.1007/BF01396415.

Nguetseng, G. (1989). "A general convergence result for a functional related to the theory of homogenization." *SIAM Journal of Mathematical Analysis* 20.3, pp. 608–623. ISSN: 0036-1410. DOI: 10.1137/0520043.

Orive, R. & E. Zuazua (2005). "Finite difference approximation of homogenization problems for elliptic equations." *Multiscale Modeling & Simulation* 4.1, pp. 36–87.

Paz-García, J. M., B. Johannesson, L. M. Ottosen, A. B. Ribeiro, & J. M. Rodríguez-Maroto (2011). "Modeling of electrokinetic processes by finite element integration of the Nernst–Planck–Poisson system of equations." *Separation and Purification Technology* 79.2, pp. 183–192. ISSN: 1383-5866. DOI: 10.1016/j.seppur.2011.02.023.

Pérez-Pardo, B. (2012). "Mathematical modeling and simulation of a microfluidic reactor." MA thesis. Chair of Applied Mathematics 1, University of Erlangen–Nuremberg.

Prechtel, A. (2005). *Modelling and Efficient Numerical Solution of Hydrogeochemical Multicomponent Transport Problems by Process Preserving Decoupling Techniques*. Industriemathematik und angewandte Mathematik. Shaker. ISBN: 9783832242954.

Probstein, R. F. (2003). *Physicochemical Hydrodynamics: An Introduction*. Wiley-Interscience. ISBN: 9780471458302.

Prohl, A. & M. Schmuck (2009). "Convergent discretizations for the Nernst–Planck–Poisson system." *Numerische Mathematik* 111.4, pp. 591–630. ISSN: 0029-599X. DOI: 10.1007/s00211-008-0194-2.

——— (2010). "Convergent finite element discretizations of the Navier–Stokes–Nernst–Planck–Poisson system." *ESAIM: Mathematical Modelling and Numerical Analysis* 44 (03), pp. 531–571. ISSN: 1290-3841. DOI: 10.1051/m2an/2010013.

Quack, M., J. Stohner, H. L. Strauss, M. Takami, A. J. Thor, E. R. Cohen, T. Cvitaš, J. G. Frey, B. Holström, K. Kuchitsu, R. Marquardt, I. Mills, & F. Pavese, eds. (2007). *Quantities, Units, and Symbols in Physical Chemistry*. 3rd ed. IUPAC & RSC Publishing. ISBN: 9780854044337. DOI: 10.1039/9781847557889.

Quarteroni, A. & A. Valli (1994). *Numerical Approximation of Partial Differential Equations*. Springer Series in Computational Mathematics Series. Springer. ISBN: 9783540571117.

Radu, F. A., N. Suciu, J. Hoffmann, A. Vogel, O. Kolditz, C.-H. Park, & S. Attinger (2011). "Accuracy of numerical simulations of contaminant transport in heterogeneous aquifers: A comparative study." *Advances in Water Resources* 34.1, pp. 47–61. ISSN: 0309-1708. DOI: http://dx.doi.org/10.1016/j.advwatres.2010.09.012.

Radu, F. A. (2004). "Mixed finite element discretization of Richard's equation: error analysis and application to realistic infiltration problems." PhD thesis. Chair of Applied Mathematics 1, University of Erlangen–Nuremberg.

Radu, F. A. & W. Wang (2011). "Convergence analysis for a mixed finite element scheme for flow in strictly unsaturated porous media." *Nonlinear Analysis: Real World Applications*. In Press. ISSN: 1468-1218. DOI: 10.1016/j.nonrwa.2011.05.003.

Radu, F. A., M. Bause, A. Prechtel, & S. Attinger (2008). "A mixed hybrid finite element discretization scheme for reactive transport in porous media." *Numerical Mathematics*

and Advanced Applications. Ed. by K. Kunisch, G. Of, & O. Steinbach. Springer, pp. 513–520. ISBN: 978-3-540-69776-3. DOI: 10.1007/978-3-540-69777-0_61.

Radu, F. A., I. S. Pop, & S. Attinger (2010). "Analysis of an Euler implicit-mixed finite element scheme for reactive solute transport in porous media." *Numerical Methods for Partial Differential Equations* 26.2, pp. 320–344. ISSN: 0749-159X. DOI: 10.1002/num.20436.

Ramachandran, P. & G. Varoquaux (2011). "Mayavi: 3D visualization of scientific data." *Computing in Science & Engineering* 13.2, pp. 40–51. ISSN: 1521-9615.

Raviart, P. A. & J. M. Thomas (1977). "A mixed finite element method for second-order elliptic problems." *Mathematical Aspects of the Finite Element Method, Lectures Notes in Mathematics* 606, pp. 292–315.

Ray, N. (2013). "Colloidal transport in porous media — modeling and analysis." PhD thesis. Chair of Applied Mathematics 1, University of Erlangen–Nuremberg. ISBN: 978-3-8440-2043-4.

Ray, N., A. Muntean, & P. Knabner (2012a). "Rigorous homogenization of a Stokes–Nernst–Planck–Poisson system." *Journal of Mathematical Analysis and Applications* 390.1, pp. 374–393. ISSN: 0022-247X. DOI: 10.1016/j.jmaa.2012.01.052.

Ray, N., T. van Noorden, F. Frank, & P. Knabner (2012b). "Colloid and fluid dynamics in porous media including an evolving microstructure." *The Preprint-Series of the Institute of Applied Mathematics* 351. University of Erlangen–Nuremberg, pp. 2–20. ISSN: 1435-5833.

——— (2012c). "Multiscale modeling of colloid and fluid dynamics in porous media including an evolving microstructure." *Transport in Porous Media* 95.3, pp. 669–696. ISSN: 0169-3913. DOI: 10.1007/s11242-012-0068-z.

Redeker, M. & C. Eck (2013). "A fast and accurate adaptive solution strategy for two-scale models with continuous inter-scale dependencies." *Journal of Computational Physics* 240, pp. 268–283. ISSN: 0021-9991. DOI: 10.1016/j.jcp.2012.12.025.

Roache, P. J. (1998a). *Verification and validation in computational science and engineering*. Hermosa Publishers. ISBN: 9780913478080.

——— (1998b). "Verification of codes and calculations." *AIAA Journal* 36.5, pp. 696–702.

Roache, P. J. (2002). "Code verification by the method of manufactured solutions." *Journal of Fluids Engineering* 124.1, pp. 4–10. DOI: 10.1115/1.1436090.

Roberts, J. & J.-M. Thomas (1991). "Mixed and hybrid methods." *Handbook of Numerical Analysis: Finite Element Methods (Part 1)*. Ed. by P. G. Ciarlet & J. L. Lions. Vol. 2. Handbook of Numerical Analysis. Amsterdam: North-Holland, pp. 523–639. DOI: 10.1016/S1570-8659(05)80041-9.

Roubíček, T. (2005a). "Incompressible fluid mixtures of ionized constituents." *Trends in Applications of Mathematics to Mechanics*. Ed. by Y. Wang & K. Hutter. Shaker, pp. 429–440.

——— (2005b). *Nonlinear Partial Differential Equations with Applications*. International Series of Numerical Mathematics. Birkhäuser. ISBN: 9783764372934.

——— (2006). "Incompressible ionized fluid mixtures." *Continuum Mechanics and Thermodynamics* 17.7, pp. 493–509.

Saaltink, M. W., J. Carrera, & C. Ayora (2000). "A comparison of two approaches for reactive transport modelling." *Journal of Geochemical Exploration* 69–70.0, pp. 97–101. ISSN: 0375-6742. DOI: 10.1016/S0375-6742(00)00012-1.

Salari, K. & P. Knupp (2000). "Code verification by the method of manufactured solutions." *Sandia National Laboratories*, pp. 3–117. DOI: 10.2172/759450.

Samson, E., J. Marchand, J.-L. Robert, & J.-P. Bournazel (1999). "Modelling ion diffusion mechanisms in porous media." *International Journal for Numerical Methods in Engineering* 46.12, pp. 2043–2060. ISSN: 1097-0207. DOI: 10.1002/(SICI)1097-0207(19991230)46:12<2043::AID-NME795>3.0.CO;2-7.

Sarkis, M. & H. Versieux (2008). "Convergence analysis for the numerical boundary corrector for elliptic equations with rapidly oscillating coefficients." *SIAM Journal on Numerical Analysis* 46.2, pp. 545–576.

Schmuck, M. (2009). "Analysis of the Navier–Stokes–Nernst–Planck–Poisson system." *Mathematical Models and Methods in Applied Sciences* 19.06, pp. 993–1014. DOI: 10.1142/S0218202509003693.

——— (2011). "Modeling and deriving porous media Stokes–Poisson–Nernst–Planck equations by a multiple-scale approach." *Communications in Mathematical Sciences* 9.3, pp. 685–710.

——— (2012). "First error bounds for the porous media approximation of the Poisson–Nernst–Planck equations." *ZAMM* 92.4, pp. 304–319.

——— (2013). "New porous medium Poisson–Nernst–Planck equations for strongly oscillating electric potentials." *Journal of Mathematical Physics* 54.2, p. 21.

Smith, D., P. Pivonka, C. Jungnickel, & S. Fityus (2004). "Theoretical analysis of anion exclusion and diffusive transport through platy-clay soils." *Transport in Porous Media* 57.3, pp. 251–277.

Spitz, K. & J. Moreno (1996). *A Practical Guide to Groundwater and Solute Transport Modeling*. John Wiley & Sons. ISBN: 9780471136873.

Squillacote, A. H. (2007). *The ParaView Guide: A Parallel Visualization Application*. Kitware. ISBN: 9781930934214.

Stroud, A. (1971). *Approximate Calculation of Multiple Integrals*. Prentice-Hall Series in Automatic Computation. Prentice-Hall.

Suciu, N., F. Radu, A. Prechtel, F. Brunner, & P. Knabner (2012). "A coupled finite element-global random walk approach to advection-dominated transport in porous media with random hydraulic conductivity." *Journal of Computational and Applied Mathematics*, in press. ISSN: 0377-0427. DOI: 10.1016/j.cam.2012.06.027.

Sun, S. & M. F. Wheeler (2005). "Discontinuous Galerkin methods for coupled flow and reactive transport problems." *Appl. Numer. Math.* 52.2–3, pp. 273–298. ISSN: 0168-9274. DOI: 10.1016/j.apnum.2004.08.035.

Sun, S., B. Rivière, & M. F. Wheeler (2002). "A combined mixed finite element and discontinuous Galerkin method for miscible displacement problem in porous media." *Recent Progress in Computational and Applied PDES*. Ed. by T. Chan, Y. Huang, T. Tang, J. Xu, & L.-A. Ying. Springer, pp. 323–351. ISBN: 978-1-4613-4929-7. DOI: 10.1007/978-1-4615-0113-8_23.

Tan, L. & N. Zabaras (2007). "Multiscale modeling of alloy solidification using a database approach." *Journal of Computational Physics* 227, pp. 728–754. DOI: 10.1016/j.jcp.2007.08.016.

Thomas, J. M. (1977). *Sur l'analyse Numérique des Méthodes d'Éléments Finis Hybrides et Mixtes*. Thèse d'Etat, Université Pierre et Marie Curie, Paris.

Van Noorden, T. L. (2009). “Crystal precipitation and dissolution in a porous medium: effective equations and numerical experiments.” *Multiscale Modeling & Simulation* 7.3, pp. 1220–1236.

Van de Ven, T. G. M. (1989). *Colloidal Hydrodynamics*. Colloid Science. Academic Press. ISBN: 9780127107707.

Wu, Z., J. Yin, & C. Wang (2006). *Elliptic & Parabolic Equations*. World Scientific. ISBN: 9789812700254.

Yeh, G. T. & V. S. Tripathi (1989). “A critical evaluation of recent developments in hydrogeochemical transport models of reactive multi-chemical components.” *Water Resources Research* 25, pp. 93–108. DOI: 10.1029/WR025i001p00093.